Development of a novel tunable hydrogel to support tissue formation in the context of full-thickness skin equivalents

Mariana Carranca Palomo

N°d'ordre NNT : 2020LYSE1124.

THESE de DOCTORAT DE L'UNIVERSITE DE LYON
opérée au sein de
l'Université Claude Bernard Lyon 1

Ecole Doctorale N° ED 205
Ecole Doctorale Interdisciplinaire Science-Santé

Spécialité de doctorat : Ingénierie Tissulaire (Peaux)
Discipline : Ingénierie Biomédicale et Biotechnologie

Soutenue publiquement le 04/09/2020, par :
Mariana Carrancá Palomo

Development of a novel tunable hydrogel to support tissue formation in the context of full-thickness skin equivalents.

Devant le jury composé de :

Dr. LETOURNEUR, Didier	Directeur de Recherche/INSERM Paris	Président
Prof. CHANIAUX-DEBACQ, Florence	Chercheur/Université de Namur	Rapportrice
Dr. DURRIEU, Marie-Christine	Directrice de Recherche/INSERM Bordeaux	Rapportrice
Dr. KANDAROVA, Helena	Directrice R&D/InvitroTox Consulting	Rapportrice
Dr. AUXENFANS, Céline	Praticien Hospitalier/UCBL	Examinatrice
Dr. SOHIER, Jérôme	Charge de Recherche/CNRS	Directeur de thèse
Dr. DEBRET, Romain	Charge de Recherche/CNRS	Invité

Université Claude Bernard – LYON 1

Président de l'Université	M. Frédéric FLEURY
Président du Conseil Académique	M. Hamda BEN HADID
Vice-Président du Conseil d'Administration	M. Didier REVEL
Vice-Président du Conseil des Etudes et de la Vie Universitaire	M. Philippe CHEVALLIER
Vice-Président de la Commission de Recherche	M. Jean-François MORNEX
Directeur Général des Services	M. Pierre ROLLAND

COMPOSANTES SANTE

Faculté de Médecine Lyon-Est – Claude Bernard	Doyen : M. Gilles RODE
Faculté de Médecine et Maïeutique Lyon Sud Charles Mérieux	Doyenne : Mme Carole BURILLON
Faculté d'Odontologie	Doyenne : Mme Dominique SEUX
Institut des Sciences Pharmaceutiques et Biologiques	Directrice : Mme Christine VINCIGUERRA
Institut des Sciences et Techniques de la Réadaptation (ISTR)	Directeur : M. Xavier PERROT
Département de Formation et Centre de Recherche en Biologie Humaine	Directrice : Mme Anne-Marie SCHIOTT

COMPOSANTES & DEPARTEMENTS DE SCIENCES & TECHNOLOGIE

UFR Biosciences	Administrateur provisoire : Mme Kathrin GIESELER
Département Génie Electrique et des Procédés (GEP)	Directrice : Mme Rosaria FERRIGNO
Département Informatique	Directeur : M. Behzad SHARIAT
Département Mécanique	Directeur : M. Marc BUFFAT
UFR- Faculté des Sciences	Directeur : M. Bruno ANDRIOLETTI
UFR (STPAS)	Directeur : M. Yannick VANPOULLE
Observatoire de Lyon	Directrice : Mme Isabelle DANIEL
Polytechnique Lyon 1	Directeur : M. Emmanuel PERRIN
Ecole Supérieure de Chimie, Physique, Electronique (CPE Lyon)	Directeur : M. Gérard PIGNAULT
Institut Universitaire de Technologie de Lyon 1	Directeur : M. Christophe VITON
Institut de Sciences Financière et d'Assurances (ISFA)	Directeur : M. Nicolas LEBOISNE
Institut National du Professorat et de l'Education	Administrateur Provisoire : M. Pierre CHAREYRON

Lieu de réalisation de la thèse :

Institute de Biologie et Chimie de Protéines (IBCP)

UMR-5305 CNRS UCBL 1 Laboratoire de Biologie Tissulaire (LBTI)

Equipe : Fonctionnalité et Dynamique du Tissue Cutané

7 Passage du Vercors

69367 LYON Cedex 07, France

Et

Laboratoire des Matériaux (MATEIS)

UMR-5510, CNRS INSA

Equipe : Interactions Biologiques et Biomatériaux

Bât. B. Avenue Jean Capelle

69621 Villeurbanne Cedex, France

Financement :

Ce travail de thèse a été finance par le Région Rhône-Alpes et CONACyT

Encadrement :

La thèse a été encadrée par Dr. Jérôme Sohier (CNRS 5510)

Remerciements

Je veux remercier le laboratoire de Biologie Tissulaire et Ingénierie Thérapeutique (LBTI), UMR 5305, CNRS/UCBL ainsi que laboratoire des Matériaux (MATEIS), UMR 5510, CNRS/INSA pour m'avoir accueilli respectivement au début et à la fin de ma thèse. Je remercie également la **Région Auvergne Rhône-Alpes** ainsi qu'au **CONACyT** pour leur financement.

Je tiens à remercier **Dr. Helena Kandarova**, **Dr. Florence Debacq-Chaniaux** et **Dr. Marie Christine Durrieu** d'avoir accepté de donner de leur temps pour évaluer et juger mon travail en acceptant d'être rapporteurs pour cette thèse. Ainsi qu'aux **Dr. Didier Letourneur** et **Dr. Céline Auxenfans** pour avoir accepté d'être membres de mon jury.

Je remercie l'ensemble des membres de mon Comité de Suivi de Thèse (CST) : **Prof. Daniel Hartmann**, **Prof. Marek Haftek**, **Prof. David Magne** et **Dr. Isabelle Bataille.** Merci pour avoir accepté de participer au CST. Merci pour leur disponibilité, leur suggestions et conseils pour le bon développement du projet de thèse. Je remercie également le **Prof. Marek Haftek** pour m'avoir permis de participer aux Cours de Biologie de la peau organisé par le COBIP, où j'ai appris énormément de choses sur la peau.

Merci également aux stagiaires don j'ai eu le plaisir d'accompagner : **Marc Lacournet**, **Vijay Sindovasane**, **Sabrine Bokhari** et **Leila Berriche**. J'espère que votre expérience dans notre laboratoire a été aussi enrichissante.

J'aimerais remercier l'ensemble de l'IBCP, LBTI et MMBS et plus spécialement tous les membres de l'équipe « Fonctionnalité et dynamique du tissu cutané » pour m'avoir accueilli dans leur équipe. Merci à mes collègues doctorants qui m'ont accueilli au sein de l'équipe depuis mon stage de M2. Merci à **Charlotte Mutter, Noëlle Remoué** et **Cecile Guillon** pour m'avoir enseigné diverses techniques. **Choua Ya** je te remercie très sincèrement de m'avoir partagé tes kératinocytes pour lesquelles tu as surement passé beaucoup de temps à isoler. **Louise Griveau**, même si tu es n'arrivée qu'après moi, tu n'as aucune idée de combien de fois tu m'as donné de bons conseils. J'étais très contente d'avoir quelqu'un avec qui partager les difficultés de travailler avec un matériau dans un univers biologique. Je voudrais aussi remercier l'équipe « Vecteurs colloïdaux et transport tissulaire » et surtout le directeur du LBTI, **Dr. Bernard Verrier**, de m'avoir ouvert les portes dans son laboratoire et de m'avoir permis de rester les derniers mois de ma thèse après notre déménagement dans un nouveau laboratoire. Merci de m'avoir donné l'opportunité de finaliser certaines expériences dans de bonnes conditions !

Merci à la team "BIOMAT" : **Aurore, Louise, Marine, Silvia, Daniel, Marc, Kevin**… La deuxième année de thèses n'aurait pas été pareil sans vous. Entre nous ça réticule !

Je remercie très sincèrement le **Dr. Romain Debret** pour avoir partagé ses connaissances et son expertise sur la peau, l'élastine et l'ELP. Merci pour l'aide et les bons conseils apportés tout au long de ma thèse, ainsi que pour avoir toujours été à l'écoute et m'avoir expliqué des concepts en biologie loin de mon domaine d'expertise initial.

Je remercie très chaleureusement **Aurore Berthier** pour son dynamisme et s'être rendu disponible et toujours prête à aider. Merci pour avoir produit l'ELP, sans laquelle je n'aurais pas pu obtenir une grande partie des résultats présentés ici.

Je tiens à remercier **Naima El Kholti** pour son expertise en histologie et pour sa grande disponibilité. De m'avoir appris plusieurs techniques d'histologie mais surtout ta participation à mon projet et à ton efficacité à inclure mes échantillons en paraffine et à vouloir tout tester pour trouver les meilleures conditions pour les marquages.

Je remercie très chaleureusement **Maxime Dzikowski** pour ses nombreux conseils en chimie, sa disponibilité et le temps qu'il m'a accordé pour m'enseigner des nouvelles techniques mais surtout de m'avoir introduit auprès de mon principal soutien, la personne qui me fait être toujours la meilleure version de moi-même, **Jérôme Busseron**. Jérôme, un immense merci pour ta patience, ton aide à corriger mon français, ton soutien indéfectible au quotidien et pour toujours être capable à me remonter le morale et me faire croire que je suis invincible.

Merci à mes colocs, amies, collègues et famille en Lyon, **Myriam Lamrayah**, **Bruna Gioia** et **Alix Danoy**, pour toutes les aventures et bons moments mais surtout leur soutien et conseil pendant ces trois dernières années très chargées.

Ma thèse a été l'occasion pour moi de travailler au sein de nombreuses collaborations. Je souhaite remercier :

- L'équipe de Biologie et Ingénierie du cartilage et plus spécialement au **Dr. Emeline Perrier-Groult** pour nous avoir permis d'évaluer le potentiel de l'hydrogel avec des chondrocytes humains. Merci pour la disponibilité et à donner une suite aux résultats avec **Pauline Dupaquier**.
- L'Ecole Centrale de Lyon qui m'a donné la possibilité de réaliser de mesures de micro-indentation et au **Dr. Cyrill Pailler-Mattei**. Merci pour la disponibilité ainsi que les conseils dans l'analyse et l'interprétation des résultats concernant les tests d'indentation sur les hydrogels.
- L'équipe RMN du solide des Protéines du **Dr. Anja Böckmann** sans laquelle l'analyse RMN n'aurait pas été possible. Je tiens à remercier **Dr. Lauriane Lecoq** pour la réalisation et l'analyse des expériences de RMN. Merci pour m'avoir permis visiter avec toi le Centre Résonance Magnétique Nucléaire à très hauts champs (CRMN) et ainsi voir en vrai leurs impressionnantes machines de RMN. Merci également pour le temps que tu m'as consacré au moment de la rédaction de la partie RMN de mon manuscrit.
- L'Institute de Génomique Fonctionnelle de Lyon merci pour me donner accès au vibratome sans lequel je n'aurais pas pu faire des dizaines et dizaines de disques d'hydrogel. Merci **Sabine Richard** pour ta disponibilité et ton aide.
- A la Banque de Tissus et Cellules de l'Hôpital Edouard Herriot, sans laquelle, nous n'aurions pas pu évaluer notre hydrogel face à un modèle déjà standardisé et bien connu. Merci **Dr. Celine Auxenfans** pour nous avoir ouvert la porte à une collaboration et à nous avoir donne accès à des échantillons de peaux reconstruites obtenus avec des éponges de Col-GAG-Chi.

Je tiens en particulier à adresser mes plus grands remerciements à mon directeur de thèse, **Dr. Jérôme Sohier**. Avant tout merci pour m'avoir confié ce projet, de m'avoir donné l'opportunité d'accomplir un grand défi personnel et professionnel. Merci de m'avoir fait confiance, pour la liberté que tu m'as donnée à faire de ce projet le mienne et au même temps être toujours à l'écoute et avec des suggestions pour amener ce projet a son succès. Également merci pour toujours écouter mes idées et m'aide à les réaliser soit avec une collaboration ou avec un peu de bricolage au laboratoire. Malgré les difficultés il avait toujours une solution. Merci pour les multiples opportunités à présenter mon travail en face d'un public national ou international. Merci pour toute ce que j'ai appris ce derniers quatre ans. Je te remercie d'avoir accepté que ma thèse soit rédigée en anglais ; même si maintenant je peux faire des blagues en français je suis encore un peu loin pour écrire un manuscrit en français !

También me gustaría agradecer a CONACyT y i^2t^2 por permitirme regresar a México cada año a realizar una pequeña estancia. Las estancias de investigación no solo me permitieron mantener el contacto con el mundo científico en México y dar a conocer mi proyecto, pero también me permitieron ver a mi familia y recargar las energías necesarias para vencer todos los obstáculos que implica vivir lejos de casa.

No podría omitir a mis papas, **Humberto Carrancá Bourget** y **Rosa Elvira Palomo Castañon**. Gracias por su apoyo y motivación. Aun estando del otro lado del mundo nunca dejaron de apoyarme y estar ahí para lo que fuera. Gracias por creer en mí y en darme los medios para lograr este éxito que sin ustedes no sería posible. Gracias por permitirme tener una educación del más alto nivel desde muy temprana edad, sus esfuerzos me han dado las herramientas necesarias para cumplir todos mis sueños personales y profesionales. Gracias por impulsarme a aprender varios idiomas, ahora entiendo la importancia de hablar no solo mi lengua materna. Los idiomas me han abierto las puertas a innumerables oportunidades. Ustedes han sido un ejemplo de fortaleza y valor durante toda mi vida, gracias por creer en mí y ensenarme a no tener le miedo a los retos. Gracias a toda mi familia por su apoyo y cariño. Gracias a mi hermano, **Humberto Carrancá Palomo,** por creer en mi e impulsarme a ser el mejor ejemplo de hermana mayor. Gracias al ejemplo de mi abuelo, **Humberto Carrancá Tommasi**, que nos demostró la importancia de salir de su zona de confort. Hace más de 60 años, tú también viajaste a Francia para realizar tus estudios en Francia, superarte profesionalmente y llevar adelante a tu familia. Gracias por compartir tu experiencia conmigo y darme la oportunidad de seguir tus pasos.

Résumé en Français

Développement d'un nouvel hydrogel modulable permettant la formation de tissus, dans le cadre des modèles de peau reconstruite

Les équivalents de peau reconstruites utilisés comme greffe pour le remplacement des tissus endommagés ou pour l'établissement de modèle de peau *in vitro* sont constitués d'une structure complexe dermo-épidermique. Le collagène, obtenu de source animale, est principalement utilisé comme matrice pour former l'équivalent dermique de ces structures. Ces matériaux d'origine animale présentent néanmoins plusieurs inconvénients : des propriétés mécaniques parfois limitées, une grande variabilité, des risques de contamination pathogène ; et ils soulèvent également un dilemme éthique. Ces inconvénients pourraient être évités par l'utilisation de matériaux synthétiques. Les hydrogels à base de Poly(éthylène glycol) (PEG) ont largement été utilisés dans les applications d'ingénierie tissulaire, de par leur biocompatibilité et leurs propriétés mécaniques modulables. Cependant, leur caractère (bio)inerte nécessite qu'ils soient associés avec d'autres séquences fonctionnelles. Nous proposons ici de réticuler les molécules de PEG à l'aide de dendrigrafts de poly-L-Lysine (DGL) qui, en plus de servir comme nœud de réticulation multifonctionnel, pourraient mettre à disposition de nouvelles propriétés biologiques, telles que l'adhésion cellulaire à la surface du biomatériau. Pour juger du potentiel des hydrogels en tant que substrat pour applications biologiques, nous avons étudiés la réponse cellulaire à la surface du matériau en lien avec sa composition. Afin de permettre une culture cellulaire tridimensionnelle, une technique de « particulate leaching » a été utilisée pour rendre l'hydrogel poreux, permettant ainsi l'infiltration et la colonisation par les cellules. L'équivalent dermique résultant a ensuite été étudié dans le contexte d'un modèle de peau reconstruite. De plus, l'incorporation dans l'hydrogel d'un polypeptide synthétique similaire à l'élastine afin d'accroître son activité biologique et lui conférer des propriétés élastiques a été évaluée. Finalement, la biocompatibilité des hydrogels a été testée *in vivo* par implantation sous-cutanée chez la souris.

Mots clés : Ingénierie Tissulaire ; Hydrogels ; Modèles de peau ; support 3D ; dendrigrafts de poly-L-lysine ; PEG-Hydrogels

Abstract

Development of a novel tunable hydrogel to support tissue formation in the context of full-thickness skin equivalents.

Full-thickness skin equivalents used as grafts for the replacement of damaged skin or for the establishment of *in vitro* skin models are composed of an epidermal layer seeded on top of a dermal compartment. While collagen is principally used as matrix to form the dermal equivalent, materials from animal sources still elicit an ethical dilemma, have weak mechanical properties, batch-to-batch variability and present risk of pathogen transfer. The use of synthetic materials as scaffolds could overcome these disadvantages. Poly(ethylene glycol) (PEG) hydrogels have been extensively used in tissue engineering applications, owing to their biocompatibility and tunable mechanical properties. However, their bio-inert properties require them to be associated with other functional moieties. We propose here to reticulate PEG molecules with poly-L-lysine dendrigrafts (DGL) that, beside serving as multifunctional crosslinkers, could provide inherent biological properties such as cell adhesion to PEG-based hydrogels. To judge the hydrogel's potential as a substrate for biological applications, the cellular response to the material surface, in relation to its composition, was determined. Subsequently, particulate leaching was evaluated as a simple fabrication technique to render the hydrogels porous and allow cell infiltration and colonization in three-dimensions, in view of forming a dermal equivalent. The resulting tissues were investigated in the context of full-thickness skin equivalents. Furthermore, a synthetic elastin-like polypeptide was incorporated to the hydrogels to increase their bioactivity and elastic properties. Finally, *in vivo* biocompatibility was assessed by subcutaneous implantation in mice.

Keywords: Tissue Engineering; Hydrogel; skin models; scaffolds; poly-L-lysine dendrigrafts; PEG-based hydrogels

Table of contents

Abbreviations

3D	Three-dimensional
BM	Basement membrane
BSE	Bovine spongiform encephalitis
Col-GAG-Chi	Collagen-glyscosaminnoglycan-chitosan
DAPI	4’,6-Diamidino-2-phenylindole dihydrochloride
DEJ	Dermal epidermal junction
DGL	Poly-L-lysine dendrigraft
DHT	Dehydrothermal treatment
DMA	Dynamical mechanical analysis
DMEM	Dubecco’s modified eagle medium
DNA	Deoxyribonucleic acid
DSS	Sodium trimethylsilylpropane sulfonate
E'	Storage modulus
E''	Loss modulus
E*	Complex modulus
E.Coli	Escherichia coli
EBP	Elastin binding protein
ECM	Extracellular matrix
ECVAM	European Center for the Validation of Alternative Methods
EGF	Epidermal growth factor
ELP	‘in house’ elastin-like polypeptide
ELPs	Elastin-like polypeptides
ELRs	Elastin-like recombinamers
ESEM	Environmental scanning electron microscope
FA	Focal adhesion
FBS	Fetal bovine serum
FDA	US Food and Drug Administration
G3	Third generation dendrigraft
GAGs	Glyscosaminnoglycans
Gly	Glycine
HA	Hyaluronic acid
HRP	Enzyme horseradish peroxidase
IHC	Immunohistochemistry
INEPT	Insensitive nuclei enhanced by polarization transfer
INV	Involucrin
IPTG	Isopropyl β-D-1-thiogalactopyranoside
IT	Integrins
ITC	Inverse transition process
K10	Cytokeratin 10
K14	Keratin 14
KGF	Keratinocytes growth factor
KGM2	Keratinocyte growth medium II

LB	Luria-Bertani agar
LB-ADSA	Imagej plugging for drop analysis
LCST	Lower critical solution temperature
MAS	Magic angle spinning
MMPs	Matrix metalloproteases
MSCs	Mesenchymal stem cells
NHDF	Normal human dermal fibroblasts
NMR	Nuclear magnetic resonance
OCT	Optimal cutting temperature
OECD	Organisation for Economic Co-operation and Development
PAA	Poly(acrylic acid)
PANAM	Poly(amidoamine) dendrimer
PAX	Paxillin
PBS	Phosphate-Buffer saline
PBT	Poly(butylene terephthalate)
PCL	Poly(caprolactone)
PDLLA	Poly(DL-lactide)
PEG	Poly(ethylene glycol)
PEG-NHS	O,O'-Bis[2-(N-Succinimidyl-succinylamino)ethyl]polyethylene glycol
PEG-SG	Succinimidyl glutarate polyethylene glycol
PEGT	Poly(ethylene glycol terephthalate)
PEO	Poly(ethylene oxide)
PFA	Paraformaldehyde
PLA	Poly-(lactic acid)
PLAGA	Poly[D(-)lactic acid-co-glycolic] acid
PLGA	Poly(lactic-co-glycolic) acid
PLL	Linear poly-L-lysine
PVA	Poly(vinyl alcohol)
RGD	Sequence Arg-Gly-Asp
RNA	Ribonucleic acid
s/p	100U/ml penicillin and 0.1mg/ml streptomycin
SC	Stratum corneum
SDS	Sodium dodecyl sulfate
SMA	Smooth muscle actin
TBST	TBS + 0.05% tween 20
TGF-β	Transforming growth factor beta
TLN	Talin rod
Tt	Transition temperature
VASP	Vasodilator-stimulated phosphoprotein
VCL	Vinculin
ZYX	Zyxin

List of Figures

List of Table

Contexte Général

Les équivalents de peau sont devenus un outil indispensable à la recherche, à l'évaluation de la sécurité de produits de soin ou de santé et comme alternative à la greffe de peau autologue. Ainsi, les équivalents de peau en tant que modèles *in vitro* sont très largement utilisés comme alternatives aux tests sur animaux dans le secteur cosmétologique et pharmaceutique [1,2]. Ils ont notamment été utilisés pour étudier la toxicité de composés chimiques et de produits finis sur la peau, mais également afin de mieux comprendre les fonctions de la peau en conditions physiologiques et pathologiques (*p. ex.* cicatrisation, psoriasis,…) [3,4]. Cliniquement, les équivalents de peau sont des options prometteuses pour le traitement des plaies s'étendant sur des zones importantes du corps (p. ex. grandes brulures) et où les zones de prélèvement sont limitées pour procéder à une greffe de peau autologue [5]. Les peaux reconstruites, constituées des composants dermiques et épidermiques proposent un grand intérêt puisque l'interaction entre le derme et l'épiderme ont un impact sur la morphologie de la peau, son homéostasie et son activité métabolique [6,7]. Ces équivalents de peau ouvrent la porte à des études *in vitro* plus complexes et améliorent le taux de réussite des greffes de 75% dans les applications cliniques [8]. Alors que l'épiderme reconstruit consiste exclusivement en une structure épidermique multicouche, les modèles dermo-épidermique sont quant à eux constitués d'une couche épidermique se développant au-dessus du composant dermique. Le composant dermique est, quant à lui, composé de fibroblastes implantés dans un réseau tridimensionnel tentant de mimer la structure, la physiologie et les fonctions mécanique de la matrice extracellulaire (MEC) native.

Etant donné que les protéines les plus abondantes à l'intérieur du derme sont les collagènes de type I et de type III, ces derniers sont largement utilisés pour générer des matrices servant de support aux fibroblastes afin de former un équivalent dermique [9–14]. Cependant, étant de sources animales, ils sont sujets à une forte variabilité et au risque de transfert d'agents pathogènes, tandis que leur utilisation dans l'industrie pose un dilemme éthique [15,16]. L'utilisation de matériaux synthétiques permettrait d'éviter ces désavantages. Par exemple, les hydrogels à base de poly(éthylène glycol) (PEG) ont été largement utilisés ces dernières décennies comme matrice pour la délivrance contrôlée de médicaments ou comme support de culture cellulaire, de par leur excellente biocompatibilité,

leur modularité fonctionnelle chimique et leurs propriétés mécaniques versatiles [17]. Cependant, leurs propriétés bio-inertes nécessitent de les associer à d'autres séquences fonctionnelles, comme des peptides RGD, afin d'accroître le taux de survie des cellules ou encore leur capacité à permettre l'adhérence cellulaire [18]. Les hydrogels de PEG peuvent être réticulées de nombreuses manières, dans lesquelles les molécules de PEG sont soit fonctionnalisées avec des groupes réactifs à leurs extrémités (*p. ex*. méthacrylate ou acrylate) puis activés par des initiateurs associés avec des monomères multifonctionnels pour éviter l'utilisation d'initiateurs [19]. Dans le second cas, les dendrimères ont montré un potentiel en tant que monomère pour réticuler du PEG fonctionnalisé [20–23]. Les dendrigrafts de Poly-L-lysine (DGL) sont intéressants dans cette optique en raison de leur grande surface de contact, leur facilité de fonctionnalisation, leur solubilité dans l'eau, leur stabilité sous conditions de stérilisation, leur dégradation partielle, leur non-immunogénicité et leur faible cytotoxicité [24,25]. De plus, leur nature polycationique à pH physiologique permet l'adhésion cellulaire, fournissant ainsi une bio-activité tout en restant synthétique et contrôlable [26,27]. De façon intéressante, notre laboratoire est le premier à évaluer les DGL comme monomère de réticulation d'un hydrogel de PEG, alors qu'un tel hydrogel pourrait bénéficier d'une bio-activité, sans besoin supplémentaire d'association avec des molécules supplémentaires.

Pour développer des construits tissulaires d'intérêt physiologique, les propriétés mécaniques de la MEC doivent être considérées. Alors que le collagène confère à la peau une résistance à la traction, son élasticité est apportée par l'élastine, un autre composant important de la MEC [28]. Les équivalents dermiques composés de collagène tendent à avoir des propriétés mécaniques plus limitées, une résistance à la traction moindre, ainsi qu'une élasticité moins importante. Ils ont montré également des phénomènes de contractions liées aux fibroblastes, qui, dans le cas d'applications cliniques, peuvent conduire à une fibrose, altérer la guérisions des blessures et induire des cicatrices importantes [9,29]. Pour apporter de l'élasticité et favoriser la synthèse d'élastine, les chercheurs ont récemment étudié l'utilisation d'élastine soluble (α-élastine) et de peptides similaires à l'élastine dans les biomatériaux [30,31]. Un polypeptide recombinant (ELP) similaire à l'élastine et aux propriétés physico-chimiques analogues à la tropoélastine (le précurseur soluble de l'élastine humaine), a été récemment développé dans notre laboratoire [32]. En plus de ces propriétés

élastiques, cet ELP possède des propriétés biologiques intéressantes de par son extrémité C-terminale semblable à celle de la tropoélastine native et connue pour interagir avec les intégrines $\alpha_v\beta_3$ des cellules. De plus, son unité répétitive VGVAPG interagit avec l'« elastin binding protein » (EBP) [33]. Quand il est supplémenté au milieu cellulaire, sa présence peut augmenter la prolifération de fibroblastes ainsi que l'adhérence cellulaire quand il est utilisé comme revêtement sur des surfaces plastiques [32]. Son incorporation dans l'hydrogel DGL/PEG pourrait donc fournir de plus amples informations sur le comportement cellulaire dans les microenvironnements élastiques, tout en permettant de produire des équivalents de peau d'intérêts pour des applications en cicatrisation et/ou comme modèle de peau *in vitro*.

Objectifs et contours de la thèse

Alors qu'un important développement a été observé dans la production de peaux reconstruites (dermo-épidermique), la plupart des supports de culture sont encore composés de collagène. Par ailleurs, si l'utilisation de matériaux synthétiques présente des avantages, peu ont été testés dans ce contexte. Tandis que le biomimétisme propose une stratégie pour se rapprocher de la MEC native tout en restant contrôlable et sans utiliser de ressources animales. En conséquence, l'objectif de cette thèse a été de développer un système synthétique mimant la MEC et fournissant un support pour la culture cellulaire et la formation de tissus dans le contexte des peaux reconstruites. Pour atteindre cet objectif, les questions suivantes ont été posées :

A) Est-il possible d'utiliser les dendrigrafts de poly-L-lysine comme nœud de réticulation pour former un hydrogel à base de PEG, qui soit modulable et disposant d'une capacité d'adhérence cellulaire inhérente ?

Les hydrogels constituent des réseaux polymères avec une haute capacité d'absorption des liquides et pouvant mimer la structure de la MEC ; cependant, les hydrogels à base de PEG ne favorisent pas l'adhérence cellulaire. L'utilisation des dendrigrafts de poly-L-lysine comme nœuds de réticulation multifonctionnelle pour former un hydrogel avec des molécules de PEG a donc été examinée et les hydrogels résultants ont été évalués en tant que support pour la culture cellulaire

en deux dimensions, en déterminant la réponse cellulaire en relation avec la composition de l'hydrogel.

B) L'hydrogel DGL/PEG peut-il être formulé en support poreux permettant l'infiltration de fibroblastes, afin de produire une matrice dermique pour une peau reconstruite ?

Pour correctement répliquer *in vitro* les conditions physiologiques, les cellules doivent être cultivées dans un microenvironnement tridimensionnel. Dès lors, la possibilité d'introduire une structure hautement poreuse dans l'hydrogel DGL/PEG avec une technique de préfabrication simple a été évaluée. L'infiltration cellulaire dans la structure poreuse et son potentiel en tant qu'équivalent dermique pour supporter la formation d'une couche d'épiderme a ensuite été étudiés.

C) Est-ce que l'incorporation d'un polypeptide similaire à l'élastine (ELP) améliore la qualité de l'équivalent dermique, en mimant mieux la MEC?

En ligne avec l'approche biomimétique, l'incorporation d'un 'élastin-like polypeptide' (ELP) inspiré de la structure de la tropoélastine native dans les hydrogels DGL/PEG a été étudiée comme moyen de mimer le composant élastique de la peau. Pour déterminer l'avantage potentiel de l'introduction de l'ELP dans l'hydrogel, l'effet de la réponse cellulaire sur le biomatériau a été étudié en deux et trois dimensions.

D) Les supports DGL/PEG montrent-ils une bonne biocompatibilité *in vivo* ?

En vue d'une application clinique potentielle des hydrogels DGL/PEG, leur biocompatibilité est d'une extrême importance. Par conséquent, la réponse de l'hôte aux hydrogels à base de DGL/PEG a été évaluée par implantations sous-cutanée chez la souris.

General Context

Engineered skin equivalents have become an important tool for basic research, toxicity or efficacy assessment and as alternatives to autologous skin grafting. Skin equivalents as *in vitro* models are widely used as alternative to animal testing in the pharmaceutical and cosmetic industry [1,2]. They have been used to study the toxicity of chemical agents or finished products but also to understand skin function in physiological and pathologic conditions (*e.g* wound healing, psoriasis…)[3,4]. Clinically, skin equivalents are promising options for the treatment of extensive burns or in the case of large-area skin injuries where donor site is limited for autologous skin grafting [5]. Full-thickness skin equivalents, formed of the dermal and epidermal component are of special interest since it's been shown that the interactions between epidermis and the dermis have an impact in skin morphology, homeostasis and metabolic activities [6,7]. Full-thickness skin equivalents favor more complex *in vitro* studies and increase grafting success up to 75% in clinical applications [8]. While reconstructed epidermis consists exclusively of a multilayered epidermal construct, in full thickness models the epidermal layer is grown on top of the dermal component. The dermal component is composed of fibroblasts embedded in a three-dimensional network that attempts to mimic the physiological, structural and mechanical functions of the native extracellular matrix (ECM).

Since the most abundant proteins within the dermis are type I and III collagen, they are widely used to generate hydrogel matrices to support fibroblasts growth and form a dermal equivalent [9–14]. However, being obtained from animal sources, their use in the industry still raises an ethical dilemma, while they are subject to batch-to-batch variability and present risk of pathogen transfer [15,16]. The use of synthetic materials could overcome these disadvantages. For instance, poly(ethylene glycol) (PEG) hydrogels have been extensively used as matrices for controlled drug delivery or as tissue engineering scaffolds over the past decades, owing to their excellent biocompatibility, chemical versatility and tunable mechanical properties [17]. However, their bio-inert properties require an association with other functional moieties (such as RGD peptides) or coating with ECM proteins (such as collagen and laminin) to promote survival and function of adherent cells [18,34,35]. PEG hydrogels can be crosslinked through various

paths, in which the PEG molecules are either functionalized with reactive end groups (*e.g*. methacrylate or acrylate) and activated by initiators or associated with multifunctional monomers to avoid the use of initiators [19]. In the latter approach, dendrimers have shown some potential as crosslinking monomers to reticulate functionalized PEG [20–23]. Poly-L-lysine dendrigrafts are of interest for this application due to their large surface area, versatility to be functionalized, water solubility, stability under sterilization conditions, partial degradability, non-immunogenicity and low cytotoxicity [24,25] Moreover, their polycationic nature at physiological pH allows cellular adhesion, therefore providing bioactivity while remaining synthetic and controllable [25–27]. Interestingly, our laboratory was the first to evaluate DGL as crosslinking monomers to form hydrogels with PEG, while such hydrogels could benefit from their inherent bioactivity, without the need for further association with functional moieties.

To develop physiologically relevant tissue engineered constructs, the mechanical properties of the ECM need to be considered. While collagen confers the tensile strength of the skin, its ability to be both compliant and resilient (elasticity) is provided by the elastin, another important component of the ECM [28]. Dermal equivalents composed solely of collagen tend to have weak mechanical properties, such as low tensile strength or elasticity, and have shown fibroblast-related contraction, which, in case of clinical applications can lead to fibrosis, impaired wound healing and extensive scar formation [9,29]. To provide elasticity and promote elastin synthesis, researchers are recently exploring the application of soluble elastin (α-elastin) and elastin-like peptides in biomaterials for tissue engineering [30,31]. A recombinant elastin-like polypeptide (ELP) with similar physicochemical properties as tropoelastin, the soluble precursor of human elastin, was recently developed in our laboratory [32]. In addition to its elastic properties, this ELP possesses interesting biological properties through its C-terminal extremity, which is similar to the one present in the native tropoelastin and is known to interact with cell integrins $\alpha_v\beta_3$. Furthermore, its repetitive unit VGVAPG can interact with the elastin binding protein (EBP) [33]. When added into the cell medium it can increase fibroblasts proliferation as well as cell adhesion when used as a coating of plastic surfaces [32]. Its incorporation to the DGL/PEG hydrogel could therefore provide information on the relations between cellular behavior and elastic microenvironment and could further be of interest to produce

full-thickness skin equivalents with potential in wound healing applications and/or as an *in vitro* skin model.

Aims and outline of the thesis

While extensive development has been observed in the production of full-thickness skin equivalents, most scaffolds are still composed of collagen. While the use of synthetic materials proposes attractive advantages, few have been evaluated in this context. To closely resemble the native ECM while avoiding the disadvantages of natural source materials, biomimicry can be used as an strategy to develop synthetic materials. Therefore, the aim of this thesis was to develop a synthetic system that mimics the ECM and provides structural support for cell growth and tissue formation in the context of skin tissue applications. To achieve this goal, the following question were thus investigated:

A) Is it possible to use poly-L-lysine dendrigrafts as crosslinker to form a tailorable PEG-based hydrogel, with inherent cell adhesion properties?

Hydrogels are highly swollen polymeric network that can mimic the structure of the ECM; however, PEG-based hydrogels do not promote cell adhesion. The use poly-L-Lysine dendrigrafts as multifunctional crosslinker to form a hydrogel with PEG molecules was therefore investigated and the resulting hydrogels were assessed as supports for cell culture in two-dimensions, by determining cell response in relation to hydrogel composition.

B) Can the DGL/PEG be formulated into porous a scaffold to allow fibroblast infiltration and to produce a dermal matrix for a full-thickness skin equivalent?

To properly replicate the physiological conditions *in vitro*, cells must be cultured in a three-dimensional microenvironment. Accordingly, the possibility to introduce a highly porous structure to the DGL/PEG hydrogels with a simple pre-fabrication technique was evaluated. Cell infiltration into the porous structure and its potential as a dermal equivalent to support the formation of an epidermal layer were then investigated and compared to a well-known full-thickness skin model.

C) Does the incorporation of an elastin-like polypeptide (ELP) improves the quality of the dermal equivalent by further mimicking the native ECM?

In line with a biomimetic approach, the incorporation of an elastin-like polypeptide (ELP), inspired from the native tropoelastin structure, into the DGL/PEG hydrogels was investigated as a mean to mimic the elastic component of the skin. To determine the potential advantage of introducing the ELP into the hydrogel, the effect on cell response to the biomaterial was assessed in two- and three-dimensions.

D) Do DGL/PEG scaffolds exhibit a good biocompatibility *in vivo*?

In view of further clinical applications of the DGL/PEG hydrogels, its biocompatibility is of extreme importance. Therefore, host response to DGL/PEG hydrogels was evaluated by subcutaneous implantations in mice.

Bibliographic Introduction

I. Tissue-Engineered Skin

The term tissue engineering was first introduced in 1988 to define the emerging approach to replace damaged or/diseased tissue with functional neo-tissue; by combining cells, scaffolds and bioactive agents [36]. This multidisciplinary field merges different areas of science such as cell biology, material chemistry and engineering. In this approach, cells are seeded in a biodegradable matrix or scaffold which provides an adequate three-dimensional structure of the target tissue. The cells proliferate and differentiate, producing their own extracellular matrix (ECM), to eventually result in the formation of a functional tissue. Regenerative medicine approaches share the same principle, but emphasize on the utilization of the patient's own cells [37]. In addition to its clinical applications, this field has also allowed the development of three-dimensional (3D) tissue models as alternatives to animal testing models and traditional bi-dimensional culture models. To properly study cell physiology, mechano-transduction, and tissue morphogenesis *in vitro*, cells should be cultured in 3D microenvironments that recapitulate the critical mechanical and biochemical cues present in the native extracellular matrix (ECM), while facilitating hierarchical processes such as migration and tissue organization [38].

Although the term tissue engineering was not yet introduced, engineered skin has been used for more than 45 years in clinical applications, offering major advances in burn and wound care [39]. Especially in recent years, *in vitro* engineering of human skin has been encouraged by legal and ethical demands in the cosmetic industry [40]. In order to be able to reproduce *in vitro* what occurs in real life, it is important to understand the structure and function of skin.

I.I. Skin structure and function

Skin is the largest organ of the human body, it serves as a barrier between the internal and external environment and is involved in series of physiological functions such as thermoregulation, immune response and sensory detection [41]. Human skin is composed of the epidermis, dermis and hypodermis, as shown in Figure 1. Each of these layers is composed of different cell types which are responsible for the different functions of the skin [42].

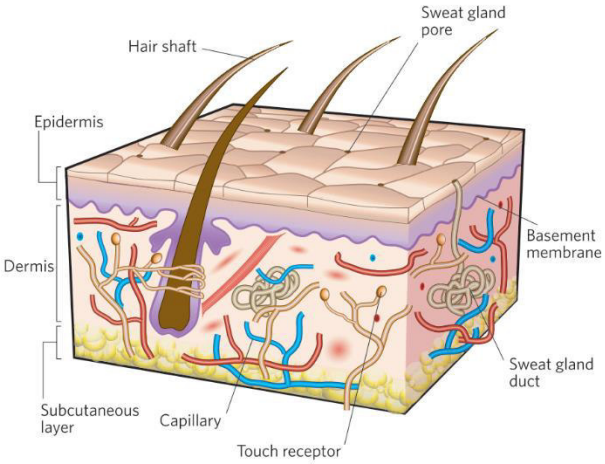

Figure 1. Human skin structure. *The three layers of the skin epidermis, dermis and subcutaneous layer or hypodermis are represented in the diagram. As observed, the upper epidermal layer is securely attached to the underlying dermis by the basement membrane. Nerve endings, capillary vessels and skin appendages such as hair follicles and sweat glands are present in the dermis. (Obtained from MacNeil et al.,* [39]*)*

I.I.I. Epidermis

The epidermis, outer layer of the skin, is principally composed of keratinocytes (90-95%), which proliferate in the deepest layer of the epidermis, the stratum basale [43]. While stem cells have an unlimited capacity of self-renewal and the ability to generate daughter cells that undergo terminal differentiation, not all proliferative cells in the basale layer are stem cells. Certain daughters, named transit amplifying cells, can first proliferate and divide a small number of times [44]. Proliferative cells remain attached to the underlying matrix, while daughter cells, product of asymmetric mitoses, migrate vertically towards the next layer, the stratum spinosum. Once in the stratum spinosum, they exit cell cycle, grow larger and establish robust intercellular connections, starting the process of differentiation [45]. Cells will gradually move upwards until reaching the most external layer, known as the stratum corneum (SC), which represents the final step of keratinocytes differentiation. During this process, keratinocytes undergo morphological and cytostructural changes, as well as express different proteins and cell junctions as observed in Figure 2. Expression of keratins and filaggrin genes, located in the epidermal differentiation complex in Human Locus 1q21, are regulated in function of the stage of keratinocytes differentiation by various external factors such as calcium concentration and growth factors [46,47]. In the stratum granulosum, the keratinocytes elongate and flatten and form the granular layer characterized by the presence of intracellular keratohyalin granules

and lamellar bodies [48]. Once the cells have reached the SC, they are no longer considered keratinocytes but corneocytes, dead cells lacking nuclei and organelles but rich in keratin and filaggrin (tightly linked to neighboring cells by desmosomes) [44]. They have a highly insoluble cornified envelop, formed by crosslinking of the soluble protein precursor, involucrin, by transglutaminase 1 [44]. Shedding of corneocytes by proteolysis, known as desquamation process, is balanced by the formation of new corneocytes in non-pathological conditions [49]. The capacity of keratinocytes to renew and maintain their ability to reconstruct the epidermis after long-term expansion is useful in engineered constructs [5]

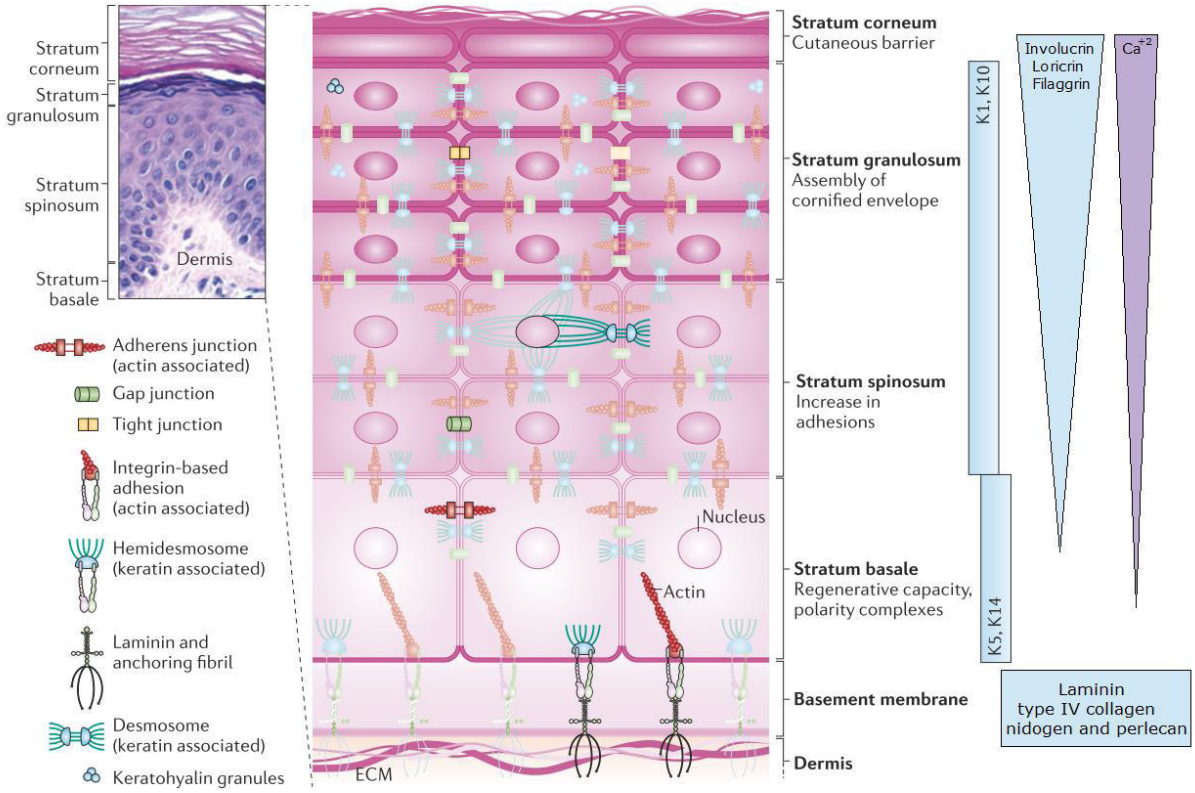

Figure 2. Epidermal structure. *The epidermis is made of a stratified cell layer, which undergoes differentiation to allow for constant renewal of the skin. Four main layers are illustrated by a hematoxylin-and-eosin stained human skin sample accompanied of a schematic representation of the stratum basale, stratum spinosum, stratum granulosum and stratum corneum. Proliferative cells in the basale layer remain in contact with the dermis through hemidesmosomes and integrin-based adhesions. During keratinocytes differentiation, cells undergo cytoskeletal changes and express different proteins and cell junctions. Differentiation is dependent of changes as calcium concentration and growth factors. At the BM proteins such as Laminin, type IV collagen, nitrogen and perlecan assure the attachment of the epidermis to the dermis. (Modified from Simpson et al.,* [45]*)*

The primary function of the epidermis is its barrier function, protecting the skin from toxic substances and pathogens. First as a physical barrier, obtained by highly compacted layers of differentiated keratinocytes joined by intercellular (tight) junctions in the epidermal sheet. The barrier function of the skin is mainly attributed to the SC, where the flattened corneocytes represent "bricks" forming a "bricks and mortar" kind of structure filled with intercellular densely packed lamellar lipids [41]. This "physical wall" formed of the corneocytes and lipid matrix withholds any external substance from easily penetrating the skin and maintains the balance of water and electrolytes inside the skin [41]. As shown in Figure 3, the stacked densely packed lipid layers (lipid lamellae) forms a three-dimensional structure where both its lamellar and lateral organization are crucial for the skin barrier function [50]. The lipids can implement such an effective barrier due to their high ordered crystalline lamellar structures [51]. During the process of cornification, plasma membrane phospholipids are hydrolyzed, and fatty acids are used to synthesize other lipids such as triglycerides, ceramides and sterols leading to the formation of the lipid matrix [52]. The lipid matrix is mainly composed of three lipid classes: cholesterol, free fatty acids and ceramides expressed in an approximately equal molar ratio [50]. The lipid sub class composition is highly complex and contains a wide range of different lipids. Changes in the proportion and organization of the lipid matrix are known to affect the skin permeability as observed in alterations of the SC of diseased skin [50,53]. Lipid analysis of *in vitro* models have shown that the lipid matrix can be formed *in vitro* but lipid proportions differ to native skin [54]. This alteration in the epidermal lipid content of tissue-engineered skin substitutes, such as different proportions of their epidermal ceramide's classes, correlates with a higher permeability observed *in vitro* compared to native human skin [55]. To create a viable permeation barrier the epidermal differentiation process and the subsequent lipid composition and organization need to be comparable to that of the human skin [43].

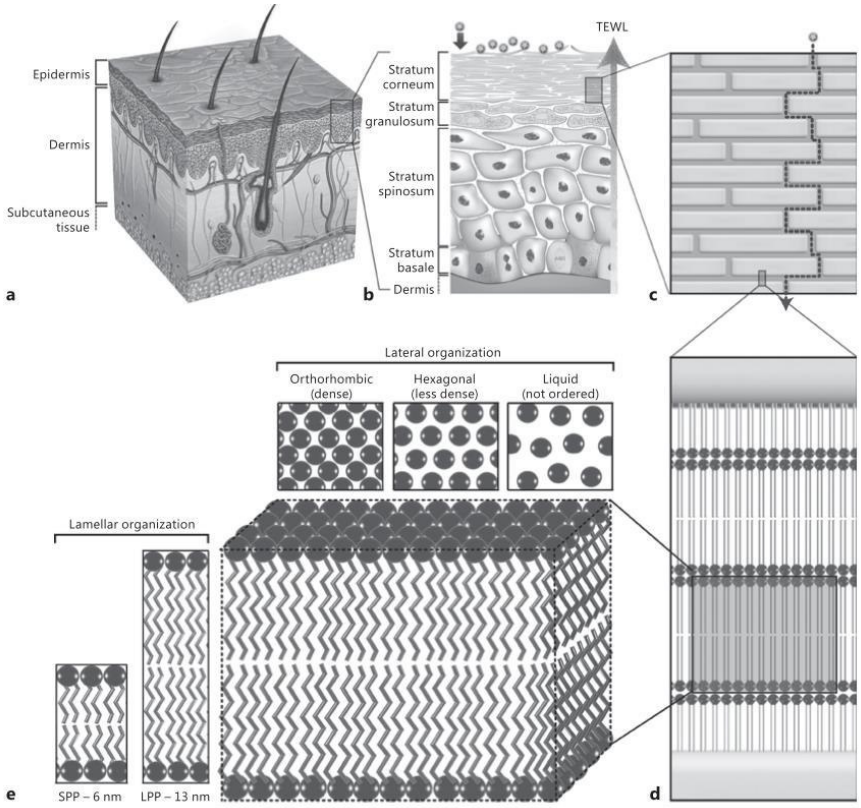

Figure 3. Lipid organization in human SC. *A) Cross-section of the skin. B) Representation of the epidermal tissue layer. C) Representation of the outermost skin layer, SC as a 'brick-and-mortar' barrier. Intercellular penetration into the deeper epidermal layers via the lipid matrix is indicated by the arrow. D-E) Stacked lipid layers in a highly ordered three-dimensional structure. Lipids adopt a lateral organization that can either be liquid, hexagonal or orthorhombic. (Obtained from Agner et al.,* [50]*)*

In addition to a physical barrier, the epidermis also has a role in other protection functions. Langerhans cells (dendritic cells present in the stratum spinosum) contribute to the barrier function by responding to exogenous substances with an innate immunological response. Another cell type present in the basale layer of the epidermis is the melanocyte, which protects the skin from UV radiation by producing melanin, an effective pigment that absorbs light across a broad spectrum of wavelengths to protect DNA in keratinocytes. Finally, Merkel-ranvier cells contribute to the sensory function of the skin [44].

I.I.II. Dermal-epidermal junction

The epidermis is tightly joined to the thick dermal layer at the basement membrane (BM) composed of proteins as laminins, collagen type IV, nidogen and perlecan [56]. The BM is characterized by two distinguishable layers at the microstructure scale: the lamina lucida (electron-lucent) and lamina densa

(electron-dense). Keratinocytes are attached to the lamina lucida by the hemidemosomes, which binds keratinocyte's keratin filaments to laminin-332 by $\alpha_6\beta_4$ integrin interaction (Figure 4) [57]. While keratinocytes produce most of the components of the BM, expression *in vitro* is weaker and delayed in the absence of fibroblasts [58]. Underneath the BM anchoring fibrils, loop structures of collagen which bind to laminin-332 and form an interwoven complex with type I and III collagen fibrils in the dermis, bind together the dermis to the lamina densa [56].

The BM provides mechanical support to the epidermis and acts as a partial barrier against the exchange of cells and large molecules [44]. The BM also acts as a reservoir for the controlled released of cytokines and growth factors crucial during wound healing [56]. In the production of skin equivalents, the integrity of the BM serves as a quality indicator, since it demonstrates the attachment between the epidermal and dermal compartment and a good cross-talk between both layers [58].

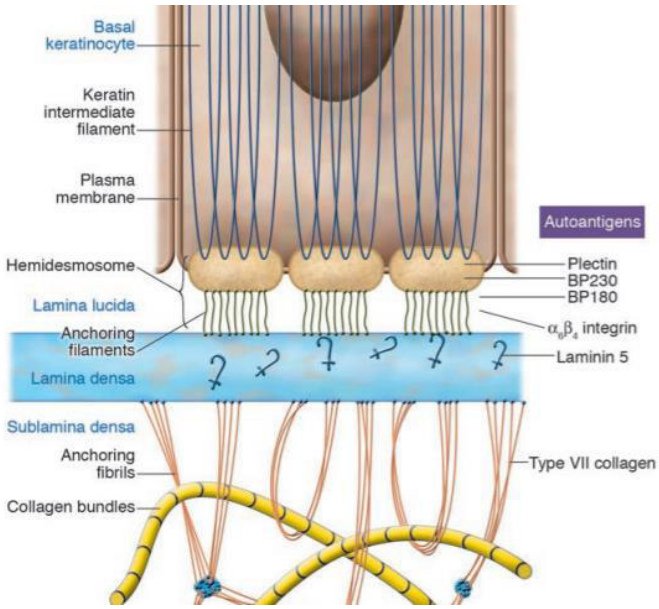

Figure 4. Components of the basement membrane at the dermo-epidermal junction. *Basal keratinocytes adhere to the BM by interactions between the hemidesmosomes with ligands such as laminin-332 (also known as laminin 5) located in the lamina lucida and lamina densa of the dermal-epidermal junction. Type VII collagen is the major component of anchoring fibrils, which link the basement membrane to the dermal collagen fibers by direct interactions with laiminin-332 in the lamina densa. (Obtained from Hertl, et al.,* [57]*)*

I.I.III. Dermis

The thick layer of connective tissue underlying the epidermis is the dermis. Most of the skin substance and structure is provided by the dermis serving as the main mechanical support of the skin [59]. This thick layer of the skin is rich in blood supply, since no blood vessels pass through the dermal-epidermal junction, dermis vascularization favors the nourishment of the epidermis [44]. Moreover, it is rich in nerve endings and various glands to carry out functions such as thermoregulation and sensation [44]. This connective tissue layer is divided between the papillary dermis formed by rete pegs and rete ridges along the dermal-epidermal junction increasing the surface contact area between the epidermis and the skin and the reticular dermis mainly composed of a dense collagen and elastic fiber network [60].

Fibroblasts, the most abundant cell type in the dermis, are subject to dynamical and reciprocal cell-cell communications and cell-matrix interactions that play an important role in skin homeostasis [61]. They are able to secrete soluble factors that impact BM organization [56,62], keratinocytes proliferation [7] and epidermal differentiation [63]. Moreover, they are responsible for the synthesis of the ECM main components and the constant remodeling of the skin. Fibroblasts secrete and organize type I and III collagens, elastin, fibronectin, tenascin and proteoglycans to form the ECM [64]. Interactions between the ECM and fibroblasts are especially crucial during wound healing, where fibroblasts are activated into contractile cells, myofibroblasts. The same ECM molecules produced by the fibroblasts simultaneously act to modify the function of fibroblasts. In this sense, the interaction of the fibroblast with the ECM can be thought of as a form of autocrine regulation that is crucial in the process of wound healing [65].

I.I.IV. The extracellular matrix

Cells are embedded in a ground substance in which polysaccharides and proteins are linked to produce a macromolecular network with a remarkable capacity to retain water, known as the ECM [44]. The extracellular components can be divided into fiber-forming structural molecules, non-fiber-forming and "matricellular proteins" which do not have a structural function but are related to cell-matrix interactions (Figure 5). Fiber-forming proteins create a complex three-dimensional framework of rigid and elastic proteins while the non-fiber-forming,

mostly proteoglycans and glyscosaminoglycans (GAGs) create a charged, dynamic and osmotically active hydrated space. Since matricellular proteins act as temporally dynamic signaling molecules, they are often absent or present in low levels in normal skin and up-regulated after tissue injury [65]. Cells are able to adhere to the ECM network via interaction with receptors such as integrins, discoidin domain receptors and heparan sulfate proteoglycans (syndecans) [66].

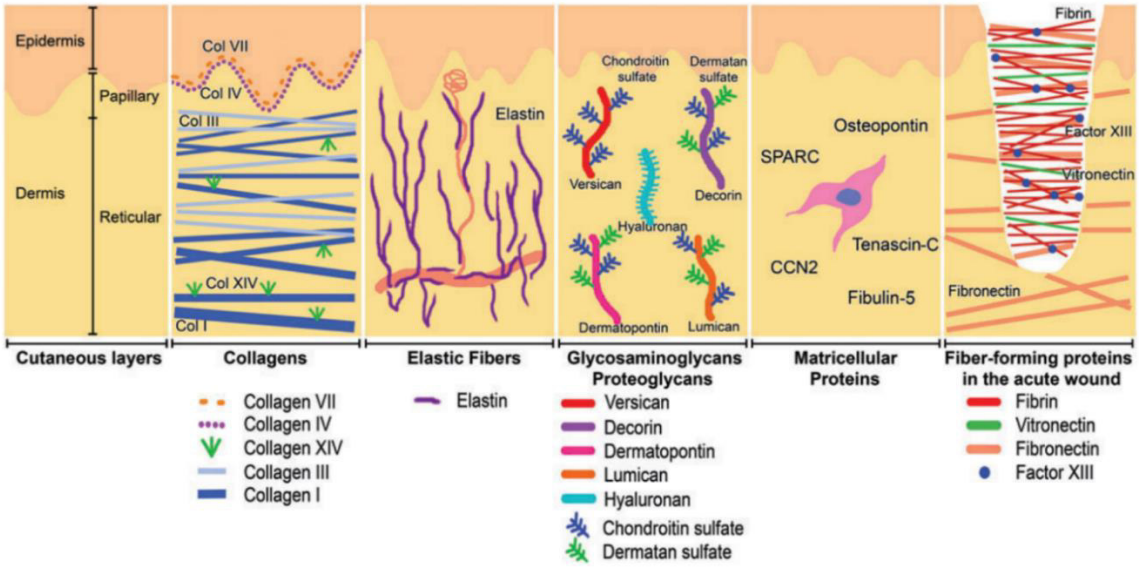

Figure 5. The extracellular matrix of normal skin. *Fiber-forming proteins and collagens define the rigid mechanical structure of the skin, while elastic fibers its elasticity. Proteoglycans and glycoproteins create an osmotically active hydrated space. Matricellular proteins do not contribute to the mechanical structure of the ECM but instead act as paracrine signaling molecules. Proteins as vitronectin, fibrin and fibronectin beside structure promote cell adhesion and are especially present during wound healing. (Obtained from Tracy et al.,* [65]*)*

i) Glycosaminoglycans

Glycosaminoglycans (GAGs) are composed of different linear polysaccharide chains composed of specific disaccharide units. They include chondroitin sulfate, dermatan sulfate, keratan sulfate, heparan sulfate, heparin, and hyaluronic acid (HA) [65]. In general, proteoglycans consist of a core protein that is bound to one or more GAG side chains. Except for HA, which is synthetized as a single polysaccharide chain without a core protein, GAGs are heavily crosslinked to a proteoglycan core protein and synthesized by glycosyltransferases and sulfotransferases. Because GAG chains contain numerous negatively charged carboxyl and sulfate groups, they are capable of hold great quantities of water molecules. In particular, HA is able to hold 1000-fold of its molecular weight in

water [67]. These hydrophilic glycoproteins and proteoglycans in conjunction with the HA are distributed throughout the dermis maintaining skin hydration [68].

ii) Collagens fibers

Collagens are the most prevalent fiber-forming proteins, comprising 77% of the fat-free dry weight of human skin [69]. Although 28 types of collagen have been identified, type I and III collagens, compose approximately 90% and 10% of the total collagen in the skin, respectively [65]. Type I collagen is observed as thick bundles in the reticular dermis, while type III collagen is observed as thin fine-woven meshwork of collagen fibers underlying the epidermis and near vascularized areas in the dermis [60]. All collagen molecules are formed by a triple helix formed of three α chains twisted around each other and mainly stabilized by hydrogen bonds and inter- and intra-molecular forces. A key motif of all triple helical structure of the collagen molecules is the repeating glycine at every third position $(Gly–X–Y)_n$ with X and Y being one of the 21 amino acids each, commonly proline and hydroxyproline [70]. Fibrillar collagens are synthesized in the intracellular space by fibroblasts in the form of precursor molecules, procollagens. Once in the extracellular space, cleavage of procollagen leads to spontaneous assembly into fibrils which are subsequently stabilized by the formation of covalent crosslinks (Figure 6). Finally the fibrils are associated as fibril bundles of fibers [70]. Collagen fibers are formed of heterogeneous mixtures of different collagen types, but as previously mentioned predominantly type I collagen [64]. Besides providing tensile strength to the dermis, collagens are also implicated in cell-ECM interactions since they can regulate cell adhesion, support chemotaxis and migrations and guide tissue formation [64].

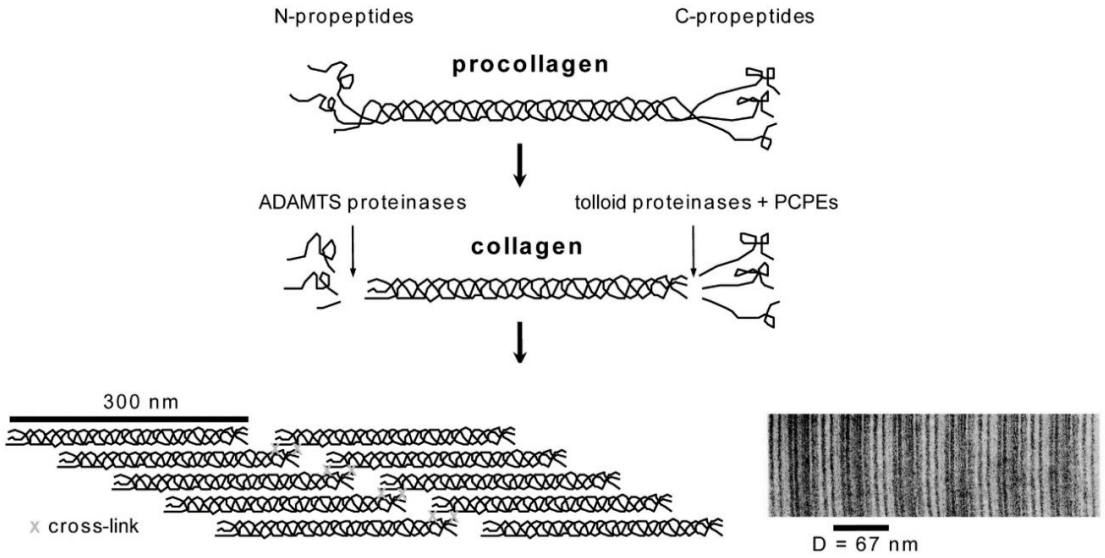

Figure 6. Fibrillar procollagens and fibril assembly. The N- and C-terminal processing of procollagen lead to a spontaneous assembly of collagen fibrils, which are subsequently stabilized by the formation of covalent crosslinks. (Obtained from Hulmes, et al., [70])

iii) Elastic fibers

To contribute to the resistance, elasticity and resilience of the skin, long crosslinked elastin fibers are intertwined with the relative rigid collagen fibers [65]. While elastin fibers are found in smaller proportions compared to collagen, they facilitate the relaxation of skin after removal of an external load giving the skin the ability to be both compliant (readily deformable) and resilient (able to recoil) [71].

Elastic fibers consist of two morphologically distinct components elastin and microfibrils [72]. Elastin is the main component of the elastic fibers and is formed of the assembly and crosslinking of its soluble precursor, tropoelastin, in a process known as elastogenesis [73]. Human tropoelastin is encoded by a single-copy gene, *ELN*, which possess 35 exons to give rise to multiple isoforms. Its amino acid sequence is divided into two major alternating domains: crosslinking and hydrophobic domains (Figure 7). Hydrophobic domains are rich in nonpolar residues glycine, valine and proline, typically occurring in repeating motif. Crosslinking domains are mainly characterized by lysine and alanine or lysine and proline [74]. Another important element of tropoelastin structure is the C-terminus, where two cysteine residues forming a disulfide bond at the final domain 36 and a terminal positively charged RKRK sequence which is implicated in fiber assembly [75]. Other motifs such as the sequence XGXXPG present in tropoelastin

play an important role binding to the elastin binding protein (EBP) and eliciting biological responses [73].

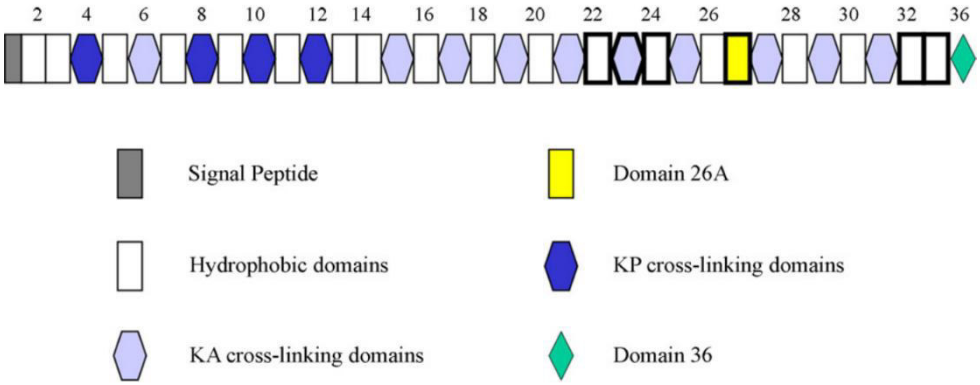

Figure 7. Domain map of human tropoelastin containing all possible exons. *Crosslinking domains are further divided into KP- and KA- rich regions. Domain 36 is assigned differently because of its unique structural features. (Obtained from Wise and Weiss et al.,* [74]*)*

In the skin, tropoelastin is secreted by fibroblasts and is chaperoned by the EBP to the plasma membrane to prevent intracellular aggregation. Once secreted in the extracellular space, tropoelastin monomers spontaneously self-assemble through a process known as coacervation [76]. This phenomenon is the result of specific interactions between the hydrophobic domains induced by an increase of its local concentration (Figure 8). Coacervation of tropoelastin is optimal at 37°C (lower critical solution temperature) in a pH range of 7-8 in physiological salt conditions [74]. The coacervates are then crosslinked to form insoluble elastin through the action of the lysyl oxidase family of amine oxidase (also implicated in collagen crosslinking). Further crosslinking and deposition onto microfibrils network, mainly composed of fibrillins, leads to the maturation of the elastic fibers [77]. Elastic fibers are arranged into three distinct types of fibers within the dermis. In the papillary dermis, oxytalan fibers, poor in elastin, are shaped into small, finger-like vertical projections. Deeply in the papillary dermis, elastic fibers gradually incorporate elastin to form elaunin fibers, while mature elastic fibers with high elastin content are located in the reticular dermis and are aligned in a horizontal network parallel to the skin surface, as shown in Figure 5 [78].

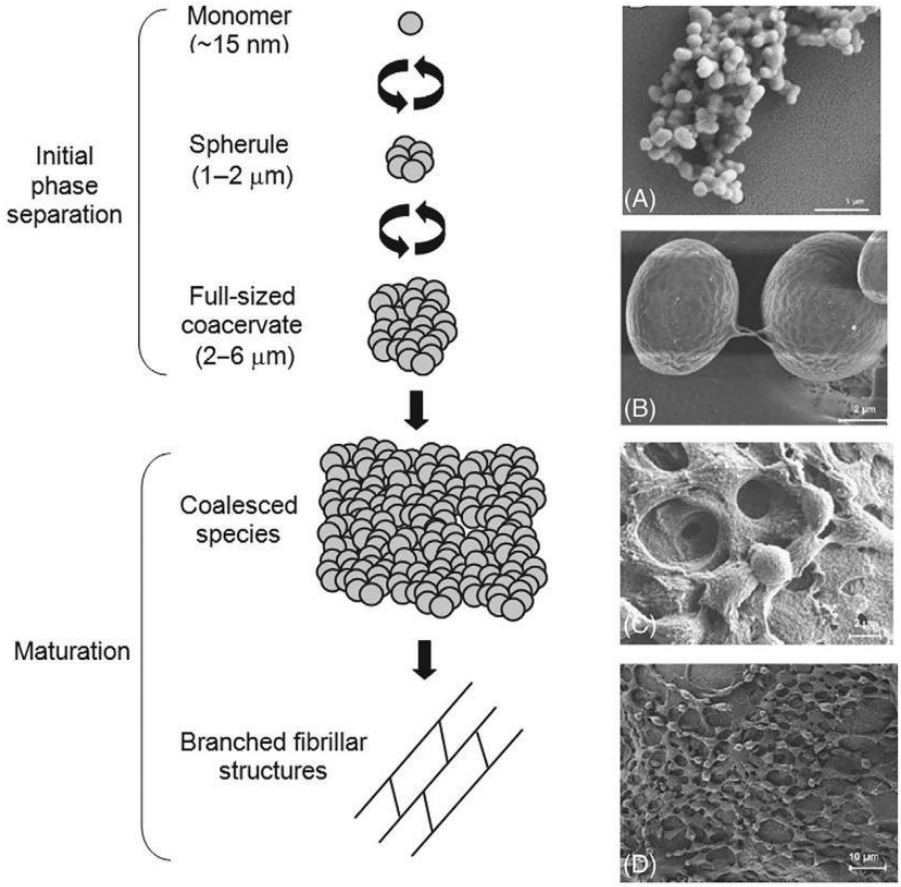

Figure 8. Coacervation of Tropoelastin. *Tropoelastin molecules undergo self-assembly in two main stages: the initial phase separation and the maturation stage. During the reversible initial phase separation stage, aqueous solutions of tropoelastin that have reached the lower critical solution temperature (LCST) form 1-2 μm spherules that aggregate in ~6 μm coacervates. Then in the maturation stage, the coacervated aggregate into larger coalesced species and then form branched fibrillar structures. (Right) Scanning electron micrographs of tropoelastin A) spherules, B) full-sized coacervates, C) and D) coalesced species. (Obtained from Wen and Weiss et al.,* [79]*)*

Elastin has a half-life of around 70 years, during which it can go through billions of extensions and relaxation cycles without losing its function [30,80]. Most of the elastin formation in mammals occurs during the late foetal and early neonatal periods, and at maturity new elastin productions ceases [74]. During injury the production of tropoelastin can be induced by a range of soluble factors such as insulin-like growth factor-1, tumor necrosis factor-α, interleukin-1β and transforming growth factor beta (TGF-β) [73]. Despite the rise in elastin expression upon injury, which can only be detected several months after the initial wound healing stages, the formation of the new elastin network is disrupted, contributing to the reduced elasticity and even loss of function of matures scars [73]. Elastin fragments generated upon injury and wound healing, which can induce biological responses as active ligands, are known as elastokines [81]. In this manner,

tropoelastin and elastin peptides are capable of interacting with cells and impacting cellular functions such as cellular attachment, proliferation, differentiation, phenotype, chemotaxis and migration [31,73,81]. The two main receptors mediating intracellular cell signaling in response to tropoelastin or its proteolytic peptides are the EBP and the $\alpha_v\beta_3$ integrin [73].

iv) Integrins

Integrins function as the principal receptors of animal cells and many of the ECM adhesion molecules. They are a large family of transmembrane cell surface molecules able to link the macromolecules of the ECM with the cell's cytoskeleton, promoting cell adhesion to the ECM. They are also involved in the binding of proteases and cell-cell adhesion mechanism [82]. Integrins are composed of non-covalently associated α and β subunits, the combination of this subunits determines the ligand specificity of the integrin [83]. A great number of integrins (*e.g.* $\alpha_v\beta_3$, $\alpha_5\beta_1$) have been shown to bind to ECM molecules via the sequence RGD (Arg-Gly-Asp) present in ECM proteins such as fibronectin, vitronectin and in a less important manner in collagen and laminin. The process of integrin mediated cell adhesion comprises a cascade of four different partly overlapping events: cell attachment, cell spreading, organization of actin cytoskeleton, and formation of focal adhesions [84].

Integrins are able to transmit information across the cell membrane through the focal adhesion kinase axis, working as critical regulators of other cell functions beside cell adhesion and migration [85]. In the epidermis for example, integrin expression assures stem cell anchorage and can regulate cell fate. Loss of contact with the ECM or reduced integrin expression in adherent cells triggers terminal differentiation of cultured epidermal cells [86].

I.I.V. Mechanical properties of the skin

The skin is subject to constant mechanical stresses, including stretch and compression due to body movement. The ECM provides the structural support, which allows the skin to withstand external forces without compromising its integrity and function [87]. Although several groups have evaluated the skin mechanical behavior, there is certain discordance in what is reported in the literature. The most widely used methods to determine the mechanical behavior of

skin are tensile, indentation, suction and torsion tests. However, new techniques like shear-wave elastography and optical coherence tomography have recently been used. When comparing the values obtained for skin, several factors must be considered as the method of measurement, experimental set up (*in vivo or in vitro*), measurement parameters and origin of the biological material (*e.g* age, body location). As shown in Table 1, Young's modulus is typically measured between 6-15 kPa by indentation tests. However, values for tensile and torsion indicated greater Young's modulus values ranging between 20 kPa to 140 MPa. Moreover, it has been extensively demonstrated that skin aging impacts the mechanical properties of the skin. With aging, collagen fibers tend to inappropriately crosslink through glycation, contributing to tissue stiffening [65]. While skin rigidity is increased, its elasticity is reduced [88].

The skin typically behaves as a viscoelastic material, which combines the term "viscous" that implies a slow deformation when exposed to an external force and the term "elastic' which implies that once the deformation has been removed, the material returns to its original configuration [59]. While the dermis provides the viscoelasticity properties to the skin, it has been shown that the epidermis also contributes to the mechanical behavior by providing an elastic rigidity that can be specially observed when comparing tensile and indentation measurements [103]. Pailler-Mattéi *et al.* investigated different mechanical models to determine the effects of the underlying tissue layers and developed a two-layer elastic model for mechanical analysis that considered the epidermis contribution [104].

Table 1. Young's Modulus of skin obtained using different techniques, parameters and sample source. *(Comparison against young and old skin when available.)*

Young modulus (kPa)	SOURCE	SAMPLE	METHOD	REF
420, 850	Young (<30 years) and old (>30 years)	*In vivo*	Torsion test ($28.6x10^{-3}$N*m)	[89]
14.38±3.6, 6.20 ±1.4	Forearm Young 24 years and old 60 years	*In vivo*	Airflow device (non-contact method) indentation	[90]
10.7±2.6, 7.2 ±2.1	Forearm young (18-30 years) and old (51-70 years)	*In vivo*	Dynamic indentation test	[91]
$14x10^3$, $14x10^4$, $35x10^3$	Forehead (85 years)	*Ex vivo*	Dynamic tensile test (2m/s) Longitudinal, transverse and shear strain	[92]
$83.3x10^3$	Back	*Ex vivo*	Dynamic tensile test (2m/s)	[93]
$4X10^3$ ± 0.3	Abdomen	*Ex vivo*	Quasistatic tensile test (0.16mm/s)	[94]
125±88	Forearm	*In vivo*	Suction 100mBar	[95]
56	Forearm	*In vivo*	Suction ultrasound detection	[96]
24.9, 101.1, 68.6	Palm, volar forearm, dorsal forearm	*In vivo*	Optical coherence tomography	[97]
20-100	Forearm between 6-61 years	*In vivo*	Torsion test	[98]
19.1 -25.2	Scalp	*Ex vivo*	Tensile test	[99]
23.5	Thigh	*Ex vivo*	Compliant supported beam	[100]
1560 – 3100	Neck	*In vivo*	Combination of resonance imaging (MRI) and finite element modeling (FE)	[101]
30.3, 14.8 and 9.5	Finger, forearm, chest	*In vivo*	Shear wave elastography (SWE)	[102]

The structural support and viscoelastic behavior of the dermis is linked to fibrillar proteins such as collagen and elastin fibers [105]. As observed in Figure 9, stress-strain behavior of the skin can be explained in three phases: first, skin shows a linear stress-strain relationship and low Young's modulus since the elastic fibers offer low resistance to the applied strain, while collagen fibers remain tangled and intertwined not contributing to the stiffness. Then collagen fibers start offering some resistance to the deformation and begin to stretch introducing non-linearity to the stress-strain curve. Finally, at higher strain, linear stress-strain relationship in once again observed until breakage of collagen fibers. In this manner, the collagen fibrils contribute to the resistance to stress and elastin ability to recoil [71].

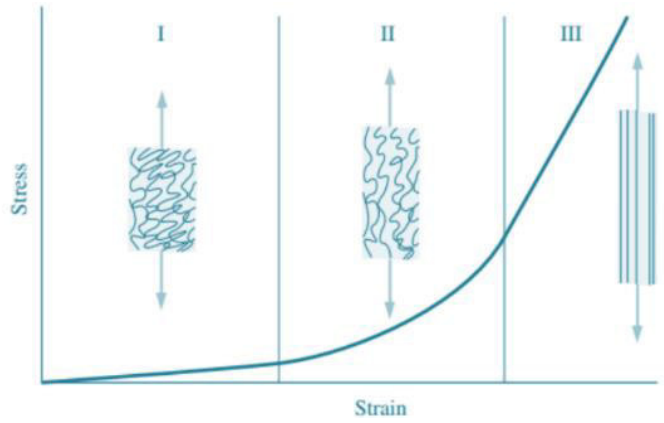

Figure 9. Schematic diagram of typical stress-strain for skin. *Showing the associated collagen fiber morphology. (Obtained from Kalra, et al.,* [59]*)*

Skin cells can actively sense the physical properties of their environment and respond by activating signaling cascades that control cell fate and function [106]. Therefore, nowadays, substrate rigidity is a critical design parameter in the development of bioengineered constructs to elicit maximal cell and tissue function.

I.II. Applications of tissue-engineered skin equivalents

In general, skin equivalents are used for three main applications: i) as skin replacement for clinical applications, ii) as models to study the effect of chemical agents or finished products on skin and iii) as three-dimensional models to study cell interactions.

I.II.I. Clinical applications

The use of engineered skin has emerged as a promising option for the treatment of skin loss, especially in the case of large area injuries such as deep burns covering more than 60% of the body when autologous transplant sources are not sufficient [107]. They have also been employed in the cases of chronic wounds associated with aging and diabetes, considered for scar revision or prevention, corrections of pigmentation defects and in the treatment against blistering diseases [5,108,109]. While some products have been shown to reduce morbidity and improve clinical outcomes after injury, no single skin substitute currently on the market has been demonstrated to fully restore normal skin structure and physiological function. Main drawbacks are lack of aesthetics and excessive scarring due to "wound contraction" and reconstruction of a poorly organized ECM network resulting in loss of functions and lack of elasticity [40].

Moreover, economic and regulatory challenges surround the application of skin engineered products. Tissue-engineering products do not fit in healthcare models for developing medical devices of pharmacological products [108]. However, in recent times rules and regulations have been the subject of considerable discussion [40]. Current available tissue-engineered skin products for clinical applications can be categorized into three groups: i) Epithelial sheets, where keratinocytes are grown into sheets, made into a suspension and sprayed onto the wound site or delivered on carriers like collagen or synthetic polymers. They are usually used in the case of superficial wounds [39]. Secondly, ii) split-thickness grafts, where grafting is done in two separate procedures, a dermal component is grafted to the patient, before applying an epidermal equivalent. Finally, small number or products have been developed that can provide both the dermal and the epidermal layers, known as iii) full-thickness skin equivalents. In this case, the reconstructed skin is produced on the laboratory securing the attachment between the keratinocytes and the dermis compartment [40].

Table 2 shows some examples of available products for clinical applications in the different groups previously described.

Table 2. Current available tissue-engineered skin products for clinical applications.

Epithelial sheet	Dermal replacement for split-thickness	Full thickness skin equivalents
• **Epicel:** biopsy of patient's cells grown into a sheet and enzymatically detached to be delivered to the patient. • **Myskin**: cells are delivered to the patient on a carrier dressing before reaching confluence. • **Epidex**: sheets formed from patient's hair follicles are delivered to the patient. • **CellSpray**: subconfluent cells are expanded and made into a suspension which is then delivered into the patient's skin as a spray. • **Celaderm**: allograft with keratinocytes from neonatal foreskin. • **Laserskin**: matrix of hyaluronic acid with patient's keratinocytes.	• **Integra**: dermal matrix of bovine collagen and glycosaminoglycan with an epidermal substitute made of thin poly(silicone). • **Alloderm**: freeze dried human donor dermis. • **Dermagraft**: synthetic knitted polymer conditioned with fibroblasts. • **Transcyte**: like dermagraft but uses a silicon nylon mesh membrane. • **Endoform**: xenograft ECM composed of a mix of biological substrates.	• **Apligraf**: allogenic keratinocytes and fibroblasts in a bovine collagen matrix. • **Permaderm**: autologous keratinocytes and fibroblasts in a reconstructed skin made of bovine collagen. • **Orcel**: neonatal fibroblasts and keratinocytes culture in a collagen sponge.

I.II.II. *In vitro* skin models

In the early 2000s the EU's 7th Amendment "Cosmetic Directive" prohibited animal testing of finished products or cosmetic ingredients regardless of the availability of alternative non-animal tests [1]. This circumstance worked as a catalyst to further develop skin equivalents as *in vitro* models. Since then, several models for the assessment of the toxicity and irritation potential of chemical agents and products topically applied in the skin have been standardized and validated by the European Center for the Validation of Alternative Methods (ECVAM) [2,40]. The first validated models simply determined the corrosion potential of chemical agents, then more complex models considering the metabolic reaction of the skin, cytokines and enzymes release were developed and are routinely used in the industry [110]. Penetration potential has also been studied in skin models; however, skin substitutes frequently exhibit higher permeability than native human skin due to differences in lipid bi-layer composition [111,112]. For the same reasons while skin equivalents are widely used in the cosmetic industry, they have

only recently been contemplated in the pharmaceutical industry for drug discovery [2,112].

Besides enabling hazard assessment, skin equivalents have also made progress in the fundamental processes of skin formation and homeostasis. Although the great majority of skin substitutes used in the cosmetic industry are only composed of an epidermal layer, the addition of the dermal layer containing fibroblasts to obtain full-thickness skin substitutes was of great value for the investigation of complex dermatological questions, where the molecular crosstalk between the keratinocytes and the fibroblasts is crucial or when the epidermis and dermis are equally involved. It was demonstrated that cell growth of both fibroblasts and keratinocytes is regulated by a double-paracrine mechanism [7]. Moreover, fibroblasts are able to secrete soluble factors that influence BM formation [62,113], epidermal histogenesis and epidermal differentiation [114,115]. These *in vitro* three-dimensional models allow the study of complex cell-cell and cell-ECM interactions since cells are arranged in a 3D physiological environment and in contact with different cell types and the surrounding matrix. While several full-thickness skin substitutes are commercially available (Table 3), researcher have developed their own models to answer more fundamental questions.

Table 3. Commercially available full-thickness skin substitutes.

Brand name/ manufacturer	Scaffold material	Cell source	Applications
EpiDermFt™/ MatTek Corporation	Collagen	Human keratinocytes (neonatal foreskin, adult breast skin), human fibroblasts (neonatal skin, adult skin)	Corrosivity, irritation, phototoxicity, anti-aging, wound healing, skin hydration and UV protection
Phenion®FT, LONG-LIFE and AGED Models/ Henkel	Bovine collagen	Human keratinocytes and fibroblasts (neonatal foreskin)	Genotoxicity, wound healing, skin penetration, UV exposure
StrataTest®/ Stratatech	Collagen I	Immortalized human NIKS® keratinocytes and dermal fibroblasts	Toxicological assays (no longer available)
T-Skin™/ EPISKIN	Collagen I	Human keratinocytes and fibroblasts (adult breast skin)	UV Exposure, genotoxicity, bacterial adhesion, omics, permeability
Advanced Skin Test 2000/ LifeLine Cell Technology	Polycarbonate collagen coated	Human keratinocytes and fibroblasts (neonatal foreskin)	Genotoxicity, phototoxicity, sensitization, drug metabolism, wound healing
MIMESKIN™/ BASF	Col-GAG-Chi	Human keratinocytes and fibroblasts	(no longer for sale, only for internal use)

Beside fibroblasts, the incorporation of other cell types in skin equivalents like melanocytes to study the reaction of skin to UV [116], Langerhans cells to test immunological reactions [3], nerves and immune cells to establish a neuro-immuno-cutaneous system [117] and endothelial cells to create angiogenesis models to study the effect of pro-angiogenic factors, have been developed [118,119]. Aside from the healthy state of the skin, it is also possible to simulate pathological conditions. Researchers have developed psoriasis skin models by using fibroblasts and keratinocytes isolated from patients afflicted by this disease or by induction of features of psoriasis in healthy keratinocytes [109]. Melanoma cells were also successfully embedded into skin substitutes to develop melanoma skin models [120,121]. Other examples are the use of skin models to study wound healing [4] and pathological infections (*e.g.* Candida albicans, herpes) [122,123]. And more recently the incorporation of the native skin microbiome into skin models is greatly attracting interest among researchers in academia and in the industry [124]. In Table 3, a list of commercially available full-thickness skin equivalents details their common routine applications in the industry, however, several research groups have also developed their own models to answer more fundamental questions, which are not available commercially.

I.III. Protocol to produce *in vitro* full-thickness skin equivalents

Reconstructed human epidermis consists exclusively of a multilayered epidermal construct, whereas full-thickness skin models constitute an epidermis grown upon a dermal layer. Usually, fibroblasts are either encapsulated within ECM components like collagen or fibrin [9,13,115] or seeded on top of a matrix (synthetic or natural scaffolds) and cultured for a few days to weeks to allow cell migration into the scaffold and obtain a dermal component [125,126]. As observed in Figure 10, keratinocytes are then seeded on top of the dermal equivalent, cultured under submerged conditions for a few days and finally exposed to the air, process commonly known as the air-lift or air-liquid interface, resulting in the formation of a differentiated and stratified epidermis.

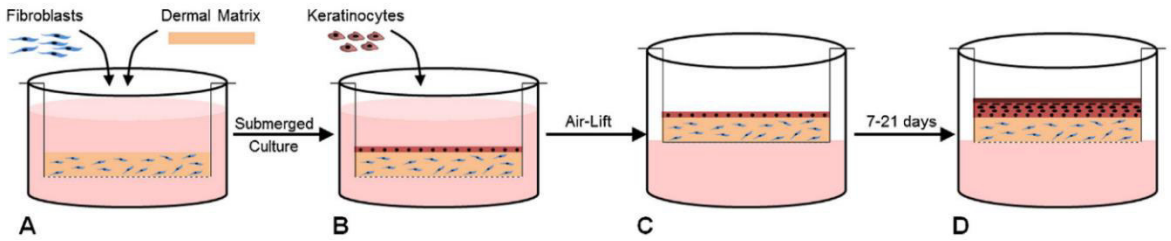

Figure 10. Culture process scheme of full-thickness skin equivalents. *A) Dermal matrices (synthetic or natural) with or without embedded fibroblasts are cultured under submerged conditions within a culture insert. B) Once the dermal equivalent is formed, keratinocytes are seeded on top of the dermal matrices. C) After a few days of submerged culture in a proliferative medium, the culture is exposed to the air allowing the media to perfuse only through the dermal compartment and a differentiation medium is used. D) Air-liquid interphase culture results in keratinocyte's differentiation and formation of a stratified and cornified epidermis. (Obtained from Sriram et al.,* [61]*)*

This delicate multistep procedure involves complex cell dynamics where the culture conditions and materials will play an essential role. Once keratinocytes are seeded, different and specific cell media are used to promote either cell proliferation or differentiation. First keratinocytes proliferation is promoted under submersion with the addition of growth factors such as keratinocytes growth factor (KGF) or epidermal growth factor (EGF) [47]. Supplements as the EGF, ensure the persistence of epidermal keratinocytes growth *in vitro,* binding specific cell-surface receptors that have been detected in the basal layer of the epidermis [44]. During air-liquid interphase, serum depletion plays an important role to form a stratified epidermis. In addition, cultivation at air-liquid interphase implies that the oxygen in the air is more directly at the disposal of epidermal cells, mimicking so the conditions of native skin and increases epidermal morphogenesis and synthesis of membrane-coating granules [127]. Since several signaling pathways involved with keratinocytes differentiation are regulated by calcium concentration, its content in the medium is increased to promote differentiation and stratification during air-lift [46]. Calcium is known to promote keratinocyte proliferation under 0.1 mM and to encourage keratinocyte differentiation at higher concentrations [46]. Other medium supplements that have been recognized in epidermal morphogenesis include hydrocortisone, triiodothyronine, vitamin D, retinoic acid, insulin and progesterone [61]. *In vitro,* vitamin D3 and triiodothyronine show antiproliferative and pro-differentiating effects [128,129]. Also Vitamin C has been shown to promote keratinocytes differentiation [130], fibroblast proliferation and collagen synthesis [115]. As well, the incorporation of essential fatty acids as media

supplements has also been evaluated to promote the formation the skin barrier to reproduce *in vitro* the lipid composition observed in native skin [55].

Protocols usually rely on complex "in-house" media containing multiple additives of the previously mentioned [131]. Cell medium volume and components need to be fine-tune to the thickness and porosity of the material. In the case of commercial models (*e.g.* Epiderm-FT, Phenion full thickness and T-skin) models arrive pre-made with their specific medium ready for a multiple of standardized tests but lack the flexibility to be tailored for more specific applications. Usually, on arrival, commercial models are just removed from transport vessels are placed on air-lift interphase as shown in Figure 11 and used following protocol instructions.

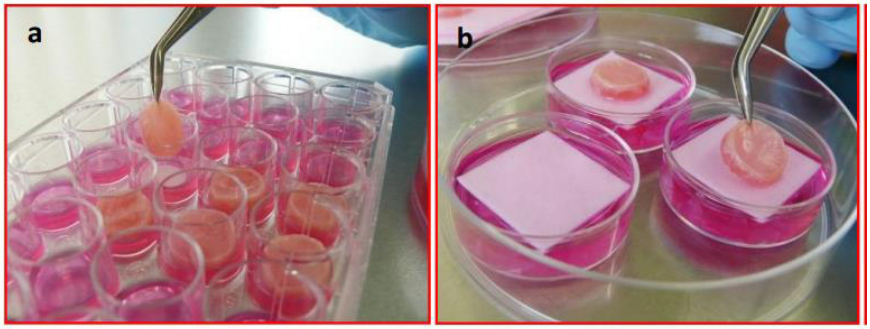

Figure 11. Phenion® FT skin model Air-Lift procedure. *A) Skin equivalent is removed from transport vessel using sterile forceps. b) Skin equivalents are placed on top of a pre-soaked filter paper for subsequent culture on the air-liquid interphase. (Modified from Phenion instruction for use,* [132]*)*

Cell source can also play a role in the ability to generate a reproducible stratified epidermis. Both donor source as well as the supplements in culture media influence the formation of a favorable lipid profile [55,133]. Most commercial *in vitro* products, as shown in Table 3, use primary cells. While primary cells can be unpredictable, attempts to use cell lines, such HaCaT cells have shown a disorganized epidermal morphology [134,135]. However, recently Reijders *et al*. were able to successfully develop a full-thickness models using TERT-immortalized keratinocytes [136].

I.IV. Current materials evaluated for tissue engineered full-thickness skin equivalents

Since the 80's when Bell *et al*. established the first skin equivalent, where fibroblasts were seeded into collagen lattices [9], few materials other than collagen have obtained as much success. Full-thickness skin equivalents available in the market for either clinical applications or as *in vitro* skin models are mostly made of collagen (Table2 -Table 3). To circumvent the main first setbacks observed with collagen lattices, such as matrix contraction and weak mechanical properties, collagen has been further crosslinked by chemical agents, either with itself or with a mixture of natural or synthetic polymers [6,12,137]. For example, crosslinking of collagen hydrogels with succinimidyl glutarate PEG (PEG-SG) reduced fibroblasts-mediated contraction and increased scaffold stability to obtain a suitable skin equivalent, however, collagen fibril structure was altered [13]. Common crosslinking agents like glutaraldehyde and formaldehyde allow a rapid crosslinking easily controlled by the acidic environment but can cause cytotoxicity [138] and techniques to eliminate residual chemical agents can be expensive and long [139]. Carbodiimide is a successful non-cytotoxic crosslinker, however, since it binds the free primary amino groups and cell-reactive carboxylates anions, it diminishes some of the essential cell-binding motif of collagen scaffolds [140,141]. Another simple way to introduce crosslinks and increase the strength of collagen networks is through physical techniques such as UV irradiation [142], heating (dehydrothermal treatment DHT) [143] or freeze drying [144]. This results in weaker bonds compared to chemical methods and require long reaction times. Although all these methods can increase tensile strength and degradation profile of collagen, its native properties can be lost during crosslinking process and encapsulation of cells can be limited [141]. Recently introduced techniques, such as enzymatic crosslinking, which does not modify the collagen structure are extremely expensive [145].

Because of its availability and biocompatibility, type I collagen main source of extraction is bovine [146]. For the moment, bovine collagen is approved by the US Food and Drug Administration (FDA) as risk of pathogen transfer is considered low when extracted from countries where herds are known to be free of bovine spongiform encephalitis (BSE) [39]. However, the spread of this disease could limit the availability of collagen in the future. Moreover, organizations against animal-

cruelty and animal testing in the cosmetic industry will eventually push towards animal-free models with synthetic alternatives [147]. Nonetheless, progress in purely synthetic materials for these types of applications is scarce. Table 4 shows a summary of the synthetic polymers that have been evaluated as scaffolds for full-thickness skin equivalents. Few innovative synthetic materials have been developed for this type of application, most of the synthetic polymers used to create dermal equivalents date from the late 90's, early 2000's. Surprisingly, few synthetic hydrogels have been evaluated in this regard, mainly synthetic polymers have been used as knitted mesh or fiber matrices. Limited clinical success of synthetic polymers is often related to the lack of biological signals to promote cell attachment and proliferation, therefore, synthetic polymers are usually combined with natural substrates to produce suitable scaffolds [148]. For instance, while in PEGT/PBT scaffolds keratinocytes migrated into the pores forming cysts, epidermis histogenesis was improved by incorporating a fibroblast-collagen mixture into the pores before seeding the keratinocytes [149]. Also polycaprolactone copolymer was evaluated as a dermal substitute [150] but further exploited as a collagen/polycaprolactone composite [151]. Just recently, Roger *et al*. evaluated the ability of dermal fibroblasts to grow and deposit ECM proteins within a polystyrene Alvetex scaffold (without introducing any exogenous ECM components) as a dermal layer to produce a full-thickness skin equivalent. While some fibroblasts infiltrated the scaffold, a majority formed 3D layers on the surface [125].

Table 4. Synthetic materials evaluated for skin engineering applications.

Scaffold material		Applications	Advantages & Disadvantages	Ref
Polyglycolic acid mesh (Dermagraft)	Knitted mesh	Skin Graft for small ulcers	-Degradable after implantation -Absorbable PLGA scaffold -Not viable for *in vitro* tests -Surface hydrophobicity and limited cell adhesion	Hart *et al*. 2012 [152]
Poly(ethylene glycol terephthalate) (PEGT) and poly(butylene terephthalate (PBT)	Porous films	Skin substitute *in vivo*	-Polymer use in clinic for other applications -Hyperproliferative epidermis -Basal lamina absent -Slow degradation	Van Dorp *et al.* 1999 [153] Glalbzouri *et al*. 2004 [149]
Polycaprolcatone (PCL)	Sponge like sheet	Dermal substitute *In vivo* studies	-Long process -Degradation after 4 weeks implantation in guinea pigs -No further studies were made	Bruin *et al.* 1990 [150]
Poly (lactic-co-glycolic acid) and polycaprolactone) PLGA-PLC	Knitted mesh	Dermal equivalent *in vitro*	-Low proliferation, difficulty to fill the space between the pores (0.5- 1 mm) -Not homogeneous cell distribution	Ng *et al.* 2004 [154]
Polyglycolic acid (PGL) and polyglactin (PGA) mesh	Knitted mesh	Dermal substitute	-Dermal equivalent evaluated *in vivo* in mice -Resorbable by the body -Decreases pH of surrounding tissues	Cooper *et al.* 1991 [155]
PEO/PBT and PLLA polyactive	Co-polymer film	Skin substitute *in vivo*	-Bilayer, fibroblasts in 2D -Low proliferation in pores -*In vitro* studies, *in vivo* biocompatibility unknown	Beumer *et al.* 1993 [156]
Poly[lactic acid-co-glycolic acid] (PLAGA) fibers	Fiber matrix	Dermal substitute	-Effect in fiber diameter -*In vitro* cytotoxicity but no evaluation *in vivo* - Epidermal formation was not evaluated	Kumbar *et al.* 2008 [157]
Poly (DL-lactide) (PDLLA)/PEG fibers	Fibrous scaffold	Dermal substitute	-Fibroblasts were more in 2D than in 3D -Epidermal formation was not evaluated	Cui et al. 2009 [158]
Electrospun Polystyrene	Fiber matrix	*In vitro* studies	-Non biodegradable -Keratinocytes formed stratified epidermis in the presence of fibroblasts (poorly defined)	Sun *et al.* 2005 [159]
Polystyrene (Alvetex)	Porous scaffold	*In vitro* studies	-Commercially available -Used as a matrix for 3D cell culture on other applications -Protocol for skin equivalents *in vitro*	Roger et al 2019 [125]

II. Development of Biomaterials

One of the key factors to develop an *in vitro* engineered tissue is the development of an adequate biomaterial that will serve as a three-dimensional architectural template to guide tissue formation and allow cell growth. There is no such thing as the perfect biomaterial, the target tissue and application will determine the optimal properties of the biomaterial [160]. However, in a general sense, these materials must mimic the native ECM, be biocompatible and have a suitable surface chemistry to allow cell bioactivity such as cell adhesion, migration, proliferation and differentiation. Different types of biomaterials have been developed and are currently used for a variety of tissue engineering applications, such as natural and synthetic polymers, ceramics, metals, composites and hydrogels [161]. Among the latter, hydrogels will be given the most consideration, due to their ability to mimic the gel-like viscous consistency of the ECM of soft tissues, such as the skin.

II.I. Hydrogels

Hydrogels are highly swollen hydrophilic polymers (Figure 12), particularly attractive as three-dimensional support for cell growth and tissue replacement, since they are capable of mimicking the highly hydrated and viscoelastic extracellular network [162]. In the skin, the ECM, mainly composed of a collagen network and water-filled ground substance, closely resembles the heterogeneous arrangement of a polymer network associated with water in a hydrogel [44]. Moreover, a wide number of hydrogels have shown to be biocompatible and permeable to oxygen and nutrients guaranteeing the maintenance of tissue formation [163–165]. Hydrogels can be prepared from various natural or synthetic materials. In addition, they can be subjected to different processing techniques to control their macro- and micro-structural properties to adequate to each application.

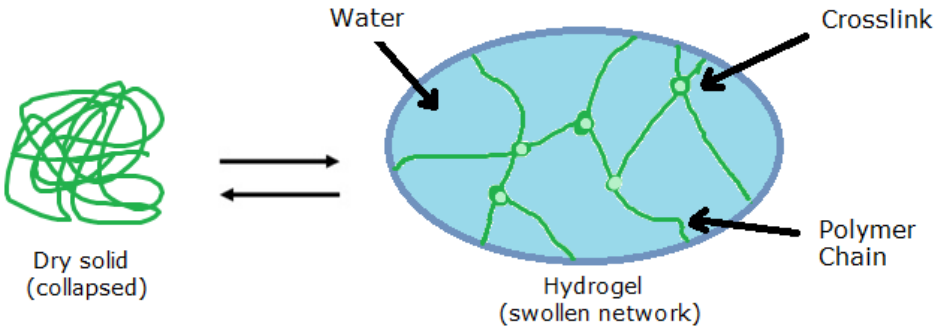

Figure 12. Representation of a hydrogel in its dry and swollen state.

II.I.I. Natural and synthetic hydrogels

Hydrogels can be produced from either natural of synthetic materials, each conferring different advantages or disadvantages to the biomaterial (Table 5). Synthetic materials used for tissue engineering scaffolds include: poly(ethylene oxide) (PEO), poly(vinyl alcohol) (PVA), poly(acrylic acid) (PAA), poly-(lactic acid) (PLA) and poly(ethylene glycol) (PEG) to name a few [166–169]. They have the advantage of having an exact composition and multi-tunable properties, but may lack bioactivity to promote cellular activities [164,170]. To address the lack of bioactivity, the polymeric networks are usually subject to surface modification to integrate cell-adhesion, degradation or growth-binding sites [84,162]. On the other hand, natural polymers confer to hydrogels their inherent ECM structure. They include; agarose, alginate, chitosan, collagen, fibrin, gelatin and hyaluronic acid [16]. However, they tend to show weak mechanical properties, batch-to-batch variability and risk of pathogen transfer [15,16]. Especially, hydrogels made of collagen for skin engineering applications tend to suffer fibroblast-mediated contraction and require further crosslinking procedures to increase its tensile strength [141]. Regardless of the progress achieved in this matter, synthetic materials display the best alternative to avoid batch-to-batch variability, risk of pathogen transfer and the ethical dilemma that emerges with the use of animal sources. Moreover, to be tailored individually towards specific medical needs, biomaterials require an improved and more flexible control over their properties which can be acquired with synthetic materials.

Table 5. Advantages and disadvantages of natural and synthetic Hydrogels. *(Modified from Ng et al.,* [154]*)*

	Natural matrix materials	**Synthetic matrix materials**
Advantages	• Mimic natural ECM structure and composition. • Emulates the ECM native stimulatory effects. • Incorporation of natural growth factors and/or other matrix proteins.	• Allow controllable degradation kinetics to suit different applications. • Control over mechanical properties, possibility to withstand cellular contraction. • Eliminate risks of pathogen transfer. • Allow controlled release of growth factors. • Control over shape, size using various processing techniques. • Reduce batch-to-batch variability
Disadvantages	• Dissolve/degrade easily, and do not allow varied degradation kinetics. • Poor mechanical forces. • Require more elaborate modifications and processing techniques due to a more complex structure and lower tolerance to heat. • Batch-to-batch variability • Possible transfer of pathogens • Mostly obtained from animal sources, ethical dilemma.	• Often do not possess natural bioactivity. • Can degrade to from by-products, which may rise to undesirable local environment. • Require surface modifications to improve cell-material interactions.

II.I.II. Methods of production of synthetic hydrogels

i) Hydrogel networks

The structural integrity of hydrogels depends on the crosslinks formed between the polymer chains that can be either chemical bonds or physical interactions [171]. Physical hydrogels are non-convalently crosslinked networks formed by molecular entanglements, such as hydrogen bonds or intramolecular interactions due to changes in the external conditions (*e.g*. pH, temperature, shear stress…). While these hydrogels benefit from reversibility and absence of chemical reactions, they have several disadvantages such as lower stability and mechanical properties compared to chemically crosslinked hydrogel [164]. For example, PNIPAAm and poly(2-oxazoline) form reversible thermoresponsive hydrogels by hydrogen bonds but collapse above a specific temperature [172]. Inspired by the understanding of protein self-assembly, recombinant peptide blocs have been

designed to form self-assembly hydrogels through the formation of physical bonds. They are of interest for biomedical applications since they are derived from recurring amino acid sequences found in proteins [173].

Contrary to physical gels, chemical hydrogels are formed by covalent bonds through Michael-type addition, click chemistry, Schiff-base crosslinking, disulfide crosslinking, photo-crosslinking and enzyme-mediated crosslinking. This reactions allow to increase the stability and mechanical strength of the hydrogel's bonds [174]. These covalent bonds form stable networks with tunable mechanical properties. However, biocompatibility and safety issues must be considered depending of the chemical reagent used during the chemical reaction [164]. The most commonly applied synthetic hydrogel polymers for tissue engineering, PEO and PEG, which share a similar chemical structure, are currently FDA approved for several medical applications [171]. PEG hydrogels can be crosslinked through various paths, in which the PEG molecules are either functionalized with reactive end-groups and activated by initiators or associated with multifunctional monomers [19].

Besides the intrinsic characteristics related to the chemical formation of the network (such as swelling, bulk mechanical properties and degradation), the ability of cells to colonize the hydrogel can play an important role in the possibility to create a new tissue [161]. In optimal conditions, crosslinking chemistry is mild and do not induce cytotoxicity, thus enabling encapsulation of cells within the hydrogel to obtain a homogeneous cell distribution [171]. To further allow cell colonization, some groups have incorporated protease-sensitive degradation sites in the polymeric network to promote cell migration [175]. Otherwise, cells can be seeded into the biomaterial after creation, but the hydrogel then needs to display sufficiently large and interconnected pores to allow the cells to penetrate and infiltrate the polymeric matrix [176]. Diverse fabrication methods can be employed to control the degree of porosity and pore interconnection to obtain an adequate macroporous structure for cell infiltration and nutrient diffusion [176–178].

ii) Macroporous structure

Porosity, pore size and interconnectivity of hydrogels can be tuned by using different pre- and post-fabrication techniques. Techniques like freeze drying, gas foaming or particulate leaching have been used to introduce macro scale pores into hydrogels [160]. Freeze drying is one of the most inexpensive ways to induce

porosity in hydrogels, but the exact size and form of pores are difficult to control, since variations of the lyophilization parameters control the porosity, pore size, architecture and final mechanical properties [144,179]. In foaming technique, high pressure CO_2 is blown into the hydrogel to form bubbles, which will form the pores [180]. This technique has the advantage of being organic-solvent-free but is expensive and often generates poorly interconnected structures. It is consequently sometimes combined with salt leaching [181]. In particulates leaching techniques, salt, wax and sugar are commonly used as porogens to create the pores. Porogens of a desired size are poured into a mold, then the polymer is cast into the mold, and porogens are dissolved using a suitable solvent, leaving behind a porous network [160,182]. For example, the use of paraffin microspheres as porogens favors the use of nontoxic solvents (such as ethanol) and results in interconnected pores [183]. Pore size can easily be tailored by controlling the amount, size and shape of the porogens [160,182]. Paraffin-leaching has the advantage to produce spherical-shaped pores with well-controlled interpore connectivity contrary to salt-leaching where pore shape is limited to the cubic crystal shape of NaCl salt [183].

II.II. Dendritic polymers

Because of their properties and versatility, dendritic polymers are ideal candidates for incorporation into tissue engineering scaffolds; however, examples on this type of application are scarce [184]. Dendritic polymers are highly branched polymers with three-dimensional architectures. Dendritic polymers can be classified into three classes: dendrimer, dendrigraft and hyperbranched polymer (Figure 13).

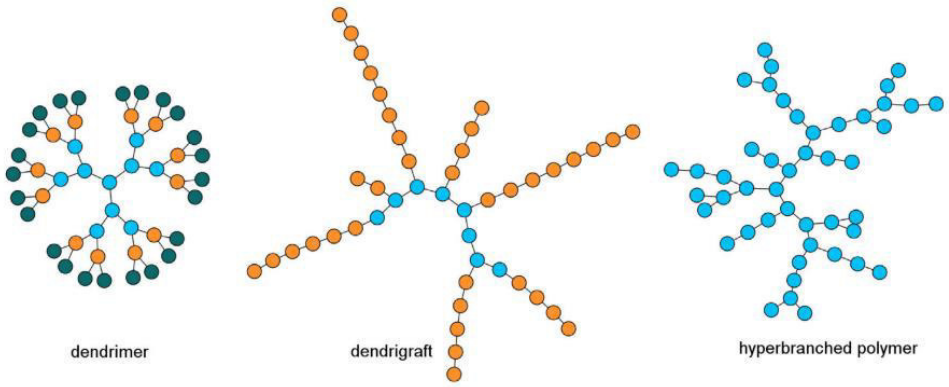

Figure 13. Dendritic polymers; dendrimer, dendrigraft and hyperbranched polymer. *Each dot represents a monomeric building block, and each generation is highlighted with a distinct color. (Obtained from Francoia, et al.,* [25]*)*

Dendrimers are macromolecules obtained after a generational synthesis, resulting into the formation of theoretically monodisperse structures. In comparison to linear polymers, the structure, molar mass, size, shape of dendrimers can be easily controlled [25]. In contrast, hyperbranched polymers are polydisperse and display random branching. Finally, dendrigrafts have a unique structure between the fully controlled and well-defined dendrimers and the uncontrolled hyperbranched polymers. They share features of both dendrimers (*e.g* generation-based growth and narrow molecular weight distribution) and hyperbranched polymers (*e.g* rapid increase in molecular weight) [25]. The molecular weight of dendrigrafts can increase more rapidly with each generation than that of dendrimers, making it possible to develop polymer possessing dendrimer-like properties at a lower cost [185]. In comparison to linear polymers that only have two functionalizable end groups per macromolecules, dendrimers polymers possess a large number of terminal functional groups which allow to incorporate new crosslinking moieties or bioactive factors [184]. Additionally, their relative empty intramolecular cavity can work as host-molecule entrapment providing opportunities for subsequent controlled drug release as synthetic carriers [24,186]. Despite their macromolecular size, dendritic polymers are theoretically single-molecule compounds; and therefore, could be used as multifunctional crosslinkers [187].

A number of dendritic polymers have been reported in the literature so far, and the poly(amine)-based have attracted the most attention for biomedical applications [188–190]. Poly(amine)-based dendritic polymers are mostly represented by poly(amidoamine) (PAMAM), however, PAMAM dendrimers have shown high cytotoxicity, few interactions with cells, low degradation and high productions cost [191]. Similarly, poly(L-lysine) and poly-ethylenimine polymers (PEI), other poly(amine)-based polymers, can benefit from their polycationic nature at physiological pH theoretically allowing cellular adhesion, endocytosis, intracellular trafficking for therapeutic delivery, genetic material transfection or imaging [26,192]. While both have been assessed for biological applications, Poly (L-lysine) has showed a superior viability of 90% compared to 50% for hyperbranched PEI at the same concentration on HeLa cells [25]. While poly(amidoamine) dendrimers (PAMAM) have been successfully evaluated as crosslinking monomers for functionalized PEG to form hydrogels for drug delivery

applications that do not require extensive interactions with cells [187,193,194], our laboratory was the first to assess DGL-G3 as crosslinking monomers with PEG. Such hydrogels could benefit from their inherent bioactivity, without the need for further association with functional moieties.

II.II.I. Poly-L-lysine dendrigrafts

Poly-L-lysine dendrigrafts (DGL) are based on naturally occurring amino acid monomers (Figure 14). They bestow additional properties to classical dendrigrafts such as water solubility, stability under sterilization conditions, partial degradability under the action of endogenous peptidases, non-immunogenicity and low cytotoxicity [24,25]. Beside the presence of multiple amino groups in the surface area, a free carboxylic acid function at the core of DGL opens the door to various modifications towards the implementation of tailored features [25]. DGL used as coatings on surfaces have been shown to increase cellular adhesion and proliferation of human skin fibroblasts by inducing the expression of integrin α5, a receptor implied in cell adhesion to fibronectin (through RGD) [27].

DGL synthesis is based on the grafting of subsequent lysine molecules onto a polymeric substructure, linear poly-L-lysine (PLL), using protect-deprotect steps. In this manner, increasing generations of DGL (G1-G5) can be obtained with a simple, scalable procedure, water-soluble reaction (pH 6.5) with low batch-to-batch variability with a typical yield of 50-60% on a multigram scale [185]. While G3 and G4 both showed an increase in cellular adhesion in comparison to linear and smaller generations lysine dendrigrafts, DGL-G3 represents the best compromise between biological activity and fabrication cost, as well as limiting the formation of aggregates observed in the G4 synthesis [27].

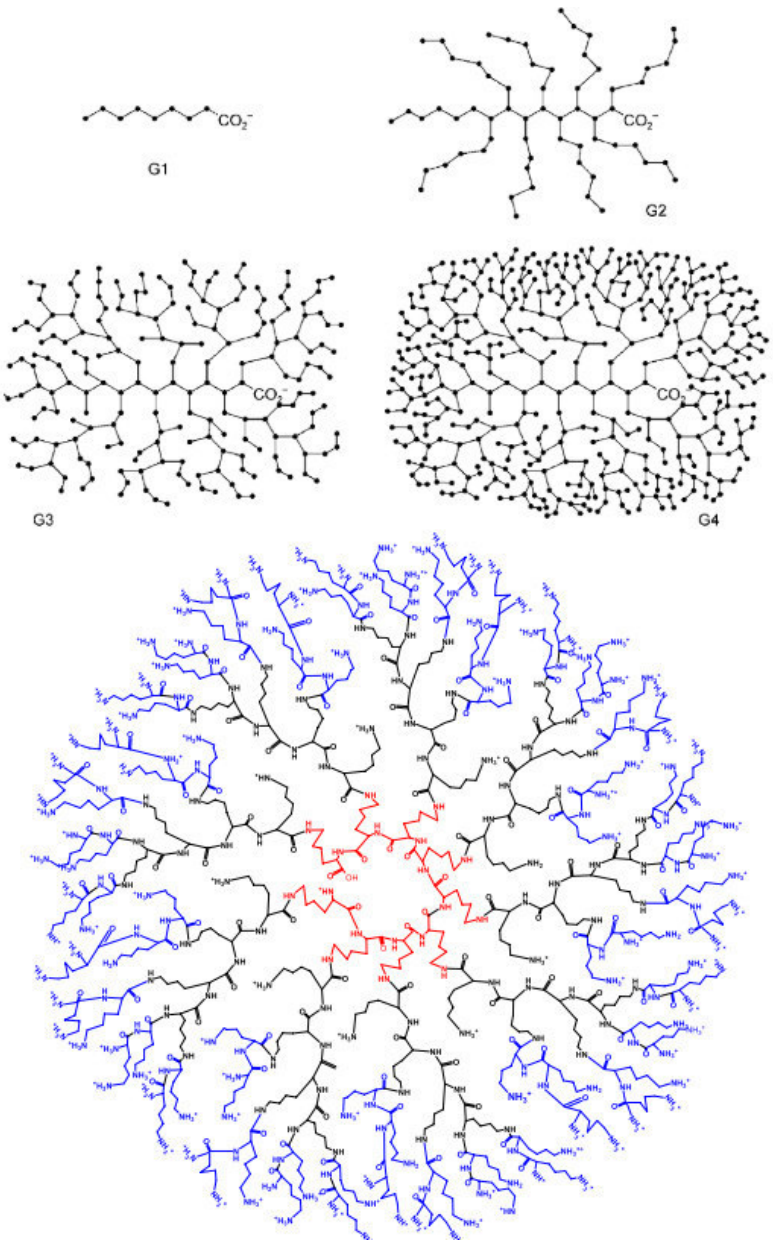

Figure 14. Schematic representation of poly-L-Lysine dendrigrafts (DGL G1-G4). At the bottom, the chemical structure of DGL G3. Each dot represents a Lysine residue. At the bottom the chemical structure of DGL G3, chemical structure in red corresponds to G1 and structure in red and black to G2. To facilitate 2D-representation of the whole structure, central part of G3 is shown in a cyclic conformation. (Obtained from Yevlampieva et al., [195])

II.III. Cell response to biomaterials

Biomaterials have a role in mimicking the native ECM to promote a proper tissue formation and homeostasis. *In vivo*, the ECM interacts with the cells by two different signaling mechanisms: ligand-induced, which depend on ECM biological

and chemical stimuli, and traction-induced signaling, which depends on the ECM mechanical stimuli and how the cells "feel" the mechanical properties of their microenvironment. In 1997, Pelham and Wang were one of the first to show that both the mechanical and biochemical cues could have a role in cellular behavior [196].

II.III.I. Mechanical cues

Studies to understand the influence of the ECM mechanical properties are still scarce compared to the biochemical signals, however, more researchers are trying to address this aspect of the ECM. As shown in Figure 15, the range of mechanical compliance of the human tissue varies from tissue to tissue. Engler *et al.* demonstrated the extreme sensitivity of naïve mesenchymal stem cells (MSCs) to tissue stiffness. MSCs were able to compromise to a specific cellular phenotype, either into neurons (0.1-1 kPa), myoblasts (8-17 kPa) or osteoblasts (25-40 kPa), depending solely of the mechanical properties of the substrate [197].

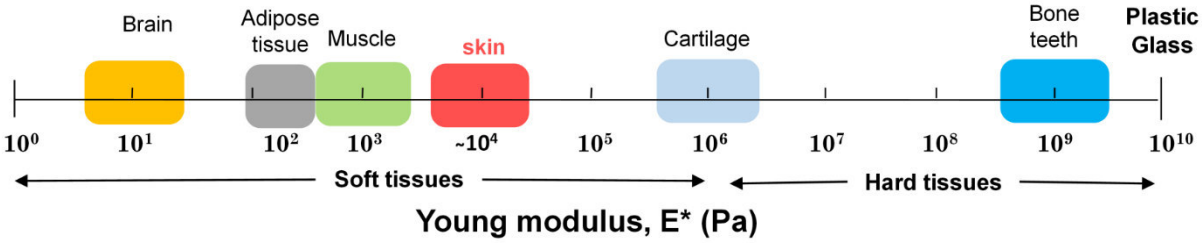

Figure 15. Range of stiffness (Young modulus, E*) of a variety of solid human tissues. *(Modified from Engler et al.,* [197]*).*

The mechanism by which cells receive mechanical stimuli and process them into biochemical or gene expression changes is called mechanotransduction [198]. Mechanosensitive molecules at the cell membrane such as integrins, stretch-activated ion channels, G protein couple-receptors and growth factor receptors perceive the mechanical stimuli and translate this mechanical signal into a biological response. The primary site of force transmission in the cellular membrane is by the formation of focal adhesion points (FA), which serve as anchorage points between the cell and the substrate, binding the transmembrane component of the ECM with the integrins and the actin cytoskeleton of the cell [199] (Figure 16). Changes in cell cytoskeleton and tight connections between the cytoskeleton and the ECM through this cell-surface receptors, translates the

mechanical signals and influence various cell functions including cell adhesion, migration, proliferation and tissue formation [198].

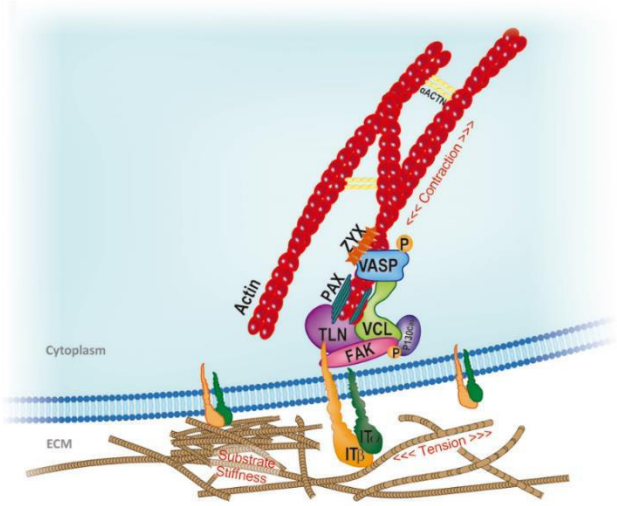

Figure 16. Schematic representation of key mechanosensing players involved in cell-ECM interactions at the focal adhesion (FA) site. *Extracellular matrix changes in stiffness, tension or other mechanical stimuli are perceived by integrin clusters whose morphology changes recruit focal adhesion kinase (FAK). Then other molecules such as Talin rod (TLN), vinculin (VCL), paxillin (PAX) and adaptor protein p130Cas anchor to each other to transfer the mechanical cues from the integrins (IT) to the actin component of the cytoskeleton. As well the vasodilator-stimulated phosphoprotein (VASP) and zyxin (ZYX) regulate actin assembly. (Obtained from Martino et al.,* [199]*).*

Accordingly, substrate stiffness has become essential in the development of tissue engineering substrates and for the *in vitro* study of the dynamics implicated in mechanotransduction [106,200,201]. Previously, researchers focused in investigating cell response to substrate stiffness using natural gels, such as collagen and Matrigel, by increasing the elastic modulus with increasing protein concentrations within the gel. However, it is complicated to assess the contribution of the mechanical component from the biological cues. More recently, scientists have developed synthetic materials of which mechanical properties can be easily modified. For example, PEG-based hydrogels and polyacrylamide systems have been widely used to study cell response to substrate rigidity [202]. The rigidity of polyacrylamide gels can be easily controlled by varying the quantity of acrylamide monomer or bisacrylamide crosslinker, however, these gels do not possess inherent biological activity. To allow cell adhesion these gels are coated with collagen or fibronectin [201,203,204]. In our group, we recently investigated substrate stiffness as a regulator of keratinocytes behavior (full article available in page 197). Proliferation and spreading were strongly decreased in keratinocytes

seeded in softer polyacrylamide gels (4 kPa) with an increased expression in late differentiation markers, however, their proliferative ability was recovered once they were put back in contact with a stiffer environment [205]. While polyacrylamide is one of the most standardized and used material for rigidity studies, it is only suitable for 2D cell culture. PEG gels enable a number of modifications and various molecular weights and can be easily engineered with adhesive or degradations ligands [206]. However, similar to polyacrylamide gels, PEG hydrogels require to be associated, functionalized or coated with supplementary proteins of the native ECM or functional moieties, such as collagen [34], laminin [35], or arginine-glycine-aspartic (RGD) peptides [207,208] to support survival and function of adherent cells [18,202]

II.III.I. Biochemical cues

As previously mentioned, interactions with the surrounding microenvironment influence cell adhesion, migration, proliferation and differentiation. One of the most basic cell functions required for cell survival is cellular adhesion [209]. Cell adhesion to a biomaterial can be promoted by simply modifying the surface chemistry of a biomaterial with certain functional groups [210] or coating with polymers or proteins that allow cell adhesion [204]. For instance, polycationic amine-based polymers, such as PLL allow cellular adhesion at physiological pH [25,27]. In the case of biomaterials made of ECM components (*e.g.* collagen, fibrin, fibronectin), the natural occurring receptor-binding ligands of their native molecules bind to cell integrins and can easily promote cell adhesion [16]. Since the identification of some of the small oligopeptide sequences within the ECM adhesion proteins that are able to interact with cell integrins, it has been possible to incorporate these peptides into synthetic networks to promote cell adhesion. For example, RGD peptides found in many ECM proteins, including fibronectin, vitronectin, osteopontin, collagen and fibrinogen has been successfully employed to provide biological activities to materials in a large range of applications [84,208,211].

Beside adhesion ligands; growth factors [212], protease-cleaving sites [213] and recognition peptides [214] can be incorporated into biomaterials to achieve a higher degree of dynamic interactions with the cells and induce specific cell and tissue responses. The native ECM also serves as a reservoir of soluble

macromolecules such as growth factors, chemokines and cytokines, protecting them from enzymatic degradations and releasing them when necessary [66]. ECM-bound growth factors could be released or presented as complexes still bound to the ECM proteins to modulate cell growth and migration, as part of a tightly controlled feedback circuit essential for normal tissue homeostasis [215]. Likewise, ECM proteins or growth factors can simply be entrapped within a synthetic hydrogel scaffolds and released upon network degradation [167]. For instance, VEGF immobilized within matrix metalloproteinase (MMP)-sensitive synthetic hydrogel network could be released and retaining its biological activity on cell demand [214]. Similarly, the use of peptide that mimic growth factors has been evaluated their smaller molecular weights and a simple orientation allows immobilization of the actives sites in biomaterials [212]. Aside from favoring the release of growth factors, controlling degradation can be of interest to be able to match biodegradation of the matrix with the formation of new tissue. Degradation can be tailored with the incorporation of MMP sensitive sites as well as by controlling the physicochemical properties of the network [162,214].

Covalently modified PEG-based hydrogels with ECM ligands, collagenase-degradable peptide and growth factors to promote specific cell functions or proteolytic degradation have been extensively investigated [17,214,216]. Another recent approach to mimic the specific features of the ECM is the incorporation of recombinant proteins [19,213]. Recombinant DNA technology allows to obtain synthetic analogs of natural ECM matrix materials without resorting to natural proteins [217]. Besides their role as recognition motif to enhance cell attachment of induce cell signaling pathways, synthetic peptide sequences have been assess as monomer to create smart bioinspired materials [218].

II.IV. Biomimicry of ECM proteins

Biomimetics seeks from nature a source of inspiration to solve complex problems. Biomimetic approaches are routinely applied in the development of synthetic materials and systems that intend to mimic biological processes. Examples of biomimetics go from the reconstruction of the mechanical properties of a tissue to the creation of synthetic sequences that reproduce the biological activity of proteins. Recombinant techniques, mostly using bacteria, provide a controllable well-defined source of synthetic proteins or polypeptides [217].

Recombinant proteins can provide cleavage sites for controlled degradation, as adhesion sites on inert synthetic materials and even as building blocks to form a synthetic network by themselves [213]. Polypeptide based hydrogels have shown promising attributes as biomaterials since they can responds to external cues such as temperature and pH [219]. For example, elastin-like polypeptides have been extensively reviewed by several research groups as building blocks [31,219,220]. While in the last couple of years there has been a slight development in the production of recombinant collagen, the yield is extremely low due to its extremely complex structure [221,222]. The correct amount of post translational modifications such as hydroxylation of proline and lysine and the heterotrimeric composition are still challenging [222]. The few recombinant collagen composites to date require more in depth studies on biocompatibility, immunogenicity and long term stability [223]. In the contrary, the structure of elastin, another main component of the ECM, can be more easily imitated with recombinant techniques [31]. Moreover, this structural protein has attracted recent attention in the development of biomaterials for tissue engineering applications thanks to a broad range of advantages.

III.I.I. Benefits of elastin-based materials

Excessive scarring and wound contraction leading to a loss of functionality and decreased aesthetics are still major drawbacks of current biomaterials used for dermal reconstruction [79]. Adult human dermal fibroblasts do not synthesize functional levels of tropoelastin, resulting in an aberrant elastic network after wound healing [74]. Elastin-based biomaterials are particularly promising alternatives to reproduce the natural elasticity of the skin and promote elastin synthesis [30,31]. While human dermal fibroblasts cultured in the absence of tropoelastin do not exhibit mature elastin synthesis, the addition of exogenous tropoelastin substantially induces *de novo* elastogenesis and deposition of elastin fibers into the ECM [224]. Likewise, Pirayesh *et al*. reported that elastin-collagen composites could induce modest levels of elastin depositions in rats with a correlated increase in elasticity in clinical trials, whereas collagen scaffolds did not show elastin synthesis [225]. As well as elasticity, the biological activity of tropoelastin and elastin derived peptides has long been established [226,227]. They have been shown to promote *in vitro* attachment, spreading and proliferation

of fibroblasts through binding integrin $\alpha_v\beta_3$ and EBP [33,228]. Incorporation of elastin into biomaterials can occur in different forms: including insoluble elastin derived from natural elastin, repeated elastin like sequences, recombinant human tropoelastin or tropoelastin fragments [30,31,79,80].

III.I.II. Elastin sources

The purification process of elastin from animal sources is a complex process since insolubility of elastin prevents it from being isolated and purified except by heterogeneous fragmentation. Once crosslinked, insoluble elastin cannot be converted into its soluble precursor form, tropoelastin [30]. In addition, elastin extracted from animal sources may be associated with microfibrillar proteins and lead to increased calcification following implantation [79]. Therefore, elastin-based biomaterials depend mainly on recombinant human tropoelastin and synthetic elastin-like polypeptides (ELPs) [31,80]. ELPs are polymer-based oligopeptides with sequences that recur in tropoelastin. ELPs may be synthesized either chemically or through recombinant techniques, best known as elastin like recombinamers (ELRs). Recombinant techniques are attractive because they can produce greater quantities of longer sequences [79]. Purification of ELPs or ELRs is typically achieved through the repetition of several rounds of inverse transition cycling (ITC), exploiting the coacervation properties of the ELPs/ELRs, which are similar to native tropoelastin. The solution is heated over its transition temperature (Tt) and centrifuged at the same temperature to collect the coacervate (usually over 37°C), then cooled below the Tt to solubilize the product in cold buffer, followed by cold centrifugation to remove insoluble cellular debris. This purification technique is simple, convenient and produces a high yield surpassing the complexity of current chromatographic techniques used to isolate other recombinant proteins, such as collagen [173,223]. ELPs/ELRs can be used by themselves to form scaffolds through methods such as coacervation, physical crosslinking, chemical crosslinking and enzymatic crosslinking [173,229], or can be incorporated into other scaffolds to enhance regeneration [226], or even used as exogenous solutions to promote elastin synthesis in burns and surgical scars [79].

III.I.III. 'In house' elastin-like polypeptide (ELP)

Recently, in our lab, an elastin-like polypeptide (ELP) was designed to present a similar structure to tropoelastin and obtained by recombinant techniques with high efficiency. Contrary to tropoelastin, the hydrophobic and crosslinking domains are built of the same amino acid units. The motifs present in native tropoelastin; VGVAPG and VGVLPG were used for the hydrophobic domains, while the motif AAAKAAAKAAK for the reticulation domains (Figure 17). Moreover, it possesses in its structure the domain 36 of human tropoelastin which is implicated in the assembly of elastic fibers. Kozel *et al*. demonstrated that the ability of tropoelastin to self-assemble and develop fibers is dramatically reduced if the disulfide bond in the domain 36 is disrupted [75]. Moreover, Lorion *et al*. demonstrated that the presence of the hydrophobic domains and the GRKRK motif in the domain 36, in the ELP, were able to interact with the two major receptors of the native tropoelastin, EBP and $\alpha_v\beta_3$ integrin [32]. When the ELP binds to the EBP, it induces a stimulating effect in fibroblasts proliferation and showed the capability to be incorporated into neosynthesized elastic fibers *in vitro* [32]. In addition, surfaces coated with the ELP showed an increase in cellular adhesion which could be slightly inhibited in the presence of L-lactose or anti-$\alpha_v\beta_3$ integrin antibody, further confirming the contribution of VGVAPG/VGVLPG and GRKRK motif in the biological activity of ELP, respectively [32].

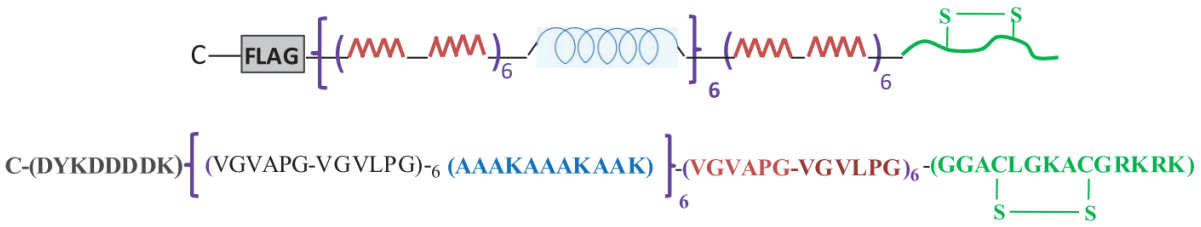

Figure 17. Structure of Elastin-like peptide developed in the laboratory. *The ELP has a FLAG tag (DYKDDDDK) right after N-terminal extremity, follow by repeated hydrophobic (VGVAPG-VGVLPG) and reticulation domains (AAAKAAAKAAK).D is for Asp, Y for tyrosine, K for Lysine, A is for Alanine, L for Leucine, P for Proline, L for lysine, V for Valine, C for Cysteine and G for Glycine. (Obtained from Lorion et al.,* [32]*)*

The ELP also presents similar physico-chemical properties to the native tropoelastin, such as its thermo-reversible transition. Under 33°C ELP is soluble in an aqueous solution, when temperature is increased over Tt, the protein forms aggregates until reaching a maximal diameter at 60°C. Once the temperature is

decreased the ELP returns to a soluble phase. ELP can form self-assembly aggregates *in vitro* in a similar manner to tropoelastin, from small spheres to filaments with a pearl-like structure (Figure 18). Moreover, once reticulated with genipin, a vegetable lysine crosslinker, to form a polymeric network, the resulting mechanical properties of the polymer showed a highly elastic behavior [32]. While possessing interesting elastic properties, the resulting crosslinked material showed excessive stiffness (1.5 MPa). Therefore, this ELP has not yet been assessed for skin engineering applications, however, its interesting properties could be beneficial when designing a scaffold for this application.

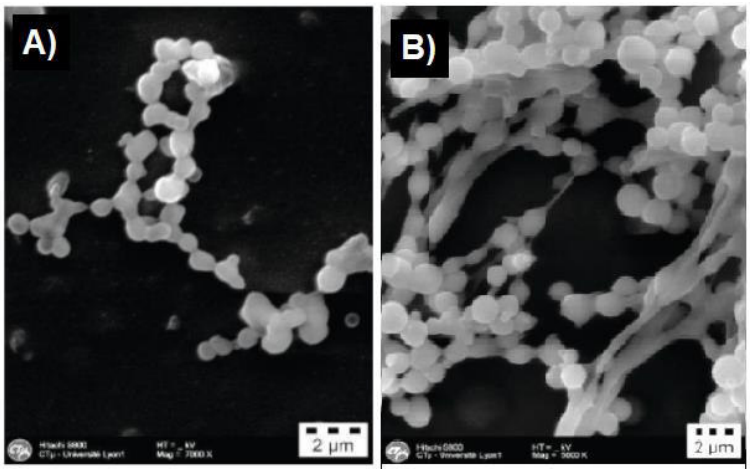

Figure 18. SEM images of ELP coacervates and reticulated with genepin. *A) SEM structure of coacervates form ELP auto-assembly B) SEM structure of ELP reticulated with genipin. (Modified from Lorion et al.,* [32]*)*

II.V. Key points in designing a scaffold for skin tissue-engineering applications.

Depending of the target tissue and applications, different key points need to be considered during the development of a novel scaffold. Generally, full-thickness skin equivalent for tissue replacement applications must above all provide a physical barrier against external agents, loss of fluids and heat [41]. This physical barrier is obtained from an adequate differentiated epidermis morphology, appropriate protein expression, similar lipid contents and lipid-lamellar structures as those of human skin [37]. The epidermal compartment must be securely attached to the dermis at the wound bed without causing any immune reaction that might result in excessive inflammation and material rejection [15]. The scaffold must favor an active vascularization of the dermal equivalent; without a

well-vascularized dermal wound bed survival of the epidermal layer is limited [108]. Likewise, the mechanical and physical properties of the scaffold should be considered to mimic those of the skin, without neglecting its elasticity [79]. Eventually, the ideal tissue engineering skin replacement for clinical use must be able to support a complete reconstruction of the skin without the formation of scar, loss of functionality or lack of aesthetics. Biodegradation is of high importance, in clinical applications all synthetic materials must eventually be discarded or replaced by alive cells and their native ECM. In principle, degradation should match the remodeling of the new tissue and the derived degradation fragments should not cause immune response or have a cytotoxic effect to the neighboring tissues [15]. Furthermore, to assure market success it must be cost-effective, easily available, user-friendly and have a long shelf life [40].

The design criteria for full-thickness skin equivalents intended as *in vitro* models is less demanding. For instance, less biodegradable materials are competent to develop *in vitro* toxicity studies [230]. In general, the scaffold should be fit for purpose. That is, they should allow skin cells to form an epithelium, to communicate with each other and to mimic as far as possible the responses of normal skin cells when exposed to a range of chemical, pharmacological, or biological agents. For this, they need to be sufficiently predictable and reproducible to allow interpretations which will unequivocally answer to a specific question. One great advantage of skin equivalents is that the cellular compositions and experimental parameters are in complete control of the operator. Consequently controlling one question at a time, contrary to the complexity of animal models, where *in vivo* situations impede the discrimination between different factors [231].

Materials and Methods

I. Production of DGL/PEG hydrogels

In general, all chemicals were purchased from Sigma-Aldrich (Saint-Quentin-Fallavier, France) unless stated otherwise. The poly(L-lysine) dendrigrafts of third generation (DGL-G3, 22000 g/mol) were bought from COLOCOM (Montpellier, France). The elastin-like polypeptide (ELP) was produced and provided by the LBTI laboratory. In general, hydrogels were prepared at 4°C by adding the desired concentration of O,O'-Bis[2-(N-Succinimidyl-succinylamino)ethyl]polyethylene glycol (PEG-NHS, 2,000) dissolved in DMF to a solution of DGL-G3 in Phosphate-buffered saline (PBS) with or without ELP. Stock solutions of DGL-G3 and PEG were performed using a 5 ml volumetric flask to avoid miscalculation due to volumetric expansion and stocked at -20°C. More detailed information on hydrogel production will be presented below.

I.I. Dense hydrogels discs

Dense hydrogel discs were prepared by adding the components (previously chilled on ice) to a final volume of 800 µl in 2 ml conic tubes (Maxymum Recovery Axygen) and vortexed for a complete homogenization. To reach high concentration hydrogels, which usually have a crosslinking time lower than 10 seconds, preparation took place in a cold room (4°C) to slow down the chemical reaction. To ease the hydrogel retrieval after crosslinking, the conical part of the tube was cut-off then the tube was immersed in ethanol for 5 min. The resulting cylindrical hydrogels were rehydrated in PBS, then sectioned at a 2 mm thickness using a vibratome (7550 Integraslice) at a frequency of 60 Hz, a 1 mm amplitude and at a slow blade speed (0.15-0.22 mm/s). Finally, hydrogel discs were stored in PBS at 4°C before use.

I.II. Hydrogel-coated coverslips

To prepared hydrogel-coated coverslips hydrophobic glass slides were required. Prior to hydrogel crosslinking, standard glass slides were hydrophobically coated using a method consisting in slow dipping the glass slides in dichlorodimethylsilane (Sigma-Aldrich) followed by overnight evaporation under a fume-hood. Finally, discs were washed by a single immersion in distilled water to eliminate the silane residues. 100 µL of hydrogel were prepared by mixing all the

required components (previously chilled on ice) then 60 µl of the obtained mixture were placed between a hydrophobic glass slide and a round coverslip (15 mm in diameter), as shown in Figure 19. After crosslinking, the hydrogel-coated coverslip was gently removed, placed in a 24 well plate and hydrated with PBS. Finally, the hydrogels were sterilized with 70% ethanol incubation overnight at 4°C, washed three times for 30 minutes with sterile PBS, and kept at 4 °C prior use. In the case of highly concentrated hydrogels (crosslinking speed lower than 10 seconds), the process was performed in a cold room to slow down the crosslinking speed and obtain a homogeneous hydrogel.

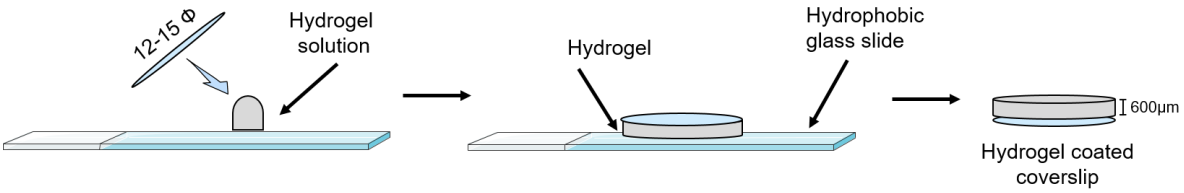

Figure 19. Representative scheme of the process to obtain a hydrogel-coated coverslip.

I.III. Porous hydrogels

Hydrogels were made porous with particulate leaching technique using paraffin microspheres as porogens, similarly to Ma *et al*. with certain modifications [232].

i) Paraffin microsphere production and characterization

Paraffin microspheres of different sizes were prepared by pouring 10 mg of melted paraffin (Histolab products AB) into 250 ml of a solution of 0.5% PVA (Sigma-Aldrich), while under high agitation (1000 rpm) at 80°C to create an emulsion. After 20 min of agitation, the mixture was transferred to a container with twice the volume of distilled water at 0°C. Microspheres were formed directly after contact with the freezing water. Then, the microspheres were sieved under vacuum with metal sieves of 50, 100 and 180 µm (Verrerie Villeurbanaise) as shown in Figure 20. Microsphere fractions were washed with distilled water, freeze dried (Freeze dryer Cosmos-80, Cryotec) and conserved at 4°C.

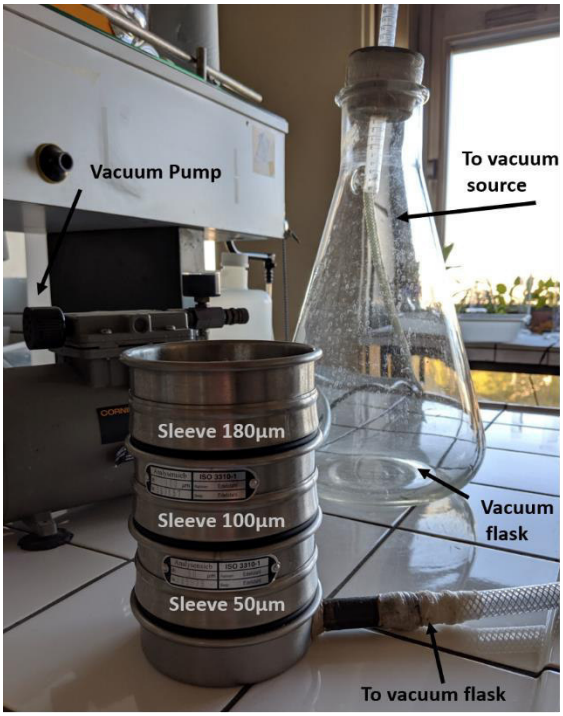

Figure 20. Vacuum filtration system for paraffin microspheres sieving

The size distribution of 5 different batches of paraffin microspheres was determined to confirm porogens size distribution. To perform the microscopical analysis, a drop of freeze-dried microspheres dispersed in 70% ethanol solution was placed on a glass slide. Six pictures of each size fraction were taken with a microscope (Leica Laborlux S) and particle size distribution was determined by image processing as shown Figure 21.

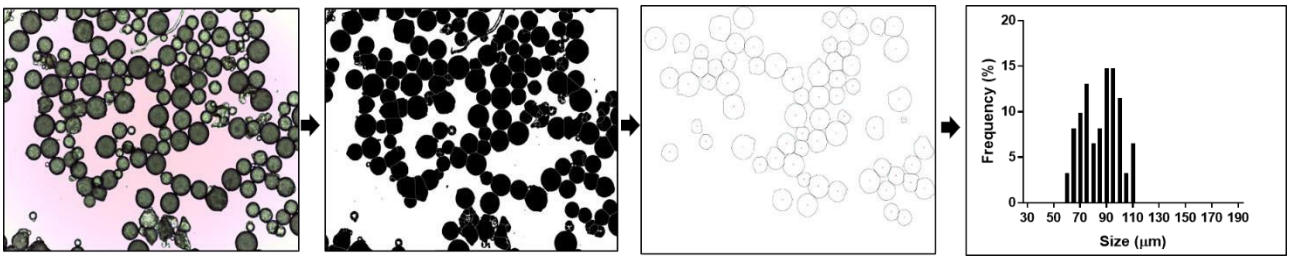

Figure 21. Image analysis processing for size distribution determination.

ii) Porous hydrogel by particulate leaching technique

To prepare porous hydrogels, 400 mg of paraffin microspheres were placed in 2 ml microtubes (Maxymum Recovery Axygen). The paraffin was compacted by centrifugation using a small table centrifuge (2000 g). To obtain a flat surface the tube was centrifuged twice, once of each side for 10 seconds. The hydrogel components, chilled on ice, were mixed by vortex and rapidly transferred to the

paraffin-containing microtubes, which were subsequently centrifuged at 2000 g for 10 seconds and placed on ice. In the case of highly concentrated hydrogels, the process was performed in a cold room to slow down the crosslinking speed and obtain a homogeneous hydrogel. Resulting hydrogels were retrieved from the microtubes by placing them in boiling ethanol under reflux for 40 minutes to extract part of the paraffin. The hydrogels were then cut into 2 mm thick discs with a vibratome (7550 Integraslice) with a frequency of 60 Hz, a 1 mm amplitude and at a slow blade speed (0.15-0.22 mm/s). The remaining paraffin was removed by immersing the hydrogels in fresh boiling ethanol under reflux for 40 minutes. This operation was repeated several times until complete extraction of the paraffin. To determine if all the paraffin was successfully removed, porous hydrogel discs were placed in distilled water and their transparency assessed. If paraffin remained, the hydrogels were subjected to another ethanol extraction as shown in Figure 22. Samples were then rehydrated and stored in PBS at 4°C. Hydrogel discs used for *in vitro* experiments were sterilized with 70% ethanol overnight and washed three times for one hour with PBS prior use.

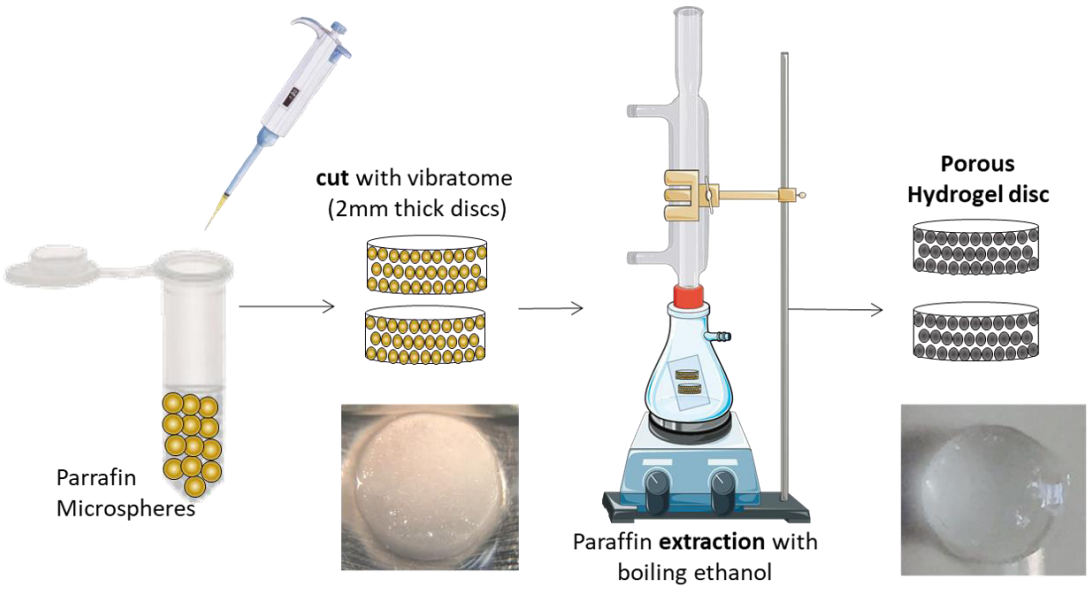

Figure 22. Hydrogel production and paraffin extraction process.

II. Production of 'in-house' elastin-like polypeptide

The 'in-house' elastin like polypeptide (ELP) was obtained by recombinant protein production. The ELP DNA coding sequence was cloned with Flag tag fusion protein using the pET30a vector backbone. BL21(DE3) *E.Coli* strain was transformed with pET30a-Flag-ELP plasmid. Single colonies were isolated on Luria-

Bertani (LB) agar medium supplemented with 50 µg/ml kenamycine (Sigma-Aldrich) and incubated at 37°C overnight. Then, 200 ml of Terrific Broth supplemented with 50 µg/ml kanamycin were inoculated with one colony and incubated at 37°C overnight while shaking (150 rpm). In a bioreactor (Minifors II, INFORS), a total of 4 L of Teriffic Broth were inoculated with preculture at DO=0,1. Bacteria were grown to log phase DO=1, in the presence of kanamycine, 1 mM trace elements and glycerol (10g/L) at 37°C under agitation at 400 rpm and 20% pO_2. The temperature of culture was decreased to 25°C and expression was induced with 1 mM IPTG for 16 hours under agitation from 400 rpm to 800 rpm at 20% pO_2, to avoid foam formation 500 µl of anti-foam was added. For the NMR experiments, ^{13}C-^{15}N-labeled ELP was prepared using M9 minimal medium containing $^{15}NH_4Cl$ and ^{13}C-glucose.

For purification, culture was harvested and centrifuged at 5000 g for 20 minutes, bacteria was resuspended in 400 ml of ultrapure water and lysed by pressure cell disruption at 2600 bar (Cell Disruption System, Constant System Ltd). The lysate was harvest, buffered with 20 mM Tris-HCl pH8,8 and centrifuge at 10000 g for 20 min. The supernatant was treated with 0,2% Polyethylene-imine (PEI) (Sigma-Aldrich) on ice, PEI was slowly added drop by drop under soft agitation and then centrifuged for 20 minutes at 10000g and 4°C to eliminate precipitated contaminants. After eliminating contaminants, 500 mM of NaCl were added to the supernatant, incubated for 10 min at 40°C and finally centrifuged for 10 minutes at 10000g and 40°C. The pellet was re-suspended in PBS overnight at 4°C and centrifuge at 5000g for 10 minutes at 4°C. Finally, the supernatant was freeze dried (freeze dryer Cosmos-80, Cryotec) and stored at -20°C before use. Stock solutions of ELP were prepared by suspending the dry protein in PBS to a maximal concentration of 10 mg/ml.

III. Characterization of dense DGL/PEG hydrogel

III.I. Crosslinking speed

To measure the crosslinking speed of hydrogels of different ratios of DGL/PEG (mM), hydrogel components previously chilled on ice, were added to a small glass vial (8x25x35 mm) to a final volume of 50 µl. The mixture was placed under agitation (300 rpm) with a small magnetic rod (5 mm) and placed at exactly

4 cm from the magnetic stirrer, as shown in Figure 23. Crosslinking time was defined, in our study, as the time needed to halt the magnetic rod after adding the last component of the hydrogel formulation (PEG-NHS). At least three hydrogels were measured for each condition.

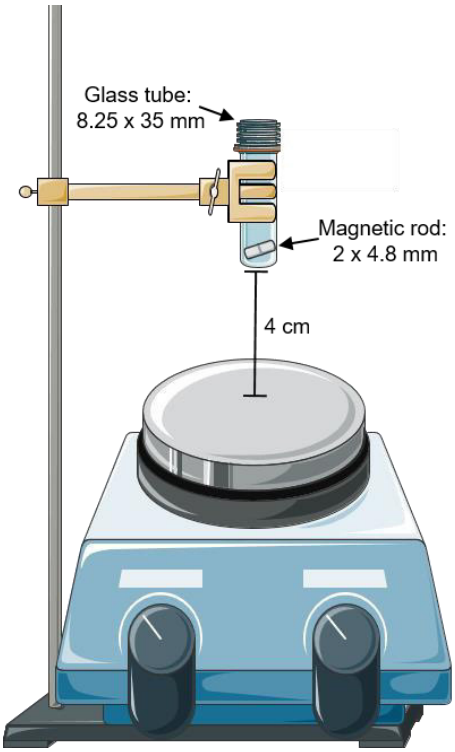

Figure 23. Representative schema to measure crosslinking speed.

III.II. Swelling ratio

The swelling ratio (Qs) of 2mm-thick dense hydrogel discs was determined in PBS at 37 °C, to mimic the physiological conditions. Prior incubation in PBS, samples were frozen in liquid nitrogen and freeze dried (freeze dryer Cosmos-80, Cryotec) to measure their dry weight (Wi). Samples were blotted before each weight measurement, performed at 1, 2, 6 and 24 hours. The swelling ratio was defined as ((Ws-Wi)/Wi), where Ws is the weight of swollen hydrogel and Wi is its initial dry weight after freeze drying. Five hydrogels were measured for each condition.

III.III. Mechanical properties

i) Micro-indentation

a) Principle

During indentation tests, a spherical indenter will apply an axial force to the surface of the material followed by a cycle of load and unloading, the sensor measure the displacement executed by the indenter for a given force (Figure 24.A). Indentation allows to determine the reduce Young's modulus of a material from the measurements of normal contact stiffness, k_z, which is the slope of the initial part of the unloading curve. For completely elastic materials the loading and unloading curve follow the same path and are therefore in distinguishable from one another. For viscoelastic materials, a difference between the loading and unloading curve is observed (Figure 24.B). This variation between the curves is related to the dissipation characteristics of a viscoelastic material.

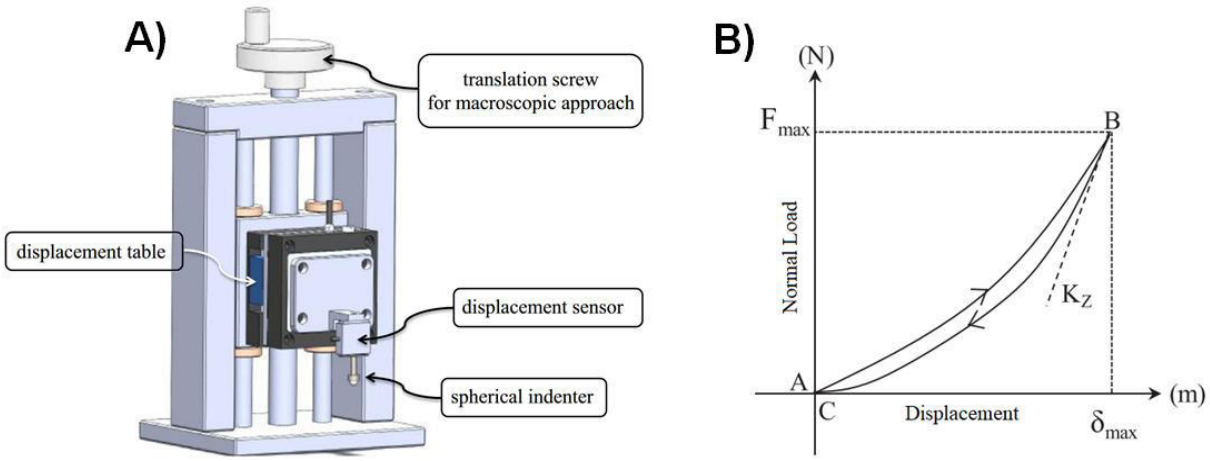

Figure 24. Micro-indentation set up and curves of a viscoelastic material.
A) Representative schema of an experimental micro-indenter B) Indentation curve obtained from a viscoelastic material. A indicated the starting contact point, B represents the maximum load applied (F_{max}) for a maximum displacement (δ_{max}). Loading curve from A-B and unloading curve B-C reflect the mechanical behavior of the material. (Obtained from C. Pailler-Mattei et al., [233]*)*

b) Protocol

For indentation tests under normal load, a spherical steel probe of radius curvature r=1.59 mm was used with a maximal load of 4 mN and a velocity of 20 µm/s. During each test one cycle of load was applied to the sample and the test was repeated 3 times in different points of each dense hydrogel disc (2x9.1 mm). The tests were not performed under submersion, meaning that there could be mild

effect of adherence of the hydrogel to the probe. The indentation curves were recorded on real time with LabVIEW (National Instruments, TX, USA). Resulting load data were analyzed to determine the complex modulus.

ii) Dynamical mechanical analysis

a) Principle

Similarly, dynamic mechanical analysis (DMA) allows to measure the viscoelastic properties of materials (Figure 25.A). The modulus of elasticity of a polymer can change in function of temperature, time and frequency of the dynamic forced applied. Therefore, DMA is capable of evaluating the viscoelastic properties during a controlled temperature and/or frequency. Samples will be subjected to a sinusoidal force (Stress σ), which in response will produce another sinusoidal deformation curve (strain ε), as shown in Figure 25.B. The shift between these two curves will be dependent of the viscoelastic behavior of the material. In this manner, the DMA can measure the stiffness and damping of a material. How much the sinusoidal wave will be deformed will be related to its stiffness, which is composed of the storage modulus and the loss modulus. The storage modulus (E') is the material's elastic behavior while the loss modulus (E'') corresponds to its viscous response. Damping or tan delta depends on how well the materials can get rid of the energy absorbed measuring the dissipation of energy and is determined by the ratio between the loss and storage modulus (E"/E').

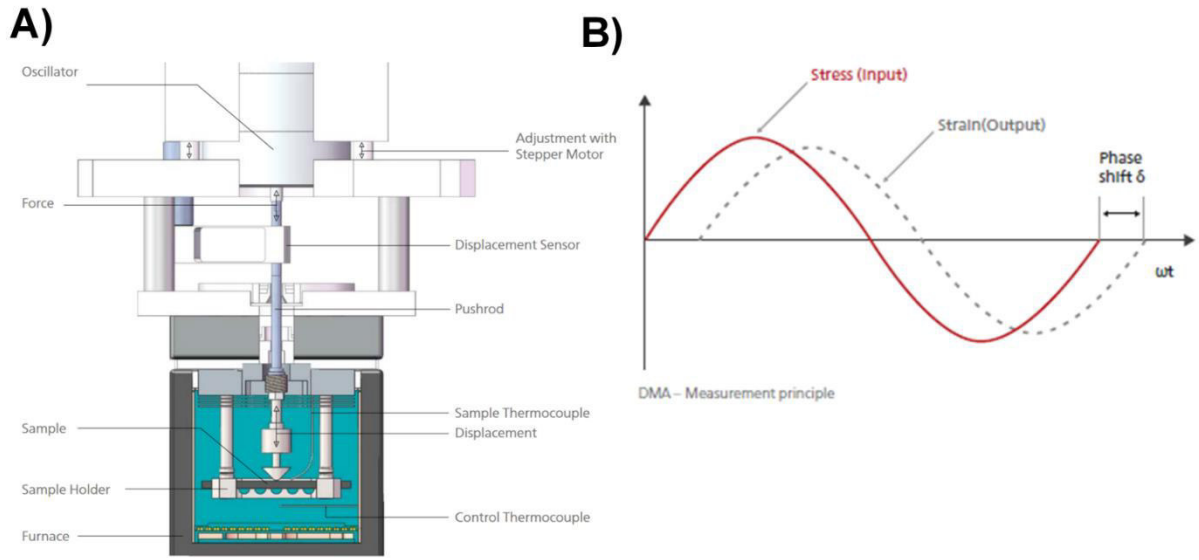

Figure 25. Dynamical mechanical analyzer system and curves. *A) Representatives schema of DMA experimental system. B) Representation Schema of sinusoidal curves detected by a DMA.*

b) Protocol

The mechanical properties of dense DGL/PEG hydrogel discs (2x9.1 mm) of different compositions were analyzed by cyclic compression with a dynamic mechanical analyzer (DMA 242 E Artemis, NEZSTCH). The hydrogels domain of linearity was first determined with a strain sweep and compression test performed in PBS immersion at room temperature. Samples were then subjected to compression at a 10% strain and an amplitude of 60 µm, with increasing frequencies (1-20 Hz) in PBS immersion and at room temperature. At least 5 hydrogel discs were measured for each condition.

III.IV. Hydrogel degradation

Hydrogel degradation was determined by monitoring the hydrogels mass loss through time under acidic, neutral and basic conditions. Hydrogel degradation profile on neutral conditions can allow an estimation of self-life. Dense hydrogel demi-disc (2x9.1 mm) were freeze dried (freeze dryer, Virtis 10-020) to determine their initial dry weight (Wi) and placed in citrate buffer (pH 5), PBS (pH 7) or sodium carbonate buffer (pH 10) at 37°C. Buffer was refreshed every two days under sterile conditions and samples were retrieved after 27 and 52 days, rinsed three times in pure water, freeze dried and weighed (Wd) using an analytical grade scale. Three hydrogels were measured for each condition. Degradation was expressed as a percentage of weight loss in relation to the initial weight, determined as:

$$\%\, weight\ loss = \frac{(W_i - W_d)}{W_d}\ X\ 100$$

IV. Effect of ELP incorporation in hydrogel properties

IV.I. Wettability/hydrophobicity

a) Principle

Measuring the contact angle by gionometry is a simple and well-known method to determine the wettability of the surface of a solid material. The contact angle is defined as the angle formed by the intersection of the liquid-solid interphase and the liquid-vapor interphase. The interphase where the solid, liquid and vapor co-exist is known as the "three-phase contact line", therefore the

contact angle will be defined as the angle at the equilibrium of these three phases. As shown in Figure 26, small contact angles (<90°) correspond to a high wettability, while larger contact angles (>90°) correspond to low wettability. When the wettability of a drop of water to a surface is determined we can also talk of the hydrophobicity of the material.

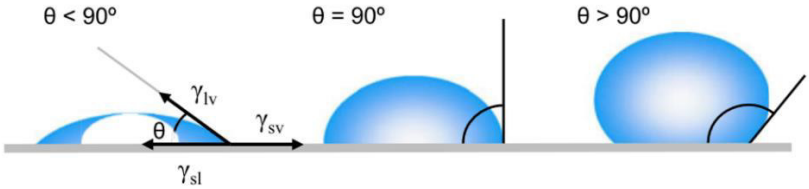

Figure 26. Illustration of contact angles formed smooth solid surface. *(Obtained of Yuan, Y. et al,* [234]*)*

b) Protocol

To measure the increase of hydrophobicity when ELP is incorporated into the hydrogels, the contact angle of a drop of distilled water placed on top of a hydrogel-coated coverslip was determined. As shown in Figure 27, hydrogels with or without ELP were placed in an elevated support in front of direct lighting. To be able to observe the contact angle, the camera with a macroscopic lens was placed looking over the sample with a slight inclination. Before placing 10 µl of distilled water, the excess liquid on the hydrogel was removed with a tissue paper. Three measurements were performed to each sample and at least 3 hydrogels per condition were measured. After image acquisition, the contact angle was determined by images analysis with Imagej plugging for drop analysis "LB-ADSA".

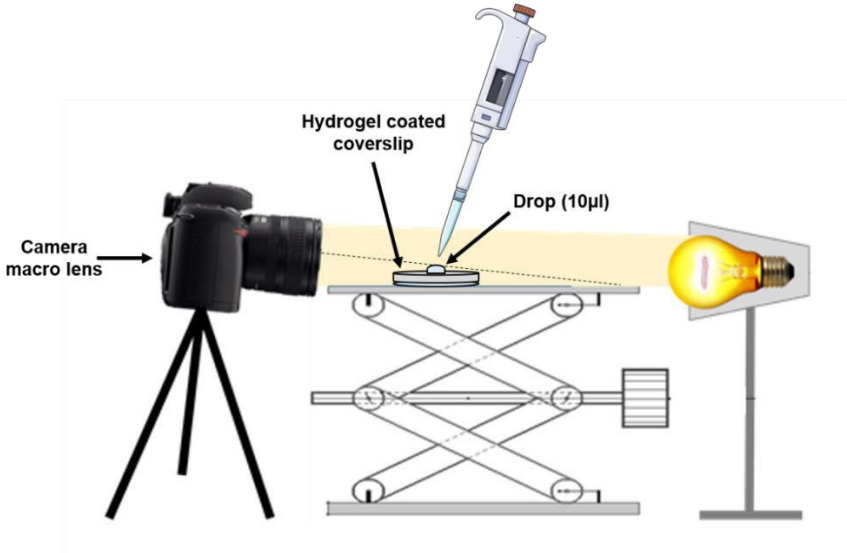

Figure 27. Graphical representation of the experimental set up to measure contact angle. *(Modified from N. Costanie and M. Dzikowski)*

IV.II. NMR spectroscopy

a) Principle

The use of NMR spectroscopy and solid-state NMR in particular, have recently greatly contributed to the characterization of polymer hydrogels as it allows to obtain detailed information on their morphology, molecular organization and intermolecular interactions. Variations of chemical shifts, spin relaxation times or intensity of the NMR signal can be used to obtain information on the nature or the intermolecular interactions [235]. During NMR spectroscopy, samples are subjected to a powerful magnetic field that will have an impact on the nuclei, producing an electromagnetic signal with a characteristic frequency depending on the different magnetic shielding caused by the surrounding electrons. This phenomenon is known as the chemical shift. Since the chemical shift of a nucleus is determined by the electron density surrounding it, if a new covalent bond is formed the electron density surrounding a specific nucleus will change, leading to a chemical shift perturbation [236]. Therefore, this technique allows to determine when covalent bonds are formed between two substances.

b) Protocol

Solid-state NMR experiments were recorded on ELP when incorporated into DGL/PEG hydrogel in order to detect whether the protein interacts covalently with the polymeric network of the hydrogel. About 40 µl of samples were loaded in 3.2 mm rotors composed of a cylindrical Zirconia tube (Figure 28.A). The rotors were then inserted in the stator of the NMR probe, where an airflow directed on the wings allows for spinning of the rotor. The rotor was then tilted by an angle of 54.74° (magic angle, Figure 28.B) inside the NMR probe inserted in the spectrometer (Figure 28.C).

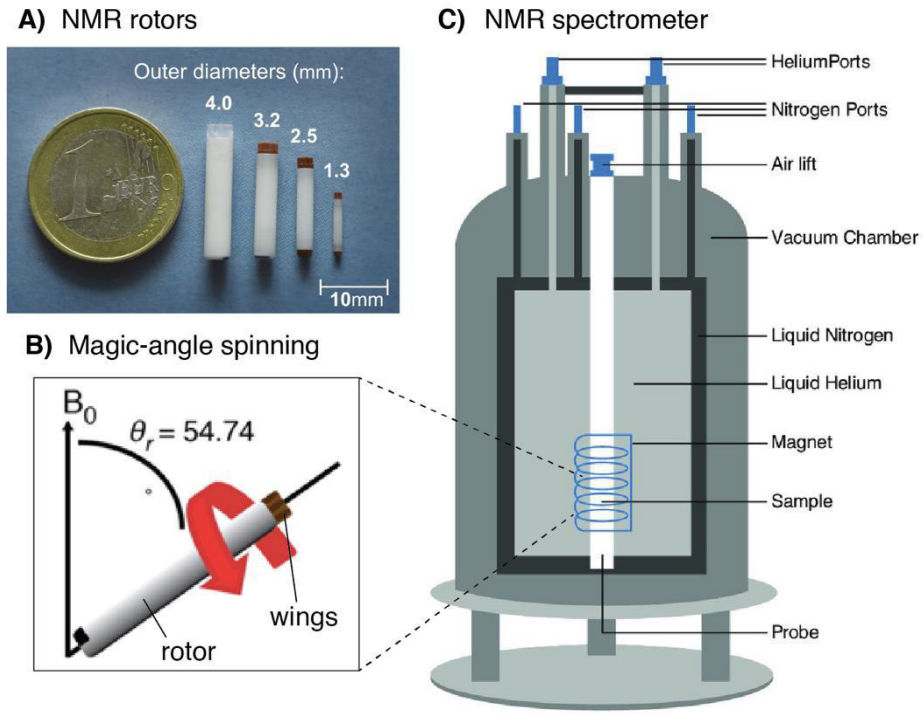

Figure 28. NMR Spectroscopy. *A) NMR rotors of different sizes. For our experiments, rotors with a diameter of 3.2 mm were used. B) Illustration of magic-angle spinning (MAS) used in solid-state NMR. B_0 represents the external magnetic field. C) Illustration showing the inside of an NMR spectrometer.*

For the free-ELP sample, 20 mg of ^{13}C-^{15}N-ELP in PBS buffer were coacervated at 40 °C for 15 minutes directly into the rotor. For the hydrogel control sample, a hydrogel composition 2 mM DGL and 19 mM PEG for a final volume of 40 µl was prepared directly into the rotor. For the ELP-hydrogel sample, hydrogel was prepared with 1.75mg of ^{13}C-^{15}N-ELP (the maximal amount of ELP that could be incorporated into a hydrogel of 1 mM DGL and 19 mM PEG with final volume of 50 µl). Another rotor of ELP-hydrogel was prepared to assess reproducibility.

All NMR experiments were conducted using a 3.2 mm triple-resonance (^{1}H-^{13}C-^{15}N) probe head at a magnetic field of 18.8 T corresponding to 800 MHz proton resonance frequency (Bruker Avance II). The MAS frequency was set to 17.5 kHz and the VT gas temperature to 278 K, corresponding to a sample temperature of around 25 °C. Two-dimensional HC-INEPT (Insensitive nuclei enhanced by polarization transfer) spectra [237] were recorded on all the samples and referenced using Sodium trimethylsilylpropanesulfonate (DSS). The J-coupling evolution delay for the INEPT step was set to $1/(4*J_{coupling})$, with a scalar J coupling set to 200 Hz. Experimental parameters are detailed in Table 6. Spectra were

processed using TopSpin 3.2 (Bruker Biospin) and spectra analysis was done with the CcpNmr Analysis package [238].

Table 6. NMR parameters of 2D INEPT spectra recorded on ELP and hydrogel samples.

Sample	**ELP**	**Hydrogel**	**ELP-hydrogel**
Experiment	**2D INEPT HC**	**2D INEPT HC**	**2D INEPT HC**
MAS frequency / kHz	17.5	17.5	17.5
Field / MHz	800	800	800
t1 increments (^{1}H)	350	256	350
Spectral width (t1) / ppm	9	9	9
Acquisition time (t1) / ms	24.3	17.8	24.3
t2 increments (^{13}C)	2802	2802	2802
Spectral width (t2) / ppm	466	466	466
Acquisition time (t2) / ms	15	15	15
Carrier ^{1}H / ppm	4.7	4.7	4.7
Carrier ^{13}C / ppm	100	100	100
Interscan delay / s	2	2	2
Number of scans	48	48	48
Experiment time	9h30	7h	9h30

IV.III. ELP embedding in the hydrogel

The release of ELP from the hydrogel after 24 hours was determined by western blot. 40 µl hydrogels containing 6 mg/ml of ELP were prepared directly in a 48 well plate. After 15 minutes, 300 µl of PBS were added and samples were incubated at 37°C for 24 hours. After incubation, 100µl of supernatant were harvested and stored at -20°C. The same quantity of ELP in PBS was used as controls and subjected to the same incubation times. To detect the ELP by western blot, 25 µl of the previously recovered supernatants were loaded into a pre-cast SDS-PAGE gel for migration (Bio-rad) with Laemli 5X buffer. After migration, transfer was performed on a PVDF membrane (Bio-Rad) with the Trans-blot turbo transfer system (Bio-rad). Blots were blocked with 5% non-fat milk in TBS + 0.05% Tween 20 (TBST) for 1 hour and then incubated with monoclonal Anti-Flag Antibody (1:3000 mouse F7425, Sigma-Aldrich) in TBST for at least 1 hour. Blots were washed three times with TBST and incubated with 1:10000 anti-mouse HRP

conjugated antibody (goat anti mouse 1706516, Bio-rad) in TBST for 1 h. Blots were again washed three times with TBST. HRP conjugates were detected with SuperSignal West Pico chemiluminescent substrate (Pierce) and blots were imaged with CCD Camera (Fusion Fx7, Vilber Lourmat).

V. Characterization of porous DGL/PEG hydrogel

V.I. Porosity with liquid displacement technique

Porous hydrogel porosity was measured using a standard fluid replacement method and a pycnometer as shown in Figure 29. PBS was used as the displacement liquid to avoid swelling or shrinkage since the hydrogels were prepared in PBS. Moreover, PBS mimics the physiological *in vivo* osmotic environment that the samples will be subjected when used in biological applications. Before use, samples were immersed in PBS for at least 2 hours to reach equilibrium. The total mass of the pycnometer (10.244ml) filled with PBS was measured using an analytical grade scale (m_1). Each swollen sample was then immersed in the pycnometer and subjected to three vacuum cycles to remove any trapped air bubbles. The pycnometer was then refilled with PBS and the total mass determined (m_2). The sample was subsequently carefully removed and the mass of the pycnometer with the remaining liquid measured (m_3). Finally, the porous hydrogel sample was quickly rinsed three times with distilled water, blotted for excess water, freeze dried (Freeze dryer, Virtis 10-020) and the dry weight measured (m_d) (Figure 29). The porosity (ε) was determined as follows:

$$\varepsilon = \frac{\boldsymbol{V_p}}{\boldsymbol{V_p + V_s}} = \frac{(\boldsymbol{m_2 - m_3 + m_s})}{\boldsymbol{m_1 - m_3}}$$

Where, V_s is the total volume of the scaffold represented by the mass of the displaced liquid by $(m_1\text{-}m_2\text{+}m_s)/\rho_{PBS}$, while the volume filling the pores of the samples (V_p) is $(m_2\text{-}m_3\text{+}m_s)/\rho_{PBS,}$ (density of the displaced liquid is represented by ρ_{PBS}). To determine the mass of the hydrogel without any liquid entrapped in the pores, the swollen mass (m_s) was calculated using the swelling ratio previously determined from the dense hydrogels since $Qs=(m_s\text{-}m_d)/m_d$.

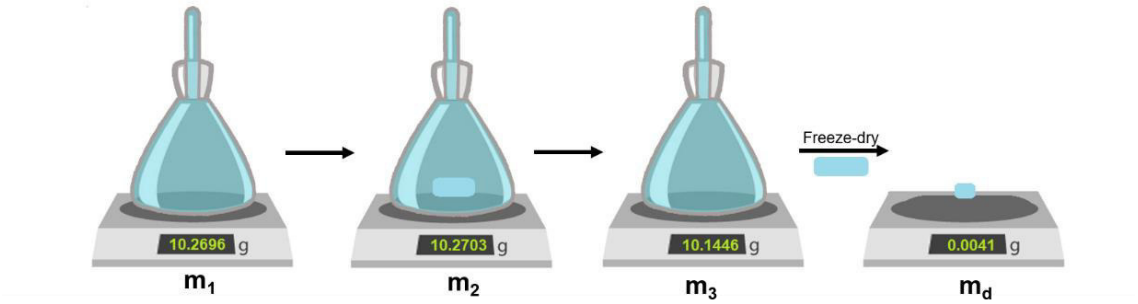

Figure 29. Representative schema of the standard liquid displacement method. *Pycnometer of 10.244ml*

V.II. Hydrogel structure by ESEM

Environmental scanning electron microscopy (ESEM) is a unique system in which wet materials can be examined with an electron beam in a chamber with pressure allowing water vapor without additional sample preparations. The surface morphology of porous hydrogels in its swollen state was observed by ESEM (FEI Quanta 250 FEG) at 10 kV and 3 torrs.

VI. Two-dimensional *in vitro* evaluations

VI.I. Cell culture

i) Human dermal fibroblasts

Normal human dermal fibroblasts (NHDF) isolated from foreskin (male/ Caucasian/ donor age <5) were obtained from Promocell (Heidelberg, Germany). Cells were stored in liquid nitrogen and thawed when needed. Cell culture from frozen stocks was performed by quickly thawing the cells and adding 10 times the volume of Dubecco's Modified Eagle Medium/Ham's F12 (DMEM-F12) 1:1 Glutamax (Life Technologies) supplemented with 10% Fetal bovine serum (FBS) (Life Technologies), 100U/ml penicillin/0.1mg/ml streptomycin (s/p) (Sigma-Aldrich). Cells were centrifuged at 1000 rpm at 4°C for 5 min and the cell pellet re-suspended in supplemented DMEM-12 at 37°C. For amplification, cells were seeded at a density of $1x10^4/cm_2$ in tissue culture flasks, with supplemented DMEM-12 and incubated at 37°C and 5% CO_2. When cells reached 70% confluence, they were once again amplified. Cell flasks were washed three times with sterile PBS

and then incubated with 60 µl/cm^2 Trypsin-EDTA 0.05% (Sigma-Aldrich) for 5 to 7 min at 37°C and 5% CO_2. Trypsin was inhibited with twice the volume of supplemented DMEM-12 with 10% FBS and detached cells were counted on a Malassez cell and trypan blue (1:1) (Sigma Aldrich), centrifuged for 5 min at 1000 rpm and re-suspended in the suitable volume of supplemented DMEM-F12 to achieve a density of 1x10^4/cm^2, which was re-plated on tissue multi-well culture plates.

ii) Human nasal chondrocytes

Primary cultures of human nasal chondrocytes were obtained from healthy septal cartilages of donors undergoing rhinoplasty. Nasal cartilage samples were collected upon written informed consent of donors and complied with local ethics guidelines, national and European Union legislation regarding human sample collection, manipulation, and personal data protection (Ethics Committee for research with human samples, CODECOH: DC-2014-2325). For chondrocytes extraction, septal cartilages were washed with PBS supplemented with 50 µg/mL streptomycin (Panpharma) then cut in small slices and digested overnight at 37°C with 0.5 mg/mL bacterial collagenase A (Roche Applied Science) in culture medium composed of DMEM-F12. Chondrocytes were then seeded on hydrogels at a density of 1.5x10^4 cells/cm^2 in culture medium supplemented with 50 µg/mL streptomycin and 10% FBS. At this stage, cells were designated at passage 0 (P0).

VI.II. Live/Dead assay

Hydrogel cytocompatibility was evaluated with live/dead assay on hydrogels of various compositions. For nasal chondrocyte studies live/dead assay was performed after 3 and 7 days of culture on the surface of dense hydrogel discs (1 mm thickness). For dermal fibroblast viability, live/dead assay was performed after 1 and 3 days of culture on fibroblasts seeded on top of hydrogels-coated coverslips (0.6 µm thickness). Cells were incubated 30 min with a solution with 6 µm propidium iodide (Sigma-Aldrich) and 1 µm Calcein (Invitrogen) in supplemented DMEM-12 medium and subsequently observed with a fluorescence microscope (Nikon TiE). The percentage of viable cells compared to the total amount of cell was calculated by image analysis (Imagej).

VI.III. Morphology evaluation

The effect of hydrogel composition on cell morphology was evaluated by phase contrast microscopy and by actin staining. Nasal human chondrocytes or dermal human fibroblasts at a density of 10,000 cell/cm^2 were seeded either in the surface of dense hydrogel discs (1 mm thickness) or hydrogel-coated coverslips and incubated at 37°C and 5% CO_2, respectively.

i) Phase-contrast microscopy

Phase-contrast microscopy pictures (Nikon TiE) were acquired after 24 and 72 hours of culture. Before acquisition, medium was refreshed to remove non-adherent cells. To compare cell morphologies; cell spreading area, circularity and Feret diameter were determined by image analysis (Imagej). Five phase contrast fields of view were analyzed of ten hydrogels after 24 hours and five after 72 hours per composition. Control were only analyzed after 24 hours since after 72 hours images analysis were not possible due to cell confluence.

ii) Actin staining

Actin cytoskeleton was stained with fluorescent dye-coupled phalloidin after 1, 3 and 8 days of culture for dermal human fibroblasts and after 7 days for nasal human chondrocytes. Cells on the hydrogels were fixed with paraformaldehyde (PFA) 4% (Electron Microscopy Science) for 10 min followed by 20 min permeabilization with a 0.1% triton solution in PBS. After washing twice with PBS, the samples were incubated for 10 minutes with a 2 µg/ml 4',6-diamidino-2-phenylindole (DAPI) (Sigma Aldrich) and 2 µg/ml phalloidin (Thermo Fischer Scientific) solution in PBS to stain the cell nucleus and actin cytoskeleton, respectively. Finally, hydrogels were observed with a fluorescence microscope (Nikon TiE). Cell number for dermal human fibroblast proliferation was determined by counting cell nuclei by images analyses (Imagej) of at least 5 randomly acquired images per hydrogel, at least three hydrogels per condition.

VI.IV. Cell migration by time-lapse

Dermal human fibroblasts were seeded in the surface of hydrogel-coated coverslips at a density of 10,000 cell/cm^2 and incubated at 37°C and 5% CO_2. After

three days of cell culture cell migration was observed by time-Lapse (Zeiss AxiObserver Z1) maintaining an environment with 5% CO_2 and 37°C, and pictures were acquired every 20 minutes for 16 hours. Images obtained were analyzed using Imagej and manual tracking plugging to determine the velocity traveled by 5-8 cell per image. Migration is expressed as the mean slope of the accumulated distance travel by the fibroblasts per condition. At least two hydrogels were measured per experiment and three separate experiments were performed.

VI.V. Metabolic activity

Hydrogels with or without ELP were prepared directly in cell culture 24-well plates, sterilized overnight with 70% ethanol in PBS and wash thoughtfully before use. Cells were seeded at a density of 10,000 cells/cm^2 on top of the hydrogels and incubated at 37°C and 5% CO_2. Metabolic activity was measured after 24 hours of culture. To do so, hydrogels were incubated with DMEM-12 supplemented with 10% alamar blue for 3 hours at 37°C in an atmosphere with 5% CO^2, following the supplier's protocol (Invitrogen). After incubation, duplicates of the working solution were transferred to a 96 black well plate and measured with a fluorimeter (TECAN, Infinite M1000) excitation at 580 nm and emission 585 nm. Two hydrogels without cells were used as blank controls and four hydrogels were measured per condition.

VI.VI. Immunocytofluorescent staining of Ki67

Fibroblasts were seeded at a density of 10,000 cells/cm^2 on top of hydrogel-coated coverslips and incubated at 37°C and 5% CO_2. After 3 days of cell culture, cells were fixed with 10 min incubation of PFA 4% and permeabilized with 10 min incubation of a solution of PBS and 0.1% triton. Proliferative cells were stained with anti-Ki67 antibodies (ab15580 – 1:200) and revealed with Alexa Fluor-conjugated anti-rabbit IgG secondary antibodies (1:1000), while cells nuclei were counterstained with 1 µg/ml DAPI. Finally, hydrogels were observed with a fluorescence microscope (Nikon TiE). After image analysis, proliferation percentage was determined as the percentage of Ki67 positive cells in relation to the total amount of cell per image (>15 images per condition). Three hydrogels were measured for each condition.

VII. Three-dimensional *in vitro* evaluations

VII.I. Human keratinocytes culture

Keratinocytes used to form the stratified epidermis on the skin equivalents formed with DGL/PEG hydrogels were isolated after enzymatic treatment of child foreskin biopsies. Skin biopsies were disinfected by a 15 minutes incubation in 10% dermal betadine, subsequently washed with a solution of PBS with 5% v/v penicillin/streptomycin. The biopsies were cut in small pieces (around 0.5 cm^2) and placed in a Petri dish with the epidermis towards the top. The biopsies were incubated overnight at 4°C in 20 ml of a trypsin/dispase solution in DMEM (5 µg/ml trypsin, 2.4U/ml dispase, 2,500U/ml streptomycin and 2.5mg/ml penicillin). After incubation the epidermis could be easily detached with the help of a pincer and scalpel and incubated with 0.5% trypsin-0.02% EDTA for 20 min in a water bath at 37°C, while every 5 minutes the cellular suspension was vortexed. The cellular suspension was homogenized and filtered through a 70 µm cell filter into a 50 ml tube to avoid cell debris and cellular aggregates. Enough supplemented DMEM medium was added to complete the 50 ml and centrifuged for 15 min ate 1800 rpm. Finally, the cell pellet was resuspended in culture medium KGM2 (keratinocyte growth medium II, Promocell) supplemented with growth factors (0.06 mM $CaCl_2$ and 0.1 mg/ml primocin), keratinocytes were counted on a Malassez cell and seeded in a cell culture flask at a cell density of $3x10^4/cm^2$ supplemented with 1% FBS to improve cell adhesion. Medium was changed every two days and cell were amplified once they reached 80% of confluence. Cells were stored in liquid nitrogen and thawed when needed. Cell culture from frozen stocks was performed by quickly thawing the cells and adding 10 times the volume of KGM2 with 1% antibiotics (penicillin/streptomycin). Cells were centrifuged at 1000 rpm at 4°C for 5 min and the cell pellet re-suspended in supplemented KGM2 medium at 37°C. For amplification, cells were seeded at a density of $1x10^4/cm^2$ on tissue culture flasks, in supplemented KGM2 medium and incubated at 37°C and 5% CO_2.

VII.II. Dermal equivalent production

i) Proliferation and colonization of dermal equivalents

Sterile porous hydrogel discs (2x9 mm) were punched with a sterile puncher (n°4) to obtain a disc with 8 mm of diameter corresponding to the size of culture inserts. Hydrogels were placed in 24 well-plates culture inserts (Falcon, pore size 8 µm). To assure that the hydrogels adhered to the bottom of the insert, the remaining liquid was vacuumed from underneath the inserts and the plate was stored at 4°C before use. Before cell seeding, hydrogels were rehydrated with 200 µl of DMEM-F12, supplemented with 10% Hyclone II FBS (Fisher Scientific) and 1% antibiotics (s/p). Normal human dermal fibroblasts were seeded on the surface of the porous hydrogels at a density of $1x10^5$/hydrogel in 50 µl, hydrogels were incubated at 37°C and 5% CO_2 for two hours, then 2 ml of supplemented DMEM-12 were added. Samples were incubated at 37°C and 5% CO^2 and the medium was changed every two days using of a vacuum pump.

For proliferation studies, samples were retrieved after 7, 14 and 21 days of cell culture and fixed in 4% PFA for 30 min. Samples were embedded in OCT compound (Sakura) by successive 10-30 min baths of increasing concentrations of OCT in PBS (50%, 75%, 85% and 100%). After embedding, samples were frozen in dry ice and cross sections (12 µm) were performed every 100 µm, collected on glass slides and dipped in glacial acetone for 20 min. To evaluate cell density, infiltration and proliferation, cell nucleus was staining with 10 min incubation of 2 µg/ml DAPI (Sigma-Aldrich) solution and observed with florescence microscopy (Nikon TiE). Cell number per section was quantified with the ITCN (image-based tool for nuclei counting) plugging for ImageJ, allowing a semi-quantification of proliferation over time. To do so, the threshold was adjusted, and the following process was performed to all images: binary image creations, fill holes, convert to mask and watershed, particle analysis with limitations to 0-1000 μm^2 size and 0.2-1 of circularity. The results were normalized to the surface of each hydrogel section, resulting in fibroblasts/mm^2. Cell homogeneity was determined by comparing the variability of the number of cells on different acquisition fields (x10) of the same slide section and between different depth sections of the hydrogel and expressed as the relative frequency of cells per section.

Cell infiltration and colonization of porous DGL/PEG hydrogel in 3D was observed by staining cells nuclei with DAPI and cytoskeleton with fluorescent phalloidin. After 21 days of cell culture, colonized hydrogels were fixed with PFA 4% overnight at 4°C and afterwards stored in PBS containing 0.4% PFA. Before staining, hydrogels were washed three times with PBS and finally incubated with a solution containing 1 µg/ml DAPI and 1 µg/ml fluorescent phalloidin in PBS for 15 min protected from light. Before observation, hydrogels were once again washed with PBS three times. Cellular infiltration into the pores was observed by confocal microscopy (ZEISS, LSM 800) reaching up to 130 µm depth in the hydrogel.

To determine the optimal seeding density cell number $1x10^5$, $5x10^5$ and $10x10^5$ cells were seeded on the surface of porous hydrogels placed in cell culture inserts and retrieved after 7 and 14 days of cell culture. Cell number was determined as previously stated.

ii) Percentage of matrix contraction

The percentage of contraction suffered by the scaffolds during cell culture was determined by image analysis. DGL/PEG hydrogel with or without ELP were compared to classical collagen gels known to retract due to fibroblasts-mediated contraction when cultured in 3D, either by encapsulating the fibroblast in the collagen gel or by seeding in the cell in the surface of the collagen gel similarly to porous hydrogels. Porous DGL/PEG hydrogel production and cell seeding was performed as previously explained for all dermal equivalents. Collagen gels were prepared with type I collagen from rat tails (Gibco) with a final concentration of 2.5 mg/ml following manufacturer protocol and poured into 24 well-plates. Fibroblasts encapsulated in the collagen matrix were mixed with the gel components before jellification at a density of $2.9x10^5$ cells per gel. Fibroblasts on the surface of collagen gel were seeded at a density of $3x10^4$ cells per gel. After 12 hours of incubation at 37°C and 5% of CO_2, all collagen gels were detached from the edges of the cell culture plate to allow matrix contraction. Colonized gels were imaged right after seeding (t0) and on days 2, 4 6 and 9 of cell culture. The difference of area of the gel at each time point compared to the initial matrix (t0) was measured and expressed as the percentage of contraction.

VII.III. Skin equivalents with DGL/PEG hydrogels

Porous hydrogels of composition 2/19 DGL/PEG with a porosity made of 75% 50-100 µm and 25% 100-180 µm porogens were prepared as previously stated. Human primary keratinocytes ($2.5x10^5$ cells/hydrogel in 100 µl) were seeded on the surface of 21-day colonized hydrogels (dermal equivalents). After 2 hours, 1.5ml of proliferation medium (DMEM-F12, 5% Hyclone II FBS, 1% antibiotics, adenine 24 µg/ml, EGF 0.2 ng/ml, hydrocortisone 0.4 µg/ml, insulin 5 µg/ml, cholera toxin 8 ng/ml and triiodothyronine $2x10^{-8}$ mM) were added and the inserts with the colonized hydrogels were maintained immersed. The medium was changed every other day. After three days of culture, the inserts were lifted to the air interface and the proliferation medium was replaced by a keratinocyte differentiation medium (DMEM-F12, 5% Hyclone II FBS , 1% antibiotics, calcium chloride 2 mM, hydrocortisone 0.4 µg/ml, insulin 5 µg/ml, cholera toxin 8 ng/ml, triiodothyronine $2x10^{-8}$ mM and ascorbic acid 50 µg/ml), keeping the upper surface of the hydrogel dry. After two days, the Hyclone II FBS percentage was reduced to 1% and the cellularized hydrogels kept in culture for 16 days. Differentiation medium was changed every day with the help of a vacuum pump. Dermis and skin equivalents obtained with the porous hydrogels were compared to a well-known and characterized model made of collagen-GAG-chitosan prepared as described by Collombel et al [10]. Both models were colonized with the same cells, however, the production the dermal and skin equivalents obtained with Col-GAG-Chi sponge were performed at the Tissue and Cell Bank of the Hospital Edouard Herriot following their internal protocols (Figure 30).

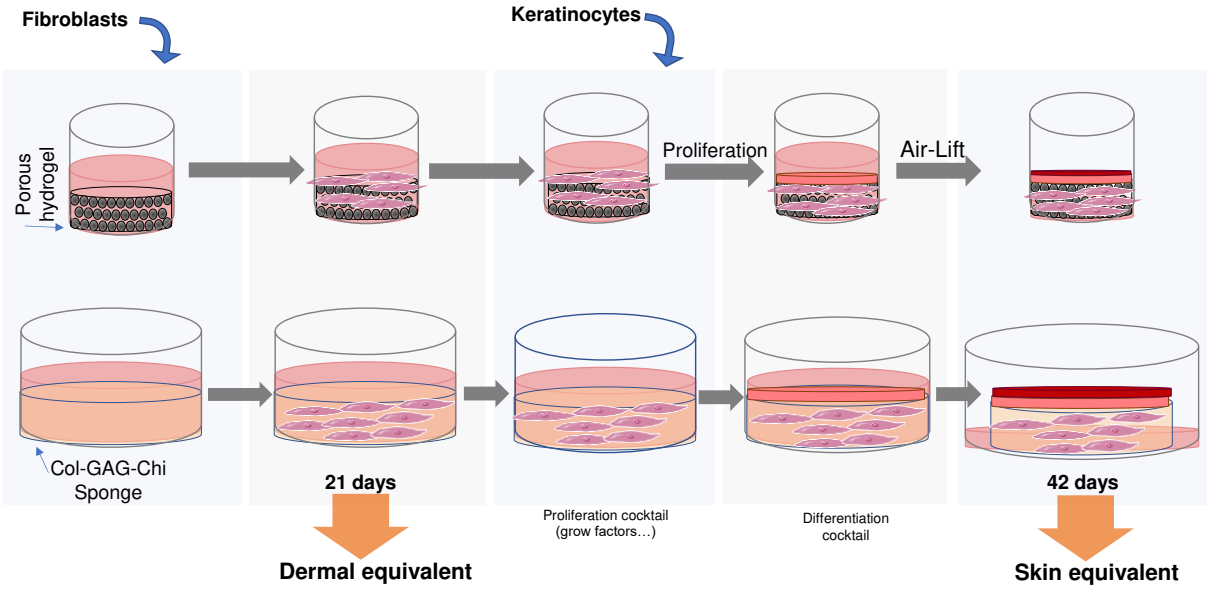

Figure 30. Process to obtain skin equivalent process with porous DGL-PEG hydrogels and Col-GAG-Chi sponges. *Fibroblasts are seeded on top of previously sterilized matrices and incubated for 21 days to obtain a dermal equivalent. Keratinocytes are subsequently seeded on top of the colonized matrices incubated with proliferation medium for 2-3 days depending of the protocol, then samples are placed at air-lift interphase and incubated with a differentiation medium. During air-lift interphase, DGL-PEG hydrogels were maintained in the inserts and transferred to a new plate to adjust medium volume and assure air-lift. In the case of Col-GAG-Chi sponges, samples were transferred and placed on top of a pre-soaked filter paper.*

For analysis, dermis or skin equivalents were retrieved and fixed with 4% PFA solution in PBS, after 21 and 42 days of cell culture, respectively. Samples were embedded in paraffin, and sections of 5 µm were prepared with a microtome (Leica RM2125RT). Skin equivalents were stained with hematoxylin and eosin to determine the epidermis thickness by image analysis (NIS Element). Synthesis of ECM components was observed by classical immunohistochemistry (IHC) of collagen type I (anti-rabbit NOVOTEC 1:4000) and elastin (anti-rabbit abcam ab23747, 1 µg/ml) and immunofluorescence of collagen type I (anti-rabbit, Novotec 20111, 1:200), laminin-332 (anti-mouse, abcam ab78286 1:500) and fibronectin (anti-rabbit, abcam ab45688, 1:250) revealed with Alexa fluor-conjugated anti-rabbit (abcam ab150079) or anti-mouse IgG secondary antibodies (Sigma-Aldrich A21236) (1:1000) while cells nuclei were counterstained with 1 µg/ml DAPI.

Furthermore, the formation of collagen fibers in skin equivalents was observed by Second Harmonic Generation (SHG) Microscopy. Epidermis

stratification was observed by IHC of cytokeratin 10 (abcam ab76318, 1:2000), Involucrin (abcam ab53112, 1:400) Keratin 14 (abcam ab181595, 1:2000). Proliferative cells were evidenced by immunofluorescence staining of Ki67 (anti-rabbit, abcam ab15580, 1:500) revealed with Alexa fluor-conjugated anti-rabbit (abcam ab150079) and cells nuclei counterstained with 1 µg/ml DAPI.

VII.IV. Mechanical properties of acellular vs colonized hydrogel

Before cells seeding, mechanical properties of the acellular porous hydrogels were measured by cyclic compression with a dynamic mechanical analyzer (DMA 242 E Artemis, NEZSTCH). Samples were subjected to penetration (rod 3 mm) at 10% strain, an amplitude of 60 µm and at a frequency of 10 Hz DMEM-F12 submersion using a water-bath at 37°C. Porous hydrogels were sterilized with 70% ethanol overnight and washed three times for one hour with sterile PBS. Fibroblasts were seeded as previously stated for the development of dermal equivalents, incubated at 37°C and 5% CO^2 and cell medium changed every 2 days. After 15 and 22 days of culture, samples were retrieved and measured once again using the same parameters as the acellular hydrogels. Three hydrogels were measured for each condition

VII.V. Gene expression analysis

i) RNA extraction

After 21 days of culture, porous hydrogels colonized by fibroblasts were cut in two pieces and immediately frozen with liquid nitrogen and stored at -80°C. RNA extraction was performed with a modified TRIzol protocol. Frozen samples were transferred to a 2 ml Potter homogenizer with 100 µl of SDS 0.5% (Sigma Aldrich) and grinded several times while keeping the homogenizer on ice (justification of SDS use described in annexes page 177). Under a fume hood, 300 µl of TRIzol (Molecular Research Center) was added before finishing homogenization. After transferring the homogenized solution to a 1.5 ml conic tube, 60 µl of chloroform (Sigma Aldrich) were added and mixed vigorously. The solution was left several minutes allowing decantation and centrifuged at 12,000 g for 15 minutes at 4°C. The aqueous phase (upper phase) was carefully recovered and transferred to a

new conic tube. The interphase and organic phase were stored at 4°C for subsequent protein extraction. To precipitate RNA, 400 µl of isopropanol was added to the aqueous phase, mixed by gently turning the tubes upside-down, incubated for 10 minutes at room temperature and centrifuged at 12,000 g for 10 minutes at 4°C. The supernatant was removed, RNA pellet was washed twice with 800 µl of ethanol 70% and centrifuged at 7,500 g for 5 minutes at 4°C. After removing all the traces of ethanol, the tubes were left to air dry under the fume hood for 5-10 minutes and RNA was re-suspended in 25 µl of RNAse-free water. RNA concentration and quality were measured by spectrometry with the Nanodrop 2000 (Thermo-Scientific) and electrophoresed at 100 V in 1% agarose gel prior revelation with ethidium bromide under UV light.

ii) Reverse Transcription

Reverse transcription was performed from 0.5 µg of total RNA using the PrimeScript RT reagent kit (Perfect real time, Takara, Ozyme) following product specifications. After thawing on ice and adding reaction mixture, reverse transcription was performed in the presence of poly(dT) oligonucleotides in thermocycler (Thermocycler T100 Bio-Rad) for 15 minutes at 37°C and stopped by enzyme inactivation for 5 seconds at 85°C, then temperature was decreased to 12°C. The obtained cDNA were transferred on ice and diluted at 1/10 in RNase free water for a final concentration of 5 ng/ml and store at -20°C.

iii) qPCR

Real time PCR was performed using Rotor-Gene Q (Qiagen) technology. cDNA was amplified using the FastStart Universal SYBR Green Master kit (ROX) (Sigma Aldrich). 5 ng of cDNA were mixed with kit reagents consisting of Taq Polymerase and its buffer, SYBR Green dye, dNTPs, and forward and reserve primers at final concentration of 300 nM (Table 7). Samples were subjected to the following qPCR program: Activation of Taq polymerase with 10 min at 95°C followed by 40 cycles of 10 seconds at 95°C and 30 seconds at 60°C as amplification cycles then 1 minute at 60°C followed by 1 minute at 90°C. Melt curves were obtained by subsequently heating from 55-95°C rising 1°C per cycle. Gene expression was normalized to the RPL13A housekeeping gene and expressed as fold ratio compared to hydrogel without ELP.

Table 7. Sequence of primers used for qPCR analysis.

Gene	*Primers*	*Sequence (5'→3')*
RPL13A	*Forward*	*GAT GGT GGT TCC TGC TGC CC*
	Reverse	*GGC TTT CTC TTT CCT CTT CTC CTC C*
COL1A1	*Forward*	*CAG CCG CTT CAC CTA CAG C*
	Reverse	*TTT TGT ATT CAA TCA CTG TCT TGC C*
FN1	*Forward*	*ATG ACG CTT GTG GAA TGT GTC G*
	Reverse	*ATT CAC CTA CAA TGG CAG GAC G*
ELN	*Forward*	*GTT GGT GGC TTA GGA GTG TCT G*
	Reverse	*CGG CAC TTT CCC AGG CTT C*

VII.VI. Gelatin zymography

a) Principle

Zymography is a technique that allows to assess the enzymatic activity. Total proteins are separated as function of their size by denaturating non-reducing SDS-PAGE containing the substrate of the enzymes of interest. After renaturation, activation and incubation, the enzymes degrade the substrate where they focalized. Finally, coomassie blue staining will show the proteolytically cleaved sites as clear white bands on a dark-blue background. More specifically, gelatin zymography allows to detect the gelatinase A (MMP-2) and B (MMP-9) activities. MMPs appear as two white bands corresponding to the pro- and activated forms.

b) Protocol

Gelatinases produced by the fibroblasts seeded in hydrogels were determined by zymography after 20 days of cell culture. At day 18, complete medium was discarded, cells were rinsed once with PBS, and DMEM-F-12 without FBS was added for the 2 last days. Conditioned medium was recovered and frozen -80°C. Medium was thawed on ice and 24 µl of conditioned medium without serum were loaded into a gelatin gel (SDS-PAGE 0.1% gelatin p/v) and run at 4°C for 30 minutes at 90V and 1 hour at 160V. After migration the gelatin gel was washed twice with Triton X-100 (2.5% v/v) and incubated for 48hrs at 37°C in activation buffer (58 mM Tris/HCL pH 7.2, 200 mM NaCl, 5 mM CaCl2 and 0.01% v/v Triton X-100). The gel was stained for 30 min (0.2% w/v colorant G-250, 20% methanol, 70% distilled water, and 10% acetic acid) and exposed with white light after discoloration (20% methanol, 70% distilled water, and 10% acetic acid) with a

Fusion Camera (Fusion Fx7, Vilber Lourmat). Gel bands were analyzed with GelAnalyser. As control HT1080 (human fibrosarcoma cell line) conditioned medium was used. The ratio of expression of pro-MMP-2 and active MMP-2 of hydrogels with ELP compared to hydrogels without ELP was determined from three different experiments.

VIII. *In vivo* biocompatibility assessment

Biocompatibility of dense and porous hydrogels was assessed by subcutaneous implantations of acellular hydrogel on the back of SKH1 mice.

VIII.I. Subcutaneous implantation in mice

After approval by local ethics committee, four hydrogel discs per condition (2x6 mm diameter) were implanted under the back skin of 8-week-old SKH1 mice (Charles River, Ecully, France) under sedation by intraperitoneal xylazin-ketamin injection (four hydrogels per mouse, as shown in Figure 31). A small incision was performed at the low back of the mice and 4 subcutaneous pockets created with a sterile spatula. The hydrogels were inserted in the pockets and the incision sutured. Mice, fed ad libitum, were monitored every day for recovery and signs of distress. After three weeks, the mice were euthanized by anesthetic overdoses (intracardiac injection of sodic pentobarbital), the hydrogel samples recovered with surrounding tissue, fixed in PFA 4% solution in PBS, embedded in paraffin, sectioned and stained with Masson's trichrome. Fibrous capsule thickness was measured from mosaic images by image analysis (Imagej) every 200 µm around the implanted hydrogels.

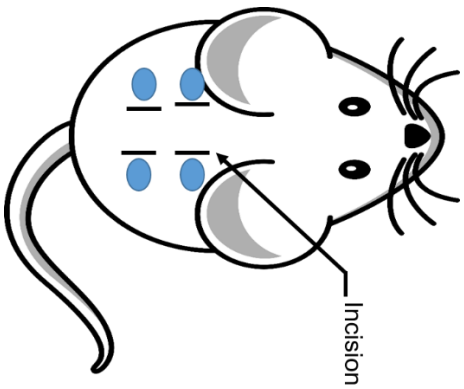

Figure 31. Subcutaneous implantation scheme for biocompatibility assessment.

VIII.II. A-SMA staining and blood vessels quantification

To highlight the penetration of blood vessels in the implanted hydrogels, paraffin-embedded sections were stained for α-SMA (anti-rabbit, abcam ab5694 – 1:250) revealed with Alexa fluor-conjugated anti-rabbit (abcam ab150079) and cells nuclei counterstained with 1 µg/ml DAPI and observed by confocal microscopy (ZEISS, LSM 800). Round blood vessels with a diameter superior to 10 µm and 25 µm per hydrogel cross section were counted of 3 sections per condition.

IX. Statistical analysis

Statistical analyses were performed with Graphpad prism or Kaleidagraph. Tests were performed using variance analysis (ANOVA), t-student or non-parametric tests (kruskal-Wallis followed by a post-hoc tests), according to the experiment and as indicated in figure legends. Data values are presented as mean ± standard errors (SE) and p-values of 0.05 and below were reported as being significant.

Results and Discussion

Is it possible to use poly-L-lysine dendrigrafts as crosslinker to form a tailorable PEG-based hydrogel, with inherent cell adhesion properties?

A successful scaffold must meet numerous and sometimes conflicting requirements. The construct may be as simple as a non-toxic two-dimensional surface upon which cells can grow, however, more sophisticated scaffolds may seek to encapsulate one or more cell types in three-dimensional structure, arrange them in spatially differentiated strata, and incorporate various bioactive factors such as hormones, cytokines, or signaling molecules [9]. Poly(ethylene glycol) (PEG) hydrogels have been extensively used as matrices for the development of tissue engineering scaffolds and in regenerative medicine [17]. However, their bio-inert properties require coating with ECM proteins or association with other functional moieties such as RGD peptides to promote survival or function of adherent cells [18]. PEG hydrogels can be crosslinked through various paths, for example by functionalization with reactive end-groups, activated by initiators, or by direct association with multifunctional monomers. For the latter, dendrimers can be used as crosslinking monomers to reticulate functionalized PEG molecules. Poly(amidoamine) (PAMAM) dendrimer for instance have been successfully associated with PEG to form hydrogels for drug delivery applications that do not require extensive interactions with cells [187,193,194]. However, they tend to exhibit unwanted features as cytotoxicity and non-degradability, low synthetic availability and non-sustainable synthesis [191].

Poly-L-lysine dendrigraft (DGL) are based on naturally occurring lysine amino acid monomers, bestowing additional properties to the versatility of dendritic polymer such as water solubility, stability under sterilization conditions, partial degradability under the action of endogenous peptidases, non-immunogenicity and low cytotoxicity [24,25]. Coating with DGL-G3 increased cellular adhesion of fibroblasts in comparison to linear poly-L-lysine (PLL) and represents the best compromise between biological activity and fabrication cost, compared to other generation DGL's [27]. Interestingly, our laboratory was the first to consider DGL as crosslinking monomers to form PEG-based hydrogels, while

such hydrogels could benefit from their inherent bioactivity, without the need for further association with functional moieties.

Therefore, in this first chapter, the use of DGL as crosslinking monomer was evaluated in the development of an innovative synthetic hydrogel composed of DGL and PEG, with extensive and straightforward tuneable mechanical properties. We hypothesized that these hydrogels will benefit from the DGL characteristics and therefore allow cell adhesion and proliferation without further coating or association with active sequences such as RGD. The characteristics of these hydrogels (crosslinking time, swelling and mechanical properties) were determined. To validate the potential of these innovative hydrogels as a synthetic substrate that supports cell function, different cell types were seeded on the surface of dense hydrogels and cell viability, proliferation and morphology were determined, in relation to the hydrogel composition.

I. Hydrogel characterization

I.I. Hydrogel formation and crosslinking speed

DGL/PEG hydrogel formation was possible through the simple and straightforward mixing of bifunctionalized polyethylene glycol-NHS (NHS-PEG-NHS) and DGL solutions. The amine groups present in high density at the DGLs surface could be swiftly used as binding sites for the PEG, to form network chains through the creation of amide bonds between PEG and DGL via N-hydroxysuccinimide (NHS), as shown in Figure 32.

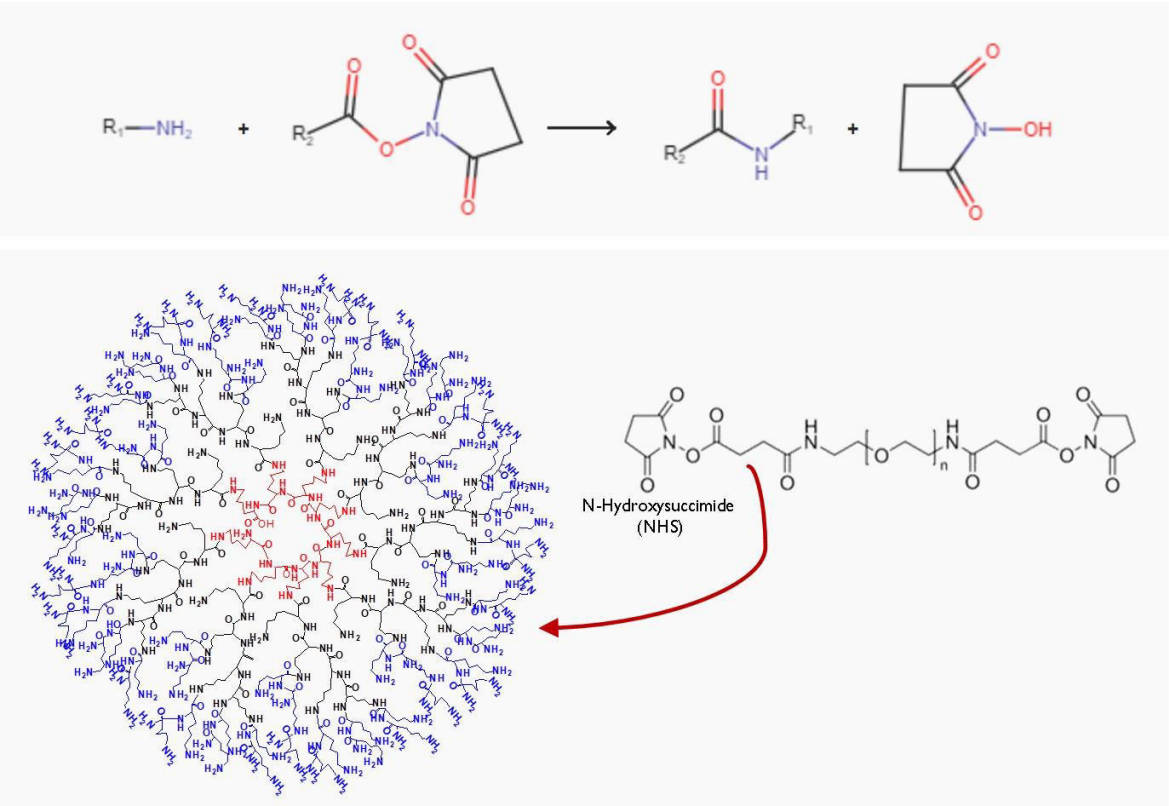

Figure 32. NHS ester reaction scheme for chemical conjugation to a primary amine. *R represents the polyethylene glycol and the one side NHS functionalization; P represents the poly-L-lysine dendrigrafts of third generation (DGL-G3) with a large surface area of primary amines.*

At room temperature, DGL and PEG-NHS solutions respectively comprised between 1 to 4 mM and 19 to 30 mM allowed to form self-standing gels, as observed in Figure 33. Concentrations of reactants under these values did not allow to form self-standing gels, while concentrations above resulted in a too rapid crosslinking to allow homogenization.

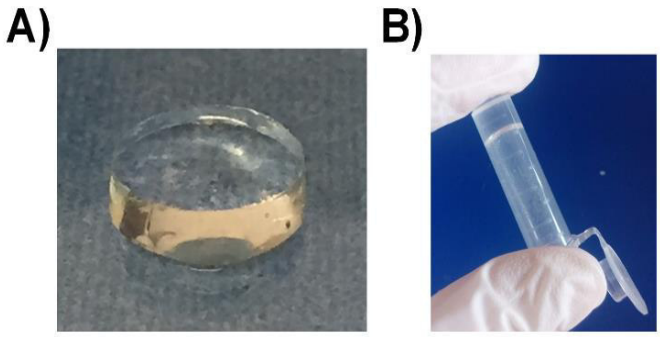

Figure 33. Photographs of the hydrogel at room temperature. *A) Dense 2/19 mM DGL/PEG hydrogel disc of 2 mm thickness and 9.1 mm diameter. B) Hydrogel in an inverted conic tube.*

The crosslinking velocity could be varied between 5 and 145 seconds by modifying the DGL and PEG-NHS concentrations (Table 8). While concentration doubling from 1 mM to 2 mM for a constant PEG-NHS concentration induced a 10-fold increase of the crosslinking velocity, a 1.6-fold increase of PEG-NHS for a constant DGL concentration only marginally decreased crosslinking speed, suggesting that DGL concentration has a predominant effect on crosslinking speed, this was supported by two-way ANOVA statistical analysis. DGL of third generation used in this study present a theoretically important density of amine groups on their surface (123), and it has been determined by Coussot *et al*. that 97.7% of this theoretical number of protonated residues are available as binding sites per molecules (114) [239]. PEG-NHS, on the contrary, possess only a double NHS functionality per molecule. However, it is unlikely that all the end groups will be able to react with the PEG molecules due to steric crowding at the surface of the DGL, which will limit the maximum number of PEGs that can be grafted to a single dendrimer [187]. The fact that an increase of PEG-NHS concentration for a constant DGL does not result in a significant increase of the crosslinking speed supports this hypothesis by indicating that a maximal number of PEG per DGL has been reached. Contrariwise, an increase of DGL at constant PEG-NHS allows to reduce the steric crowding by increasing the availability of amine-bearing molecules, and therefore increases crosslinking velocity.

Interestingly, by considering the amount of amine groups and NHS functions theoretically available for the covalent reaction to occur, similar ratio of amine to NHS resulted in different crosslinking velocities, which increased with a global increase of reactant concentrations. This general effect of both reactants concentration on crosslinking velocity can be similarly ascribed to the probability

of covalent reaction between PEG and DGL. Aside from a logical increase of reactive groups density, once a PEG molecule is attached to the surface of the dendrigraft, the second NHS function on the other end of the PEG chain will have a lower mobility, which will increase its probability to react with an amine function on the same dendrigraft and form intramolecular loops [190]. Therefore, the dilution of the reaction mixture increases the space between the dendrigrafts, forming many intramolecular loops at the expense of effective networks chains. Conversely, concentrating the mixture results in the opposite and increases the crosslink velocity [187].

Table 8. Crosslinking time to form self-standing gels in relation to the final concentration of DGL and PEG-NHS and ratio of available amine/NHS functions (two-way ANOVA between PEG and DGL concentration, * indicates that there is a statistically significant difference when DGL concentration is modified, for any given PEG concentration, $p<0.05$, n=3).

Time (s) *(Ratio amines/NHS)*		PEG-NHS (mM) *(Available NHS)*		
		19 *(38)*	28 *(56)*	30 *(60)*
DGL (mM) * *(Available amines)*	1 *(114)*	144.6 ± 23.3 *(3)*	122.0 ± 24.0 *(2.03)*	140.2 ± 15.8 *(1.9)*
	2 *(228)*	14.94 ± 1.1 *(6)*	13.17 ± 1.9 *(4.07)*	12.28 ± 3.5 *(3.8)*
	3 *(342)*	10.47 ± 4.5 *(9)*	8.4 ± 1.2 *(6.1)*	7.66 ± 1.1 *(5.7)*
	4 *(456)*	6.77 ± 0.9 *(12)*	4.76 ± 0.6 *(8.14)*	5.47 ± 0.6 *(7.6)*

I.II. Swelling, mechanical and degradation properties

Since hydrogels can absorb great quantities of liquids, the swelling ratio of hydrogels of different DGL/PEG compositions was evaluated. To mimic the physiological conditions, swelling ratio was determined in PBS at 37°C. The gel formed from the crosslinking of DGL and the PEG molecules is effectively a hydrogel since it absorbs between 1200 to 2200 times its weight in liquid. As observed in Figure 34, the swelling was decreased with an increased concentration of DGL or PEG. After 2 hours, most of the water had been absorbed by the hydrogel, which reached an equilibrium after 6 hours. The composition with lowest concentration of both components (1/19 mM DGL/PEG) showed the greatest ability

to absorb PBS, with a swelling ratio of 22.89 ± 1.95 after 24 hours. While no direct relationship was observed for an increase in DGL for a constant PEG or, inversely, an increase in PEG concentration for a constant DGL concentration, the swelling was decreased by an increase of the total hydrogel concentration.

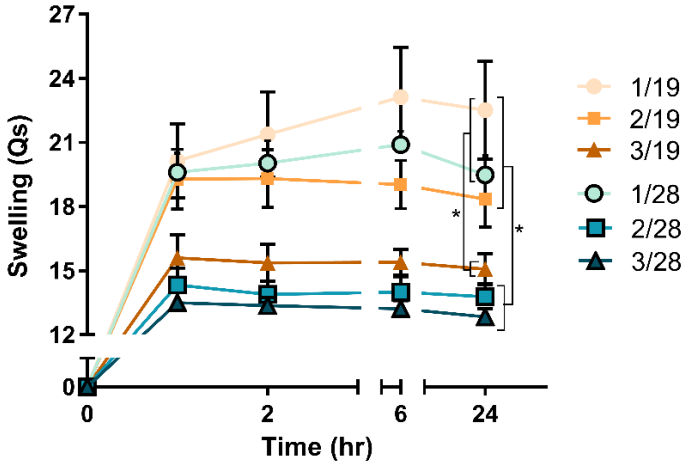

Figure 34. Swelling ratio in PBS at 37°C of hydrogels of different compositions. *Hydrogel concentration is expressed as the ratio DGL/PEG in mM (five hydrogels per condition, two-way ANOVA, p<0.05 * at 24hrs).*

A similar effect was observed when the relationship of hydrogel composition and their resulting rigidity was determined by mechanical dynamic analysis. The loss modulus (E''), storage (E') and complex modulus (E*) were determined at increasing frequencies between 1 and 10 Hz. Overall, the complex modulus of the different hydrogels was increased with an increased concentration of PEG and DGL, varying from 7.7 ± 0.7 KPa to 90.4 ± 28.8 KPa (Figure 35.A). Like the swelling ratio, the rigidity of the hydrogels was modified by the increase of total hydrogel concentration and not related specifically to an increase of DGL or PEG. For all hydrogels, the storage modulus (E') was greater than loss modulus (E'') over the entire frequency range, confirming the typical viscoelastic behavior of hydrogels. As shown in Figure 35.B, the ratio of the moduli (E''/E') that describes the viscous energy dissipation relative to the stored elastic energy of the hydrogel, also known as tan delta, was always lower than one. While E' was constant for all applied frequencies, E'' increased with frequency, a typical behavior of rubbery elastic materials [241].

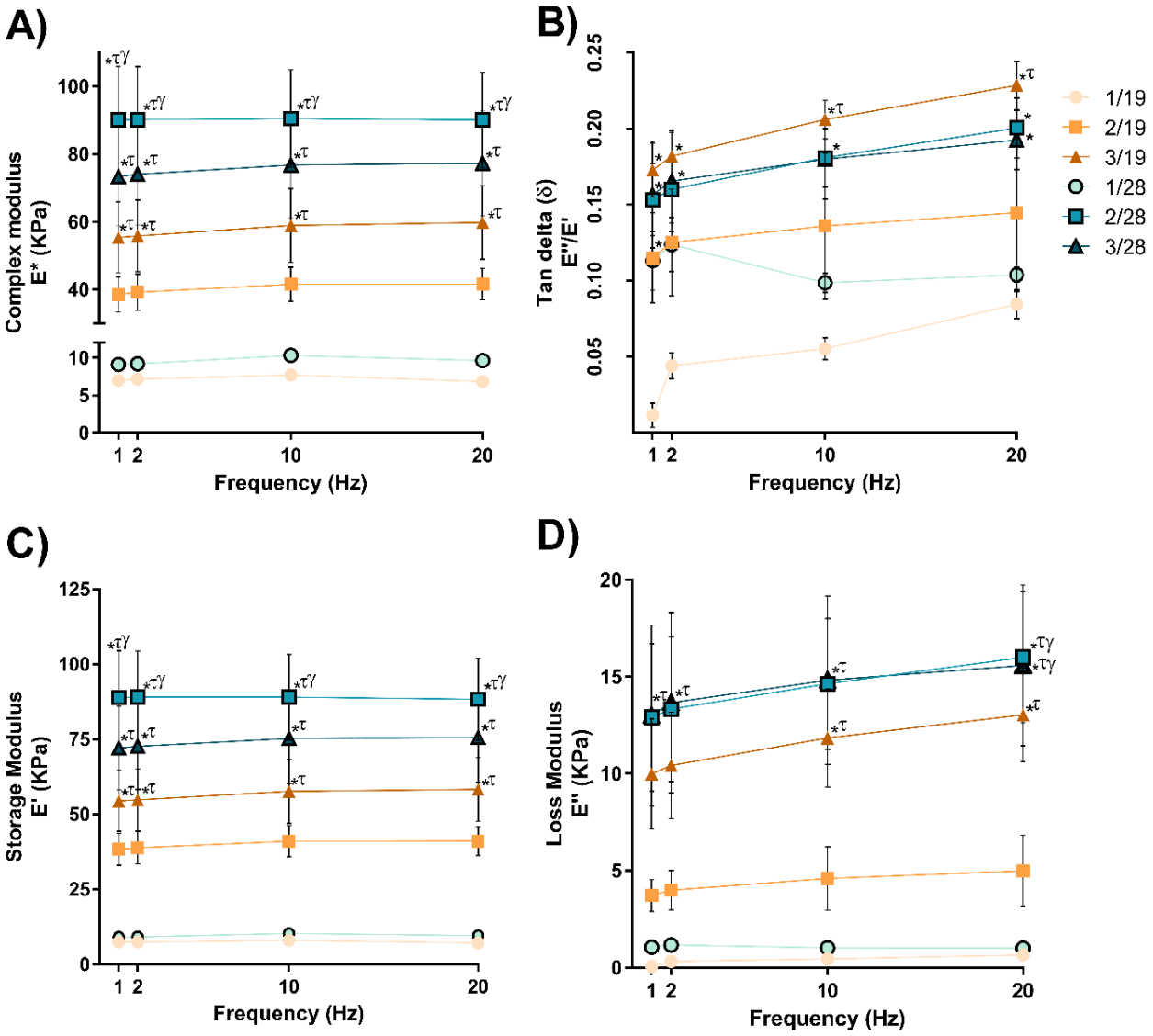

Figure 35. Mechanical properties of dense DGL/PEG hydrogel. *Hydrogel discs (2x9.1mm) of different compositions were measured at room temperature under PBS immersion by dynamic mechanical analysis in compression at a 10% strain and 60 µm of amplitude (Hydrogel concentration is expressed as the ratio DGL/PEG in mM). A) complex modulus, B) tan delta, C) storage modulus and D) loss modulus. (At least five hydrogels per condition, two-way ANOVA, p<0.05, *compared to 1/19, τ compared to 1/28 and γ compared to 2/19).*

In summary, solutions of increasing DGL and PEG-NHS concentrations but of similar ratios resulted in increasing crosslink velocities and mechanical properties but decreased swelling. As previously mentioned, the dilution of the components for a similar ratio of available amines per NHS group can have an impact in the intermolecular bonds formed. One PEG molecule that has already attached to one dendrigraft will have greater probabilities to react with another amine group of the same molecule, compromising the strength of the network but

increasing its swelling properties. Therefore, the effect of the polymer content could be logically ascribed to an increase of crosslinking density due to a closer presence of the amine (DGL) and NHS (PEG) reactive species. Since the arborescent molecules function as junction points in the crosslinking system, an increase in crosslinks density will limit the expansion of the network, meaning a more compact mesh that leads to a decrease in swelling and an increase in rigidity. This has also been observed for other hydrogels where the Young's modulus tends to decrease with an increased swelling [190,242]. Similarly, Gitsov *et al.* observed that the swelling properties of hydrogels prepared from PEG and various dendritic fragments were not related to the PEG concentration or the dendrimer generation but mainly to the total increase in component concentration [243].

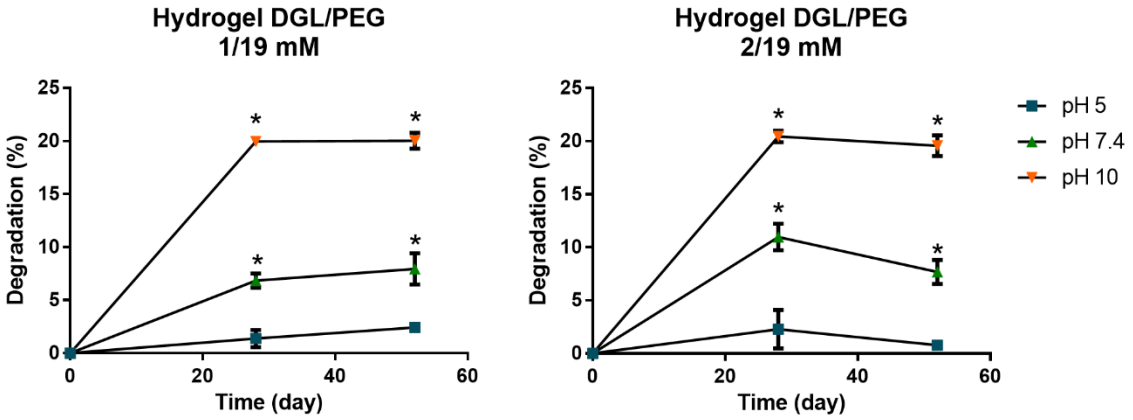

Figure 36. Hydrogel percentage of degradation in different environments. *Degradation expressed as the weight loss through time in different buffers, citrate buffer (pH 5), phosphate buffered saline (pH 7.4) and carbonate-bicarbonate buffer (pH 10). (at least three hydrogel per conditions, two-way ANOVA, $p<0.05$ * compared to hydrogel before degradation)*

Finally, the *in vitro* degradation of two hydrogel compositions were evaluated in citrate buffer (pH 5), carbonate-bicarbonate buffer (pH 10) or phosphate buffer saline (pH 7.4) by measuring their weight loss over time. As shown in Figure 36, both hydrogel compositions, 1 and 2 mM of DGL for 19 mM PEG showed a similar degradation rate. After two months, just a marginal decrease in weight mass was observed for hydrogels in PBS (pH 7.4) and citrate buffer (pH 5). However, a 20% weight loss was observed for both compositions in a carbonate buffer (pH 10) after just one month of incubation, indicating a potential hydrolysis. This hydrolysis could occur on the secondary amides in the PEG chain in basic conditions [244], as depicted in Figure 37. While no difference was observed by

increasing the DGL concentration, the effect of PEG concentration in degradation rate was not determined.

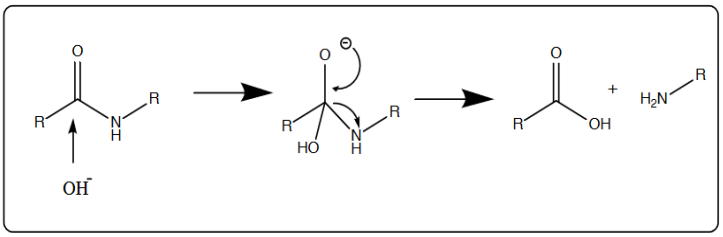

Figure 37. Scheme of secondary amide hydrolysis in basic conditions.

To further determine the biodegradation of the polymer, other *in vitro* studies in the presence of enzymes or *in vivo* degradation tests must be performed. Nevertheless, the degradation studies performed in different buffers indicate that the polymer is stable and does not extensively degrade or dissociate in physiological conditions. This can also indicate that the hydrogels can have a self-life of at least 52 days under physiological conditions without suffering degradation.

II. Cell response to the biomaterial

To assess the potential of the DGL/PEG hydrogels as cell substrate that allows cell adhesion without further coating or moiety incorporation, different cell types were seeded on the surface of dense hydrogels of different compositions. The behavior of the cells was investigated to validate if DGL can convey biological properties to the hydrogel, similar to coated surfaces.

II.I. Human nasal chondrocytes preliminary response to the hydrogel

First, the viability and morphology of freshly extracted nasal human chondrocytes on 1/19 and 2/19 mM DGL/PEG hydrogels was evaluated with a life/dead assay and DAPI/phalloidin staining. After 7 days of culture, chondrocytes could adhere on the surface of the hydrogels and no sign of cytotoxic effect on either composition was noticeable (Figure 38.B). An increase of cell number was observed over culture time by phase contrast images suggesting that cells were able to proliferate, however, proliferation was not measured (Figure 38.A). Interestingly, as shown in Figure 38.C, a higher fraction of chondrocyte round morphology was maintained by the soft hydrogel composition (1/19 mM DGL/PEG

– 7 kPa) while chondrocytes appeared to dedifferentiate in more rigid hydrogels and displayed elongated morphologies (2/19 mM DGL/PEG- 40 kPa). Similarly, when seeded in culture plastic dishes chondrocytes tend to dedifferentiate to a more fibroblastic-like morphology, losing their spherical shape [245].

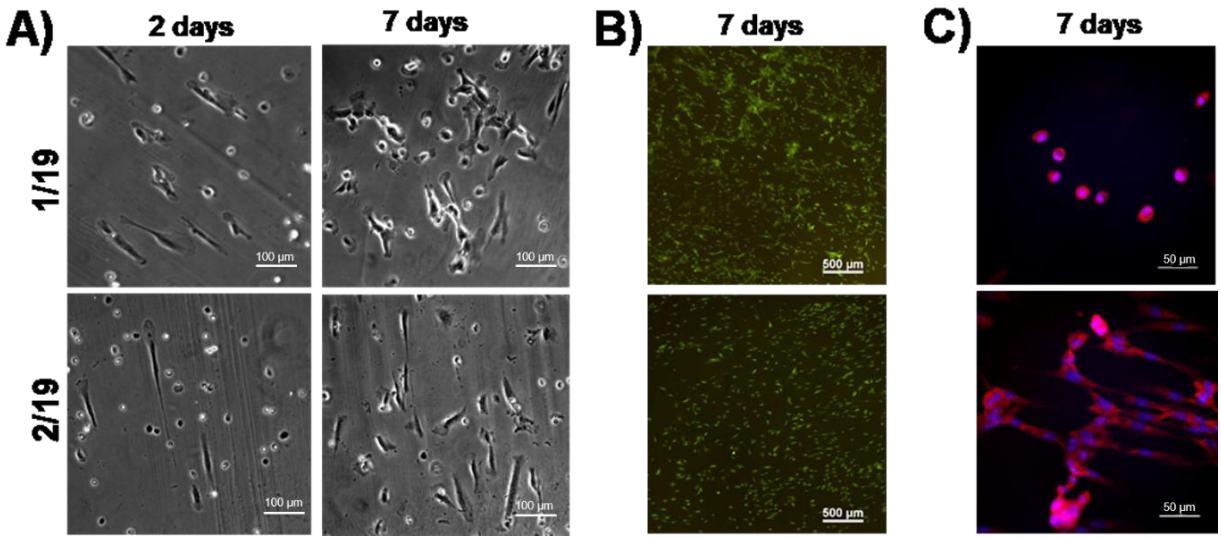

Figure 38. Response of Human nasal chondrocytes seeded in the surface of hydrogels of different compositions. *(Hydrogel concentration is expressed as the ratio DGL/PEG in mM) A) Phase contrast images after 2 and 7 days of culture (scale bar 100 µm. B) Cell viability by live/dead assay after 7 days. Live cells are observed in green and dead cells in red (scale bar 500 µm). C) Cytoskeleton structure observed by DAPI-Phalloidin staining after 7 days of culture. Cell nuclei appear in blue and actin fibers in red (scale bar 50 µm).*

Benya *et al*. were able to re-express the native chondrocyte phenotype after serial monolayer dedifferentiation by suspension culture on the surface of agarose gels. They hypothesized that this was due to the maintenance of a spherical shape of cells in the gels, as opposed to the flattened shape in monolayer culture [246]. Moreover, it has been widely stated that cells are able to sense the mechanical cues of their microenvironment and commit to a specific phenotype depending of its mechanical properties [197]. In this manner, Schuh *et al*. demonstrated that substrates with low elastic modulus (4 kPa) could help to maintain the chondrogenic phenotype independently from the availability of adhesion sites [247]. While morphology is a good indicator of the chondrocyte phenotype, these results are still preliminary. To better determine the potential of these hydrogels as a substrate to maintain the normal chondrocyte phenotype, the type of extracellular matrix synthesized by the chondrocytes must be assessed. For example, a higher type II collagen expression as compared to type I collagen would further indicate a proper chondrocyte phenotype [245,247]. Nevertheless, these

results clearly indicate a lack of the DGL/PEG cytotoxicity and the ability for chondrocytes to adhere on their surface.

II.I. Human dermal fibroblasts response to hydrogel

a) Viability and cell adhesion

To further assess the potential of DGL/PEG hydrogels to interact with cells and its potential as a substrate in skin engineering, human dermal fibroblasts were seeded on the surface of dense hydrogels of a broader composition range. Cell viability was evaluated with a life/dead assay (Figure 39.A). After 1 day of culture, an overall very low cytotoxicity was observed, as the majority of cells that adhered on the hydrogels were alive; except for the composition 3/19 mM DGL/PEG, which showed a mortality of 79.3 ± 5.9%. After 3 culture days, compositions 1/19, 1/28 and 2/19 mM DGL/PEG presented around 85% of viability while more concentrated compositions 2/28 and 3/28 mM DGL/PEG showed no difference to control cells seeded on polystyrene culture dish, with a viability of 97.9 ± 0.7 and 96.0 ± 2.3%, respectively (Figure 39.B).

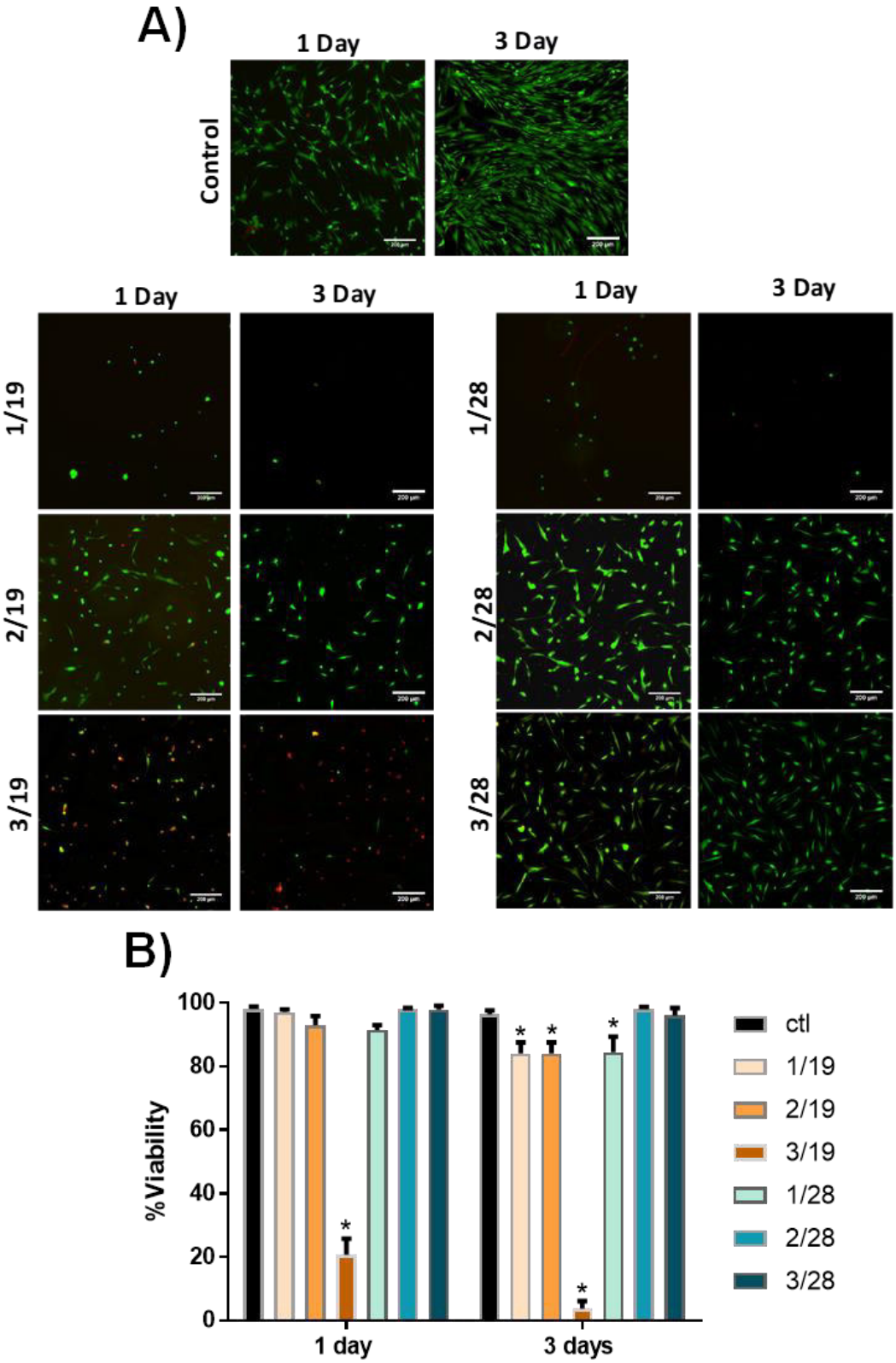

Figure 39. Dermal human fibroblast viability. *(Hydrogel concentration is expressed as the ratio DGL/PEG in mM). A) Cytotoxicity by live/dead assay after 1 and 3 days of culture on the surface of hydrogels of different compositions (scale bar 200 μm). Live cells are observed in green and dead cells in red B) Viability percentage obtained from image analysis (at least seven hydrogels, one-way ANOVA, $p < 0.05$ * compared to control, culture plastic).*

Hydrogel composition had an apparent effect on cell adhesion, as shown in Figure 40. With an increase of DGL concentration, the total number of cells that adhered to the hydrogel's surfaces was increased, regardless if they were alive or dead. Cells adhesion was minimal when the DGL concentration was low (1 mM) regardless of the associated PEG concentration, indicating that a minimal DGL concentration is necessary to favor cell attachment to the hydrogel. Similarly to DGL coated surfaces [27], the ability of cells to attach and spread to DGL-containing hydrogels could be attributed to early electrostatic interactions between the polyanionic cell surfaces and the polycationic charges brought by amine groups of the DGL.

While the concentration of DGL plays a major role on the adhesion to the surface of the hydrogels, viability was dependent of the ratio between DGL and PEG. Indeed, mortality was observed where the ratio of amines to NHS groups was greater than nine. The cationic nature of DGL that provides them their cell adhesion properties is possibly also the cause of their cytotoxic effect since excessive cationic charges can affect the integrity of the cell membranes [248]. When coupled with PEG molecules, PEG might shield the dendritic cationic charges and improve the DGL viability, since an increase in PEG concentration resulted in an increase of adhered cell viability. Similarly, Tang *et al*. showed that PEG-gelation of DGL vectors for gene therapy allowed to decrease the vectors toxicity [249].

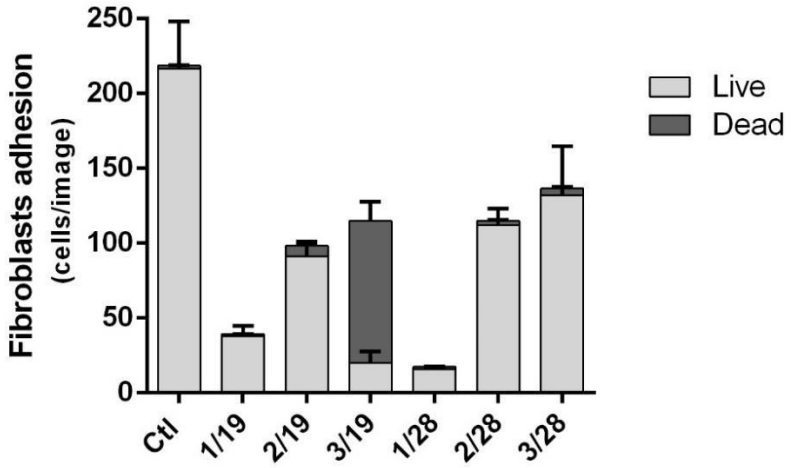

Figure 40. Fibroblast cell adhesion after 24hrs of cell seeding on top of hydrogels of different compositions. *(Hydrogel concentration is expressed as the ratio DGL/PEG in mM). Number of cells obtained from image analysis of live/dead (at least seven hydrogels per condition One-way ANOVA, $p<0.05$, *compared to control, culture plastic, τ compared to 1/19 mM DGL/PEG and γ compared to 1/28 mM DGL/PEG).*

b) Cell proliferation

Human dermal fibroblasts seeded on top of hydrogels were able to proliferate over time in certain compositions. An increase in cell number was observed for hydrogels with viability over 84% and a minimum of 2 mM DGL, while hydrogels with low concentrations of DGL (1 mM) showed proliferation rates close to zero (Figure 41). Compared to controls (135.2 ± 26.19), proliferation rates were lower at large, although hydrogel compositions 2/28 and 3/28 mM DGL/PEG showed similar proliferation rates of 69.9 ± 8.1 and 66.7 ± 14.6, respectively.

In vivo, fibroblasts are in quiescent/secretory state unless induced into proliferation by the release of stimulating factors as a result of tissue damage [250] or by culturing then *in vitro* on glass or tissue culture plates. Likewise, when seeded on collagen substrates, fibroblasts proliferation rate was decreased compared to plastic controls [250–252]. Sarber *et al*. suggested that the difference of proliferative activities when fibroblasts were seeded on collagen lattices was attributed to the similarities to a tissue-like environment [250]. Similarly, a decrease of proliferation has been observed in other biomaterial composites without collagen. Mekhail *et al*. showed a significantly lower count of fibroblasts seeded on top of chitosan/Poly-L-lysine gels, compared to plastic controls [253].

On the other hand, the different proliferation rates between DGL/PEG compositions can be explained by their differences in rigidity. Proliferation of fibroblasts has indeed been widely demonstrated to be modified by substrate mechanical properties, an increase in rigidity resulting in an increase in proliferation in both 2D and 3D models [202,254,255].

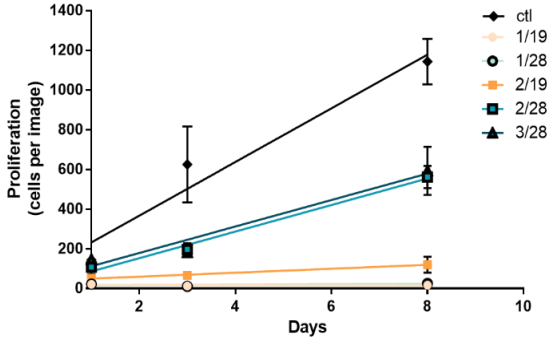

Proliferation rate (slope)	
Control	135.2 ± 26.19
1/19 (*)	-0.3671 ± 1.043
2/19 (*)	9.981 ± 4.951
1/28 (*)	0.9532 ± 1.776
2/28 (*τγ)	66.95 ± 8.143
3/28 (*τγ)	66.72 ± 14.65

Figure 41. Cell proliferation rate of fibroblasts seeded on the surface of hydrogels of different compositions. *(Hydrogel concentration is expressed as the ratio DGL/PEG in mM). Proliferation rate obtained from cell nuclei counting after 1, 4 and 8 days of culture is expressed as the slope obtained from cell quantification through time (at least three hydrogels per condition, one-way ANOVA, p<0.05, *compared to control, τ compared to 1/19 and γ compared to 1/28).*

c) Cell morphology

The morphology of fibroblasts seeded on hydrogels was evaluated by determining the spreading area, circularity and ferret diameter from phase contrast images of cells 24 and 72 hours post-seeding (Figure 42). Cell morphology was modified by hydrogel composition, with a slight increase of cell spreading for all hydrogels after 72 hours (Figure 42.B). The morphological parameters of fibroblasts seeded on tissue culture controls could not be determined at 72 hours since confluence was then already reached, preventing to perform accurate image analysis of individual cells. While the effect of DGL concentration on cell adhesion and the effect of the DGL/PEG ratio on cell viability was clear, the influence of hydrogel composition on cell morphology and proliferation seems to be related to the overall substrate rigidity, similarly to what was observed with chondrocytes. Cells on hydrogels with smaller concentrations of DGL (1 mM) and therefore smaller percentage of adhesion and low rigidity (7-10 kPa) presented a round morphology similar to non-adherent cells, as shown in Figure 42.A, with a mean circularity of 0.8, the smallest ferret diameter (26.9 – 28.9 µm) and no proliferation. Conversely, an increase in DGL concentration for a given PEG concentration resulted in a more spread morphology and an increase in proliferation only when the mechanical properties were also increased, as for hydrogel composition 1/19 and 2/19 or 1/28 and 2/28 mM DGL/PEG. However, when there was no significant increase of substrate rigidity, fibroblasts showed similar morphology and proliferation rate, as could be observed for compositions 2/28 and 3/28 mM DGL/PEG, were both compositions showed a similar spreading area, circularity and ferret diameter. On the other hand, when PEG concentration was increased for a constant DGL concentration (2 mM), the hydrogel rigidity increase was reflected in a higher proliferation, fusiform-like spreading morphology, ferret diameter (108 µm compared to 75.4 µm) and in a lower circularity (from 0.6 to 0.42). Similarly, compositions 2/19 and 3/28 mM DGL/PEG with a similar amine/NHS ratio, but different overall polymer concentrations and therefore substrate rigidity (respectively, 41.5 ± 5.0 to 76.7 ± 15.5 kPa) showed different cell proliferation and spreading.

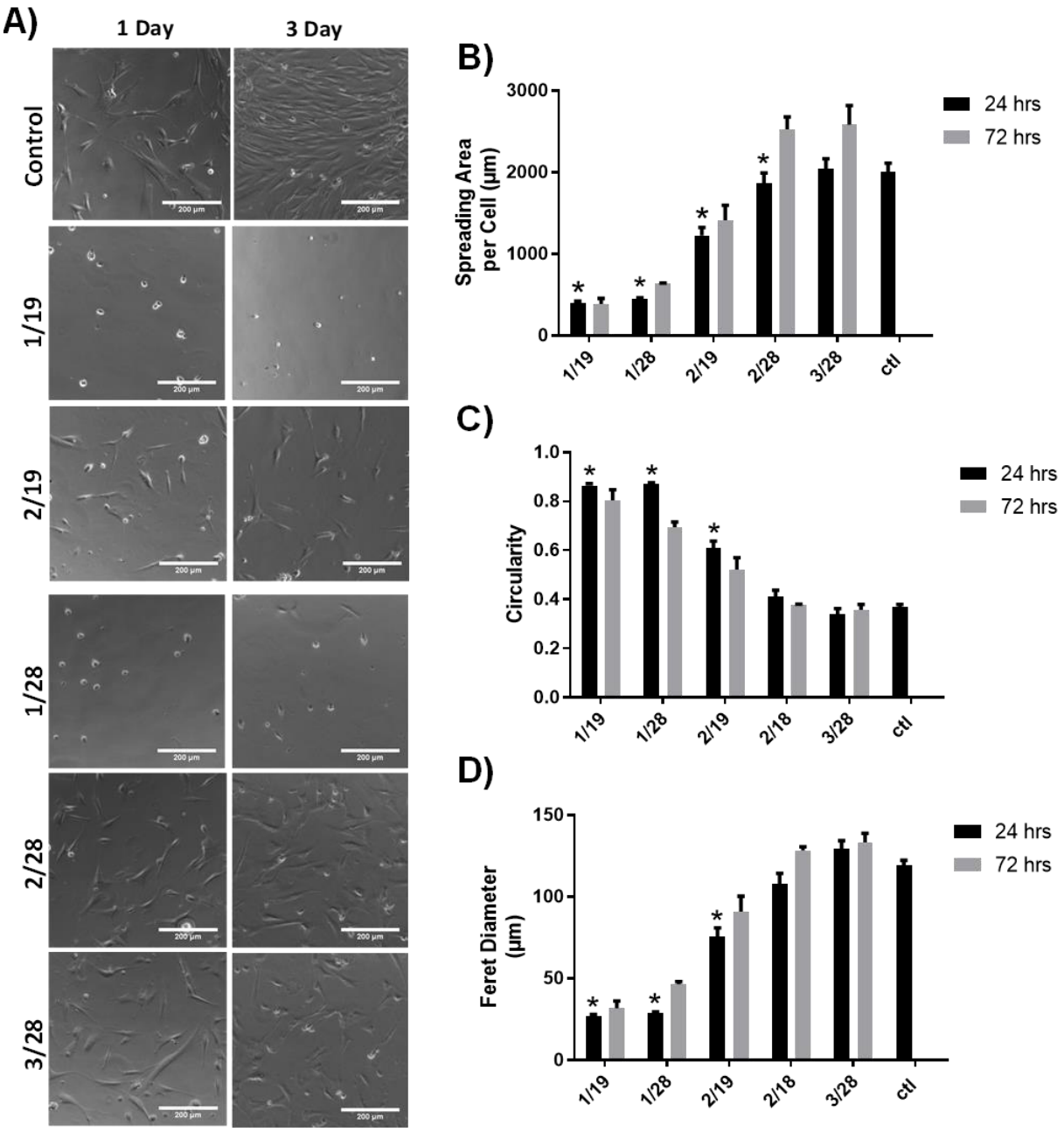

Figure 42. Dermal fibroblast morphology when cultured on the surface of hydrogels of different compositions. *(Hydrogel concentration is expressed as the ratio DGL/PEG in mM). A) phase contrast photos after 24 hours and 72 hours of cell seeding (scale bar 200 µm). B) Spreading area per cell. C) Circularity and D) Ferret diameter. Morphology parameters were obtained from images analysis of phase contrast photos of at least ten hydrogels per conditions at 24 hours and five hydrogels after 72 hours. Control was analyzed only after 24hrs since cells had reached confluence after 72 hours. (One-way ANOVA, $p<0.05$, * compared to control at 24 hours).*

The effect of hydrogel composition on cell morphology and F-actin stress fiber formation was further confirmed by staining with fluorescent phalloidin after 1, 3 and 8 days of culture. The presence of actin fibers was consistent with cell spreading area as observed in Figure 43. Several groups have studied how different

cell lines "feel" and respond to the mechanical properties of their environment, showing an increase in spread area and stress fibers with an increase in substrate rigidity [200,202,203,254]. For instance, Lo *et al*. showed that 3T3 fibroblasts were able to easily migrate across soft-rigid boundaries upon the same polyacrylamide gel with an increase in spreading and traction forces [256]. Solon *et al*. further showed that fibroblasts were able to increase their internal stiffness to match that of their substrate, proving what substrate stiffness is a crucial regulator of cell morphology and behavior [257]. Similarly, Ghosh *et al.* showed evidence that cells sense the substrate mechanics and undergo arrangement to match the substrate and reach a new equilibrium, resulting in a proliferation increase of dermal fibroblasts with an increase in substrate rigidity [254].

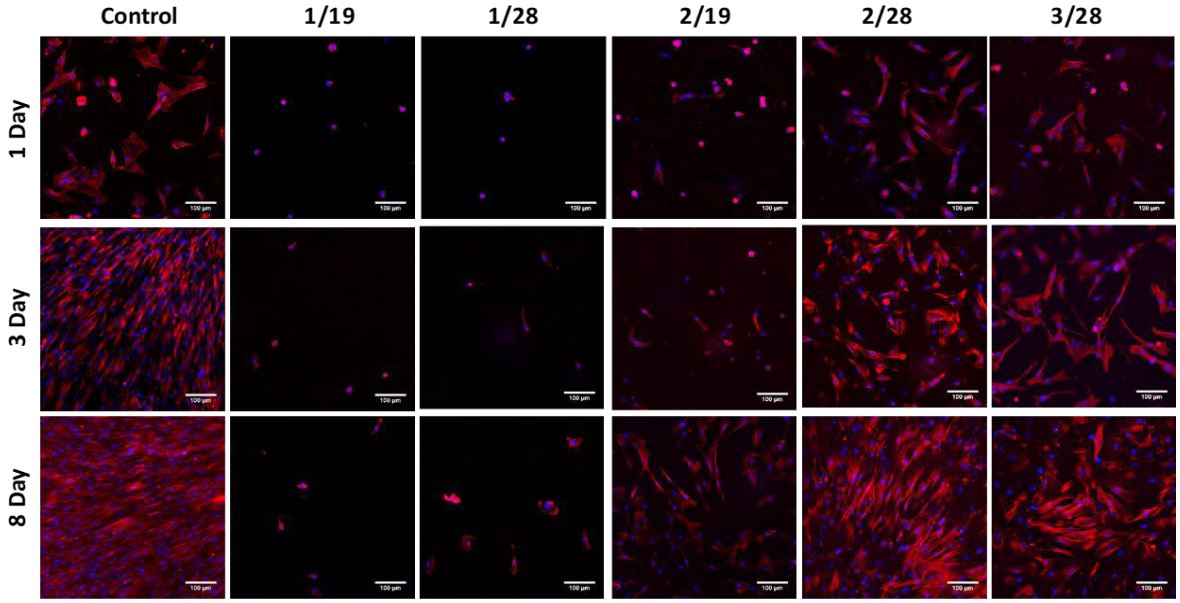

***Figure 43. Cytoskeleton structure of dermal fibroblasts seeded in the surface of hydrogel of different compositions (hydrogel* concentration is expressed as the ratio DGL/PEG in mM*) by* DAPI-Phalloidin staining after 1, 4 and 8 days of culture**. Cell nuclei appear blue and actin fibers red (scale bar 100 μm).

Critical evaluation and conclusion

We have demonstrated that DGL-G3 can serve as a multifunctional crosslinker to form through straight forward approaches a novel and stable PEG-hydrogel system. While crosslinking velocity of the hydrogel was mainly dependent of DGL concentration, hydrogel's properties such as swelling and mechanical properties were modified by an increase in total concentration. A dilution of the same amine/NHS ratio decreases the substrate rigidity and increases the swelling ratio. Moreover, the crosslinking of PEG-NHS with DGL facilitates cellular attachment and proliferation of human nasal chondrocytes and human dermal fibroblasts. As expected, cell adhesion of different cell types on the hydrogels surface was mainly dependent of the concentration of DGL, however, minimal concentration of PEG in relation to DGL is needed to sustain the viability of the adhered cells. Contrarily, cell behavior and morphology appear linked to substrate rigidity rather than hydrogel composition. While human nasal chondrocytes preserved their round morphology on softer hydrogels, fibroblasts showed a spindle-shaped morphology and the ability to proliferate in more rigid hydrogels. The possibility of controlling the hydrogel mechanical properties by modifying its components opens their potential for a wide range of soft tissue applications. However, DGL/PEG hydrogel crosslinking is not optimal for the encapsulation of cells (data non shown), therefore, to properly study its potential as a substrate to mimic the ECM and support cell culture as a three-dimensional matrix, hydrogel should be made porous to allow cell infiltration.

Can the DGL/PEG hydrogel be formulated into a porous scaffold to allow fibroblast infiltration and to produce a dermal matrix for a full-thickness skin equivalent?

Most full-thickness equivalents are based on a collagen-matrices as the support to produce the dermal component. However, while natural polymers confer biomaterials with their inherent ECM structure and biochemical activities, they tend to have weak mechanical properties, batch-to-batch variability and risk of pathogen transfer [15,16]. Moreover, the use of animal source ingredients, especially in the cosmetic industry is subjected to an ethical dilemma [1]. We previously introduced a novel synthetic DGL/PEG hydrogel which demonstrated inherent biological activity; by allowing cell adhesion and viability on a two-dimensional environment. While it's been shown that bulk material properties have an important impact on cell interactions with the biomaterials, another important factor to consider is the macroscopic properties, such as pore size, interconnection and porosity [176,258]. Therefore, to properly study the interactions with the biomaterial in a more physiological condition and to be able to support co-culture and tissue formation, cells must be cultured in a three-dimensional microenvironment. To do so, the transformation of the DGL/PEG hydrogel into a porous scaffold was evaluated using a particulate leaching technique with paraffin microspheres as porogens. The use of paraffin as porogens favors the use of nontoxic solvents (such as ethanol) [183]. This technique has demonstrated to be able to direct pore size by controlling the porogen size distribution, with a good correlation when using paraffin microspheres [232]. The cellular infiltration of dermal human fibroblasts into the macroporous structure was evaluated in relation to pore size, porosity and interconnection between pores to obtain a dermal equivalent. Furthermore, to evaluate the potential of the porous hydrogels as a matrix to support full thickness skin equivalents, the ability of fibroblasts to proliferate within the hydrogel and produce their own ECM to form a dermal equivalent was assessed. Finally, to validate the use of the porous hydrogels in the development of skin-engineering, keratinocytes were seeded on top of the fibroblast-colonized hydrogels and the resulting full-thickness skin equivalents were compared to skin equivalents obtained with well-known Collagen-GAG-Chitosan model, which supports a properly stratified epidermis [126].

I. Hydrogel as a porous scaffold

I.I. Pore size, macrostructure and interconnectivity

In addition to the intrinsic characteristics of the polymer that will determine cell viability and cell adhesion, the macrostructure (*e.g*. porosity, pore size, interconnectivity and surface area) plays an important role in biocompatibility and cell infiltration of tissue engineering scaffolds; since these characteristics are important to recapitulate the cues present in the native extracellular matrix and therefore mimic the cell microenvironment [164]. Accordingly, a particulate leaching using paraffin microspheres as porogens was evaluated as fabrication technique to render the hydrogel porous. As shown in Figure 44.A, porogens obtained after emulsion-based process have a spherical shape. Paraffin-leaching has the advantage to produce spherical pore shapes with well-controlled interpore connectivity contrary to salt-leaching where pore shape is limited to the cubic crystal shape of NaCl salt [183]. Moreover, the use of paraffin as porogens instead of salt or sugar porogens avoids the dissolution of porogens during reticulation in aqueous medium. Here, two sieved paraffin microspheres populations (50-100 and 100-180 µm) used to create the pores contained 80.7 and 72.6% respectively of the expected size population (Figure 44.B), probably due to the difficulty to properly sieve out of range populations.

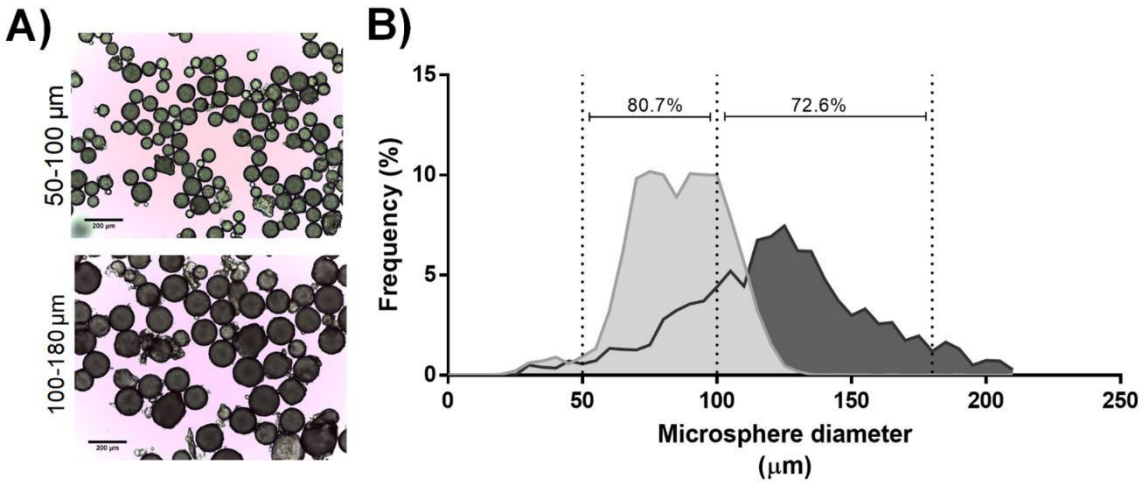

Figure 44. Porogens for particle/leaching technique. *A) Paraffin microspheres used as porogens obtained after sieving between 50-100 µm and 100-180 µm. B) Size distribution of paraffin microspheres obtained from images analysis of five different production batches.*

After pouring the hydrogel mixture into a template of compacted microspheres, paraffin could be effectively removed producing a homogeneous porous structure, as observed in Figure 45. This technique allows to control the pore size by varying the size of the porogen. Ma *et al.* demonstrated that by using paraffin as porogens it is possible to obtain a macroporous structure replica of the compacted paraffin microspheres used as a casting template [183].

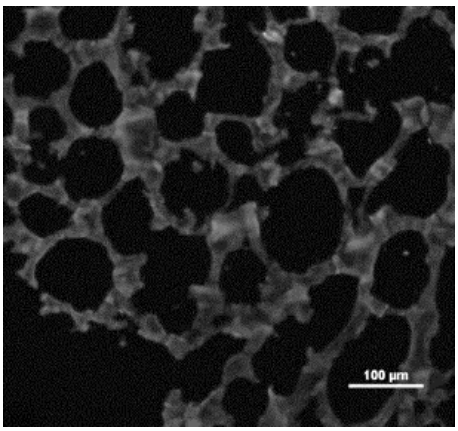

Figure 45. Porous hydrogel slide after paraffin extraction. *Hydrogel prepared with a range of paraffin microspheres of 50-180 µm. Hydrogel autofluorescence in white (scale bar 100 µm).*

Beside pore size, a key factor determining the potential of a porous material as a scaffold is the interconnection within its porous structure. Indeed, interconnectivity between pores has been related to cell ingrowth, vascularization and nutrient diffusion [176–178]. To evaluate the presence of interconnection between pores in the formed hydrogels, the macrostructure of two different hydrogel compositions with a similar ratio of available amines/NHS was observed by environmental scanning electron microscopy (ESEM). As shown in Figure 46, images clearly indicate the presence of fenestrations between the pores. Interestingly, no apparent difference could be noticed between the two hydrogel compositions, suggesting that paraffin template is the predominant factor in providing the macrostructure organization independently of hydrogel composition.

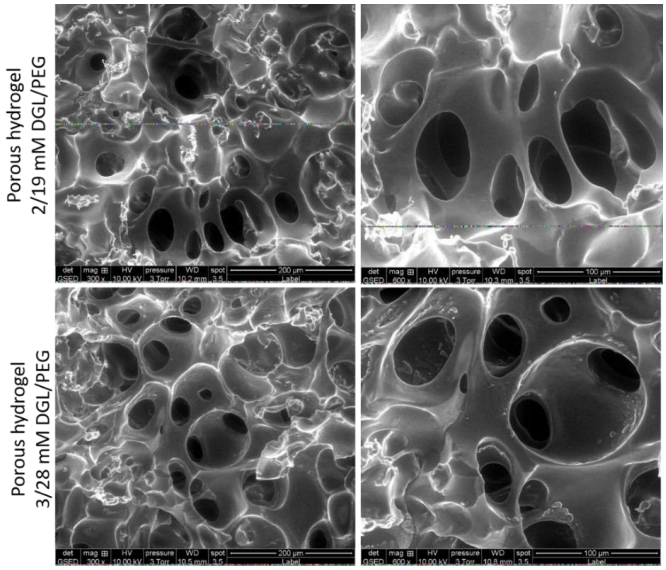

Figure 46 Environmental scanning electron microscopy (ESEM) images of porous hydrogels of different compositions. *Hydrogel concentration is expressed as the ratio DGL/PEG in mM. Both hydrogels were prepared with 75% 50-100 µm and 25% 100-180 µm paraffin microspheres. Left magnification x300 and right x600.*

I.II. Mechanical properties of porous hydrogels

In order to mimic the mechanical properties reported for the skin, the mechanical properties of two different DGL/PEG porous hydrogels prepared with increasing DGL/PEG concentrations were measured by compression mode with dynamic mechanical analysis (DMA). The complex modulus (E*) and tan delta (tan δ), were determined at increasing frequencies (1 and 20 Hz). As observed in Figure 47.A, both hydrogels behaved as elastic materials since tan delta was smaller than one. Complex modulus was increased with an increase in frequency from 1 to 10 Hz, then stabilized at 10 Hz**.** While both hydrogel compositions have a similar ratio of available amines for NHS groups (see Table 8, in page 105), more concentrated hydrogels showed an increase in rigidity. As shown in Figure 47.B, rigidity of porous hydrogels at 10 Hz varied from 15.2 ± 2.0 to 34.39 ± 20.6 kPa for hydrogel compositions 2/19 and 3/28 mM DGL/PEG, respectively. Hydrogel variability was increased in higher concentration hydrogels (3/28) due to an increase of the crosslinking speed. Even though highly concentrated hydrogels were produced in a cold room to slow down the reaction (<10 seconds at room temperature) hydrogel homogeneity was decreased. Overall, macroscopic mechanical properties of 2/19 and 3/28 mM DGL/PEG porous hydrogel were decreased to 63.4% and 54.5%, in comparison to their dense counterparts (see Figure 35.A, page 107)**.**

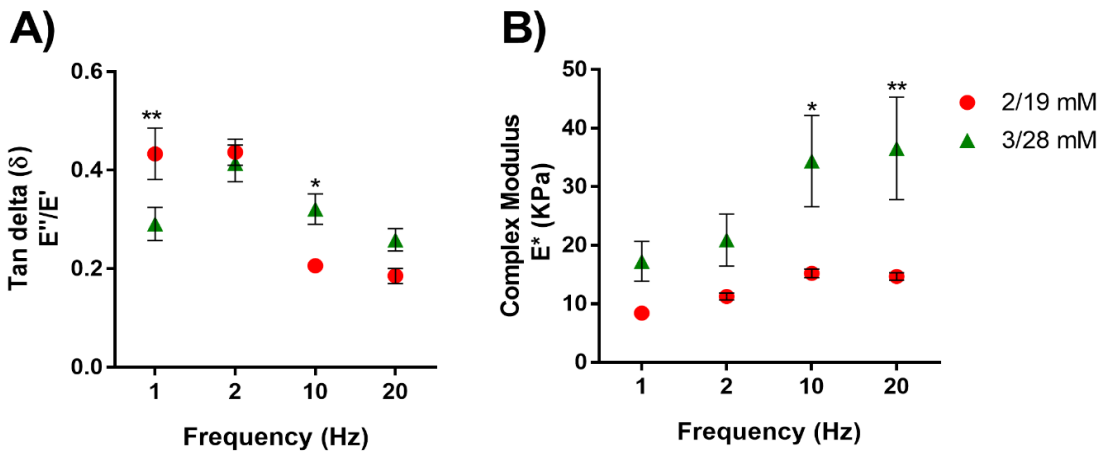

Figure 47. Mechanical properties porous DGL/PEG hydrogel discs (2x8mm) of different compositions *(hydrogel concentration is expressed as the ratio DGL/PEG in mM) measured at room temperature under PBS immersion by dynamic mechanical analysis (DMA) using compression mode at a 10% strain and 60 µm of amplitude. A) Tan delta B) Complex modulus (at least seven hydrogels per hydrogel composition, t-student *p<0.05)*

Depending of age, human skin complex modulus has been reported in the range of 6-15 kPa by indentation techniques (see Table 1 in page 41). This suggests that hydrogel 2/19 mM display a mechanical behavior closer to what is observed in vivo for skin. Moreover, the input provided by cells and ECM component after seeding most be considered. Dermal equivalents have shown to increase up to 22% the mechanical properties of acellular matrices due to the cellular components and the matrix deposition [259].

I.III. Cellular infiltration and hydrogel porosity

To determine the capacity of the porous hydrogels to allow cell infiltration and determine the most suitable structure in this respect, mixtures of 50-100 and 100-180 µm paraffin microspheres populations were used. The ability of fibroblasts, deposited on the surface of the porous matrices, to infiltrate over time was then assessed to confirm the interconnection between pores. As observed in Figure 48, at early culture times (7 days after seeding), fibroblast penetration appeared deeper in porous hydrogels prepared with a higher fraction of 100-180 µm paraffin beads. This tendency was inversed between 7 and 14 days of culture as the most effective cell colonization was observed for hydrogels with a higher fraction (75%) of 50-100 µm paraffin beads. Bigger pores allowed a rapid

infiltration at 7 days; however, cell infiltration was probably interrupted due to the lack of interconnected pores throughout the hydrogel.

To investigate the role of DGL/PEG hydrogels porosity on cellular infiltration, a standard liquid displacement method using a pycnometer was employed. Hydrogels prepared with microsphere fractions between 50-100 and 100-180 µm resulted in a porosity of 70.8 ± 1.9 % and 76.0 ± 3.2 %, respectively. Larger porogen spheres seemed to induce a slight increase in hydrogel porosity, however, not significantly. An intermediary value of 74.1± 4.9 % porosity was obtained for the composition that allowed the best cell infiltration (75% 50-100 µm and 25% 100-180 µm). The lack of an important difference in terms of porosity confirms that the difference in cell infiltration is probably due to a better interconnection between pores. It is possible that by compacting a broader size distribution of paraffin microspheres, the void space between bigger microspheres is decreased due to the presence of intercalated smaller spheres, consequently increasing the interconnection between pores [260].

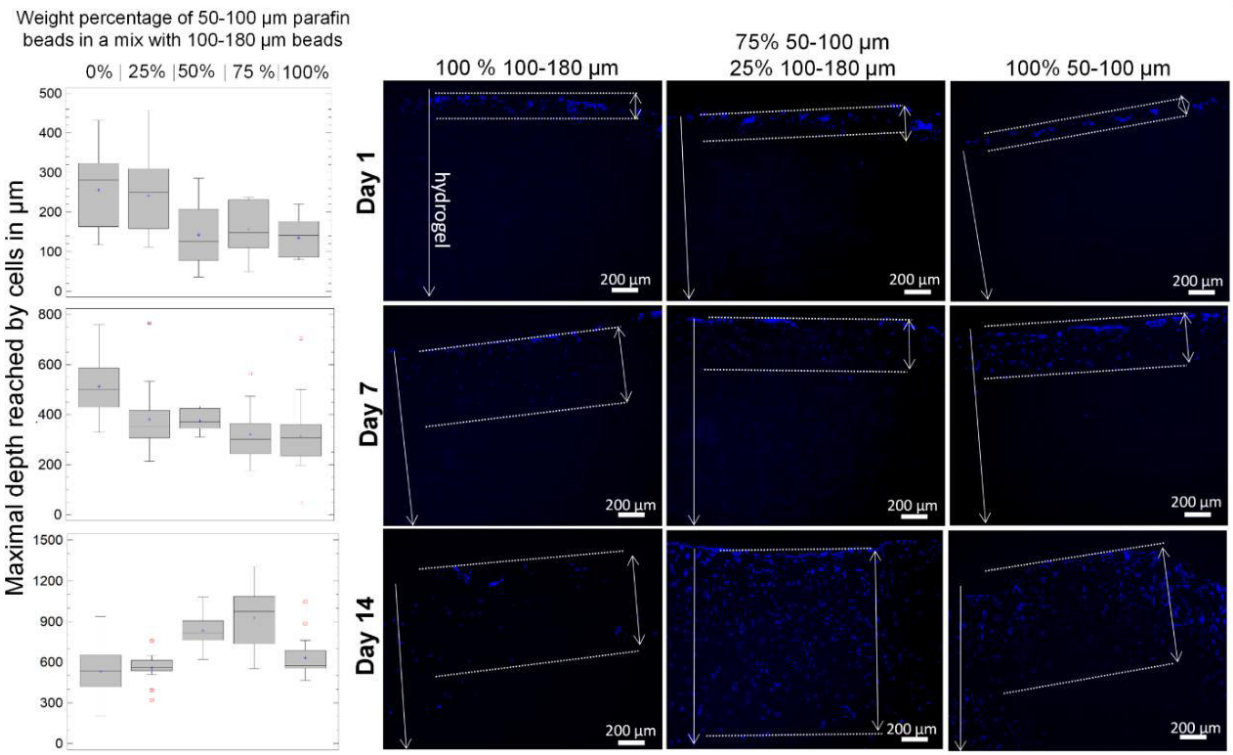

Figure 48. Cellular infiltration of human dermal fibroblast (NHDF) seeded in porous hydrogels with different pore size distributions. *Pore size distributions were prepared by increasing the weight percentage of 50-100 µm paraffin beads in a mix with 100-180 µm beads in hydrogel composition 2/19 DGL/PEG. A) Maximal depth reached by fibroblasts over time obtained from image analysis. Non-parametric tests (Kruskal-Wallis followed by a test post-hoc the Nemenyu). B) Representative images of cell infiltration, cells nuclei stained in blue (scale bar 200 µm). Graph obtained by intern Céline Tournier.*

II. Porous hydrogel as a three-dimensional matrix to produce dermal and skin equivalents

To assess the potential use of the porous hydrogels as a three-dimensional scaffold to produce dermal and skin equivalents, hydrogel composition with the mechanical properties closest to the values reported for human skin and with the porous structure that showed the most important cell infiltration were employed (2/19 mM DGL/PEG with 75% of 50-100 µm paraffin beads). The use of this hydrogel as a three-dimension matrix to obtain skin equivalents was compared to a well-known and widely use collagen-GAG-chitosan model [10,261]. Control models were performed as described by Collombel *et al*, at the Tissue and Cell Bank of the Hospice de Lyon following their cell culture protocols [2].

II.I. Fibroblast proliferation within DGL/PEG porous hydrogel

Human dermal fibroblasts seeded on top of porous hydrogels were able to proliferate and colonized the porous structure. As shown in Figure 49.A, the number of fibroblasts within the porous hydrogel steadily increased up to 4.2 folds after 3 weeks of culture, clearly highlighting the role of cellular proliferation in the porous hydrogel colonization. Additional fibroblast infiltration could be observed after 21 days of cell culture indicating that cells could reach more than 900 µm with longer culture times. As observed in Figure 49.C, fibroblasts form a three-dimensional network within the pores. In comparison to two-dimensional cell culture (Figure 41, see page 114), when cultured in a three-dimensional microenvironment fibroblast proliferation is increased. In a three-dimensional environment, cells are not only in contact with the biomaterial but also with each other and the newly synthesized extracellular matrix, consequently inducing a better proliferation rate.

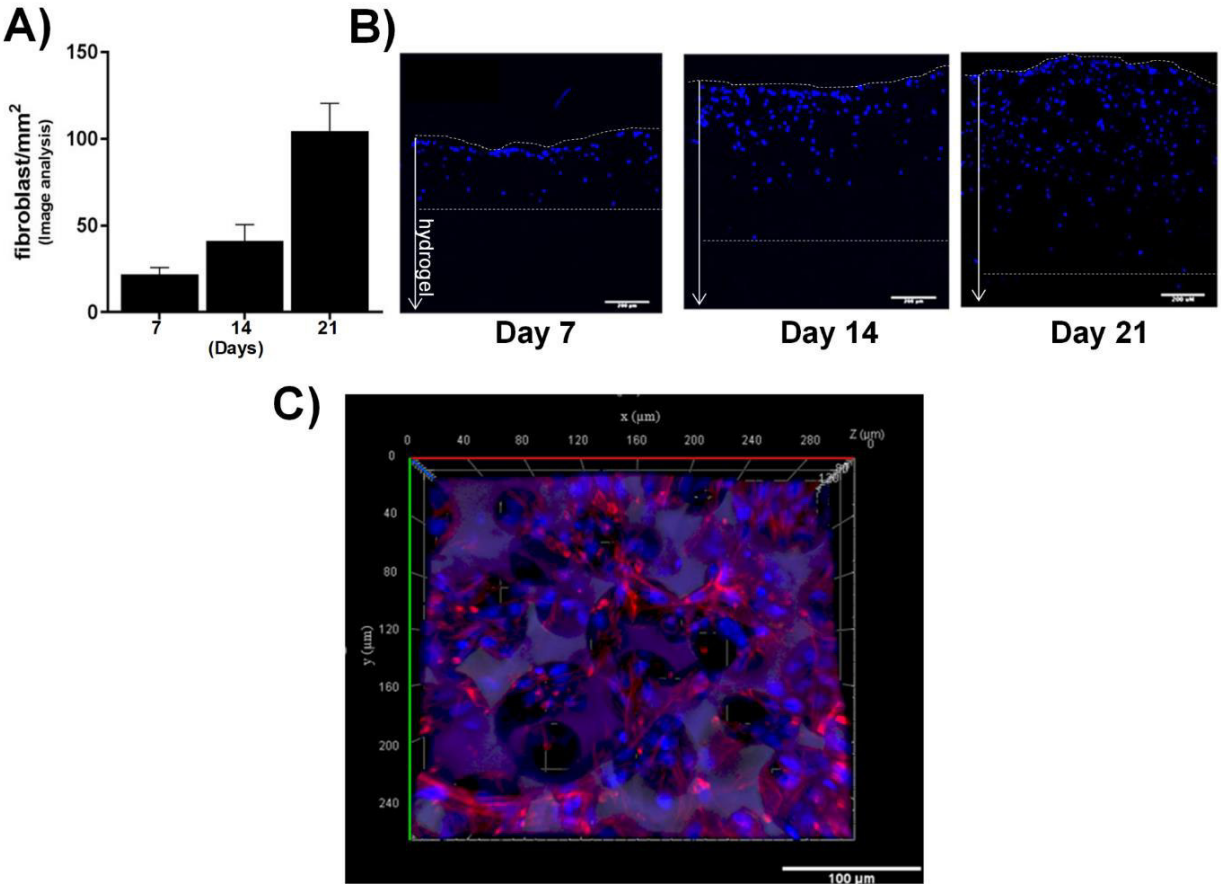

Figure 49. Porous DGL/PEG hydrogels (2/19 mM DGL/PEG) as a matrix to form dermal equivalents in vitro. *A) Semi quantitative cell proliferation expressed as fibroblasts/mm2 determined by images analysis after 7, 14 and 21 days of cell culture. B) Representative images of cell proliferation over time, cell nucleus stained in blue and dotted lines delimit the surface of the hydrogel where the fibroblasts were seeded, and the maximal distance traveled (scale bar 200 µm). C*) Stacked image (130 µm deep) of colonized hydrogel after 21 days of culture, cell nucleus in bright blue and cytoskeleton in red. Hydrogel can be distinguished by the combination of autofluorescence in blue and green (scale bar 100 µm).

After 21 days of culture, the 2 mm-thick porous hydrogels were homogeneously colonized by the fibroblast as shown by the representative image in Figure 50.A. Variability between different acquired fields (x10) within the same hydrogel slide and sections obtained at different depths of the hydrogel showed a normal population distribution (Figure 50.B) which indicates that most of the image section showed a mean of 350 cells/image. A bimodal distribution would suggest that, while sections of the hydrogel show a high density of fibroblast other sections are poorly colonized by the fibroblasts.

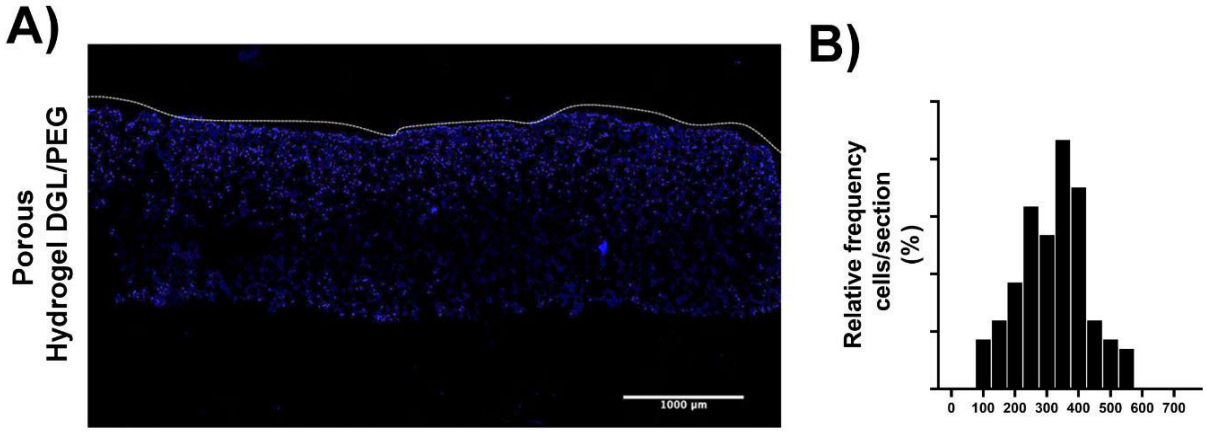

Figure 50. Porous DGL/PEG hydrogels homogeneous colonization after 21 days of cell culture. *A) Representative mosaic image of a complete slice of hydrogel colonized by dermal human fibroblasts after 21 days of cell culture. Dotted line delimits the hydrogel surface were cells were seeded (scale bar 1000 µm). B) Variability of the cell number observed at randomly acquired fields (x10) expressed as the relative frequency of cells per section (12 µm slides were obtained every 100 µm and randomly acquired fields within a same slide and between slides were analyzed by image analysis, at least 50 images)*

To determine the optimal cell seeding conditions to obtain a dermal equivalent, increasing cell seeding densities were evaluated. Interestingly, an increase in cell seeding number did not speed up the hydrogel colonization by the fibroblasts. For instance, a five-fold increase of seeded cells resulted in a loss of cell number during the first 7 days of culture, and a lack of proliferation after 14 days. Cell proliferation was even reduced when the seeding density was increased by ten-folds, as shown in Figure 51. It is possible that increase in cell density only increased the cell number on the surface of the hydrogel, resulting in contact inhibition of proliferation before cells were capable of infiltrating the hydrogel. Also, an increase in cell number on the surface of the hydrogel could limit availability of nutrients, inducing cell death and explaining the decrease in fibroblasts/mm^2, explaining the reduction of cell number after 14 days of culture. Similar

observations were reported by Brown *et al*. for collagen matrices where they showed that proliferation rate was seeding density-dependent [255].

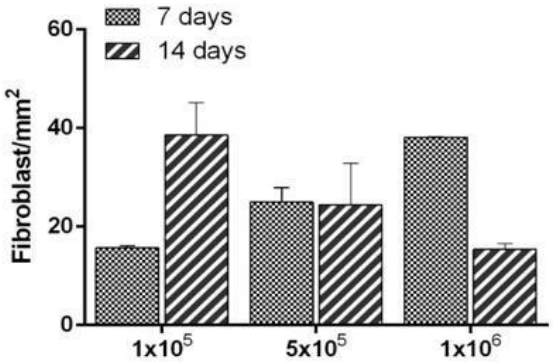

Figure 51. Cell seeding optimization of porous DGL/PEG hydrogels (2 mM DGL and 19 mM PEG) as a matrix to form dermal equivalents in vitro. *Obtained from images analysis nuclei counting (three hydrogels per condition).*

II.II. Synthesis of extracellular matrix

The ability of the fibroblasts to synthesized ECM within the porous DGL/PEG hydrogel to form a dermal equivalent and subsequent skin equivalent were compared to those obtained with Col-GAG-Chi sponges. In both models, 21 days after cell seeding on the surface of the matrices, fibroblasts migrated and filled the pores with neosynthesized ECM, thus forming a dermal equivalent (Figure 52.A). By subsequently seeding keratinocytes on the surface of the dermal equivalent, it was possible to obtain full-thickness skin equivalents, with both a dermal compartment and an epidermal layer. An increase in collagen expression was observed after 42 days, once the keratinocytes were added. However, scare evidence of elastin expression was observed in both skin equivalents (Figure 52.B). Besides its structural and mechanical contribution, the ECM provides anchoring sites for the cells and regulates intracellular communication to ensure a normal cell growth and differentiation [64]. While the synthetic DGL/PEG scaffolds can provide a proper mechanical support, the synthesis of ECM components is an important requisite to allow the native skin tissue formation in 3D.

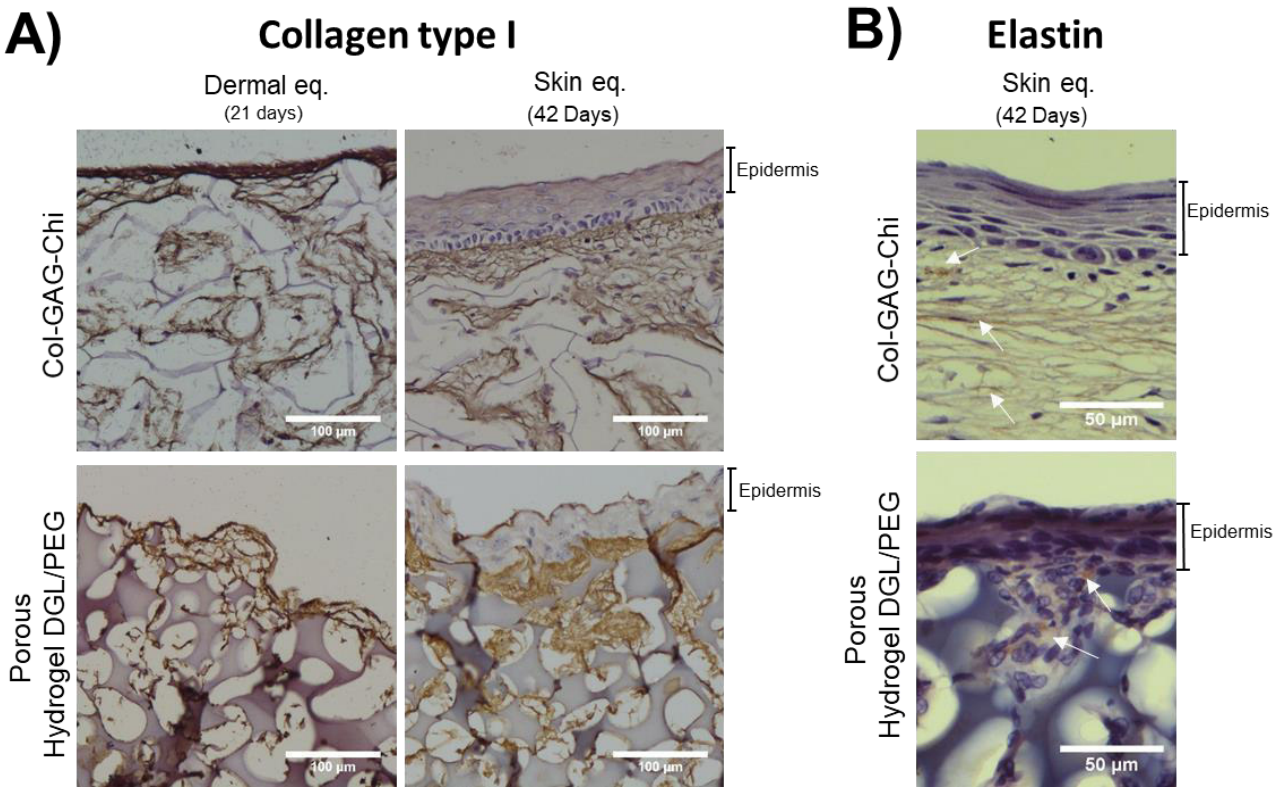

Figure 52. Synthesis of the native extracellular matrix in dermal and skin equivalents. *A) Immunostaining of type I collagen after 21- and 42-days of cell culture (scale bar 100 µm). B) Immunostaining of elastin after 42 days of cell culture of skin equivalents, arrows indicate the presence of elastin (scale bar 50 µm).*

Moreover, fibrillar collagen in skin equivalents obtained with DGL/PEG hydrogels was evidenced by second-harmonic generation microscopy (Figure 53). Organized collagen fibers are known to provide skin with its mechanical properties and structural framework [65]. After 21 days of culture with only fibroblasts, no fibrillar collagen was visible indicating that collagen fibers formation occurred once dermal equivalents were cultured with keratinocytes. Similarly, Duplan-Perrat *et al*. showed with TEM images that collagen and elastin were more abundant and better organized in skin equivalent compared to matrices containing only fibroblasts and cultured for the same amount of time. They further demonstrated that keratinocytes are important in the maturation of the ECM [262].

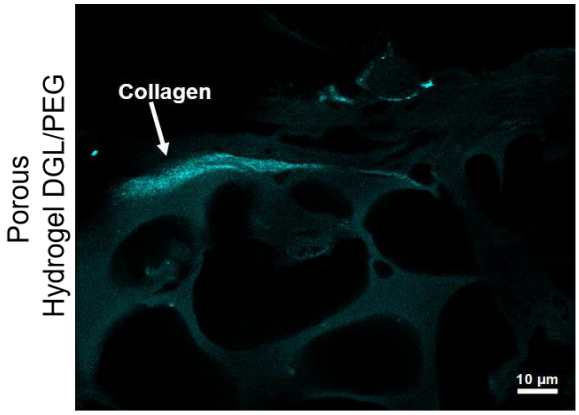

Figure 53. Second-harmonic imaging microscopy of collagen fibers skin equivalents. *After 42 days of cell culture with fibroblasts and keratinocytes in porous DGL/PEG hydrogels (scale bar 10 µm).*

II.III. Epidermal Stratification

Keratinocytes seeded on top of the dermal equivalents were able to differentiate to from a stratified epidermis *in vitro*. However, the total epidermis thickness obtained with DGL/PEG hydrogels was lower than what was observed for Col-GAG-Chi skin equivalents (39.2 ± 2.6 µm and 47.25 ± 1.41 µm, respectively; Figure 54). The latter being closer to the epidermis thickness observed for human skin *in vivo*, which is around 40-50 µm [263].

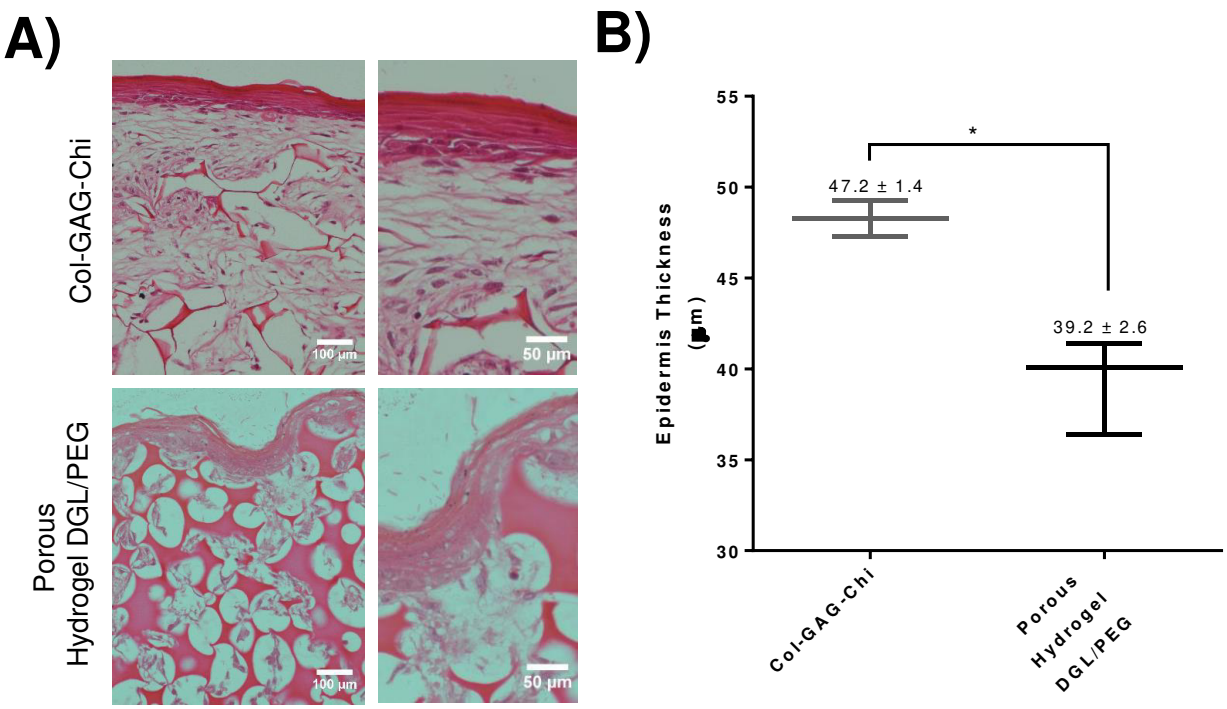

Figure 54. Epidermis thickness of skin equivalents. *A) Hematoxylin & Eosin images of skin equivalents obtained with porous DGL/PEG hydrogel and Col-GAG-Chi (scale bar 100 µm left and 50 µm right). B) Mean epidermis thickness measured from image analysis (three hydrogel per condition and two controls, t-student, *p<0.05).*

Interestingly, as observed in Figure 55, DGL/PEG porous hydrogels were able to more closely mimic the structure of the papillary dermis formed by rete pegs and rete ridges along the dermal-epidermal junction [44], while the epidermis formed in Col-GAG-Chi sponges forms a uniform flat structure.

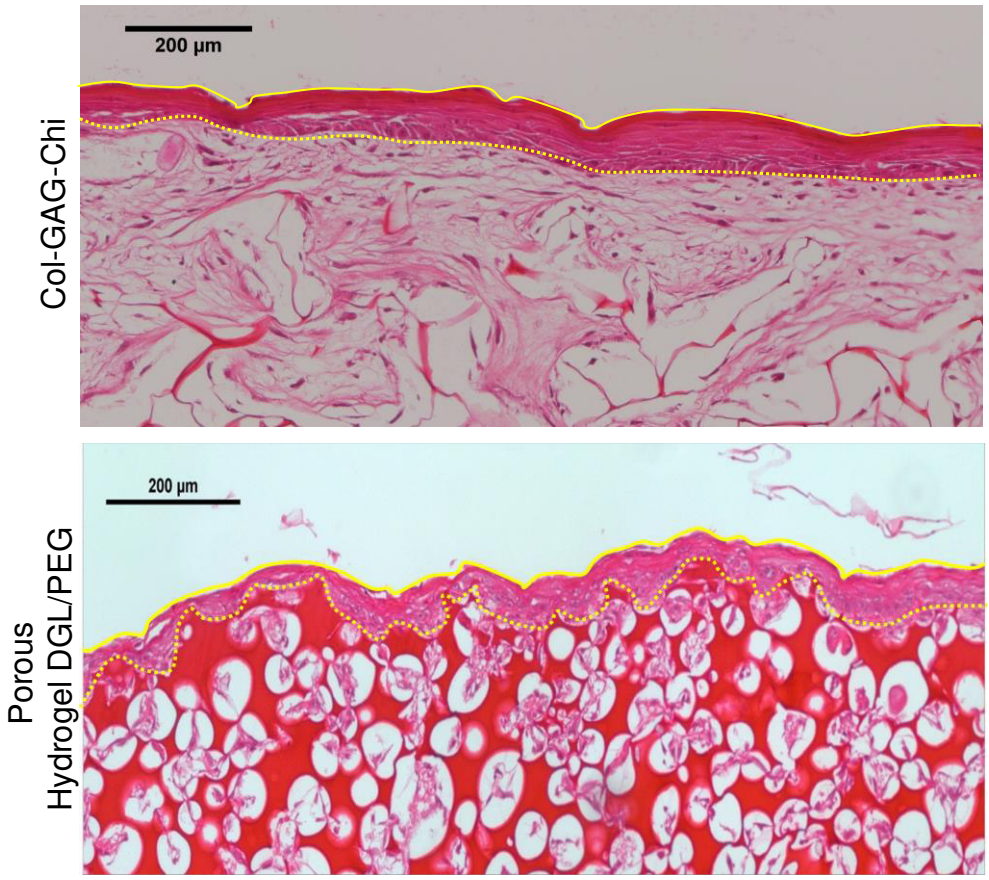

Figure 55. Mosaic H&E image of skin equivalents. *Yellow lines delimit the epidermal layer (scale bar 200 µm).*

To further characterize the formed epidermis, different markers of epidermal stratification and keratinocyte differentiation were evaluated. While proliferative cells are confined to the basal layer, daughter cells will steady migrate upwards and differentiate into subsequent epidermal layers. The presence of proliferative keratinocytes solely in this basal layer was demonstrated by the immunostaining of Ki67, a nuclear marker of cellular proliferation, as observed in Figure 56.A. Indeed, keratinocytes differentiation in the epidermis forms a well-organized multilayered structure. Keratinocyte terminal differentiation was evaluated as observed in Figure 56.B. As expected, cytokeratin 10 (K10) was present in all layers but the stratum basale, while involucrin (Inv) was observed in the intermediary layers and keratin 14 (K14), a marker of early differentiation, was

present only in the stratum basale. However, the epidermal layers of the skin equivalent obtained with DGL/PEG hydrogels were less defined compared to Col-GAG-Chi sponges and lacked the uppermost layer, the stratum corneum (SC). This can explain the difference in epidermis thickness of 8 µm observed between the porous DGL/PEG hydrogels and Col-GAG-Chi sponges. The SC could have been detached from the epidermis because of a less cohesive attachment or due to conditions that do not promote the formation of the SC. Of note, the air-liquid interphase period during culture was not performed in the most optimal conditions for the DGL/PEG hydrogels. During the air-lift interface protocol for Col-GAG-Chi sponges, samples are removed and placed over a gauze as observed in Figure 11 (see page 48), while skin equivalent performed in DGL/PEG porous hydrogels were maintained in the inserts even after air-lift interphase. Even though the volume of medium was reduced to avoid contact with the epidermal component, the hydrogels absorb a high amount of liquid and it was therefore difficult to completely avoid humidity inside the culture inserts that contained the hydrogels. It has been stated that the air-liquid interphase and serum depletion are important for a suitable cell differentiation since it allows a higher expression of high-molecular weight keratins, indicators of a complete differentiation [127]. Both media composition and volume should be fine-tuned for each specific substrate type, thickness, and porosity.

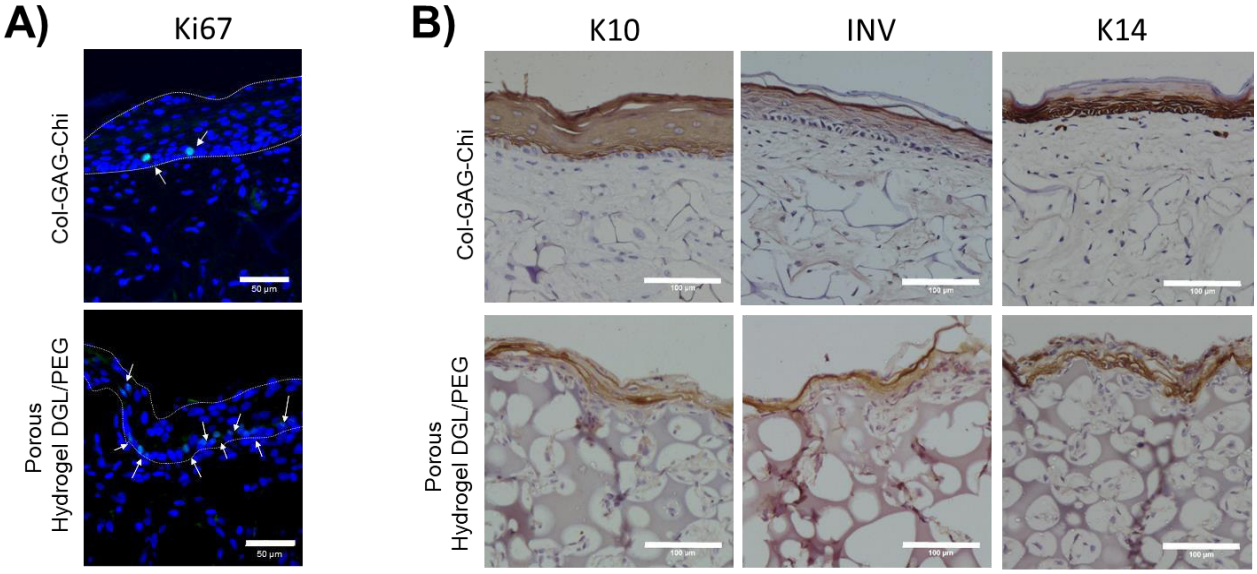

Figure 56. Epidermal stratification of skin equivalents. *A) Immunostaining of proliferative cells in the basal membrane. Ki67 positive cell in green, cell nucleus in blue (scale bar 50 µm). B) Immunostaining of markers of keratinocyte differentiation; Cytokeratin 10 (K10), Involucrin (Inv) and Keratin 14 (K14) (scale bar 100 µm).*

The epidermis layer is tightly bound to the underlying dermis layer via the basement membrane (BM) at the dermal-epidermal junction (DEJ) [43]. One key component of the BM is the laminin 332, which is essential for epidermal cell attachment [264]. As can be observed in Figure 57, laminin expression was greater in the first layers of the epidermis close to the DEJ. As expected, laminin was mainly observed in the epidermis since keratinocytes express and synthesize the majority of the basal membrane components [73]. However, laminin-332 is expected to be restricted to the DEJ and here it was observed in the whole viable epidermis, even with the Col-GAG-Chi model. It is possible that the specificity of the antibody was not adequate. A proper DEJ could also be evaluated by observing the expression of type VII collagen.

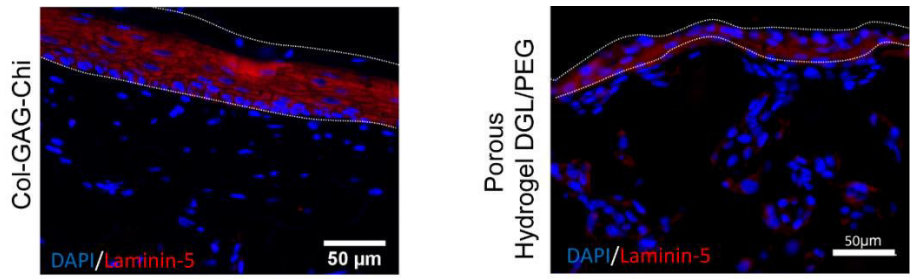

Figure 57. Expression of laminin-332 in skin equivalents. *Immunostaining of laminin-332 (also known as laminin-5) in red and cell nucleus counter stained with DAPI in blue (scale bar 50 µm).*

Critical evaluation and conclusion

The DGL/PEG hydrogel was able to promote dermal human fibroblasts infiltration by introducing interconnected pores within the hydrogel through the particle/leaching technique. The use of paraffin microspheres as porogens allowed to obtain a homogeneous porous structure. Optimal cellular infiltration was obtained with a mixture of 50-100 and 100-180 µm paraffin microspheres, probably due to a better interconnection between pores. Hydrogel mechanical properties could be modified in relation of the component's concentration, allowing to target different tissue rigidities. Once the hydrogels were rendered porous their mechanical properties were decreased in comparison to the bulk material, acquiring a three-dimensional matrix which mimics the mechanical properties reported for skin's indentation measurements *in vivo* [90,91]. After 21 days of culture, dermal human fibroblasts seeded on top of the porous hydrogels were able to infiltrate and homogeneously colonize the porous matrix. Moreover, once fibroblasts migrated within the hydrogel, they synthesized their own extracellular matrix since collagen synthesis was evidenced. Beside structure, native ECM is implicated in cell-ECM interaction regulating cell function and tissue formation [64]. Here, hydrogels can provide the main architecture while fibroblasts synthesized their own ECM components. Therefore, the resulting dermal equivalents composed of fibroblasts embedded in their own ECM within the hydrogel allowed the formation of a stratified epidermis with structure imitating the rete pegs and rete ridges observed in native skin. However, in comparison to a well-known model (Col-GAG-Chi) the layers of the epidermis were less defined and no evidence of a stratum corneum was observed. We hypothesized that difference between the models could be related not only to the material but to the cell culture process and a possible improper air-liquid interphase during the porous hydrogel culture. Of note, each protocol was performed with the same source of fibroblasts but in different laboratories following their specific handling procedures. However, a similar collagen synthesis was observed in both models, suggesting that keratinocytes seeded on top of the matrices are in contact with neosynthesized ECM in a similar manner. Overall, we have demonstrated the potential of the synthetic DGL/PEG hydrogel as a porous scaffold to promote tissue formation in three-dimensions. This system could further profit of biomimetic approaches by incorporating recombinant components inspired from the ECM.

Does the incorporation of an elastin-like polypeptide (ELP) improve the quality of the dermal equivalent by further mimicking the native ECM?

In the previous section, the potential of the porous DGL/PEG hydrogel as a support to guide cell growth in three-dimensions and to produce a dermal equivalent was demonstrated. Fibroblasts colonized the synthetic matrix and were able to fill the pores with neosynthesized type I collagen, supporting the formation of an epidermal layer. Whereas collagen is produced in abundance *in vitro*, production of elastin in tissue-engineered constructs is scarce [80]. Both are main components of the ECM and play an important role in its structure providing either the skin's tensile strength or elasticity [59]. Lack of elasticity has demonstrated to be a fundamental factor related to excessive scarring and wound contractions of skin engineered grafts, therefore, the introduction of the elasticity component with the use of native elastin derivatives, elastin-like peptides of synthetic elastomers has attracted great interest [79]. Contrary to collagen, the procurement of elastin from natural sources for tissue engineering applications is highly challenging [80,146]. However, the structure of tropoelastin can be easily reproduced by recombinant techniques, allowing to obtain a synthetic but biomimetic polypeptide. Elastin-like polypeptides (ELPs), synthesized through recombinant techniques, provide a controllable and well-defined source of polymer-based oligopeptide with sequences that recur in tropoelastin for tissue-engineered applications [31]. Several groups have evaluated the incorporation of ELPs in dermal substitutes to provide elasticity and to promote biological activity in a similar manner to native tropoelastin [31,265,266]. In this context, the incorporation of an 'in-house' ELP developed in our laboratory in the DGL/PEG hydrogels and the resulting dermal equivalents were evaluated. First, the interaction of ELP with the polymeric network and its contribution to the material properties were assessed. Moreover, biological activity of ELP was observed in two- and three-dimensions to determine if the sequences contained in the ELP and able to interact with the two major receptors of the native tropoelastin (EBP and $\alpha_v\beta_3$) are still available and have an effect when incorporated into the hydrogel. The association of the elastin component of the ECM to the synthetic matrix could improve the dermal equivalents and increase its potential for tissue engineering applications.

I. Hydrogel characterization

When incorporating the ELP to the hydrogel mixture, no apparent changes in crosslinking were observed. Self-standing hydrogels were swiftly obtained in a similar manner to hydrogels without the addition of ELP.

I.I. Mechanical and wetting properties

When crosslinked with genipin, ELP shows a highly elastic behavior, with a Young's modulus between 1.4-1.5 MPa [32]. Its incorporation to the hydrogel could then grant further elasticity properties to the DGL/PEG hydrogels. In order to assess the contribution of the ELP to the mechanical properties, two techniques were used. When the hydrogels were measured by micro indentation, an increase of the complex modulus with 3.75 mg/ml of ELP was observed (Figure 58.A). However, this effect was not concentration-dependent since no significant difference was observed when the ELP concentration was doubled.

On the contrary, hydrogels measured with dynamic mechanical analysis showed a slight decrease of the complex modulus in presence of ELP, albeit not significantly (Figure 58.B). While contradictory results were obtained concerning the effect of the ELP on mechanical properties, the complex modulus of hydrogels without ELP was in the same order of magnitude for micro-indentation and DMA: 58.9 ± 3.3 and 41.5 ± 5.0 kPa respectively.

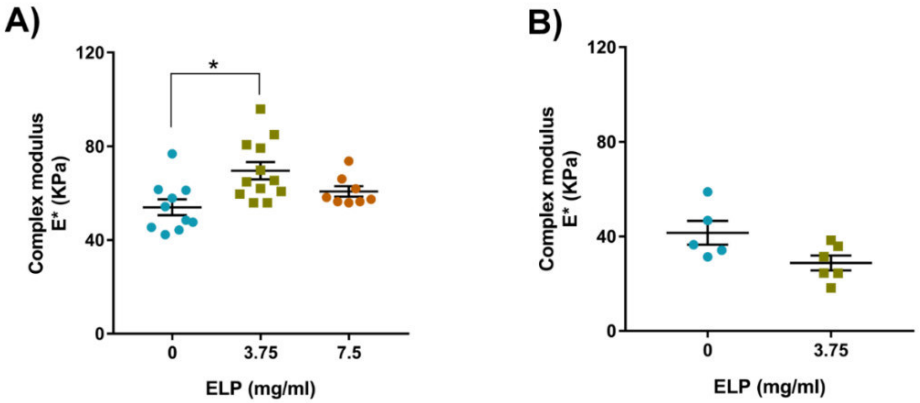

Figure 58. Effect of the ELP on the mechanical properties of the hydrogel (2 mM DGL/ 19 mM PEG). *A) Micro-indentation tests performed with an original light load indentation device as reported in* [104]*, in collaboration with the Ecole Centrale de Lyon. Indentation test was performed under normal load of 4 mN using a spherical steel probe of radius curvature r=1.59 mm and at a velocity of 20 µm/s (at least eight hydrogels per condition, One-Way ANOVA, Dunnett's multiple comparison test *p<0.05 compared to hydrogel w/o ELP). B) Dynamical Mechanical Analysis (DMA 242 E Artemis, NEZSTCH) by compression mode at room temperature under PBS immersion with a 10% strain and 60 µm of amplitude (five hydrogels per condition, t-student).*

The discrepancies observed between the two different measurement techniques can be probably related to their respective parameters. For instance, DMA measurements were performed in immersion, the hydrogels being then in a complete swollen state. Contrarily, micro-indentation tests were performed in air and the samples were therefore subjected to a greater adhesion phenomenon of the indentation probe and to evaporation during the measurement. Indeed, adhesion forces recorded during the indentation procedure clearly showed a higher negative pull-off adhesion recorded when the indenter was being retracted from the surface of ELP-containing hydrogels (Figure 59). Hydrogel with ELP therefore showed greater adhesion forces than hydrogels without ELP.

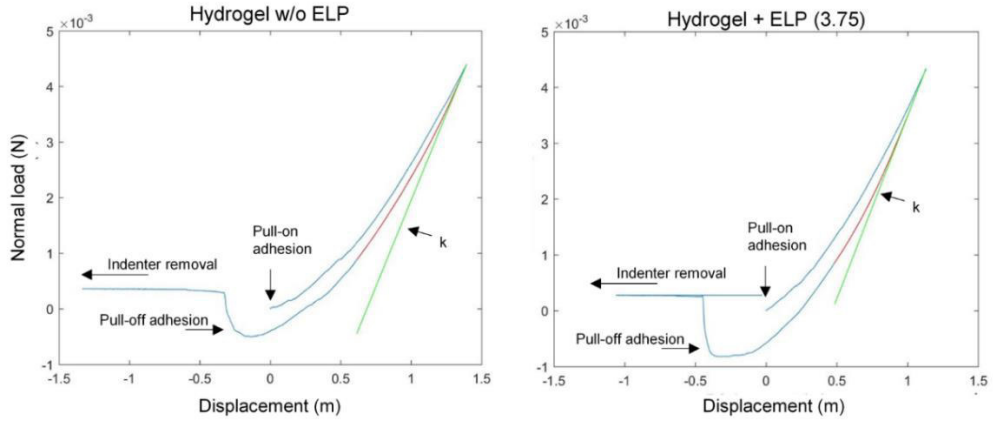

Figure 59. Comparison between representative curves obtained by micro indentation. *A) Representative curve of hydrogel 2 mM DGL and 19 mM PEG without ELP. B) Representative curve of hydrogel 2 mM DGL and 19 mM PEG with 3.75 mg/ml ELP. 4mN of normal load were applied at a constant speed of 20 µm/s with spherical indenter r=1.6 mm.*

The modification on the hydrogel surface properties in the presence of ELP was as well indicated by contact angle measurement. The ELP-containing hydrogels contact angle and hydrophobicity was slightly increased in a concentration manner, as observed in Figure 60. This is in good agreement with the physico-chemical properties of the ELP, as it is mainly composed of hydrophobic domains in a similar manner to native human tropoelastin [32]. Hui *et al*. stated that surface tension of materials such as gels could provide a resistance to deformation by indentation forces [267]. The increase in the hydrophobicity could therefore be related to the increase in adhesion forces observed in the micro-indentation measurements.

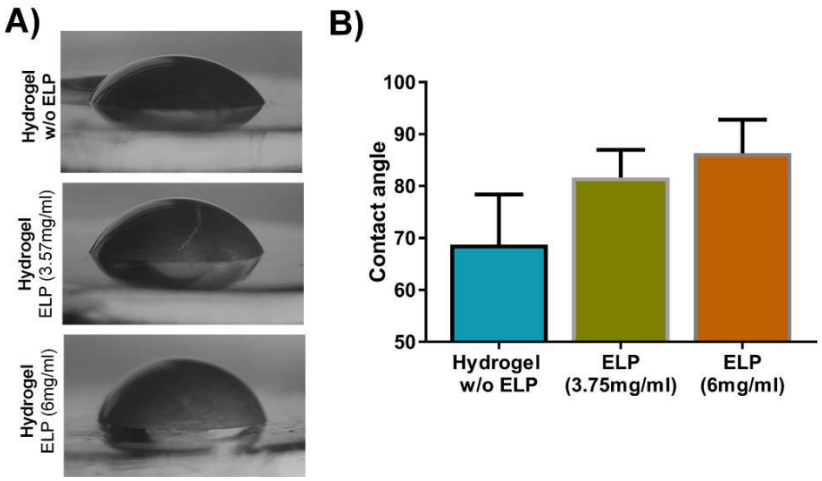

Figure 60. Contact angle at the surface of hydrogel coated coverslips with increasing concentrations of ELP measured by gionometry. *Image analysis performed with Imagej plugging "LB-ADSA" (at least three hydrogels per condition, One-Way ANOVA).*

Overall, the incorporation of ELP in the DGL/PEG hydrogels did not provide a significant and clear effect on the resulting mechanical properties of the matrices. However, the presence of the ELP was reflected in the modification of the hydrogel's hydrophobicity. The lack of mechanical effect of the ELP suggests that the recombinant protein might not be integrated in the hydrogel polymer mesh. To assess this hypothesis, nuclear magnetic resonance (NMR) studies were performed.

I.II. ELP interaction with the polymeric network

NMR is a highly sensitive method that provides detailed information of the structure and chemical environment of molecules. When placed in a powerful magnetic field it is possible to measure the interactions of the nuclear spin of atoms such as ^{13}C and ^{1}H. Since the chemical shift of a nuclei is determined by the electron density surrounding it, if a new covalent bond is formed the electron density surrounding a specific nucleus will change, leading to a chemical shift perturbation [236]. Therefore, this technique allows to determine if the ELP is incorporated into the polymeric network through a covalent bond. NMR was recorded using insensitive nuclei enhanced by polarization transfer (INEPT) spectra as this type of transfer allows to enhance the signal resolution, increase ^{13}C sensibility and provide excellent selectivity [237].

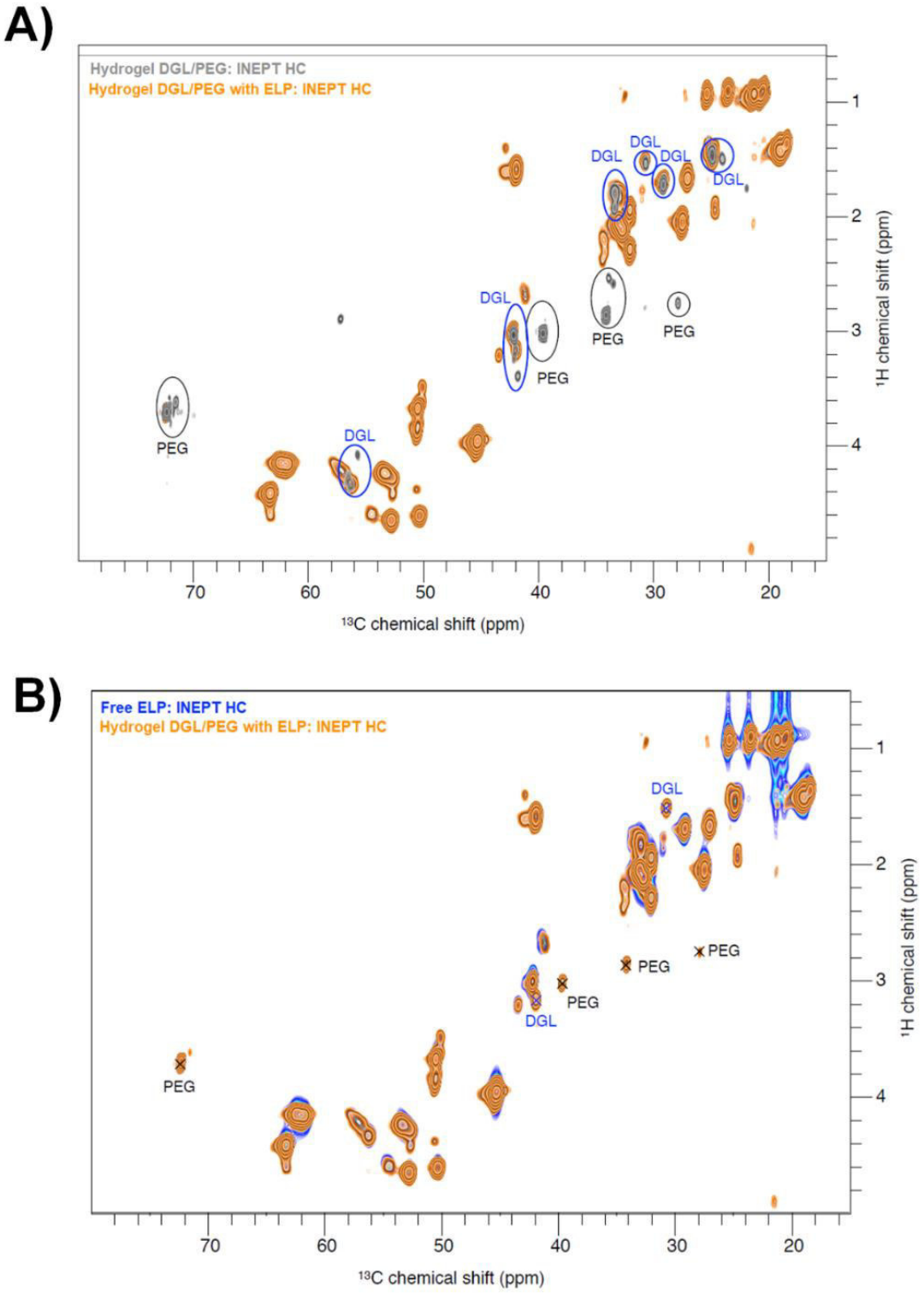

Figure 61. NMR spectrum of free ^{13}C-^{15}N ELP and hydrogel with and without ^{13}C-^{15}N ELP. *A) Overlay of INEPT spectra of DGL/PEG hydrogel without ^{13}C-^{15}N-ELP (in grey) and of hydrogel with ^{13}C-^{15}N-ELP (1.75mg) (in orange). The hydrogel is observed in natural abundance, and the NMR resonances corresponding to DGL and PEG are circled. B) Overlay of INEPT spectra of free ^{13}C-^{15}N-ELR (20 mg) (in blue) and in presence of hydrogel (in orange). Results obtained in collaboration with the group of Protein Solid State NMR, UMR 5086, MMSB.*

The comparison of both hydrogel spectra with and without ELP allowed to identify the resonances coming from the DGL and PEG molecules (Figure 61.A). No changes in chemical shift were observed when the hydrogel was in presence of ELP, suggesting no intermolecular interactions. This was further confirmed by the perfect overlay of the spectrum of the free ELP with the spectrum of hydrogel with ELP (Figure 61.B), which means that there were no chemical shift perturbations induced in the ELP when incorporated into the hydrogel, and therefore that there is no covalent binding between the protein and the polymeric network of the hydrogel. In addition, the intensity of signals in INEPT spectra indicate that the free ELP is highly flexible, and that it remains highly flexible when incorporated into the hydrogel. *In vivo*, within the crosslinked structures of mature elastin, the tropoelastin moieties are quite flexible and show an elastic behavior [80].

I.III. Preliminary assessment of ELP embedding

NMR analysis demonstrated that the ELP is not bound to the polymeric network though a covalent bond. To determine if the ELP stayed embedded in the hydrogel after crosslinking, hydrogels with or without ELP were submerged in PBS for 24 hours at 37°C and the presence of ELP in the supernatant was observed by western blot. While ELP was detected at around 55 kDa for the control solutions, the lack of detection bands when ELP was incorporated into the hydrogel suggests that ELP remains embedded in the hydrogel after its crosslinking (Figure 62).

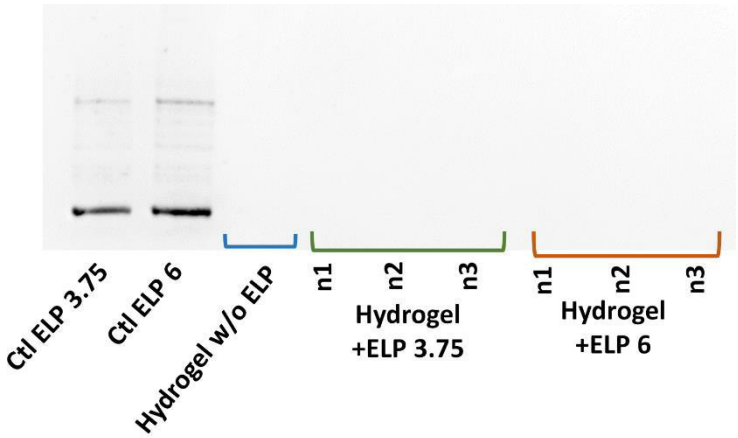

Figure 62. Western blot detection of ELP released after 24 hours incubation in PBS at 37°C. *Hydrogel composition 2 mM DGL and 19 mM PEG with or without ELP (3.75 and 6 mg/ml). For controls the same quantity of ELP was incubated in PBS at 37°C without hydrogel.*

II. Effect of ELP on the behavior of dermal human fibroblasts in two-dimensions

Although the ELP does not appear to be integrated in the hydrogel polymer network covalently, its integration in the hydrogel bulk still induces modification of its hydrophobicity. Combined with the presence of cell-interacting motifs in its primary sequence via $\alpha_v\beta_3$ integrin and EBP, the presence of ELP could modify the way the hydrogel interacts with cells. To assess this, the effect on cell behavior when the ELP is incorporated in the hydrogel was first assessed in two-dimensions. by seeding. The effect of ELP on cell adhesion, morphology, proliferation and migration of fibroblasts seeded on top of dense hydrogels prepared directly in tissue culture plate or on top of coverslips was evaluated.

II.I. Effect of ELP on cell adhesion, morphology and proliferation

Cell activity of fibroblasts seeded on top of dense hydrogels was measured after 24 hours with alamar blue. As observed in Figure 63.A, fluorescence signal was increased when ELP was incorporated into the hydrogels, indicating a greater amount of metabolically active cells on the surface of hydrogels with ELP. This could suggest that a greater number of cells were able to adhere to the surface of hydrogels with ELP. A similar effect was observed by phase-contrast microscopy (Figure 63.B), cell number was increased 1.3-folds and 1.2-folds 24 hours post-seeding with 3.75 mg/ml and 6 mg/ml of ELP, respectively. Concomitantly, cells seeded onto hydrogels with ELP showed a higher spreading area, with a more spindle shaped morphology since circularity was decreased and Feret diameter increased in comparison to hydrogels without ELP (Figure 63.C). However, no further differences were observed with an increase of the ELP concentration. The effect of the ELP appears to be noticeable only at early time points, suggesting an effect in the early adhesion of fibroblasts to the surface of the hydrogels. This effect could be related to an increase of anchoring sites for the cells linked to the presence of ELP, which do not impact cell morphology at longer culture time points. Two of the bioactive domain of the native tropoelastin are present in the ELP, the C-terminal GRKRK and the hydrophobic repeated unity VGVAPG [32]. These sequences are known to interact with $\alpha_v\beta_3$ integrin and the EBP, respectively [73]. Previous studies in our group showed that plastic-coated surfaces with this ELP

increased fibroblast adherence and that this effect was related to the contribution of the motifs VGVAPG and GRKRK of the ELP. When inhibitors for either $\alpha_v\beta_3$ integrin and EBP were added, cell adhesion was decreased a 50% and 78%, respectively [32]. It is therefore likely that some molecules of the ELP are available at the surface of the hydrogels, enhancing cell adhesion.

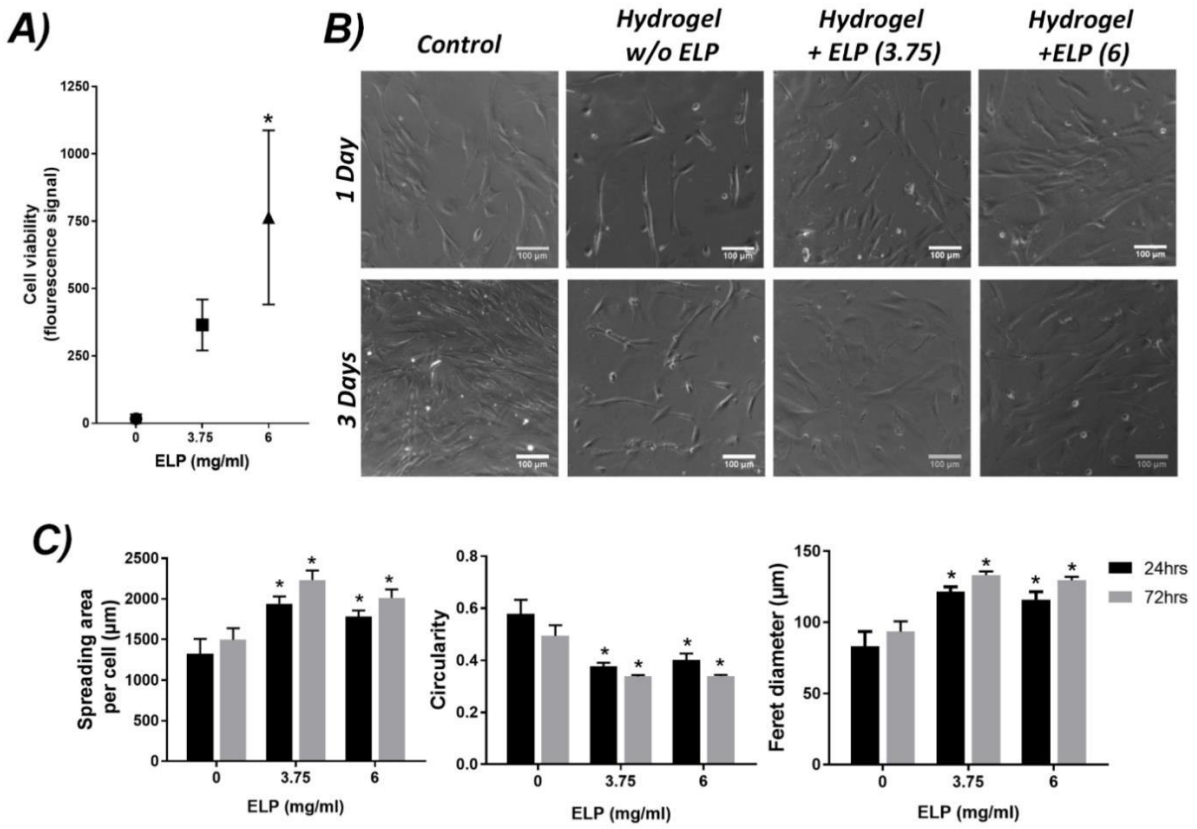

Figure 63. Dermal human fibroblast adhesion and morphology when cultured on the surface of hydrogels (2 mM DGL and 19 mM PEG) with different concentrations of ELP (0, 3.75 and 6 mg/ml). *A) Fluorescence signal obtained from metabolic assay, alamar blue, after 24 hours of cell seeding on hydrogels prepared directly in cell plate. (four hydrogels per condition, one-way ANOVA, Dunnett's multiple comparisons test *p<0.05 compared to hydrogel w/o ELP). B) Phase contrast images after 24 hours and 72 hours of cell seeding, cell number was counted of ten randomly acquired images per sample of at least five hydrogels per condition (scale bar 100 µm). C) Morphology parameters obtained from images analysis of phase contrast photos: spreading area per cell, circularity and ferret diameter (four hydrogels per condition, one-way ANOVA, p<0.05, * compared to plastic control at 24 hours).*

Since Tajima *et al*. demonstrated that the same motif implicated in cell adhesion (VGVAPG) was able to stimulate fibroblast proliferation [33], the effect of ELP when incorporated into the hydrogel on cell proliferation was evaluated by measuring the percentage of proliferative cells (ki67 positive cells). As observed in Figure 64.B, a slight increase in the number of proliferative cells could be observed when ELP was incorporated to the hydrogels, albeit not significantly. It is important

to mention that while cells seeded in plastic controls could be easily distinguished during images analysis, hydrogel autofluorescence rendered the determination of Ki67 and nucleus staining co-localization a difficult and unreliable task.

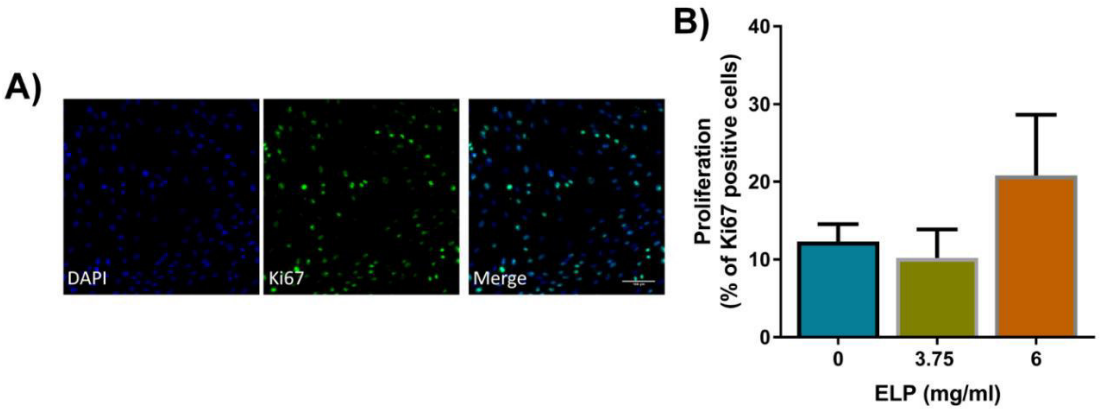

Figure 64. Effect of the ELP on cellular proliferation of fibroblasts seeded on top of hydrogels with or without ELP. *A) Representative image of immunofluorescence of Ki67 in green and nuclei counter-staining with DAPI in blue of cell seeded in plastic controls. B) Percentage of ki67 positive cell after 3 days of seeding fibroblasts on top of hydrogels with or without ELP (one-way ANOVA, at least three hydrogels per conditions).*

II.II. Effect of ELP on human dermal fibroblasts migration

Aside from adhesion and proliferation, an increase in anchoring sites on the hydrogels could also be reflected on cell migration. Therefore, the movement of fibroblasts seeded on top of hydrogels without or with ELP was followed for 16 hours by time-lapse microscopy. As observed in Figure 65.A, fibroblasts seeded on hydrogels with 3.75 mg/ml of ELP traveled longer distances in comparison to cells seeded on ELP-free hydrogels. Mean cell migration, expressed as the slope of the accumulated distance traveled by fibroblasts, was statistically increased in the presence of ELP (Figure 65.B).

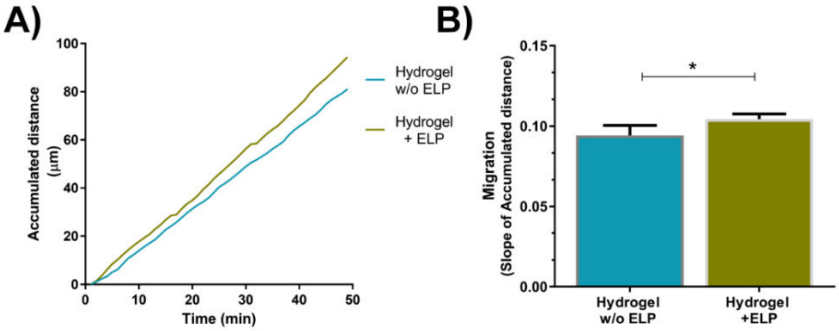

Figure 65. Dermal fibroblast migration followed by a 16-hour time-lapse.
*A) Representative image of accumulated distance travel by cell seeded on top hydrogels (2 mM DGL/19 mM PEG) without or with ELP (3.75 mg/ml). B) Migration expressed as the mean slope of the accumulated distance of at least 5 cells per hydrogel (four hydrogels per condition, t-student *p<0.05).*

III. Effect of the ELP on the behavior of dermal human fibroblasts in three-dimensions as dermal equivalents

Reports on elastin expression in full-thickness models are scarce. However, elastin plays a fundamental role in the ECM, by providing the skin with its elasticity and promoting several biological activities. The incorporation of elastin or elastin-based peptides into scaffolds to mimic the natural elasticity of the skin is an attractive alternative to avoid contraction and fibrosis [79]. While the ELP use in this study has elastic properties by itself, once incorporated into the DGL/PEG hydrogel it did not have a significant impact on the mechanical properties of the hydrogel. However, the biological activities observed in two-dimensions could nevertheless have a positive impact on the dermal equivalents obtained. Therefore, the effect of ELP in 3D porous hydrogels to obtain dermal equivalents was evaluated.

III.I. Matrix contraction

A common setback of collagen matrices is fibroblast-mediated contraction [148]. To evaluate the resistance of our scaffolds against fibroblasts-mediated contraction and the impact of the ELP in this contraction, fibroblasts were seeded on the surface of porous DGL/PEG hydrogels (±ELP) and on collagen gels as positive controls, and the percentage of contraction over culture time was measured. The original area considered as 100% was measured immediately after cell seeding. Unlike collagen gels, in which fibroblasts caused an important contraction, colonized DGL/PEG hydrogels with or without ELP showed significantly less shrinkage after only 2 days of culture (Figure 66). Although no difference could be measured between hydrogel compositions, the lack of contraction in the DGL/PEG porous structures is noteworthy. Indeed, contraction of collagen gels is swift (in the first 12 hours) and characterized by an exponential rate until reaching a constant value [29]. As a result, contraction can reduce the efficacy and grafting potential of a scaffold and may result in severe wound contraction, tissue immobility, loss of function and fibrosis *in vivo*. Minimizing contraction, limits the possibilities of scar formation after healing [148]. Moreover contraction *in vitro*, impedes the standardization of full-thickness models, limiting their use as reliable tools for toxicity studies [13].

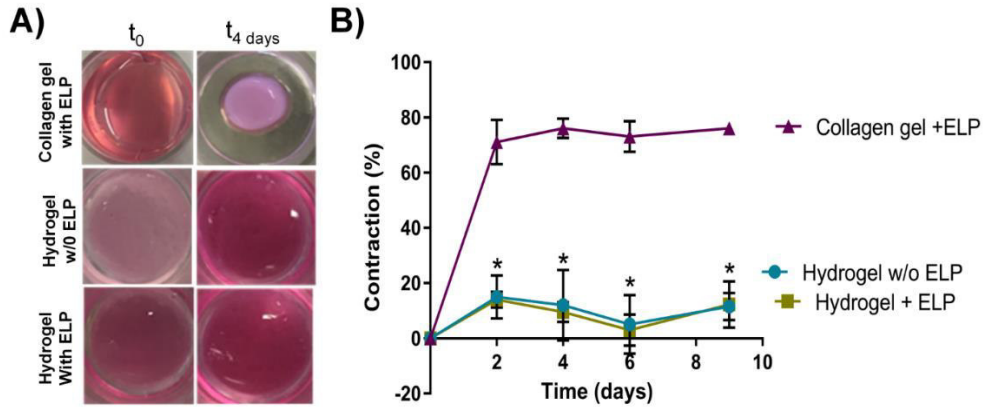

Figure 66. In vitro contraction percentage of porous hydrogels. *Photographs were taken right after cell seeding and on days 2, 4, 6 and 9. Percentage of contraction is expressed as the area of any given time compared to the area immediately after seeding (t0). Collagen gels (2.5mg/ml) were used as contraction controls, fibroblasts were seeded in the surface of collagen similarly to DGL/PEG hydrogels (composition 2 mM DGL and 19 mM PEG) with or without ELP (3.75 mg/ml) (two-way ANOVA, *p<0.05, four gels for each condition).*

III.II. Effect of ELP in cell density and cellular infiltration

Interestingly, fibroblasts seeded on the surface of porous DGL/PEG hydrogel with ELP were able to infiltrate further into the porous matrix. After 14 days of culture, we could observe a mild improvement of fibroblast colonization in the presence of 6 mg/ml of ELP, while no difference was observed at lower ELP concentration (Figure 67). Contrarily to cell migration in two-dimensions, greater amounts of ELP were necessary to observe an increase in three-dimensions. Since surface area in porous hydrogels is increased compared to dense hydrogels, it is possible that some ELP is more easily lost during the production process. The release profile of the ELP in the porous hydrogel could clarify the discrepancy of biological effects observed.

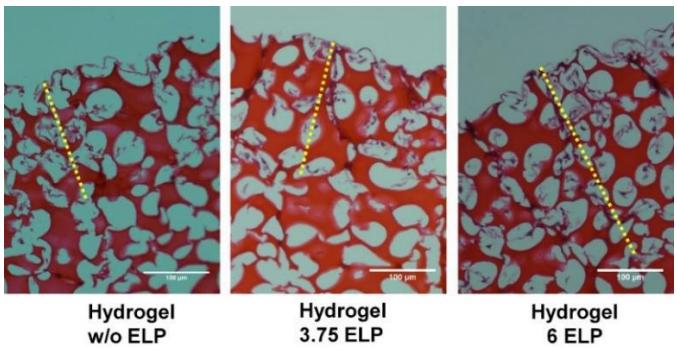

Figure 67. Hematoxylin and Eosin staining of porous hydrogels after 14 days of cell culture. *Infiltration of fibroblasts seeded in the surface of porous hydrogels (composition 2/19 mM DGL/PEG) with increasing concentrations of ELP (3.75 and 6 mg/ml). Yellow line marks maximal distance traveled by human dermal fibroblasts (scale bar 100 µm).*

After 21 days of culture, cell infiltration and cell density in fibroblast-colonized porous hydrogels with or without 6 mg/ml ELP were evaluated. While the effect of ELP incorporation in the hydrogels on cellular proliferation was unclear in two-dimensions, a strong effect on cellular proliferation was visible in a three-dimensional porous environment. As presented in Figure 68.B, cell density in porous hydrogels with ELP was increased up to 137% (770.1 ± 38.12 fibroblasts/mm^2 compared to 351.1 ± 59.8 fibroblasts/mm^2). Although Miller *et al*. estimated that cell density of normal human dermis is comprised between 2000 and 4000 cells/mm^3 [268], we could not infer a volumetric value for our system, due to the limitations of image analysis of the hydrogels cross sections. Another potential technique to measure cell density in the scaffolds could have been to measure DNA content after cell culture. However, DGL strongly binds with nucleic acids through electrostatic interactions, producing inaccurate quantitative results (see Annexes page 177 for more information).

Furthermore, as shown in Figure 68.A, after 21 days of cell culture, fibroblasts in hydrogels with ELP (6 mg/ml) were able to reach further inside the porous structure: median distance of 314.2 ± 36.11 µm, twice more than fibroblasts in hydrogels without ELP (Figure 68.C). The maximal distance attained by the fibroblasts was 1062 ± 36.9 µm, as compared to 745.7± 163.2 µm for the hydrogels without ELP. In comparison, when seeded on top of collagen matrices, fibroblasts have shown to migrate up to 400 µm since cells need to remodel the collagen network to migrate [269,270].

These results demonstrate that the presence of ELP promotes cellular colonization of the porous scaffold. The sequences of the ELP that interact with fibroblasts $\alpha_v\beta_3$ integrin or the EBP might be accessible along the large porous surface area. However, it is not possible to distinguish between the contribution on cell migration, adhesion or/and proliferation. In a similar manner to fibroblasts seeded in two-dimensions, ELP showed a positive impact in cell migration observed by the distance travelled by fibroblasts. Nevertheless, an increase in cell density also suggests an increase in cell proliferation. While not statistically, a slight increase in cell proliferation was observed in two-dimensions when 6 mg/ml of ELP was introduced to the hydrogel. However, the increase in cell density could also be related to an increase in cell adhesion at early time points in cell culture. In this case, if an increase in migration did not play a role in cell colonization, we would observe only an increase in cell number in the surface of the hydrogels and not

necessary throughout the hydrogel. To identify the contribution of cell adhesion, migration or proliferation in the porous hydrogel colonization more clearly it would be interesting to follow cellular infiltration through time.

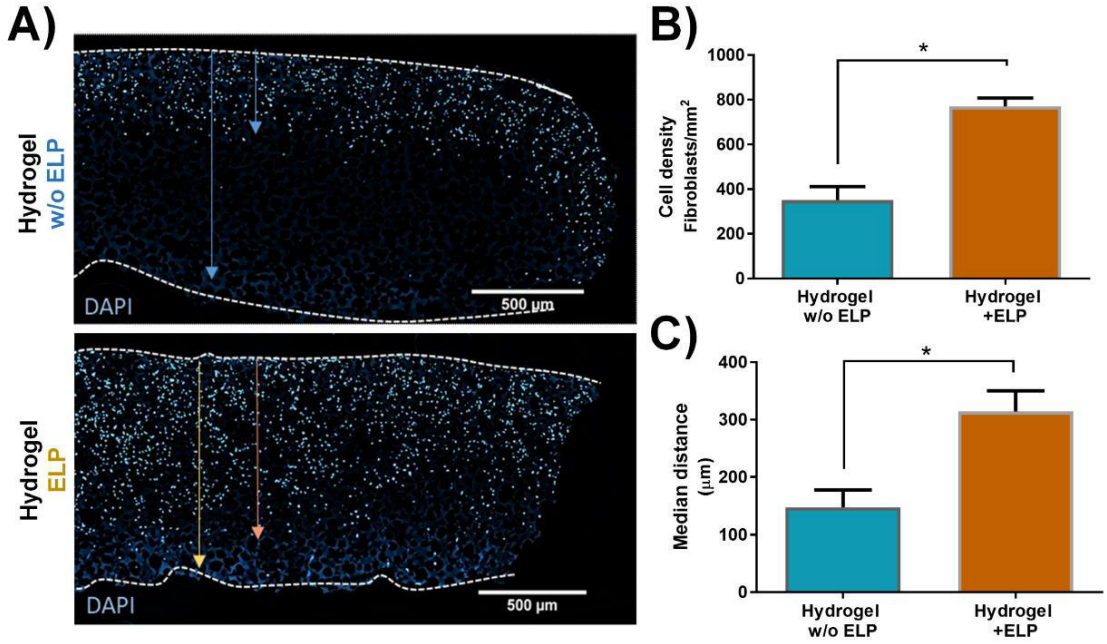

Figure 68. Cell density and infiltration after 21 days of cell culture in porous hydrogels (2/19 mM DGL/PEG) with or without ELP (6 mg/ml). *A) Representative images of hydrogel cross sections used for quantification. Cells nuclei are stained with DAPI (blue), white lines denote the upper and lower surfaces of the hydrogels and arrows stand for the total depth of the hydrogel and the maximal distance traveled by the fibroblasts. B) Cell density obtained from image analysis, by counting cell nuclei in several slides of at least three slides per hydrogel and three hydrogels per condition. B) Median distance traveled by human dermal fibroblasts after being seeded on the surface of the hydrogel obtained by image analysis (three hydrogels per condition, t-student, *p< 0.05).*

III.III. Effect of the ELP on the synthesis of the extracellular matrix in dermal equivalents

In the context of improving the dermal equivalents obtained with the porous DGL/PEG hydrogels, the synthesis of different ECM components by fibroblasts seeded on the porous hydrogels with or without ELP was evaluated by immunohistochemical staining (IHC) and gene expression.

As observed in Figure 69.A, a greater expression of type I collagen was observed when fibroblasts were seeded and cultured for 21 days in porous hydrogels with ELP. However, when fluorescence intensity was normalized to the number of cells in each image, no significant difference was observed between both conditions (Figure 69.B). Similarly, no significant difference was observed

when comparing the type I collagen gene expression after 21 days of cell culture (Figure 69.C).

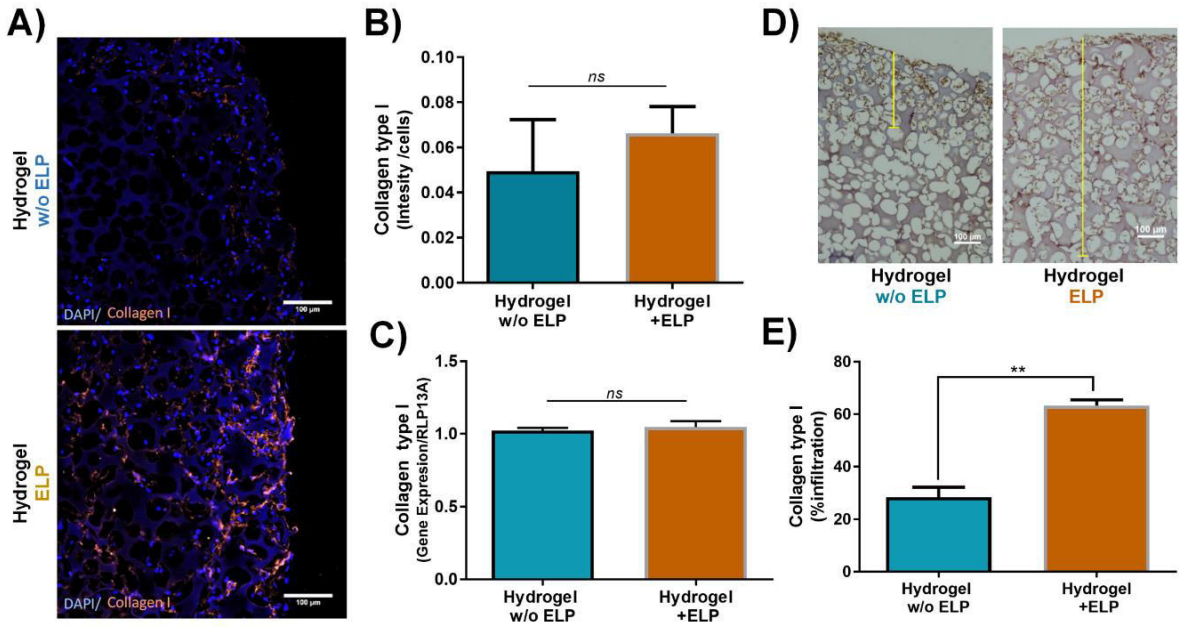

Figure 69. Synthesis of type I collagen by fibroblasts seeded in porous hydrogels (2/19 mM DGL/PEG) with or without ELP (6 mg/ml) after 21 days of culture. *A) Representative image of IHC detection of type I collagen (red) with immunofluorescence and cells nuclei with DAPI counterstaining (blue). B) Type I collagen intensity obtained from image analysis of immunofluorescence images normalized by the total number of cells per image (three hydrogels per condition, t-student). C) Type I collagen gene expression after 21 days of culture obtained from qPCR (normalized to RL13A gene expression, t-student, *p<0.05, three hydrogels per condition). D) IHC detection of type I collagen using brown precipitating HRP substrate DAB. Yellow lines denote the range of collagen type I staining (scale bar 100 µm) E) Percentage of collagen infiltration in relation to the total hydrogel thickness, obtained by image analysis of IHC (three hydrogels per condition, t-student, *p<0.05).*

While collagen synthesis was not increased, we did observed a greater quantity of type I collagen deposited and a deeper presence of type I collagen inside the hydrogel with ELP (Figure 69.D). Collagen could be found at a 63.2 ± 2.1 % of the hydrogel thickness compared to 28.4 ± 3.7 % in hydrogels without ELP (Figure 69.E). This result is in good agreement with the cellular infiltration shown previously and possibly indicates that cellular infiltration occurred at early time points, allowing the fibroblasts that had migrated deeper into the hydrogel to synthesize collagen.

While the amount of collagen produced by the cultured cells *in vitro* is abundant, the amount of elastin is limited [76]. Elastin-based scaffolds have demonstrated an elastogenic potential by stimulating elastin synthesis [80]. However, few granular and randomly scattered staining of elastin were observed

in both porous systems, with no visual enhancement when ELP is present in the hydrogel (Figure 70.A). Similarly, no statistical difference was observed for elastin gene expression (Figure 70.B). This is disappointing, as Tajima *et al*. demonstrated that the peptide VGVAPG not only stimulates fibroblasts proliferation, but also has an effect on elastin expression [33]. Since the elastin synthesis is scarce, the effect of the ELP might not be noticeable. Nevertheless, the low expression of elastin in the DGL/PEG porous hydrogels is of interest in the context of skin equivalents production. Expression of elastin in skin equivalents is nearly exclusive of skin models cultured with collagen-chitosan-glycosaminoglycan matrix, and the formation of fibers is then solely visible after co-culture with keratinocytes in air-lift [126,271]. In a similar manner, Mewes *et al*. was able to observe the gene expression of elastin only after keratinocytes were seeded on top of the collagen dermal equivalent [271]. An improvement of elastin synthesis with ELP could be better evidenced once keratinocytes were seeded on the dermal equivalents.

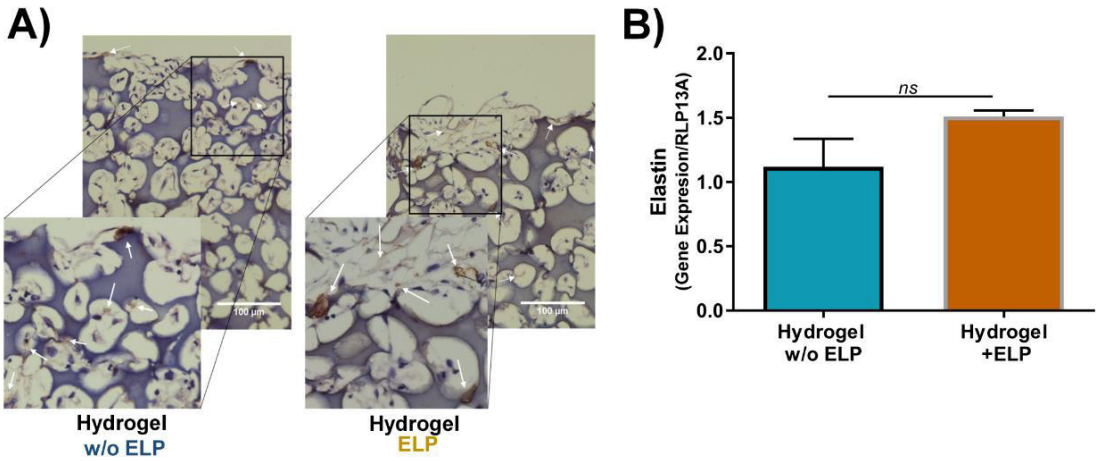

Figure 70. Synthesis of elastin by fibroblasts seeded on porous hydrogels (2/19 mM DGL/PEG) with or without ELP (6 mg/ml), after 21 days of culture. *A) IHC detection of elastin using brown precipitating HRP substrate DAB (scale bar 100 µm) and magnification of the images to allow better observation. Arrows indicate elastin staining. B) Elastin gene expression after 21 days of culture obtained from qPCR normalized to RL13A gene expression (three hydrogels per condition, t-student, *p<0.05).*

A third important and abundant component of the skin ECM that plays a critical role in matrix organization and stability specially during wound healing is fibronectin [65]. Also, *in vitro* studies revealed that fibronectin is required for the deposition of type I collagen and other structural proteins [65]. As observed in Figure 71.A, fibronectin was expressed in greater abundance after 21 days of culture in the upper part of the dermal equivalent, which corresponds to its physiological location. In skin, fibronectin is principally found in the dermo-

epidermal junction and papillary dermis, where it has an important role in keratinocytes attachment to the dermal compartment [148]. IHC images suggest that a greater quantity of fibronectin was present in the ELP-containing hydrogels. However, when the signal intensity was normalized to the number of cells, a significant increase in fibronectin synthesis was measured for hydrogels without ELP (Figure 71.B). Lorion *et al*. demonstrated that DGL induces α5β1 integrin in fibroblasts [27]. This integrin is known to bound to fibronectin with a positive feedback loop for fibronectin assembly [272]. Indeed, the presence of DGL may indirectly induce fibronectin expression. However, surprisingly no correlated difference in fibronectin gene expression could be detected (Figure 71.C). During tissue remodeling fibronectin and fibrin are the first proteins produced by the fibroblasts to remodel the extracellular matrix [273]. For instance, Bouvard *et al*. detected fibronectin in dermal equivalents as early as 4 days [274]. It is therefore possible that the increase in fibronectin synthesis occurred at earlier time points and that fibronectin gene expression was normalized after 21 days.

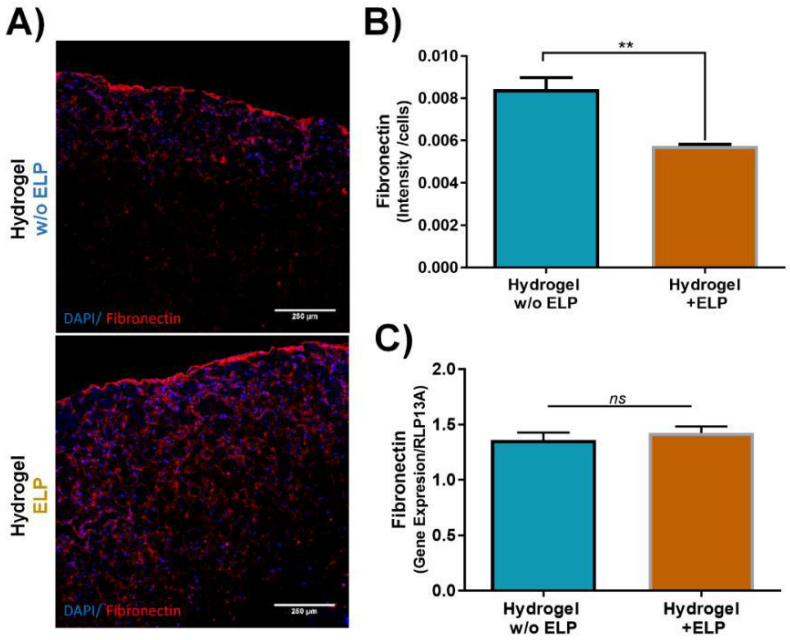

Figure 71. Synthesis of fibronectin by fibroblasts seeded on porous hydrogels (2/19 mM DGL/PEG) with or without ELP (6 mg/ml) after 21 days of culture.
*A) IHC detection of fibronectin (red) by fluorescence detection and cells nuclei by DAPI counterstaining (blue). B) Fibronectin intensity obtained from image analysis of IHC images normalized by the number of cells (three hydrogels per condition, t-student *p<0.05). C) Fibronectin gene expression after 21 days of culture obtained from qPCR normalized to RL13A gene expression (three hydrogels per condition, t-student).*

III.IV. Mechanical evolution of dermal equivalents over time

The contribution of the neosynthesized ECM to the mechanical properties of the dermal equivalents was measured by dynamic mechanical analysis (DMA), comparing the mechanical behavior of colonized-hydrogels after 15 and 22 days of culture to acellular matrices at 10 Hz, in the physiological frequency range [103]. As depicted in Figure 72.A, the complex modulus increased in a time dependent manner, hydrogel rigidity was increased from 17.0±3.1 to 56.5±6.5 for hydrogel without ELP and from 18.9±3.3 kPa 49.7±6.3 kPa for hydrogel with ELP after 22 days of cell culture. This increase was due only to an increase of the storage modulus (Figure 72.B), while the loss modulus was maintained constant even after 22 days of cell culture. The fibroblasts might therefore introduce an elastic component to the mechanical behavior of the materials by migrating into the porous structure and by filling the pores with neosynthesized ECM. Likewise, Rolin *et al* showed an increase in rigidity of 22% between dermal equivalents obtained with acellular 3D polyester matrices [259] while Pailler-Mattei *et al*. observed a significant effect on the rheological behavior of dermal equivalents compared to collagen-glycosaminoglycan-chitosan scaffolds alone, the cellular component increased by 2-folds the mechanical properties [233]. In the case of the DGL/PEG porous hydrogels mechanical properties were increased around 3-fold after 22 days in comparison to the acellular matrix.

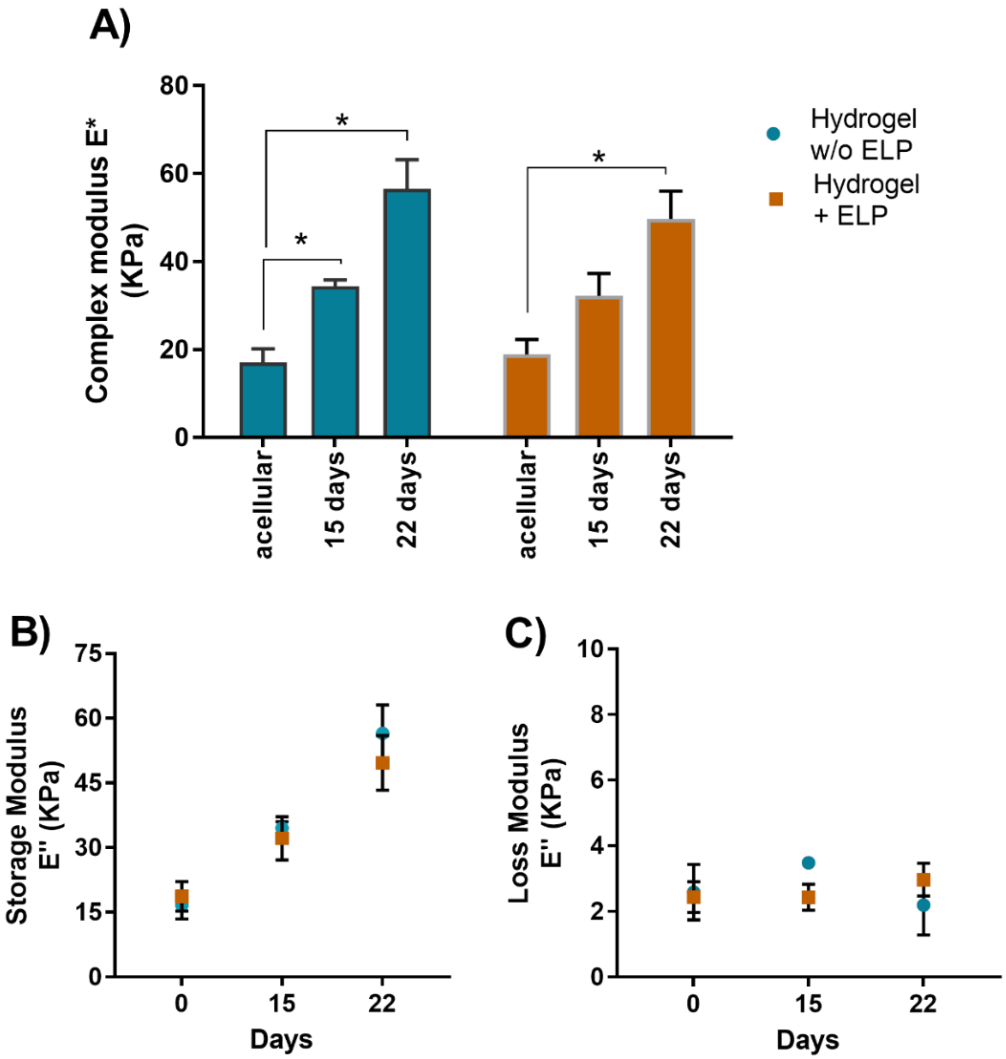

Figure 72. Mechanical evolution of colonized hydrogels obtained by dynamic mechanical analysis with a penetration probe (3 mm). *Measurements were performed at 37°C under immersion in DMEM-F12 medium with a 10% strain, 60 µm of amplitude at 10 Hz. Acellular hydrogels (0 days) were measured in the same conditions before sterilization and cell seeding. A) Complex modulus, B) Storage modulus and C) Loss modulus (at least three hydrogels per condition, two-Way ANOVA Turkey's comparison test *p<0.05).*

III.V. Dynamical remodeling of the neosynthesized extracellular matrix

In the course of wound healing, fibroblasts produce matrix metalloproteinases (MMPs) to control the remodeling of the newly formed granulation tissue [19]. More specifically, MMP-2 is able to degrade different types of collagens, gelatin, elastin, fibronectin, vitronectin, to name a few proteins [275]. The activity of gelatinases A and B secreted by dermal fibroblasts seeded on porous DGL/PEG hydrogels with or without ELP was observed by zymography of serum-free culture medium. Bands at 72 and 66kDa of gelatinase A were detected, corresponding respectively to pro MMP-2 and activate MMP-2 (Figure 73.A). No

bands at 92 and 88kDa, corresponding to gelatinase B (MMP-9) forms, were observed except for the HT1080 (human fibrosarcoma cell line) conditioned medium used as control. Contrary to primary cell lines, cancerous fibroblasts are able to produce MMP-9 besides MMP-2. As can be observed in Figure 73.B, a great majority of the pro-peptides synthesized by the fibroblast in the DGL/PEG porous hydrogels remained inactive. No significant difference was observed between conditions with or without ELP. In a similar fashion, no bands corresponding to gelatinase B were observed when fibroblasts were seeded on collagen lattices, however, the ratio of activated and pro-form MMP-2 was greater than one [270,276]. Scott *et al*. showed that MMPs pay an important role in fibroblast-mediated contraction of collagen lattices. When fibroblasts are seeded on top of collagen matrices, instead of embedded into them, collagen hydrolysis is necessary for cells to penetrate the network, which results in the activity of collagenase 1 (MMP-1) and gelatinase A (MMP-2) [270]. In our case, fibroblasts seeded on top of porous hydrogels do not need to degrade the matrix to penetrate into the porous structure, which is neither subjected to contraction forces.

Elastin peptides have been reported to have a role in MMP-2 stimulation in tumor invasion and metastasis [277,278], which Toupance *et al*. suggested is not mediated by EBP nor $\alpha_v\beta_3$ integrin but rather by a fourth receptor poorly described which binds to peptides AGVPGFGAG and AGVPGLGAG of tropoelastin [279]. Landeau *et al*. reported an enhancement in MMP-2 secretion when culturing fibroblasts with soluble elastin (k-elastin) [280]. However, the ELP incorporated into the porous hydrogels only possess the sequences VGVAPG and GRKRK that interact with the EBP and integrin $\alpha_v\beta_3$ [32], which could explain why no difference was observed in the hydrogels with ELP.

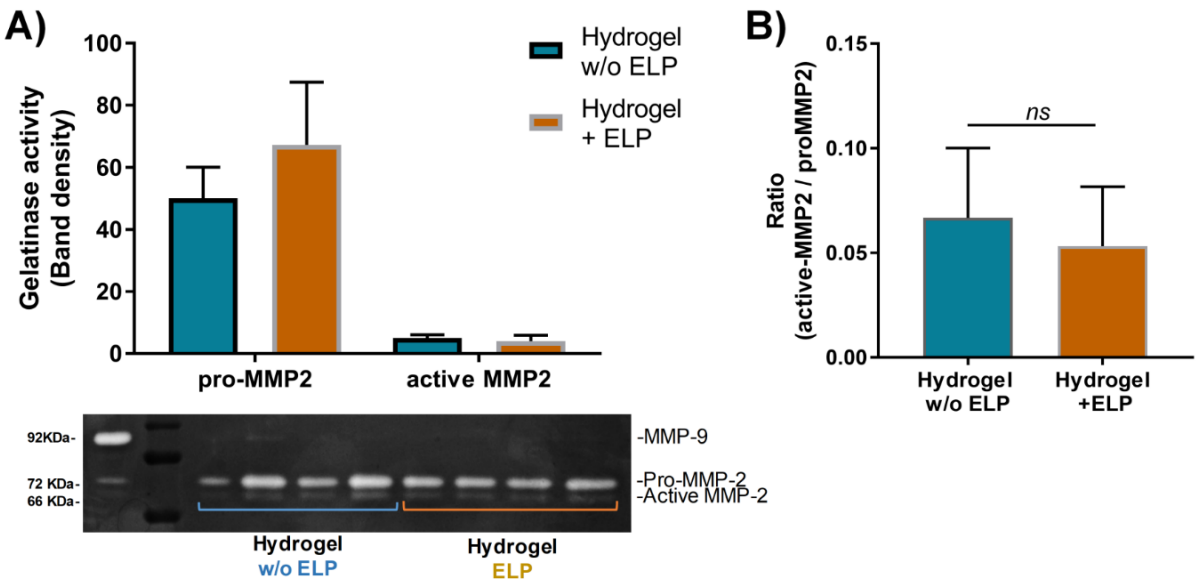

Figure 73. Activity of gelatinase A (MMP-2) by fibroblasts seeded on top of porous DGL/PEG hydrogels (2/19 mM DGL/PEG) with or without ELP (6 mg/ml) observed by zymography of culture medium after 20 days of cell culture.
A) Gelatinase activity expressed as band density (Representative results of one gel) SDS-PAGE 0.1% gelatin p/v gel, as control conditioned medium obtained from HT1080 cells was used to observe the activity of gelatinases. B) Ratio of active and pro MMP2 of three separate experiments (four hydrogel per experiment, t-student).

Critical evaluation and conclusion

Contrary to what was expected, the contribution of ELP to the mechanical behavior was not clear. Young's modulus was not significantly increased with the incorporation of the ELP, probably due to a lack of covalent bonds between the polymeric network and the ELP. In contrast, when crosslinked with genipin, ELP shows an interesting elastic behavior [32]. If the ELP does not participate in the reticulation process, it stays however embedded in the polymer network. It is possible that the relative empty intramolecular cavity of the DGL could work as a carrier for the ELP, bestowing further biological properties to the hydrogel without modifying its tailorable properties. This biological activity showed a clear effect in the cell response to the biomaterial. When fibroblasts were seeded in the surface of dense hydrogels, a significant increase in cell adhesion and migration was observed suggesting that the active sequences of the ELP (GRKRK and VGVAPG) are available in the surface of the hydrogel. This was further illustrated when fibroblasts were seeded on top of porous hydrogels, since cellular infiltration was increased within the hydrogel with a consequent increase in cell density. This could also indicate an increase in proliferation, since release of the motif VGVAPG from the porous hydrogels could stimulate fibroblasts proliferation [33].

IHC images suggest and increase in ECM synthesis, however, the effect of the ELP is unclear as no significant difference was observed in gene expression. The increase in ECM synthesis could just be related to an increase in cell density. However, the increase in cell density and ECM components were not sufficient to elicit a difference in the overall mechanical properties of the colonized hydrogel. Indeed, both conditions showed a similar mechanical evolution and resistance to fibroblast-mediated matrix contraction. While the effect of elastin peptides on collagen and fibronectin has not been reported, they have demonstrated an elastogenic potential [80]. However, no difference was observed in elastin synthesis in the dermal equivalents, which could be related to the absence of an epidermal layer. Keratinocytes have demonstrated to be key participants of the maturation and organization of the elastin network in skin equivalents. Since keratinocytes have an influence on maturation and organization of elastin network [262], to clearly observe the influence of ELP in elastin synthesis, samples should be analysed after the incorporation of the epidermal component. Moreover, the incorporation of ELP could improve the formation of the epidermal layer of full-

thickness skin equivalents, as Fujimoto *et al*., demonstrated that elastin peptide VGVAPG induced migration and terminal differentiation of culture keratinocytes via elastin-binding receptors [281]. In addition, the slight increase in ECM components observed in the hydrogels with ELP in the dermal equivalent could promote keratinocytes adhesion to the DEJ resulting in a more stable skin equivalent.

Do DGL/PEG scaffolds exhibit a good biocompatibility *in vivo*?

A combination of mechanical functionality, biological activity, and biocompatibility of tissue engineering scaffold is of great importance for the translation of biomaterials into clinical applications. The mechanical properties and ability to promote cell adhesion and proliferation of the DGL/PEG hydrogels has been previously described. To further judge the sustainability of the hydrogels for tissue regeneration applications, the *in vivo* biocompatibility and possible biodegradation of DGL/PEG hydrogels in physiological condition were investigated. In regenerative medicine applications, a proper rate between the formation of new tissue and hydrogel degradation should be acquired [171]. Moreover, the vascularization of a dermal compartment is of great importance for the survival of the epidermal layer, since nutrition at the wound bed of the epidermis its solely dependent of a well vascularized dermis [61]. In this context, the potential of neovascularization within the hydrogel was also evaluated.

I. *In vivo* biocompatibility of dense DGL/PEG hydrogel

As could be expected from PEG-based materials [282], no intense immune reaction was observed upon implantation of the DGL/PEG hydrogels under the back skin of mice for three weeks. Consequently, neither the presence of DGL nor ELP seemed to induce a specific inflammatory reaction as observed in Figure 74. All hydrogels exhibited a mild foreign body reaction with the formation of a fibrous capsule of 60.1 ± 2.3 µm and 67.9 ± 15.27 µm for hydrogels without or with ELP, respectively. While slight signs of hydrogel degradation by macrophages at the rim of the hydrogels (highlighted in close-ups) were observed, cells were not able to completely degrade and infiltrate the dense hydrogels within three weeks. No noticeable difference was observed between both conditions.

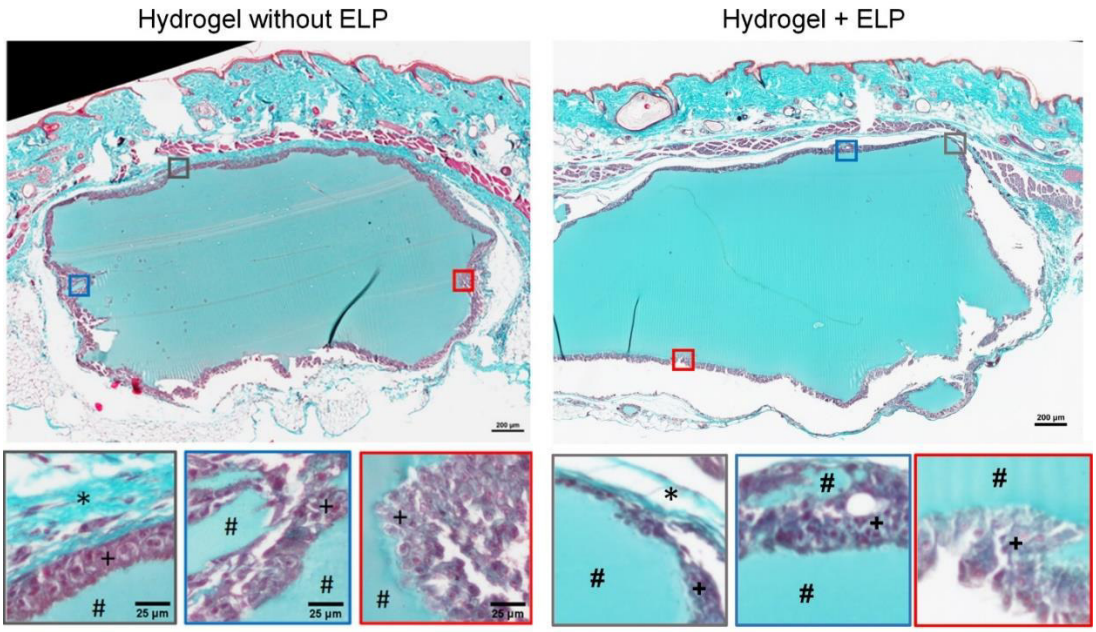

Figure 74. Subcutaneous implantation of dense DGL/PEG hydrogels. *Hydrogel composition 2/19 mM DGL/PEG with or without ELP (3.75 mg/ml) were subject to subcutaneous implantation in the back of SKH1 mice for three weeks. Fibrous capsule was measured for at least three hydrogels. Masson's trichrome staining of the full explants and close-ups highlighting the hydrogel (#), the fibrous capsule (*) and macrophages (+).*

II. *In vivo* biocompatibility and cellular infiltration of porous DGL/PEG hydrogel

To promote cell infiltration, the *in vivo* response of porous hydrogels was also evaluated. All porous hydrogels were deeply infiltrated by cells, contrarily to dense hydrogels. An important population of macrophages were visible, highly concentrated at the rim and within the porous implants, contrary to the dense hydrogels where they were only present on the external edges of the hydrogels. All porous implants showed signs of degradation after 3 weeks implantation, reflected by distortion of the outer dimensions and erosion of inter-porous walls, probably through macrophages phagocytosis and further opening the pores, as exemplified in the blue close-ups on Figure 75. Consequently, cells consisting of macrophages, fibroblasts and endothelial cells have filled the labyrinth of macropores after three weeks of implantation. Interestingly, no granulocyte or lymphocytes could be observed, suggesting a mild inflammatory reaction. However, to properly identify the presence of macrophages, IHC staining for anti-MAC3 should be performed. Resolution of acute and chronic inflammatory responses can be indicated by the formation of granulation tissue, the infiltration of fibroblasts and neovascularization [283].

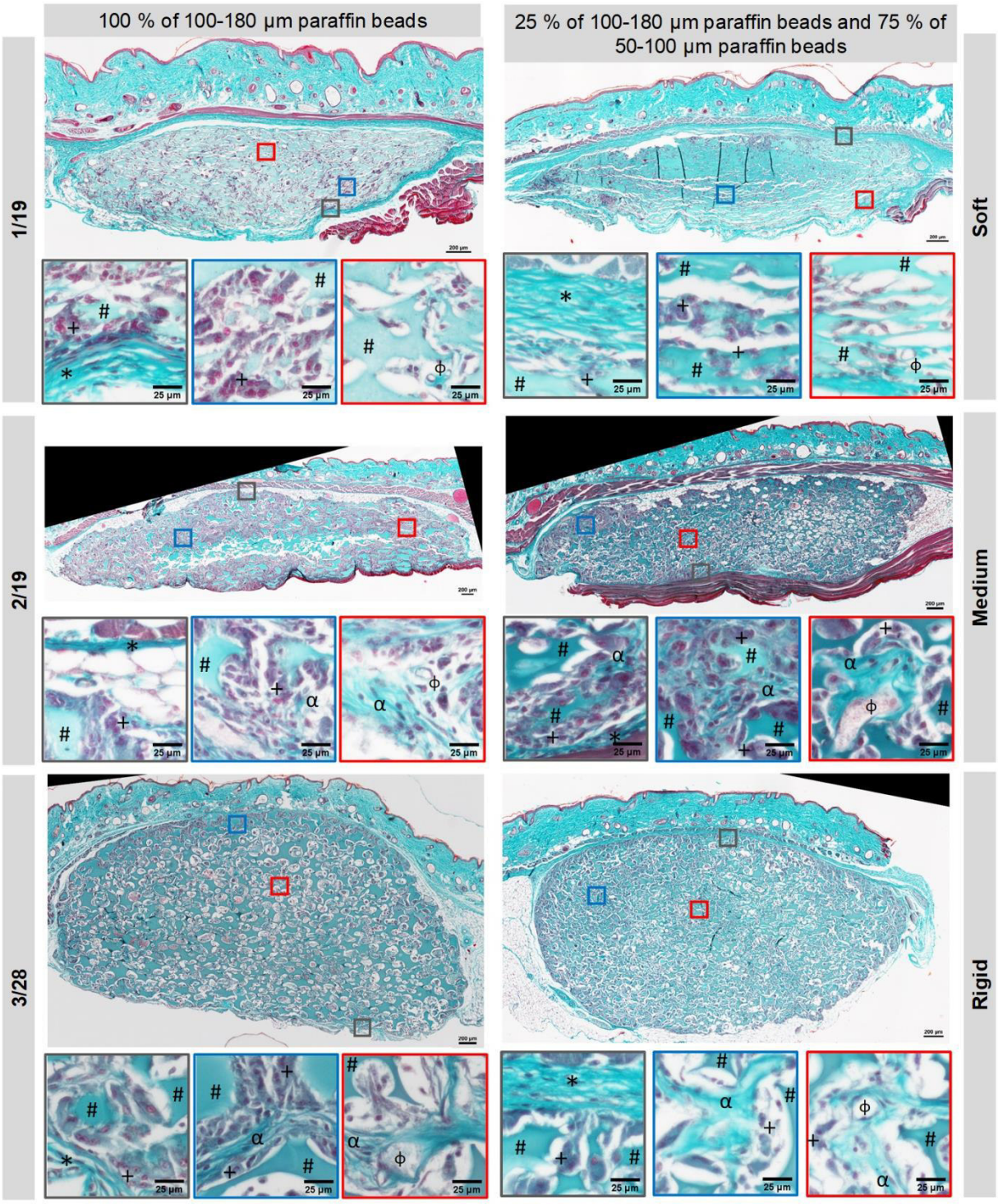

Figure 75. Subcutaneous implantation in mice for three weeks of DGL/PEG porous hydrogels of different compositions without ELP. *Masson's trichrome staining of the full explants and close-ups highlighting the hydrogel (#), the fibrous capsule (*), macrophages (+), synthesized collagen (α) and blood vessels (Φ). Hydrogel composition is expressed in as the ratio in mM of DGL/PEG concentration and with different pore sizes distributions (composition 1/19 is soft, 2/19 medium and 3/28 rigid, 7.7 ± 0.4, 41.5±5.0 and 76.7 ± 15.5 kPa, respectively).*

While the different porosities did not result in apparent differences of cellular infiltration, the hydrogel composition clearly induced structural and degradation-related variations in the implants retrieved after 3 weeks. Softer hydrogels with composition 1/19 mM DGL/PEG (7.7±0.4 kPa) appeared condensed while harder ones with composition 2/19 and 3/28 mM DGL/PEG (41.5±5.0 and 76.7±15.5 kPa) conserved their initial porous structure. Similar observations were made in regards of phagocytosis, with harder hydrogels being less prone to degradation by macrophages. The presence of neo-tissue within the hydrogels, revealed by areas of deposited collagen, followed a similar pattern with an increased occurrence in harder hydrogels than in soft ones.

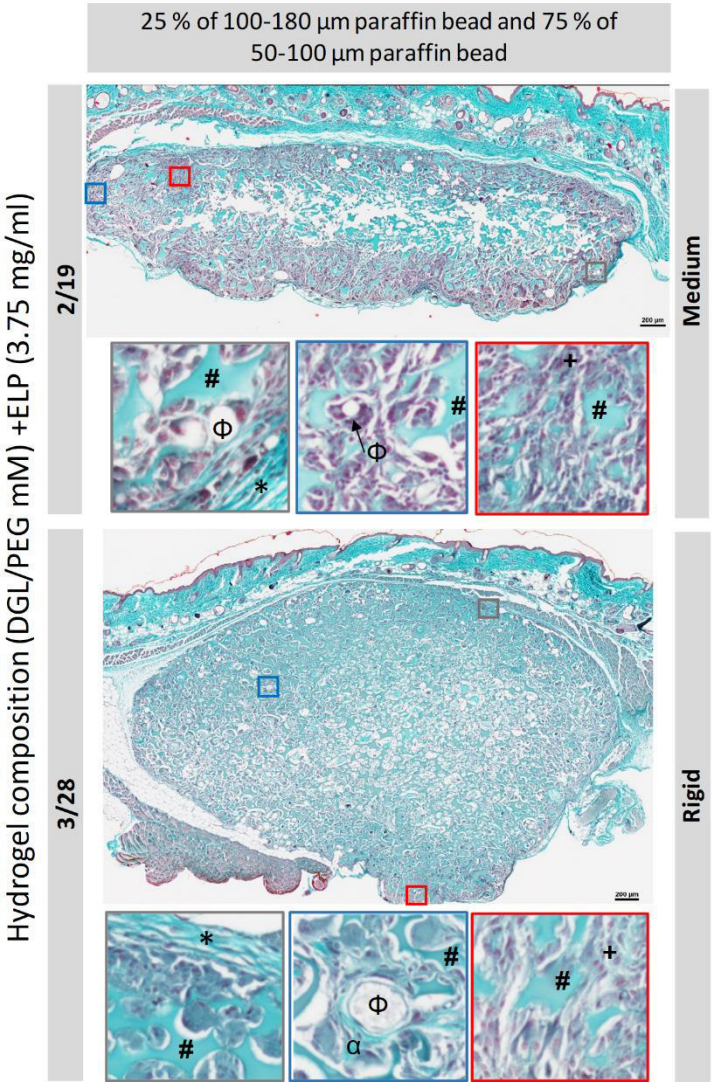

Figure 76. Subcutaneous implantation in mice for three weeks of DGL/PEG porous hydrogels of different compositions with ELP (3.75 mg/ml). *Hydrogel composition is expressed as the ratio in mM of DGL/PEG concentration with 3.75 mg/ml of ELP. Masson's trichrome staining of the full explants and close-ups highlighting the hydrogel (#), the fibrous capsule (*), macrophages (+), synthesized collagen (α) and blood vessels (Φ).*

Porous hydrogel with ELP showed a similar biocompatibility reaction, no distinct difference could be observed between the hydrogel without or with ELP (Figure 76). To comprehend the effect of ELP on biocompatibility more clearly further studies should be performed. Moreover, this *in vivo* biocompatibility study was performed with a low concentration of ELP (3.75 mg/ml). While a clear effect in cell adhesion and migration was observed in two-dimensions with this concentration, higher quantities of ELP were necessary to elicit an effect in three-dimensional studies using porous hydrogel scaffolds.

III. Neovascularization in DGL/PEG hydrogels implants

In the skin, the dermis is well vascularized favoring the nutrition of the epidermis [44]. A proper neovascularization of tissue engineering scaffolds will have an impact on the success of a skin graft. In this context, the formation of capillaries or vascular structures deep in the pores of the implant was assessed by IHC of α-SMA (Figure 77). Interestingly, an important amount of blood vessels was present within and throughout the porous hydrogels after three weeks of implantation. In accord to current standards, slit-thickness grafts, it usually takes three weeks for the materials used as dermal equivalents to be vascularized, which is needed prior the application of the epidermal layer [39].

Fewer blood vessels were present in soft hydrogels compared to more rigid compositions, with a preference to porous hydrogels with a broader range of pore size (50-180 µm). When considering only the blood vessels with a diameter over 25 µm, a preference to bigger pores was observed for more rigid compositions (Figure 77.B). Logically, bigger pores allow bigger blood vessels to penetrate the hydrogels; however, this could only be observed in rigid hydrogels since they were able to maintain their structure during implantation. This is in agreement with the observation made by Wake *et al*. who suggested that the introductions of larger pore size into scaffolds enhances angiogenesis by promoting faster vascularization [284]. On the contrary, softer porous hydrogels appear deformed and compressed after 21 days and fewer blood vessels are present. Although the appropriate pore size for tissue engineering applications is still debatable, Yannas *et al.* showed that an average pore size of 20-125 µm in collagen-glycosamininoglycan graft allows the regeneration of skin [285], while Wang *et al.* proposed a scaffold for

human dermal connective tissue with bigger pores (90-360 μm) [286]. Here we propose an intermediate range of 50-180 μm.

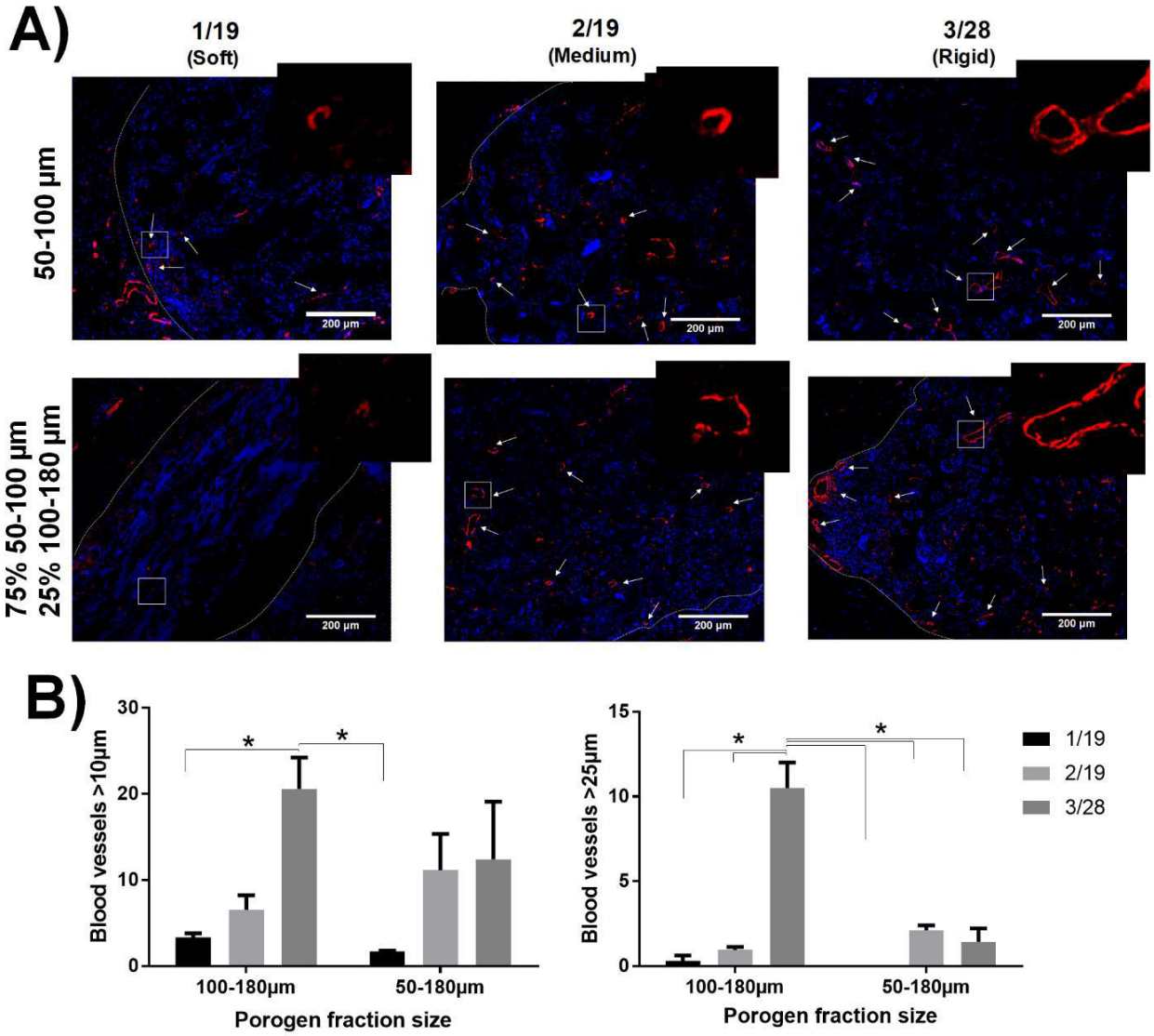

Figure 77. Blood vessels present after three weeks of subcutaneous implantation in mice in porous hydrogels of different compositions. *A) IHC α-SMA in red, indicating blood vessels present within the porous hydrogels, while cells nuclei are stained with DAPI in blue; white lines delimit the border of the hydrogel and arrows point to sectioned blood vessels. B) Number of blood vessels present in the hydrogel of a diameter greater than 10 μm or 25 μm obtained from image analysis of mosaic images of complete slides of porous hydrogels. Hydrogel composition expressed as the ratio DGL/PEG in mM, rigidity 7.7±0.4, 41.5±5.0 and 76.7±15.5 kPa for soft, medium and rigid, respectively (three hydrogels per condition, two-way ANOVA, * p<0.05*).

Critical evaluation and conclusion

DGL/PEG hydrogels exhibited an adequate biocompatibility response *in vivo* as expected for PEG-based hydrogels [282], non-immunogenic DGL [24] and bioinspired ELP [32,80]. While no noteworthy difference was observed between hydrogels without or with ELP, this must be confirmed by more precise evaluations such as identifying cell types by specific markers, determining the degree of cell infiltration and neo-synthesized ECM. Moreover, an increase in ELP concentration, potentially eliciting a response in the porous scaffolds, must be considered. Indeed, in two-dimension hydrogels containing 3.75 mg/ml were able to induce a response in cell behavior, while greater quantities of ELP were necessary in three-dimensional *in vitro* studies.

The fabricated 3D porous scaffolds have proven to possess a highly interconnected structure, sufficient to allow cell ingrowth, vascularization and nutrient diffusion, which are important prerequisite for tissue engineering applications [176–178]. However, long-term biocompatibility and biostability of hydrogels has yet to be fully defined. Longer implantation periods could be performed to better understand the biodegradation profile of the hydrogels. Images suggest degradation of hydrogels by macrophages; however, more detailed information could be acquired with specific markers to distinguish macrophage and further confirm the lack of monocytes and lymphocytes related with chronic inflammatory reaction. Nonetheless, in addition to a good cellular infiltration, the important presence of blood vessels in the porous hydrogels is a further suggestion of the potential use of these novel hydrogels to support tissue formation.

Conclusion and Perspectives

Tissue engineered skin development has been greatly catalyzed by economical and ethical turning points in the cosmetic industry. As well as providing alternative tools to animal testing, skin equivalents have greatly contributed to the fundamental knowledge of skin homeostasis and epidermal formation. Furthermore, they provide an attractive alternative to autologous skin grafting when patient's skin is not sufficient [40]. Most of the current materials used as scaffolds to reproduce the dermal compartment are made of collagen. Although collagen scaffolds benefit from their inherent ECM properties, they still bear certain disadvantages since they are still obtained from animal sources [146]. In this regard, the development of an innovative synthetic scaffold that mimic the ECM and circumvent issues from natural molecules was explored throughout this thesis.

First, the possibility to use poly-L-lysine dendrigrafts (DGL) as multifunctional crossliking points to form a PEG-based hydrogel was demonstrated. The hydrogel properties could be varied in relation to hydrogel concentration, notably hydrogel rigidity could be tailored between 7.7 ± 0.7 KPa to 90.4 ± 28.8 KPa. The family of hydrogels demonstrated a viscoelastic behavior and great swelling capacity, both characteristic of highly hydrated polymers. In comparison to synthetic materials previously evaluated as dermal matrices (mostly comprised of fiber forming polymers and knitted meshes, as shown in Table 4) hydrogel's polymeric network can absorb great quantities of liquids, therefore mimicking better the ECM.

Indeed, in physiological conditions fibroblasts are embedded in an ECM mainly composed of a collagen network and water-filled ground substances. While some classes of synthetic hydrogels allow a homogeneous cell encapsulation through a sufficiently quick and mild crosslinking chemistry, others need cells to be seeded on their surface and favor cellular infiltration. In our case, although the reticulation between NHS function of the PEG and the available amines at the surface of the DGL allows cell encapsulation, the cells are then trapped and unable to further invade the hydrogel matrix. Nonetheless, cell response to the material in relation to hydrogel composition could be easily studied in two-dimensions.

The ability of DGL to confer inherent bioactivity to the PEG-based hydrogel was demonstrated, since cell adhesion was obtained without further functionalization or coating steps. While the adhesion could be associated to DGL concentration, a minimal concentration of PEG in relation to DGL was nevertheless necessary to sustain cell viability. Cell behavior such as morphology and

proliferation could not be correlated directly to hydrogel composition but to an overall substrate rigidity. In accordance with the literature, an increase in substrate rigidity resulted in an increase in cell spreading area [203]. Gels with tailorable mechanical properties have indeed been widely used to study cell response to substrate rigidity in two-dimensions [202]. For instance, rigidity of polyacrylamide gels can easily be controlled by varying the quantity of acrylamide monomer or bisacrylamide crosslinker, followed by collagen or fibronectin coating to allow cell adhesion without modifying the mechanical properties [201,205]. Although DGL/PEG hydrogel rigidity could be tailored with increasing concentration of hydrogel components, the dependence of cell adhesion to DGL impedes to clearly distinguish between the contributions of mechanical properties and biological cues. A similar problem is observed when natural gels are used as tools to study mechanosensitive cell response (*e.g*. collagen, Matrigel), as their Young's modulus is increased with increasing concentrations of protein, concomitantly to their biological activity [202].

Considering that the project explored the potential of a novel hydrogel for skin engineering applications, human dermal fibroblast response to the biomaterial was the primary focus. Nonetheless, different cell types were able to adhere to the hydrogel, indicating a wider potential of soft tissue applications. Although only a couple of hydrogel compositions were investigated in relation to nasal human chondrocytes, preliminary results suggest their interest in conserving physiological chondrocyte phenotype, as *in vitro* cell culture substrates. These results being only based on morphological observations require a more comprehensive investigation considering a broader range of compositions. Moreover, the evaluation of chondrocyte differentiation markers must be performed to properly assess this potential. For example, the ratio of collagen II compared to collagen I should be determined to properly indicate the cell phenotype, since a higher collagen II expression would confirm the normal chondrocyte phenotype.

Cell viability and behavior in two dimensions provides basic information on the cell interactions with the material's inherent properties. However, to properly allow the reconstruction of a dermis, cell must be able to infiltrate the hydrogel. For dense DGL/PEG hydrogels, cells seeded on the surface are not able to migrate into its matrix. It would be of interest to determine the mesh size of the different hydrogel compositions, in relation with their mechanical and swelling properties. A

broader mesh size could allow cell infiltration through the dense material. This could be obtained by using higher molecular weight PEG molecules. However, the mechanical properties and biocompatibility would also be modified and would need further study. PEG molecules are versatile synthetic building blocks that can be easily functionalized to incorporate adhesion sequences and degradation sites to promote 3D cell behavior [287]. Incorporating peptide sequences susceptible to cleavage by cell-secreted proteases to allow cell mediated degradation of the synthetic materials when encapsulating cells could be further studied in the future as a technique to colonize the hydrogel. Besides incorporating degradation sites into the polymeric network to provide cell-remodeling abilities to the matrix, another approach to bypass the lack of cellular infiltration is to process the material before cell seeding. For the latter, simple post-fabrication techniques can be employed to introduce a controlled porous structure into a scaffold without modifying the hydrogel formulation and bulk properties. In our case, the use of a particulate leaching technique, with paraffin microspheres as porogens, resulted in highly porous scaffolds. Naturally, the mechanical properties of the porous materials were decreased in comparison to the bulk materials, which resulted in scaffolds with mechanical properties close to the ones reported for native skin, when measured by indentation methods. The mechanical properties allowed to discriminate between two hydrogel compositions with a similar ratio of available amines per NHS groups but with increasing concentrations of DGL and PEG and therefore different rigidities.

The porous structures demonstrated their potential as a scaffold to support cell growth and tissue formation. Confirming a sufficient interconnection between pores, fibroblasts were able to swiftly infiltrate and proliferate within the hydrogel while synthesizing their own ECM. Evidence of type I collagen and fibronectin expression suggests that fibroblasts have filled the uppermost pores with neosynthesized ECM effectively producing a dermal equivalent. The contribution of the ECM component to the newly formed matrix could also be observed by an increase in storage modulus of the cellularized hydrogels. The potential of the obtained dermal equivalent was validated by comparing it to the well-known Col-GAG-Chi sponges, in the context of full-thickness skin models. The production and culture protocol of these scaffolds have been optimized for more than 30 years, ensuring the formation of a stratified epidermis in full-thickness skin equivalents. Like DGL/PEG hydrogels, cells were seeded on the surface of Col-GAG-Chi sponges

and allowed to infiltrate and colonize the matrix over three weeks to obtain a dermal equivalent. The keratinocytes were then seeded on the surface of this dermal component, to produce a reconstructed full-thickness skin. Unlike Col-GAG-Chi controls, however, the stratified epidermis formed in DGL/PEG hydrogel was significantly thinner and less defined. The difference in thickness could be related to the lack of the stratum corneum, which could have detached on account of a less cohesive epidermis. Interestingly, the porous structure of the DGL/PEG hydrogel encouraged the formation of rete pegs and rete ridges along the dermal-epidermal junction, mimicking the skin structure. Although skin equivalents obtained with DGL/PEG hydrogels did not perform better than those obtained with Col-GAG-Chi sponges, their potential as a matrix for full-thickness equivalents cannot be completely excluded. Neither material can be exactly compared to each other, as some specific cell culture steps differed (*e.g*. air liquid interphase, size of the matrix, sterilization...). These differences bring forth an opportunity for improvement of the cell culture protocol with the DGL/PEG hydrogels. Epidermis stratification is a complex process; media composition and volume need to be fine-tuned for each specific substrate, its thickness and porosity. DGL/PEG hydrogels were considerably smaller than the Col-GAG-Chi sponges, making their transfer from the inside of the inserts to another support during air-lift impossible. Further optimization of media parameters and modulation of the humidity in the incubator in the terminal phase of cell culture could improve the quality of the epidermis. Few synthetic materials have been evaluated for skin engineering applications (Table 4). Mainly synthetic polymers have been studies as knitted mesh of fiber matrices which do not mimic the highly hydrated ECM. Limited success of this synthetic materials is often related to the lack of biological signals to promote cell function; therefore, they were further exploited as composites formed from synthetic polymers and natural components. Only recently, a polystyrene scaffold without exogenous ECM components has demonstrated its potential to produce a full-thickness skin equivalent [125]. They were able to obtain a well-defined and highly stratified epidermis and a good epidermal junction, however, in comparison to our model, few fibroblasts infiltrated the scaffold, a majority of cells formed 3D layers on both surfaces of the material.

Another opportunity of improvement to enhance the cellular response to the material is through biomimicry. Instead of focusing on reproducing the collagen

properties, which can easily be synthesized *in vitro* by the fibroblasts, elastin is an attractive alternative. Elastin synthesis *in vitro* is quite limited and its extraction from natural sources is complicated, yet its structure can be replicated by recombinant techniques [31]. Along this line, the incorporation of an 'in-house' elastin-like polypeptide (ELP) to the hydrogel composition was evaluated. Contrarily to our expectations, the ELP had no influence on the mechanical properties of the material, possibly because of a lack of the peptide integration within the hydrogel polymeric network. Nevertheless, our results suggest that the ELP could be embedded and remain sequestrated within the hydrogel matrix. It would be interesting to better understand the immobilized density of the ELP and protein release over time. Usually simple techniques such as BCA and UV absorption and use to quantify proteins, however, the ELP is not detectable with classical techniques. Further work should nevertheless be performed to understand the long-term release profile of the ELP, which could provide more ground to understand the effects of ELP that were observed on fibroblasts *in vitro*. More complex techniques, such as liquid chromatography, are being evaluated as quantification techniques for ELP. The release profile over time will help understand the differences in ELP concentration needed to elicit an effect in two- and three-dimensions. While two possible mechanisms were proposed to explain the biological action of the ELP on cells, additional analysis with the DGL/PEG hydrogels should be performed to distinguish between the relative contribution of both ELP bioactive sequences (GRKRK and VGVAPG). In a wider view, it would also be interesting to assess the entrapment of other molecules in the polymer network, such as growth factors of cytokines, to promote tissue regeneration besides providing structural support.

While three-dimensional *in vitro* studies suggest that ELP improves hydrogel colonization, the advantages of the incorporation of ELP in the context of full-thickness skin equivalents should also be evaluated in the presence of an epidermal layer. Indeed, a faster colonization and ECM synthesis could be advantageous. For instance, a greater abundance of ECM proteins at three weeks could increase epidermal adhesion to the dermal equivalent, since keratinocytes will be in direct contact with the native ECM components and not the synthetic material. In addition, the possible effect of VGAVAPG on keratinocytes migration and differentiation should be assessed. Although, the ELP did not increase the elasticity of the polymeric network, its effect in elastin synthesis cannot be rule out. Despite

the fact that no difference could be observed after 21 days of culture in the presence of ELP, elastin expression is usually reported once keratinocytes are incorporated [126,271]. To accurately evaluate the effect of ELP on elastin synthesis, samples should be assessed after the complete formation of a full-thickness skin equivalent.

In a more general view, criteria such as barrier function, morphology, reproducibility and quality control should be addressed to validate the potential of the DGL/PEG hydrogel with or without ELP as an alternative to other *in vitro* skin models. The lipid profile characterization is essential in the case of the development of new tissue models. Further studies on lipid composition by FT-IR spectrometry or RAMAN spectrometry should be performed in correlation with permeability studies. While further characterization should indeed be performed, our synthetic model could benefit of its straightforward reticulation process and low degradation profile in physiological and acid conditions, which suggest an important shelf-life. Moreover, the ELP can be produced in bioreactor with a simple purification process and quite a high production yield in contrast to other recombinant proteins.

Unlike *in vitro* applications, the degradation rate of a supporting material must be pared with the formation of a new tissue *in vivo*, while it should not generate an extensive immunological response. In this regard, DGL/PEG hydrogels showed a mild inflammatory reaction, with a normal foreign body reaction. Although no differences were observed between hydrogel with or without ELP, further experiments should be performed with greater quantities of peptides to rule out any toxicity and elicit a visible effect. Similarly to *in vitro* experiments, cell infiltration *in vivo* was only observed when the hydrogels were rendered porous. Evidence of degradation was reflected by the erosion of inter-porous walls through macrophages phagocytosis; however, this must be confirmed with specific markers to distinguish macrophages and complete degradation profiles should be assessed through longer implantation times. While a-SMA staining suggested the formation of blood vessels on the hydrogels implanted for three weeks, it would be interesting to better evidence the neovascularization with specific markers of endothelial cells, such as CD31, CD34 or VEGF. Moreover, to further study the potential of this biomaterial in regenerative medicine, experiments targeting the improvement of wound healing should be performed. The important presence of blood vessels in the porous hydrogels let foresee the possibility to obtain a vascularized dermal

equivalent, which would enable the adhesion and nourishment of the epidermal compartment. While preliminary studies were performed with such hypothesis in mind, no concrete data could be obtained. Following the application of acellular porous hydrogels in skin wounds of mice, it was either removed rapidly by the animal or evacuated with the scab. An adequate protocol should therefore be developed to properly investigate the potential of the hydrogel in would healing, and the use of previously cellularized hydrogels should be considered.

Annexes

Technical difficulties-Nucleic acid extraction

Several techniques to study cell response to a biomaterial require the isolation and extraction of nucleic acids. For example, DNA quantification is routinely used as an accurate technique to determine cell density in a biomaterial and therefore cell proliferation. Likewise, gene expression can provide relevant information of cell interactions with a given biomaterial. To do so, techniques such as qPCR and microarrays require the isolation and extraction of RNA from the cells present on the surface or within a biomaterial. If several protocols for the extraction of nucleic acids from cells cultured on plastic cultures plates or commercially available 3D models are readily available, the extraction of nucleic acids from DGL/PEG resulted, however, in unreliable results. DNA quantification with classic techniques (*e.g*. bisbenzimide H33258, Qubit DNA assay and absorbance measurement at 230/260) showed an underestimated DNA content that did not correspond with the increase in cell density observed by microscopy observations or to the initial DNA content of cell seeded on the porous hydrogels (Figure 78.A).

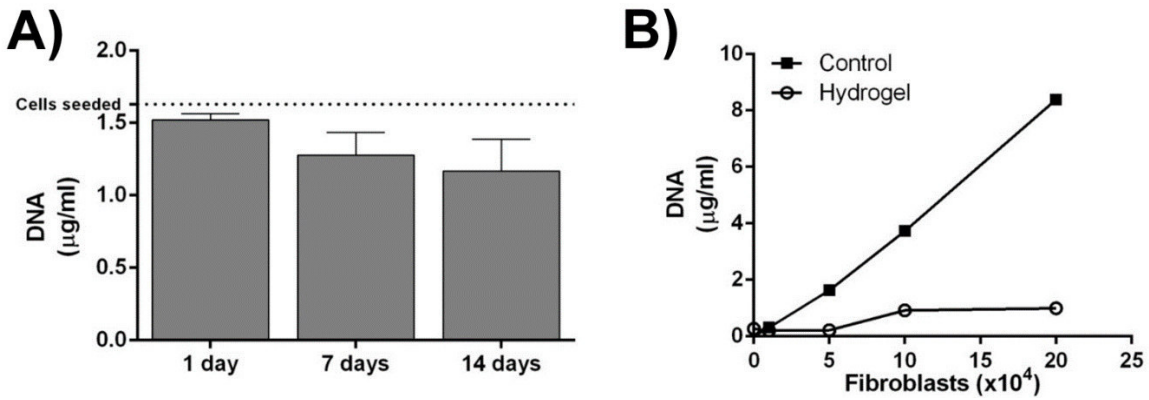

Figure 78. DNA quantification under estimation due to interactions with DGL.
A) DNA content obtained from fibroblast-colonized porous DGL/PEG hydrogels after 1, 7 and 14 days of cell culture. For extraction a Sigma kit (DNAQF) was used followed by DNA quantification using bisbenzimide H33258 assay. B) Quenching effect in DNA extraction and quantification of DGL/PEG hydrogel in the presence of a known number of cells.

Dendritic polymers, such as DGL, have been studied as vectors for gene delivery thanks to their ability to bind nucleic acids via electrostatic interactions and compact DNA into polyplexes [25,26]. While for certain applications these interactions are certainly of great interest, it represented in our case a serious difficulty. To confirm that the effect observed in DNA extraction and quantification

of fibroblasts seeded in porous hydrogel was not due to a cytotoxic effect of the hydrogel, the DNA from increasing cell densities were extracted in the presence of the hydrogel, as shown in Figure 78.B, DNA quantification was underestimated in comparison to control.

To limit the interactions between the nucleic acid and DGL molecules during the extraction process several techniques were assessed. To do so, increase concentrations of NaCl, the use of an anion exchange resin (BIO-Rad) and sodium dodecyl sulfate (SDS) were evaluated to saturate the positively charged DGL molecules and avoid their interactions with the negatively charges nucleic acids. The use of SDS showed an adequate potential to avoid DNA-DGL interactions as can be observed in Figure 79. The addition of SDS to a final percentage of 0.5% and 0.2% allowed to properly separate DNA (1 µg) from 4 µg of DGL. When DGL concentration was increased ten times, 0.5% SDS was still able to show a similar effect, however, smaller concentrations (0.2% SDS) were inefficient (data not shown). Here, all reagents were incorporated at the same time and incubated for 30 min at room temperature before loading in agarose gel. In a similar manner, the addition of SDS after incubation of DGL with DNA showed the ability to separate DNA from DGL molecules (data not shown).

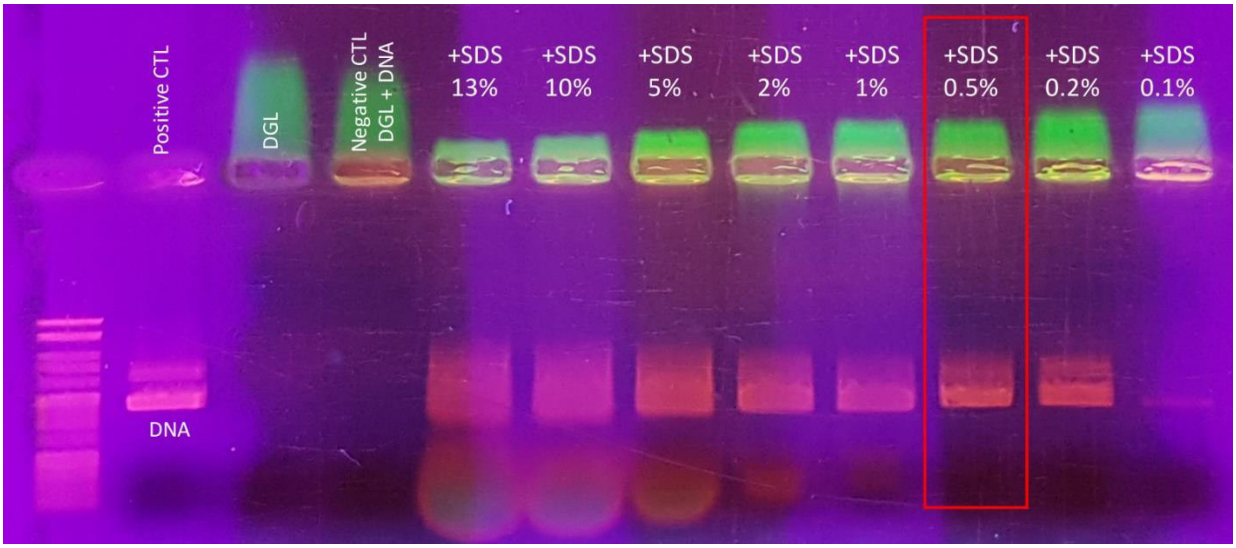

Figure 79. Effect of SDS percentage in DNA extraction from interactions with DGL by electrophoresis. *Before loading agarose gel, fluorescent DGL (4 µg) was mixed with DNA (1 µg) and incubated for 30 minutes at room temperature with increasing concentrations of SDS. SDS concentration is expressed as its final percentage. Fluorescent DGL appear in green at the load point, while DNA migrated and is observed in pink.*

To validate the DNA extraction from the formed hydrogel with SDS, cryogenically grinded hydrogels and known DNA amounts were incubated in presence of SDS and loaded into an agarose gel. As observed in Figure 80, 10 µg of DNA were able to properly be separated with 0.5% SDS from grinded hydrogels. Accordingly, nucleic acid extraction protocols were modified by incorporating SDS into classic TRIzol protocol (page 94).

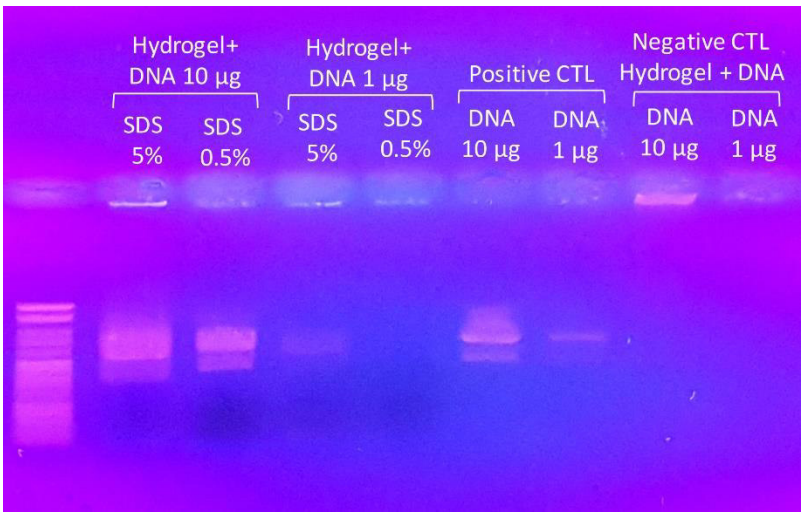

Figure 80. Validation of DNA extraction from hydrogel. *Before loading in agarose gel, hydrogel 2/19 mM DGL/PEG was cryogenically grinded and mixed with DNA (1 and 10 µg) and different SDS concentrations (5% and 0.5%), in a final volume of 200 µl for 5 minutes at room temperature. SDS concentration is expressed as its final percentage.*

Poster and oral presentations

Oral presentations

National

1. *Skin models in Cosmetic Science:* Bridging Established Methods and Novel Technologies Conference, December 2-4, 2019. (Tours, France): **"Evaluation of a novel tunable lysine dendrimers and polyethylene glycol hydrogel as a three-dimensional matrix to support tissue formation and the development of full thickness skin models."**
2. *3rd BIOMAT Congress*, June 3-4, 2019. (La Grande-Motte, France): **"Dermal equivalents produced with an innovative elastino-mimetic hydrogel"**
3. *2nd BIOMAT Congress*, June 12-15, 2018 (Ambleteuse, France): **"Characterisation and evaluation of elastino-mimetic hydrogels for soft tissues applications"**

International

1. *27th Tissue Engineering and Regenerative Medicine (TERMIS) European Chapter Meeting*, May 27-31, 2019 (Rhode, Greece): **"Dermal equivalents produced with an innovative elastino-mimetic hydrogel"**
2. *7th Symposium Fellowship CONACYT*, April 11-13, 2018 (Strasbourg, France): **"Characterisation and evaluation of elastino-mimetic hydrogels for soft tissues applications"**
3. *28th Annual Conference of the European Society of Biomaterials (ESB)*, September 4-8, 2017 (Athens, Greece): **"Characterisation and evaluation of elastino-mimetic hydrogels for soft tissues applications"**

Poster Presentations

National

1. *Skin and Formulation 5th Symposium & 17th Skin Forum*, September 23-24, 2019 (Reims, France): **"Skin equivalents producedwith an innovative hydrogel and the potential of a synthetic elastin protein to improve cell growth in dermal equivalents."**
2. *Annual Scientific Day of the Laboratory of Tissue Biology and Therapeutic Engineering (LBTI)* February 12, 2019 (St-Foy-lès-Lyon, France): **"Innovative matrix for the development of dermal and epidermal equivalents"**
3. *23rd Scientific Day of Doctoral School (EDISS)*, October 11, 2018 (Villeurbanne, France): **"Innovative matrix for the development of dermal and epidermal equivalents"**

International

1. *29th Annual Conference of the European Society of Biomaterials* (ESB). September 9-13, 2018 (Maastricht, The Netherlands): "**Innovative matrix for the development of dermal and epidermal equivalents"**
2. *1st Forum Franco-Quebecois de l'Innovation en Santé*, October 11-12, 2016 (Montreal, Canada): **"Evaluation of a Biomimetic Hydrogel as a Support for Reconstructed Skin "**

Awards

Best oral presentation at the *27th Tissue Engineering and Regenerative Medicine (TERMIS) European Chapter Meeting*, May 27-31, 2019 (Rhode, Greece) by the Journal of Materials Chemistry B.

Innovative matrix for the development of dermal and epidermal equivalents

Mariana Carrancá[1], Céline Tournier[1], Marc Laucournet[1], Sabrine Bokhari[1], Leila Berriche[1], Romain Debret[1], Jérôme Sohier[1]
[1]Laboratory of Tissue Biology and Therapeutic Engineering (LBTI), UMR 5305, CNRS, Lyon, France

INTRODUCTION

Full-thickness skin models created using 3D matrices are of great interest for cosmetic screening applications, transdermal delivery systems or to study cell-to-cell and cell-to-matrix interactions[1]. However, they still face setbacks such as contraction, inadequate viscoelastic properties and low complexity compared to skin[2-3]. To circumvent these drawbacks, an innovative porous mechanically versatile hydrogel composed of dendrimers of poly-L-lysine (DGL) and poly ethylene glycol (PEG-NHS) was developed and evaluated to develop dermal and skin equivalents.

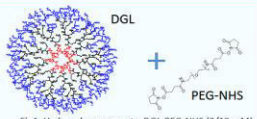

Fig1. Hydrogel components. DGL-PEG-NHS (2/19 mM)

EXPERIMENTAL METHODS

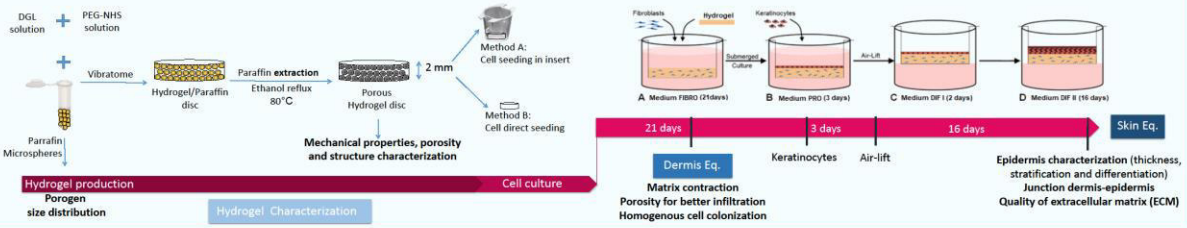

RESULTS AND DISCUSSION

Hydrogel Characterization

Complex modulus E* (kPa) of porous hydrogel

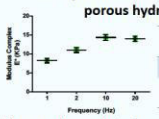

DMA compression 10Hz hydrogel (2x8mm)	
E*	Tan delta
14.3±2.1	0.2 ± 0.003

E* of skin as reported in the literature (*in vivo*)

Young	Old	Technique	Ref
14.3±3.6	6.2±1.4	Air flow device	[4]
10.7±2.6	7.2±2.1	Dynamic indentation	[5]

The complex modulus increased by applying a greater frequency and stabilized at 10Hz. At this frequency the complex modulus is similar to the reported in the literature for *in vivo* human skin.

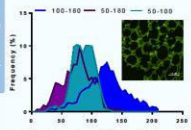

Paraffin microspheres size distribution and fluorescence microscopy image of hydrogel after paraffin extraction

Hydrogel **pore size** was controlled by porogen (paraffin microspheres) size distribution.

Hydrogel **Porosity** reach up to 75% measured with liquid displacement method.

Interconnected porous hydrogel structure was visualized with ESEM.

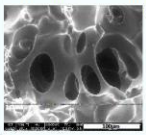

Interconnectivity between pores allows cell infiltration and transfer of nutrients trough the hydrogel.

Dermis equivalent

Optimal pore size distribution

Fibroblast infiltration was maximal (1mm after 14 days) for a pore size distribution of 75% (50-100µm) and 25% (100-180µm). Possibly due to a higher pore interconnection.

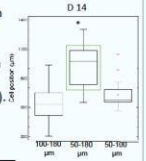

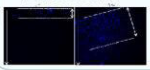
Image example of cell infiltration after 1 and 14 days cell culture.

Optimal cell seeding number

Seeding 1x10^5 cells per hydrogel disc allowed a good infiltration and proliferation. Increase in cell seeding density inhibited cell proliferation probably due to contact inhibition as cells reached confluence on the surface.

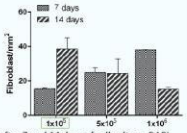

Cell proliferation after 7 and 14 days of cell culture. DAPI staining images analysis

Optimal support and method to produce dermis eq.

Two seeding methods were compared (A: seeding in insert or B: direct seeding). Only method A allowed fibroblast to proliferate and colonized homogenously the whole hydrogel after 21 days.

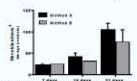
Proliferation by image analysis

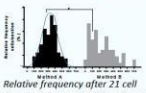
Relative frequency after 21 cell culture days determined from image analysis every 100µm

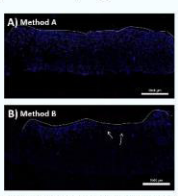

Microscope image of hydrogel colonized by fibroblast after 21 days cell culture DAPI staining

Matrix contraction

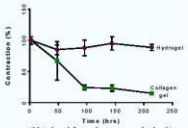

Obtained from image analysis, % contraction express in relation to t0.

While one common setback of collagen gels matrices is contraction cause by fibroblasts, our hydrogel does not show contraction after 10 culture days.

Skin Equivalent

Epidermis thickness of skin equivalents

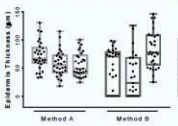

Epidermis Thickness (µm)	
Method A	62.04 ± 8.5
Method B	56.4 ± 24.1
In vivo skin [6]	68.9 ± 17

Epidermis thickness with method A resembles that of *in vivo* skin. While, mean epidermis of method B was slightly thinner and highly variable.

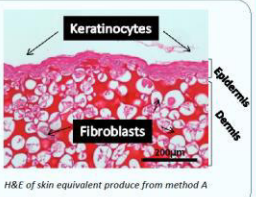

H&E of skin equivalent produce from method A

Quality of the dermis-epidermis junction

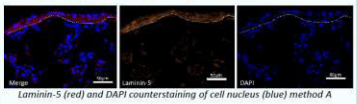

Laminin-5 (red) and DAPI counterstaining of cell nucleus (blue) method A

A suitable junction dermis-epidermis was supported by the expression of Laminin-5 (red), an essential protein for epidermal cell attachment, and evidence that proliferative keratinocytes (Ki67 green) remained attached to the basal membrane.

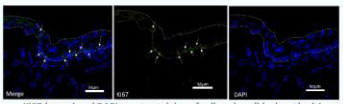

Ki67 (green) and DAPI counterstaining of cell nucleus (blue) method A

Quality of ECM synthetized *in vitro*

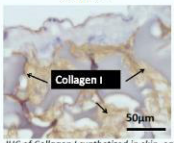

IHC of Collagen I synthetized in skin eq. produced by method A

The hydrogel not only served as a matrix that mimics the *in vivo* ECM but also promoted the synthesis of native ECM proteins. Collagen type I is the most abundant in skin and one of the primary components of the ECM.

Epidermis stratification and keratinocytes differentiation

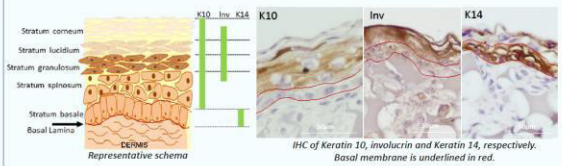

Representative schema

IHC of Keratin 10, involucrin and Keratin 14, respectively. Basal membrane is underlined in red.

While the differentiation markers were expressed in the produced skin equivalents, we could observe few stratum corneum, the outmost epidermis layer. Detachment of the delicate stratum corneum during fixation and embedding steps could be the cause.

CONCLUSION AND PERSPECTIVE

- PEG-DGL hydrogel demonstrated to have potential as a 3D matrix for culture of skin organotypic models.
- Mechanical properties resemble those of the skin *in vivo* and it's high water content, porosity and microporous structure allow for dermal fibroblast proliferation and colonization.
- The epidermis was close to physiological skin, although a lack of stratum corneum was observed.

Further work aim to improve the hydrogel by addition of a recombinant elastic protein to mimic the elastic component of the skin.

PhD Student – UCBL
2nd year
mariana.carranca@ibcp.fr

REFERENCES

1. Rami A. et al. JACS. 2013 217(3): 533-555
2. Goeber F. et al Adv Drug Deliv Rew. 2011 63(4-5): 352-366
3. Yildirimer, L. Trends in Biotech. 2012 30(12):638-648
4. Boyer et al, Med Eng Phys. 2012 Mar;34(2): 172-8
5. Boyer et al. Skin Res Technol. 2009 Feb;15(1):55-67
6. Sandby-Møller et al. Acta Derm Venereol. 2003; 83:410-3

ACKNOWLEGMENTS

The Rhone-Alpes and CONACyT are acknowledged for financial support.

Skin equivalents produced with an innovative hydrogel: potential of a synthetic elastin protein to improve cell growth

Mariana Carrancá[1,2], Leila Berriche[1], Aurore Berthier[1], Celine Auxenfans[1], Romain Debret[1], Jérôme Sohier[2]
[1]Laboratory of Tissue Biology and Therapeutic Engineering (LBTI), UMR 5305, CNRS, Lyon, France
[2]Biological Interactions and Biomaterials Laboratory, MATEIS, UMR 5510, CNRS, Lyon, France

INTRODUCTION

Full-thickness skin models created using 3D matrices are of great interest for cosmetic screening applications, transdermal delivery systems or to study cell-to-cell and cell-to-matrix interactions[1]. However, they still face setbacks such as contraction, inadequate viscoelastic properties and low complexity compared to skin[2-3]. To circumvent these drawbacks, an innovative porous and mechanically versatile hydrogel, composed of dendrimers of poly-L-lysine (DGL) and polyethylene glycol (PEG-NHS) was developed to create dermal and skin equivalents. To further mimic the dermal extracellular matrix, a elastin derived peptide (EDP) was incorporated in the hydrogel formulation. The effect of this protein (EDP), with similar physicochemical properties as tropoelastin, in de development of dermal equivalents was studied.

EXPERIMENTAL METHODS

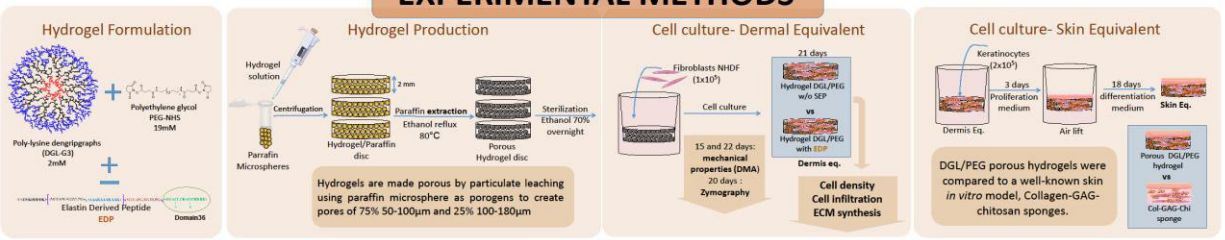

RESULTS AND DISCUSSION

Development of a porous scaffold as a 3D matrix

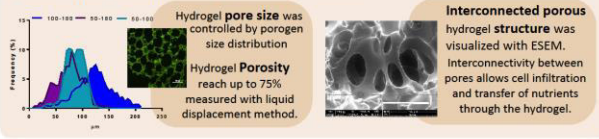

Hydrogel **pore size** was controlled by porogen size distribution

Hydrogel **Porosity** reach up to 75% measured with liquid displacement method.

Interconnected porous hydrogel **structure** was visualized with ESEM. Interconnectivity between pores allows cell infiltration and transfer of nutrients through the hydrogel.

It is possible to use the porous DGL/PEG hydrogel as a matrix to obtain a full thickness skin model

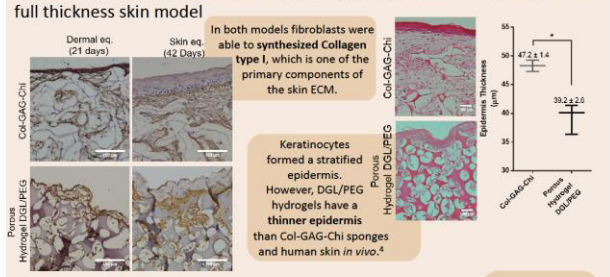

In both models fibroblasts were able to **synthesized Collagen type I**, which is one of the primary components of the skin ECM.

Keratinocytes formed a stratified epidermis. However, DGL/PEG hydrogels have a **thinner epidermis** than Col-GAG-Chi sponges and human skin *in vivo*.[4]

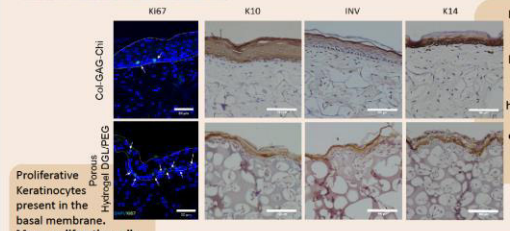

Differentiation markers are observed in both matrices. However, DGL/PEG hydrogels show a **less defined epidermis** and lack a stratum corneum.

Proliferative Keratinocytes present in the basal membrane. **More proliferative cells** are observed in DGL/PEG hydrogels.

DGL/PEG porous hydrogels have demonstrated to be a suitable matrix to develop dermal and skin equivalents *in vitro*. However, epidermis stratification needs further improvement.

An EDP in the hydrogel formulation could improve the dermal equivalent and therefore serve as a better support for keratinocytes

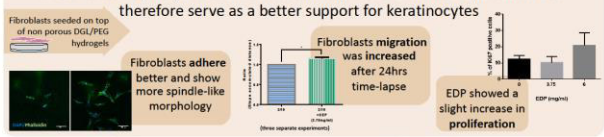

Fibroblasts **adhere** better and show more spindle-like morphology

Fibroblasts **migration** was **increased** after 24hrs time-lapse

EDP showed a slight increase in **proliferation**

EDP increases cell density and infiltration in DGL/PEG dermal equivalents.

Cell density was **increased** as observed by cell nuclei staining. Fibroblasts penetrate deeper inside the hydrogel, reaching 300µm of mean distance compared to 150µm. Suggesting an effect in migration and proliferation in the 3D matrix

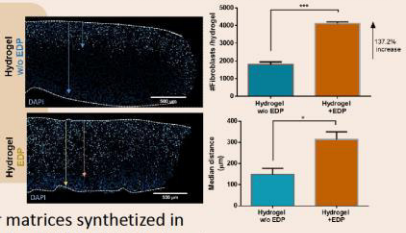

Quality of extracellular matrices synthetized in dermal equivalents made with DGL/PEG hydrogels

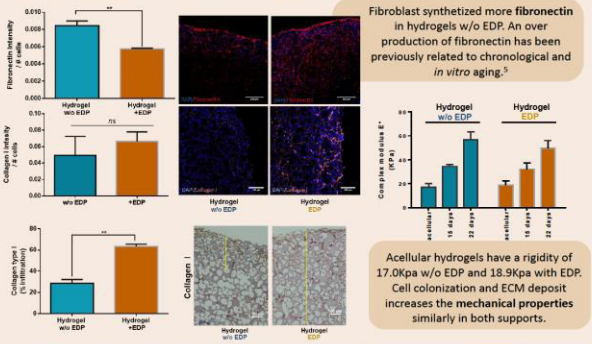

Fibroblast synthetized more **fibronectin** in hydrogels w/o EDP. An over production of fibronectin has been previously related to chronological and *in vitro* aging.[5]

Acellular hydrogels have a rigidity of 17.0Kpa w/o EDP and 18.9Kpa with EDP. Cell colonization and ECM deposit increases the **mechanical properties** similarly in both supports.

No difference in the synthesis of **collagen**, however, the expression of collagen was visible further in the hydrogel with EDP.

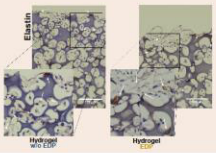

Elastin expression was evidenced by histology. However, no direct effect of EDP in elastin synthesis could be seen.

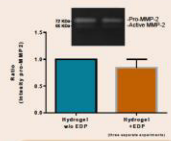

No difference was observed in the synthesis of Pro-MMP2 or its activation.

CONCLUSION AND PERSPECTIVES

- DGL/PEG porous hydrogels allow 3D tissue formation and therefore dermal and skin equivalents
- The skin equivalent obtained with DGL/PEG hydrogels still needs improvement to obtain a more defined epidermal stratification
- The EDP improves cell adhesion, migrations and proliferation and therefore allows to obtain a dermal equivalent with a greater cell density and a better ECM quality.
- Further studies on the effect of the EDP in skin equivalents formation must be carried out

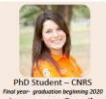

PhD Student – CNRS
Final year- graduation beginning 2020
mariana.carranca@gmail.com

REFERENCES
1. Rami A. et al. IACS. 2013 217(3): 533-555
2. Goeber F. et al Adv Drug Deliv Rew. 2011 63(4-5): 352-366
3. Yildirimer, L. Trends in Biotech. 2012 30(12):638-648
4. Sevcova, M. et al. Ces. Dermatologie, 1978, 53(4) 223-228
5. Robert, L. et al. Pathologie Bio, 2009, 57: 336-341

The Rhone-Alpes Region and CONACyT are acknowledged for financial support.
CONACYT
La Région Auvergne-Rhône-Alpes

Scientific Articles

1. **"Versatile lysine dendrigraft and polyethylene glycol hydrogels with inherent biological properties: in vitro cell behavior modulation and in vivo biocompatibility."** Mariana Carrancá, Louise Griveau, Noëlle Remoué, Chloé Lorion, Pierre Weiss, Valérie Orea, Dominique Sigaudo-Roussel, Clément Faye, Daniel Ferri-Angulo, Romain Debret, Jérôme Sohier. Accepted for publication at the *Journal of Biomedical Materials Research: Part A.* August 2020. (DOI:10.1002/jbm.a.37083)
2. **"Substrate softness promotes terminal differentiation of human keratinocytes without altering their ability to proliferate back into a rigid environment."** Choua Ya, Mariana Carrancá, Dominique Sigaudo-Roussel, Philippe Faure, Bérengère Fromy & Romain Debret. *Archives of Dermatological Research*. December 2019, Volume 311, Issue 10, pp 741-751. (DOI.org/10.1007/soo403-019-01962-5)

Received: 5 February 2020 | Revised: 27 July 2020 | Accepted: 3 August 2020
DOI: 10.1002/jbm.a.37083

ORIGINAL ARTICLE

Society For Biomaterials WILEY

Versatile lysine dendrigrafts and polyethylene glycol hydrogels with inherent biological properties: in vitro cell behavior modulation and in vivo biocompatibility

Mariana Carrancá[1,2] | Louise Griveau[1,2] | Noëlle Remoué[1] | Chloé Lorion[1] | Pierre Weiss[3] | Valérie Orea[1] | Dominique Sigaudo-Roussel[1] | Clément Faye[4] | Daniel Ferri-Angulo[2] | Romain Debret[1] | Jérôme Sohier[1,2]

[1]Laboratory of Tissue Biology and Therapeutic Engineering, IBCP, CNRS Université, Lyon, France

[2]Laboratory for Materials Engineering and Science, CNRS INSA, Villeurbanne, France

[3]INSERM, Laboratory of Osteo-Articular and Dental Engineering, Nantes, France

[4]COLCOM, Bat CAP ALPHA, Villeurbanne,, France

Correspondence
Jérôme Sohier, CNRS INSA, UMR 5510, Laboratory for Materials Engineering and Science, Bat. B. Pascal, 7 Avenue Jean Capelle 69621, Villeurbanne Cedex, France.
Email: jerome.sohier@insa-lyon.fr

Present address
Clément Faye, GLPBiocontrol, Bat CAP ALPHA, Clapiers, France

Funding information
Agence Nationale de la Recherche, Grant/Award Number: TECSAN 016-01; Consejo Nacional de Ciencia y Tecnología; Région Auvergne-Rhône-Alpes, Grant/Award Number: grant 17 002601 ARC 2016

Abstract

Poly(ethylene glycol) (PEG) hydrogels have been extensively used as scaffolds for tissue engineering applications, owing to their biocompatibility, chemical versatility, and tunable mechanical properties. However, their bio-inert properties require them to be associated with additional functional moieties to interact with cells. To circumvent this need, we propose here to reticulate PEG molecules with poly(L-lysine) dendrigrafts (DGL) to provide intrinsic cell functionalities to PEG-based hydrogels. The physico-chemical characteristics of the resulting hydrogels were studied in regard of the concentration of each component. With increasing amounts of DGL, the cross-linking time and swelling ratio could be decreased, conversely to mechanical properties, which could be tailored from 7.7 ± 0.7 to 90 ± 28.8 kPa. Furthermore, fibroblasts adhesion, viability, and morphology on hydrogels were then assessed. While cell adhesion significantly increased with the concentration of DGL, cell viability was dependant of the ratio of DGL and PEG. Cell morphology and proliferation; however, appeared mainly related to the overall hydrogel rigidity. To allow cell infiltration and cell growth in 3D, the hydrogels were rendered porous. The biocompatibility of resulting hydrogels of different compositions and porosities was evaluated by 3 week subcutaneous implantations in mice. Hydrogels allowed an extensive cellular infiltration with a mild foreign body reaction, histological evidence of hydrogel degradation, and neovascularization.

KEYWORDS
biocompatibility, cell interaction, mechanical properties, PEG based hydrogels, poly(L-lysine) dendrimers

1 | INTRODUCTION

The interest in hydrogels has grown rapidly in the past decade due to their vast potential in tissue engineering, tissue regeneration, and drug delivery.[1] These hydrophilic polymer networks are of interest through their biocompatibility, viscoelasticity, permeability to oxygen and nutrients, and high water content.[2–4] While natural hydrogels (e.g., collagen, gelatin, fibrin) confer their inherent extracellular matrix (ECM) structure and qualities, they often show weak mechanical properties, batch-to-batch variability,[5] and risk of pathogen transfer.[6] Conversely, synthetic hydrogels have an exact composition and multitunable properties, but may lack bioactivity to promote cellular

activities.[3,7,8] Among these, PEG hydrogels have been extensively used for controlled drug delivery, as cell vehicles or tissue engineering scaffolds over the past decades, owing to their excellent biocompatibility, chemical versatility, and tunable mechanical properties.[9] However, in the context of tissue engineering, a corollary setback of their bio-inert nature is that they require to be associated, functionalized or coated with supplementary proteins of the native ECM or functional moieties, such as, collagen,[10] laminin,[11] or arginine-glycine-aspartic (RGD) peptides,[12,13] to support the survival or function of adherent cells.[7,14–16] This necessity induces a complexification of the PEG-based hydrogel approaches for tissue engineering, which would benefit from inherent and native interactions with cells, without added factors.

PEG hydrogels can be obtained via covalent cross-links between PEG molecules through different paths, in which the PEG molecules are either functionalized with reactive end groups (e.g., methacrylate, acrylate),[7,17] and activated by initiators or associated with multifunctional monomers to avoid the use of initiators. In the latter approach, dendrimers have shown potential as cross-linking monomers, thanks to their versatile chemical composition, highly organized 3D arborescent structure and ease of surface functionalization.[18–21] Poly(amidoamine) (PAMAM) dendrimers, for instance, have been successfully associated with PEG to form hydrogels for drug delivery applications that do not require interactions with cells[22–24] since they tend to exhibit unwanted features such as cytotoxicity and non-degradability.[25]

Conversely, other dendritic structures with amine end groups, such as, poly(L-lysine) dendrigrafts (DGL), have recently developed interest in several applications, due to their large surface area, versatility to be functionalized, water solubility, stability under sterilization conditions, partial degradability under the action of endogenous peptidases, non-immunogenicity, and low cytotoxicity.[26,27] Moreover, their polycationic nature at physiological pH allows cellular adhesion,[27,28] which could be of high interest to provide cell interaction to inert materials. Indeed, DGL used as coatings on surfaces have been shown to increase cellular adhesion and proliferation of human skin fibroblasts by inducing the expression of integrin α5, a receptor implied in cell adhesion to fibronectin (through RGD). In this manner, the DGL could provide a bioactivity to the otherwise bio-inert material, while remaining synthetic and controllable.[29] DGL synthesis is based on the grafting of subsequent lysine molecules onto a polymeric substructure, linear poly-L-lysine (PLL), using protect-deprotect steps. In this manner, increasing generations of DGL (G1-G5) can be obtained with a simple, scalable procedure, water-soluble reaction (pH 6.5) with low batch-to-batch variability with a typical yield of 50–60% on a multigram scale.[30] While DGL-G3 and G4 showed a better cellular adhesion compared with PLL, in this study we focused on G3 since it presented the best compromise between biological activity and fabrication cost, as well as limits the formation of aggregates observed in the G4 synthesis.[29]

Interestingly, DGL-G3 has never been evaluated as cross-linking monomers to form PEG hydrogels, while such hydrogels could benefit from their inherent bioactivity, without the need for further association with additional functional moieties. To create such PEG hydrogels with intrinsic interactions with cells, we hypothesized that the amine groups present in high density at the DGLs surface could be used as binding sites to form network chains through of amide bonds between activated PEG-NHS ester and DGL-G3.

We here assess these possibilities through the development of a novel hydrogel composed of DGL-G3 and PEG, with extensive and straightforward tuneable mechanical properties, to serve as matrix or cell support for soft tissue engineering applications.[15] The characteristics of these hydrogels as cross-linking time, swelling, and mechanical properties were determined. Cell interactions with the hydrogels (adhesion, viability, proliferation, and morphology of dermal fibroblasts on dense hydrogels) were determined, in relation to hydrogel composition. Additionally, to allow cell colonisation and infiltration, hydrogels were rendered porous by particulate/leaching technique and their biocompatibility was determined by in vivo subcutaneous implantations in mice.

2 | MATERIALS AND METHODS

2.1 | Preparation of dense DGL/PEG hydrogels

Dense hydrogels of different ratios of DGL/PEG were prepared by adding the desired concentration of PEG-bis(N-succinimidyl succinate) (PEG-NHS, 2000 g/mol, Sigma–Aldrich) in anhydrous dimethyformamide (DMF, Sigma–Aldrich), to a solution of DGL (third generation, 22,000 g/mol, COLCOM)[31] in phosphate-buffered saline (PBS), at 4°C. For mechanical and swelling testing, 800 μl hydrogels were prepared in 2 ml conic tubes (Maxymum Recovery, Axygen). After cross-linking, the conical bottom of the tubes was cut off, and the tubes were immersed in ethanol for 5 min to subsequently retrieve the hydrogels. The resulting cylindrical hydrogels were then sectioned (2 mm thickness) using a vibratome (7550 Integraslice, Campden Instruments Ltd.) into flat hydrogel cylinders (thickness 2 mm, diameter 9 mm) and finally rehydrated and stored in PBS at 4°C. For 2D cellular in vitro studies, hydrogels of flat surfaces were prepared on top of coverslips for convenient handling (12 mm in diameter). The desired concentrations of DGL-G3 and PEG were mixed to prepare a final volume of 100 and 60 μl of the resulting solution were swiftly deposited between a hydrophobic glass slide and a round coverslip (for a hydrogel thickness of 0.6 mm). Hydrophobic glass slides were obtained by dipping in dichlorodimethylsilane (Sigma–Aldrich) followed by overnight evaporation under a fume hood. After cross-linking, the hydrogel-covered coverslips were gently removed, sterilized overnight in EtOH:PBS (70:30, v/v) solution, washed 3 × 30 min with sterile PBS and kept at 4°C prior use. Concentrated hydrogels, which cross-linking time was faster than 10 s, were prepared in a cold room to slow down cross-linking.

2.2 | Cross-linking speed

To monitor cross-linking speed, hydrogel components were added to a glass vial (8 × 25 × 35 mm) under agitation (300 rpm) with a magnetic rod (5 mm) placed at exactly 4 cm from the magnetic stirrer. Cross-linking time was defined, in our study, as the time needed to halt the magnetic rod after adding all the hydrogel components. Three hydrogels per condition were used.

2.3 | Swelling ratio (Qs)

The swelling ratio (Qs) of 2 mm-thick dense hydrogels discs was determined in PBS at 37°C. Prior incubation in PBS, samples were frozen in liquid nitrogen and freeze-dried to measure their dry weight. Samples were blotted before each weight measurement, performed at 1, 2, 6, and 24 hr. The swelling ratio was defined as, $([W_s\text{-}W_i]/W_i)$, where W_s is the weight of swollen hydrogel and Wi is its initial dry weight after freeze-drying. Five hydrogels per condition were measured.

2.4 | Mechanical testing

The mechanical properties of DGL/PEG hydrogels (2 × 9.1 mm) of different compositions were analyzed by cyclic compression with a dynamic mechanical analyzer (DMA 242 E Artemis, NEZSTCH). The hydrogel's domain of linearity was first determined with a strain sweep and compression test. Samples immersed in PBS were then subjected to compression at 10% strain and 60 μm amplitude, with increasing frequencies (1–20 Hz) at room temperature. At least five hydrogels per condition were measured.

2.5 | In vitro cell culture studies

Human dermal fibroblasts (Promocell, Heidelberg) were seeded at a density of 10,000 cell/cm^2 on the surface of hydrogel-covered coverslips and cultured in DMEM-F12 medium (Gibco) supplemented with 10% FBS (Life Tecnologies) and 1% penicillin/streptomycin (PAA Laboratories) at 37°C and 5% CO_2. Culture medium was refreshed every second day.

Hydrogels cytocompatibility was evaluated with a live/dead assay. Cells were washed once with sterile PBS and incubated 30 min with a 6 μM propidium iodide (Sigma Aldrich) and 1 μM Calcein (Sigma–Aldrich) solution and subsequently observed with a fluorescence microscope (Nikon TiE, Nikon Instruments). After observation, samples were washed with PBS, culture medium refreshed and cultured at 37°C and 5% CO_2 until next measurement. The number of alive and dead cells was determined from image analysis (Imagej[32]), using 5 different fields of view randomly acquired per replicate of at least 7 hydrogels per condition. Viability was determined as the percentage of alive cells from the total number of cells. Cell adhesion was expressed as the total number of cells (alive or dead) present on the surface of the hydrogels 24 h post-seeding. The effect of hydrogel composition on cell morphology was evaluated by phase contrast microscopy (Nikon TiE) and by actin staining. Phase contrast microscopy pictures were acquired after 24 h for 10 hydrogels per condition and at 72 h of culture for 5 hydrogels per condition. Cell spreading area, circularity, and feret diameter of cells seeded were determined to compare cell morphologies. Control were only analyzed after 24 h, since cell confluence impeded images analysis after 72 h. Factin cytosqueleton was observed by phalloidin (Sigam–Aldrich) staining after 1, 3, and 8 days of culture. Cells on the hydrogels were fixed with 4% paraformaldehyde (PFA, Thermo Fischer Scientific) for 10 min followed by 20 min permeabilization with a 0.1% triton solution in PBS. After washing twice with PBS, the samples were incubated for 10 min with a 2 μg/ml 4′,6-Diamidine-2′-phenylindole dihydrochloride (DAPI, Sigma–Aldrich) and 2 μg/ml phalloidin (Thermo Fischer Scientific) solution in PBS to stain the cell nucleus and actin cytosqueleton, respectively. Finally, hydrogels were observed with a fluorescence microscope (Nikon TiE). Cell proliferation was determined by counting DAPI stained cell nucleus after 1, 3, and 8 days of culture of 3 hydrogel per condition.

2.6 | Preparation of porous hydrogels

Porous hydrogels were prepared by particulate/leaching technique using paraffin microspheres as porogens.[33] Briefly, 10 g paraffin (Histolab AB, Västra Frölunda) and 250 ml 0.5% poly(vinyl alcohol) (PVA, Sigma–Aldrich) were heated to 80°C under stirring. After 20 min, the suspension was poured into ice water. The paraffin microspheres formed were sieved at 50, 100, and 180 μm and the resulting fractions were washed with distilled water, freeze-dried and conserved at 4°C.

To prepare porous hydrogels, 400 mg of paraffin microsphere, previously prepared, were compacted by centrifugation in 2 ml microtubes (2000 g, 10s) to obtain a flat surface. Consecutively, DGL and PEG-NHS solutions were mixed by vortex and rapidly transferred to the microtubes containing the paraffin at 0°C. After cross-linking, the conical bottom of the microtubes was sectioned, paraffin was extracted with boiling EtOH for 40 min and the hydrogels were removed from the microtubes. Finally, hydrogels were cut into 2 mm thick discs with a vibratome. After that, the remaining paraffin was removed by several cycles (40 min) in reflux EtOH. The obtained scaffold discs were sterilized overnight in EtOH 70%, washed 3 × 1h with sterile PBS, and kept at 4°C prior use.

2.7 | Biocompatibility

Biocompatibility of synthetized hydrogels was assessed by subcutaneous implantation of acellular hydrogels. After approval by local ethics committee, 5 hydrogels discs per condition (2 × 6 mm diameter) were implanted under the back skin of 8-weeks old SKH1 mice (Charles

River, Ecully) under sedation by intraperitoneal xylazin-ketamin injection (four hydrogels per mouse). A small incision was performed at the low back of the mice and 4 subcutaneous pockets created with a sterile spatula. The hydrogels were inserted in the pockets and the incision sutured. Mice, fed ad libitum, were monitored every day for recovery and signs of distress. After 3 weeks, the mice were euthanized by anesthetic overdoses (intracardiac injection of sodium pentobarbital), the hydrogel samples recovered with surrounding tissue, fixed in 4% paraformaldehyde (PFA) solution in PBS, embedded in paraffin, sectioned and stained with Masson's trichrome. To highlight the penetration of blood vessels in the implanted hydrogels, sections of three different hydrogels per condition were stained for α-SMA (Abcam #ab5694 1:250) by immunohistochemistry, cell nuclei were counter-stained with 2 μg/ml DAPI solution and observed by confocal microscopy (ZEISS, LSM 800). Round blood vessels with a diameter superior to 10 and 25 μm per hydrogel cross section were counted by image analysis.

2.8 | Statistical analysis

Statistical analyses were performed with Graphpad prism or Kaleidagraph. Test were performed using the variance analysis (ANOVA). Data values are presented as mean ± standard error (SE) and p-values of 0.05 and below were considered significant.

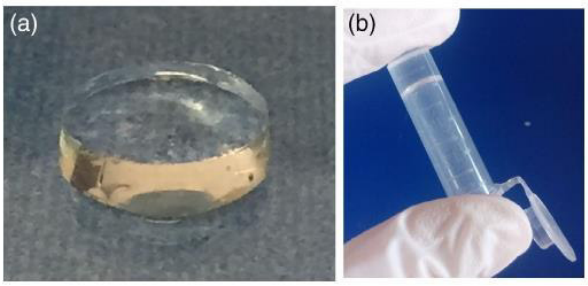

FIGURE 1 Photographs of the hydrogel at room temperature A, Dense 2/19 mM DGL/PEG hydrogel disc of 2 mm thickness and 9.1 mm diameter. B, Hydrogel in an inverted conic tube

3 | RESULTS

3.1 | Effect of reactants concentration on the formation of self-standing hydrogels

DGL/PEG hydrogel formation was straight forward. Concretely, hydrogels were obtained by covalent reaction between amine groups in the DGL and the NHS ester ends groups in PEG by simply mixing the solutions at room temperature (Figure 1.). Cross-linking velocity could be varied between 5 to 145 s by modifying reagent concentrations (between 1 to 4 mM for DGL and 19 to 30 mM for PEG-NHS), predominantly through the DGL concentration, as presented in Table 1. Interestingly, by considering the amount of amine groups and NHS functions theoretically available for the covalent reaction to occur, similar ratios of available amine to NHS functions resulted in different cross-linking velocities.

3.2 | Swelling ratio

To mimic the physiological conditions, swelling ratio was determined in PBS at 37°C. As observed in Figure 2, the swelling was decreased with an increased concentration of DGL or PEG-NHS. After 2 hr, a great quantity of liquid has been absorbed and reached equilibrium after 6 hr. The composition with lowest concentration of both components showed the greatest swelling ratio of 22.89 ± 1.95 after 24 h.

3.3 | Mechanical properties of dense DGL/PEG hydrogels

The mechanical properties of hydrogels of different compositions were measured with mechanical dynamical analysis. The loss (E"), storage (E'), and complex modulus (E*) were determined at increasing frequencies between 1 and 20 Hz. Figure 3 shows that for all hydrogels, E' was greater than E" over the entire frequency range studied. This was further expressed by tan delta, which is the ratio of moduli (E"/E') that describes the viscous energy dissipation relative to the stored elastic energy. While E' was constant for all applied frequencies, E" increased with frequency, which is a typical

TABLE 1 Crosslinking time to form self-standing gels in relation to the final concentration of DGL and PEG-NHS and ratio of available amine/NHS functions (Two-way ANOVA between PEG and DGL concentration, *indicates that there is a statistically significant difference when DGL concentration is modified, for any given PEG concentration, $p < 0.05$, $n = 3$)

		PEG-NHS (mM) (Available NHS, mM)		
Time (s) (Ratio amines/NHS)		19 (38)	28 (56)	30 (60)
DGL (mM)* (available amines, mM)	1 (114)	144.6 ± 23.3 (3)	122.0 ± 24.0 (2.03)	140.2 ± 15.8 (1.9)
	2 (228)	14.94 ± 1.1 (6)	13.17 ± 1.9 (4.07)	12.28 ± 3.5 (3.8)
	3 (342)	10.47 ± 4.5 (9)	8.4 ± 1.2 (6.1)	7.66 ± 1.1 (5.7)
	4 (456)	6.77 ± 0.9 (12)	4.76 ± 0.6 (8.14)	5.47 ± 0.6 (7.6)

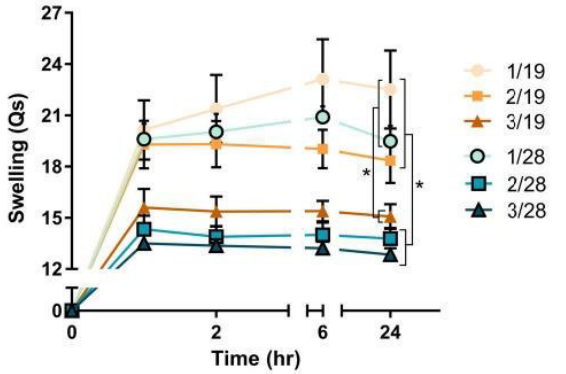

FIGURE 2 Swelling ratio of hydrogels of different compositions (hydrogel concentration is expressed as the ratio DGL/PEG in mM) swelling measured in PBS at 37°C. (n = 5, Two-way ANOVA, $p < 0.05$, *at 24 hr)

behavior of rubbery elastics.[34] Overall, the complex modulus of the different hydrogels was increased with an increased concentration of PEG-NHS and DGL, varying from 7.7 ± 0.7 to 90.4 ± 28.8 kPa.

3.4 | Cytocompatibility of the DGL/PEG hydrogels and effect of hydrogel composition on cell morphology and proliferation

To assess the potential of the DGL/PEG hydrogels as a cell substrate, the adhesion and viability of human fibroblasts seeded on the flat surface of hydrogels of different compositions were evaluated with a live/dead assay (Figure 4A). Seeded cells readily adhered on the hydrogels surface after 24 hr with a very low cytotoxicity, except for the hydrogel 3/19 mM (DGL/PEG), which showed a mortality of 79.4%. As shown in Figure 4B, the hydrogel

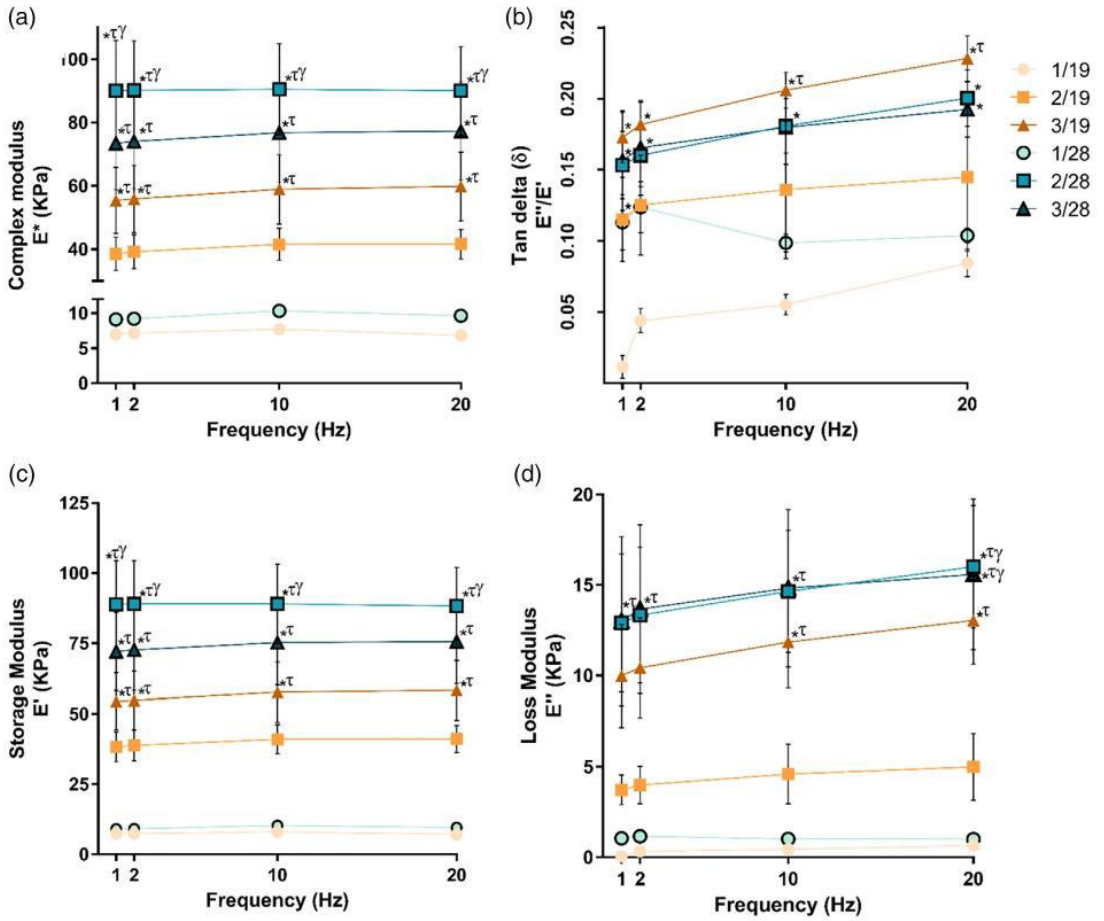

FIGURE 3 Mechanical properties of dense hydrogel discs (2 × 9.1 mm) of different compositions (hydrogel concentration is expressed as de ratio DGL/PEG in mM) measured at room temperature under PBS immersion by dynamical mechanical analysis in compression at a 10% strain and 60 μm of amplitude. A, complex modulus, B, tan delta, C, storage modulus, and D, loss modulus. (n = 7, Two-way ANOVA, $p < 0.05$, *compared with 1/19, τ compared with 1/28, and γ compared with 2/19)

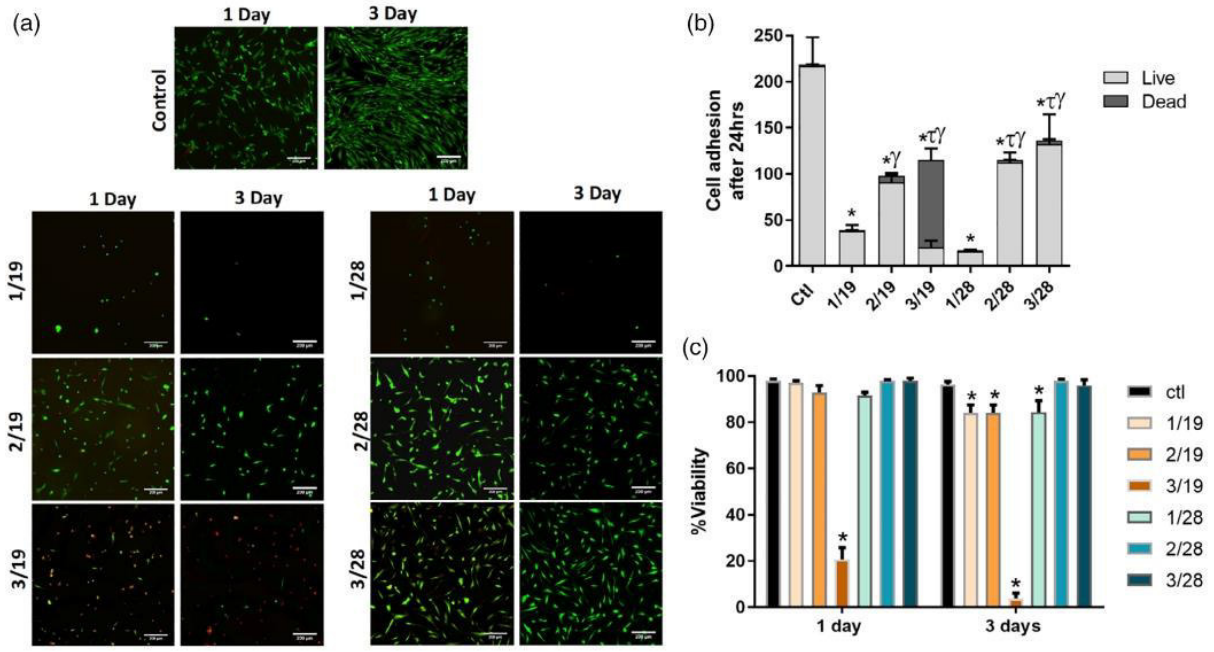

FIGURE 4 Dermal human fibroblast viability. A, Cytotoxicity by live/dead assay after 1 and 3 days of culture on the surface of hydrogels of different compositions (hydrogel concentration is expressed as de ratio DGL/PEG in mM). Live cells are observed in green and dead cells in red B, Total cell adhesion after 24 hr of cell seeding on top of hydrogels of different compositions. (n = 7, One-way ANOVA, $p < 0.05$, *compared with control, τ compared to 1/19, and γ compared with 1/28) C, Viability percentage obtained from images analysis (n = 7, $p < 0.05$ * compared with control)

composition had an apparent effect on cell adhesion, concretely, with DGL concentration. With an increase of DGL, the total number of adhered cells was increased while adhesion was minimal when the DGL concentration was 1 mM. After 3 days of culture, compositions 1/19, 1/28, and 2/19 mM DGL/PEG presented around 84% of viability while more concentrated compositions (2/28 and 3/28 mM DGL/PEG) showed a viability of 97.9 and 96%, respectively (Figure 4C), with no difference compared to controls (tissue culture plastic). Of note, an increase in PEG-NHS concentration resulted in an increase of the viability of the adhered cells.

Cell morphology was also modified by hydrogel composition (Figure 5A). Cells on hydrogels with lower concentrations of DGL (1 mM) and therefore lower percentage of adhesion presented a round morphology similar to non-adherent cells, with a mean circularity of 0.8 and a small ferret diameter (26.9–28.9 μm). An increase in hydrogel concentration had an impact on cell morphology. Except for hydrogel composition 2/28 and 3/28 (DGL/PEG), which showed a similar cell morphology. After 72 hr, cell spreading area was increased in all compositions (Figure 5B). The effect of hydrogel composition on cell morphology and spreading was further confirmed by phalloidin staining of f-actin fibres after 1, 3, and 8 days of culture (Figure 6A.).

Regarding proliferation, seeded cells were able to proliferate over time (Figure 6B), except for hydrogels with the lower concentration of DGL, where cells stayed round and showed proliferation rates close to zero. While hydrogels 2/28 and 3/28 mM showed similar proliferation rates of 69.9 ± 8.1 and 66.7 ± 14.6, respectively, which were lower than tissue culture plastic controls (rate of 135.2 ± 26.19).

3.5 | Biocompatibility

The behavior of DGL/PEG hydrogels of different compositions and porosities was evaluated in vivo by subcutaneous implantation in mice. As shown in Figure 7, regardless of pore size or composition, all hydrogels exhibited a mild foreign body reaction with the formation of a fibrous capsule after 3 weeks of implantation. All porous hydrogels were deeply infiltrated by cells, contrarily to dense hydrogels (Supplementary Figure 1). An important population of macrophages were visible, highly concentrated at the rim and within the porous implants and on the external edge of dense hydrogels. The macrophages were able to degrade the hydrogel through phagocytosis, further opening the pores, as exemplified in the blue close-ups on Figure 7. Interestingly, no granulocyte or lymphocytes could be observed, suggesting a mild inflammatory reaction. While the different porosities did not result in differences of cellular infiltration, the hydrogels composition clearly induced structural and degradation-related differences in the retrieved implants after 3 weeks. Softer hydrogels (7.7 ± 0.4 kPa) appeared condensed while harder ones

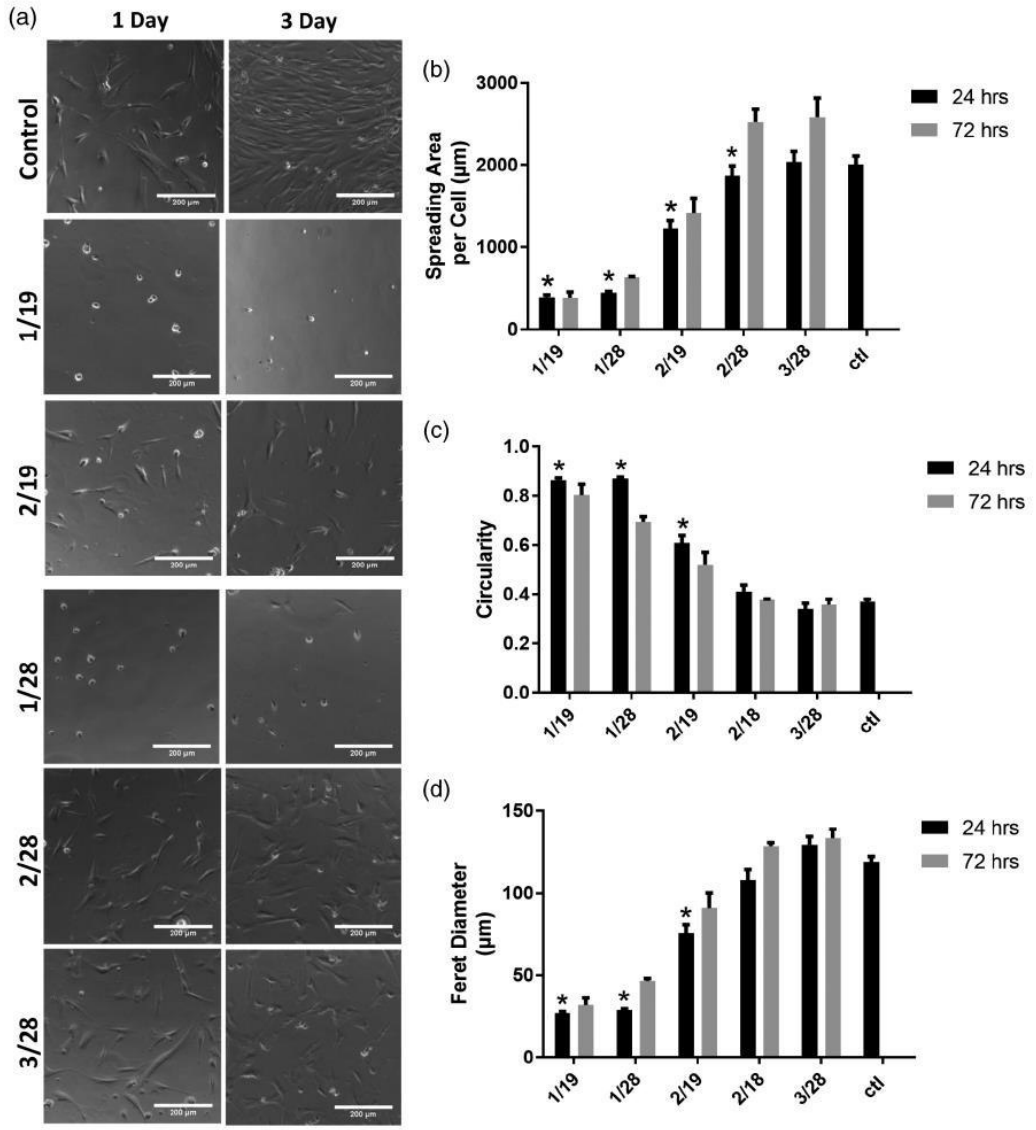

FIGURE 5 Dermal fibroblast morphology when cultivated on the surface of hydrogels of different compositions (hydrogel concentration is expressed as de ratio DGL/PEG in mM) A, contrast phase photos after 24 hr and 72 hr of cell seeding B, Morphology parameters (spreading area, circularity, and feret diameter) obtained from image analysis of contrast phase photos of 10 hydrogels at 24 hr and five hydrogels after 72 hr. Control was only analyzed after 24 hr since after 72 hr images analysis was not possible due to cell confluence. ($p < 0.05$, *compared with control at 24 hr)

(41.5 ± 5.0 and 76.7 ± 15.5 kPa) conserved their initial porous structure. Similar observations were made in regards of phagocytosis, with harder hydrogels being less prone to degradation by macrophages. The presence of neo-tissue within the hydrogels, revealing deposits of collagen, followed a similar pattern with an increased occurrence in harder hydrogels than in soft ones.

Curiously, an important amount of blood vessels were present within and throughout the porous hydrogels, as could be observed by IHC staining of α-SMA (Figure 8). Fewer blood vessels were present in soft hydrogels compared with more rigid compositions, with a preference to porous hydrogels with a broader range of pore size (50–180 µm). When considering only the blood vessels with a diameter over 25 µm, a preference to bigger pores was observed for more rigid compositions (Figure 8B).

4 | DISCUSSION

PEG-based hydrogels have been the focus of much attention for various tissue engineering applications over the past years.[9] However,

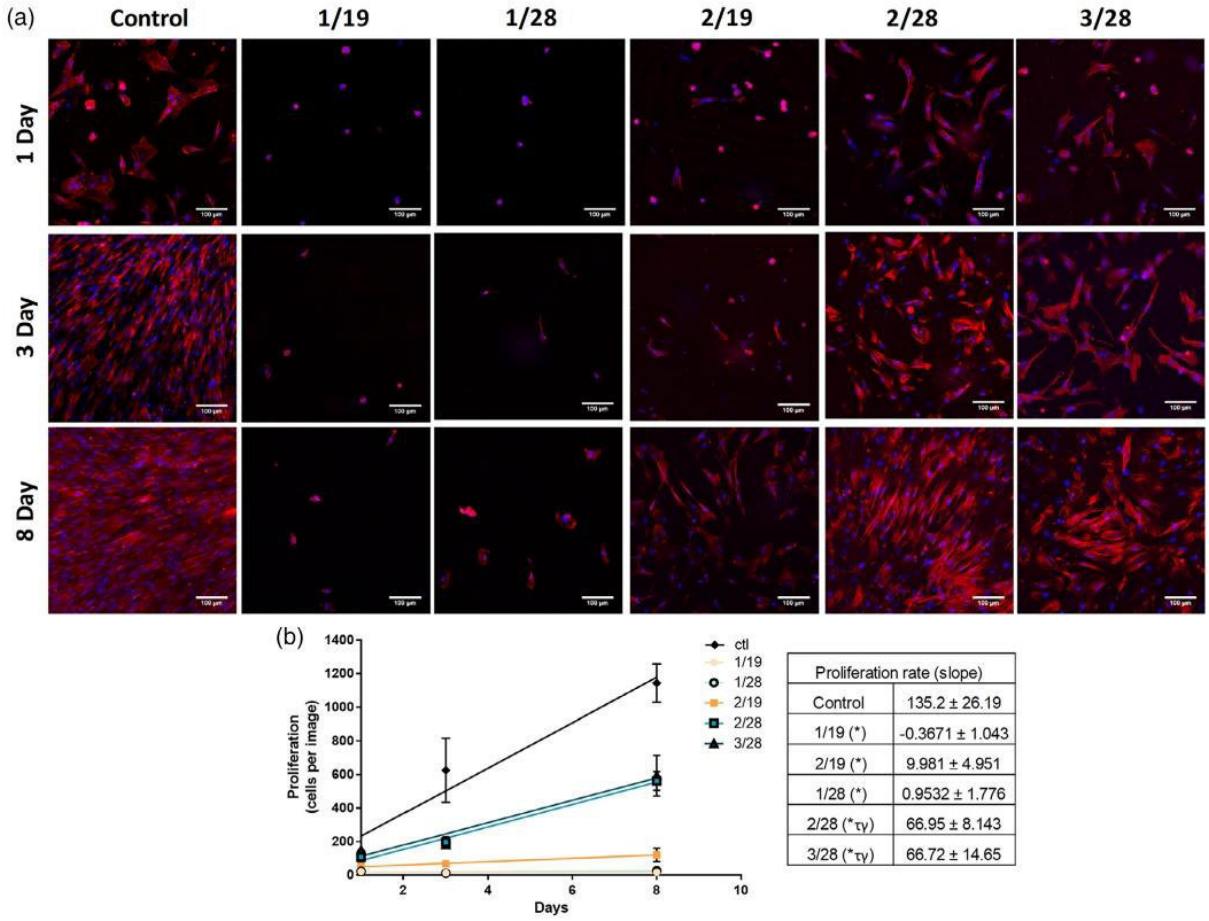

Proliferation rate (slope)	
Control	135.2 ± 26.19
1/19 (*)	-0.3671 ± 1.043
2/19 (*)	9.981 ± 4.951
1/28 (*)	0.9532 ± 1.776
2/28 (*τγ)	66.95 ± 8.143
3/28 (*τγ)	66.72 ± 14.65

FIGURE 6 A, Cytoskeleton structure of dermal fibroblasts seeded on the surface of hydrogel of different compositions (hydrogel concentration is expressed as de ratio DGL/PEG in mM) observed by DAPI-Phalloidin staining after 1, 4, and 8 days of culture (in blue cell nuclei and in red actin fibers). B, Cell proliferation rate of fibroblasts seeded on the surface of hydrogel of different compositions (hydrogel concentration is expressed as de ratio DGL/PEG in mM) obtained from cell nuclei counting after 1, 4, and 8 days of culture. (n = 3, One-way ANOVA, $p < 0.05$, *compared with control, τ compared with 1/19 and γ compared with 1/28)

their use with adherent cells requires them to be functionalized or coated with other molecules and moieties to allow cells attachment and proliferation, which increase their complexity and decrease their practical applicability. With the aim of further broadening their potential by providing them with inherent cellular adhesion and interactions, we therefore defined and evaluated a novel hydrogel where homobifunctionalized PEG-NHS is cross-linked by poly(L-lysine) dendrigrafts (DGL). The straightforward mixing of PEG-NHS with DGL in aqueous solutions indeed results in the swift formation of self-standing hydrogels. Among the various dendrimer structures that have been associated with PEG to form hydrogels,[20] DGL was so far never evaluated in this respect.

By varying the concentrations of hydrogel components, the cross-linking velocity, swelling, and mechanical properties can be tailored. DGL of third generation used in this study presents an important density of amine groups on their surface (123), and it has been determined that only 97.7% of these amines residues are available as binding sites per molecules (114).[35] PEG-NHS, on the contrary, possess only two able NHS ester group per molecules. Hence, the ratio of available amines groups versus NHS is always higher than 1, but we did not observe a relationship between this ratio and the cross-linking speed, mechanical properties or swelling ratio. Indeed, solutions of increasing DGL and PEG-NHS concentrations but of similar amines/NHS ratios resulted in increasing cross-link velocities and mechanical properties. Similarly to PEG-PAMAM gels, the effect of the polymer content could be logically ascribed to an increase of cross-linking density due to a closer presence of the amine (DGL) and NHS (PEG) reactive groups. Once a PEG molecule is attached to the surface of the dendrimer, the second NHS function on the other end of the PEG chain will have lower mobility, which will increase its probability to react with an amine function on the same dendrimer and form intramolecular loops.[36] Therefore, the dilution of the reaction mixture increases the space between the dendrimers, forming many intramolecular loops at the

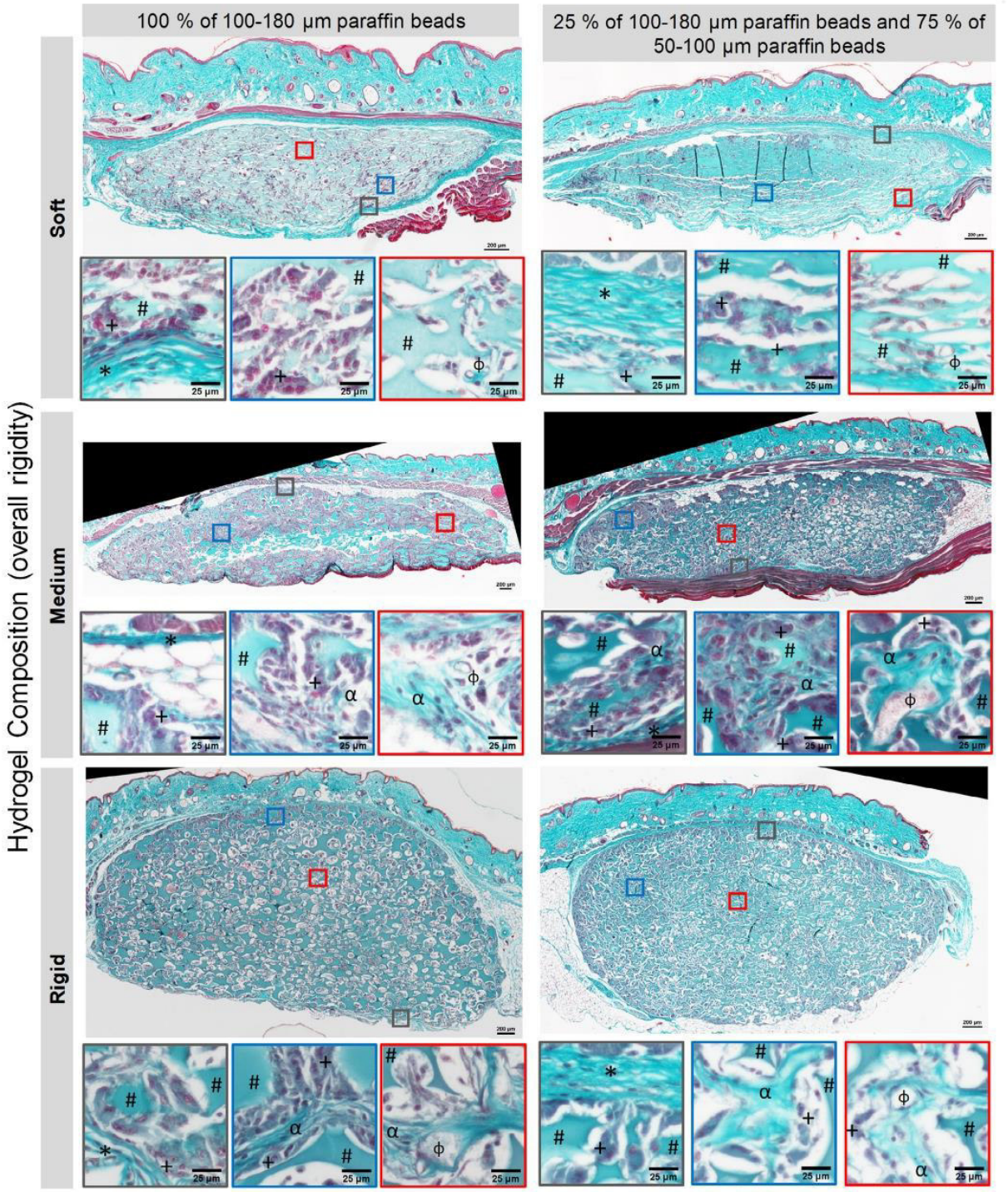

FIGURE 7 Subcutaneous implantation in mice for 3 weeks of DGL/PEG porous hydrogels of different compositions (soft, medium, and rigid, 7.7 ± 0.4, 41.5 ± 5.0, and 76.7 ± 15.5 kPa, respectively) and with different pore sizes distribution. Masson's trichrome staining of the full explants and close-ups highlighting the hydrogel (#), the fibrous capsule (*), macrophages (+), synthesised collagen (α), and blood vessels (Φ)

3.

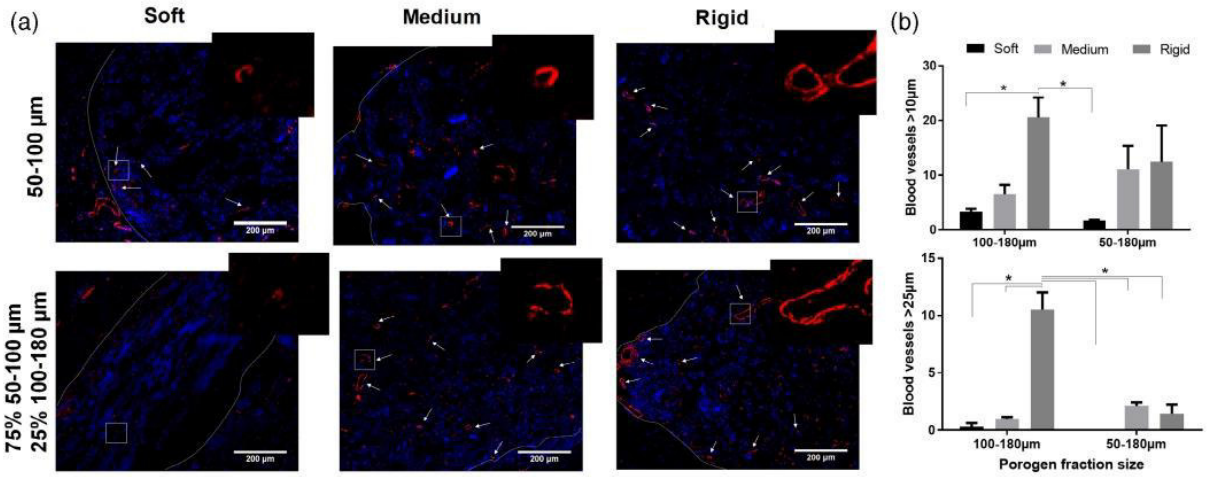

FIGURE 8 Blood vessels present after 3 weeks of subcutaneous implantation in mice in porous hydrogels of different compositions (soft, medium and rigid, 7.7 ± 0.4, 41.5 ± 5.0, and 76.7 ± 15.5 kPa, respectively) A, Immunofluorescence staining of α-SMA (red) indicating blood vessels present within the porous hydrogels while cell nuclei are stained with DAPI in blue; white lines delimit the border of the hydrogel and arrows point to sectioned blood vessels. B, Number of blood vessels present in the hydrogel of a dimeter greater than 10 or 25 µm obtained from image analysis of mosaic images of complete slides of porous hydrogels. (n = 3, Two-way ANOVA, $^*p < 0.05$)

expense of effective networks chains. Conversely, concentrating the mixture results in the opposite and increases the cross-link velocity.[24] This hypothesis is further reflected in the concomitant increase of mechanical properties and decrease of swelling observed in our hydrogels when increasing the polymer concentration. Since the arborescent molecules function as junction points in the cross-linking system, an increase in cross-links density will limit the expansion of the network, meaning a more compact mesh that leads to a decrease in swelling and an increase in rigidity. Similarly, Gitsov et al observed that the swelling properties of hydrogels prepared from PEG and various dendritic fragments were not related to the PEG concentration or the dendrimer generation but mainly to the total increase in components concentration.[37]

In addition to global polymer concentration, the DGL appears to have a predominant control of the hydrogel cross-linking. While its concentration doubling from 1 to 2 mM for a constant PEG-NHS concentration induces a 10-fold increase of the cross-linking velocity, a 1.6-fold increase of PEG-NHS for a constant DGL concentration only marginally decreases cross-linking speed. Although a DGL presents 114 amine groups to act as a cross-linker, it is unlikely that all the end groups will be able to react with the PEG molecules due to steric crowding, which will limit the maximum number of PEGs that can be grafted to a single dendrimer.[24] The fact that an increase of PEG-NHS concentration for a constant DGL does not result in a significant increase of the cross-linking speed supports this hypothesis by indicating that a maximal number of PEG per DGL has been reached. Contrariwise, an increase of DGL at constant PEG-NHS allows to reduce the steric crowding and increases further the cross-linking velocity.

To provide to PEG hydrogels the ability to inherently interact with cells, our hypothesis that DGL bioactivity could be conveyed to the hydrogel bulk was confirmed, as human fibroblasts were able to adhere and proliferate on the surface of DGL/PEG hydrogels prepared without supplementary coating or functionalization before seeding. Similarly to DGLs coated on surfaces,[29] the ability of cells to attach and spread to DGL-containing hydrogels can be attributed to early electrostatic interactions between the polyanionic cell surfaces and the polycationic charges brought by the DGL's amino groups. This was further supported by the increase in cell adhesion with an increase in DGL concentration.

While the concentration of DGL plays a role in cell adhesion to the hydrogels, their viability seems dependent of the ratio between DGL and PEG-NHS. Mortality was indeed observed when the ratio of amines to NHS groups was greater than 9. The cationic nature of DGL that provides cell adhesion properties is possibly also the cause of their cytotoxic effect, since excessive cationic charges can affect the integrity of cell membranes.[38] When coupled with PEG molecules, PEG might shield the dendritic cationic charges and improve the DGL viability, similarly to Tang et al who showed that PEG-gelation of DGL vectors for gene therapy allowed to decrease toxicity.[39]

Unlike cell adhesion and viability, cell morphology, and proliferation appear related to the overall hydrogel rigidity. For instance, for a constant DGL concentration (2 mM), an increase of PEG-NHS concentration from 19 to 28 mM results in an increase of substrate rigidity (from 41.5 ± 5.0 to 90.4 ± 14.4 kPa) that is correlated with an increase of cell proliferation and a fusiform spread-like morphology. Similarly, an increase in DGL concentration for a given PEG (1/19 and 2/19 or 1/28 and 2/28 mM DGL/PEG) resulted in a more spread morphology and an increase in proliferation, only when the mechanical properties were also increased. Furthermore, without significant increase of substrate rigidity, fibroblasts showed similar morphology and proliferation rate, as could be observed for compositions 2/28 and 3/28 mM DGL/PEG. The importance of substrate rigidity, over

hydrogel composition on cell morphology and proliferation was further underlined in hydrogels of similar amine/NHS ratio but different overall polymer concentrations. For example, compositions 2/19 and 3/28 mM DGL/PEG have different rigidity (respectively, 41.5 ± 5.0 to 76.7 ± 15.5 kPa) and showed different cell proliferation and spreading. These observations are in good agreement with several groups that have showed an increase in cell spreading area, stress fibers, and proliferation with an increase of substrate rigidity.[15, 40–44] In our case, cell proliferation was indeed considerably lower on the DGL/PEG hydrogels as compared to the plastic controls. This is in good agreement with reported studies that showed a similar decrease of fibroblasts proliferation rate when seeded on collagen substrates,.[45,46] In this regard, fibroblasts low proliferation rate on hydrogels can be considered closer to the physiological situation, where fibroblasts display a quiescent/secretory phenotype unless induced into proliferation by the release of stimulating factors as a result of tissue damage.[47]

As could be expected from PEG-based materials,[48] no intense immune reaction was observed upon implantation of the DGL/PEG hydrogels under the back skin of mice for 3 weeks. Consequently, the presence of DGL does not seem to induce a specific inflammatory reaction. The controlled porosity in the hydrogels showed sufficient interconnection to allow cell ingrowth, vascularization, and nutrient diffusion, which are important prerequisite for tissue engineering applications.[49–51] Interestingly, broader pores size distribution in the hydrogels resulted in a higher vascularization, especially of vessels greater than 25 μm in diameter. Logically, bigger pores allow bigger blood vessels to penetrate the hydrogels; however, this could only be observed in rigid hydrogels since they are able to maintain their structure during implantation. In addition to a good biocompatibility and a good cellular infiltration, the important presence of blood vessels in the porous hydrogels is a further suggestion of the potential of these novel hydrogels to support tissue formation.

5 | CONCLUSIONS

Through straight forward approaches, we have developed a novel PEG-hydrogel system cross-linked with DGL, which inherently allows human dermal fibroblasts attachment and proliferation, without the need for any additional moieties. Macroscopically, the hydrogels cross-link velocity, swelling, and rigidity can be tailored by the concentration of both components. As was hypothesized from the bioactive properties of DGLs, the ability of cells to adhere on the hydrogels surface appears solely dependent of the concentration of DGL while a minimal concentration of PEG is needed to sustain the viability of the adhered cells. Conversely, cell behavior and morphology appear linked to substrate rigidity rather than hydrogel composition. Of note, the resulting PEG-based hydrogels are biocompatible and allow cell infiltration and blood vessels invasion when porous. All these elements emphasize the potential of these novel hydrogels for a vast range soft tissue applications, while the presence of multiple amine groups and of a free carboxylic acid function in the DGL opens the door to further modifications toward tailored features.[27]

ACKNOWLEDGMENTS

This work was supported by la Région Auvergne-Rhône-Alpes (grant 17 002601 ARC 2016), CONACyT, i^2t^2 and the French national research grant DHERMIC (ANR TECSAN 016-01). The authors would like to thank the platform PriMaTiss for the histological sample preparation and the IGFL (UMR 5242) for the access to the vibratome.

CONFLICTS OF INTEREST

The authors declare no conflict of interest.

ORCID

Mariana Carrancá https://orcid.org/0000-0002-6088-8676

REFERENCES

1. Tibbitt MW, Anseth KS. Hydrogels as extracellular matrix mimics for 3D cell culture. *Biotechol Bioeng*. 2009;*103*:655-663.
2. Jia X, Kiick KL. Hybrid multicomponent hydrogels for tissue engineering. *Macromol Biosci*. 2009;*9*:140-156.
3. Park S, Park K. Engineered polymeric hydrogels for 3D tissue models. *Polymers*. 2016;*8*:23.
4. Figueiredo L, Pace R, D'Arros C, et al. Assessing glucose and oxygen diffusion in hydrogels for the rational design of 3D stem cell scaffolds in regenerative medicine. *J Tissue Eng Regen Med*. 2018;*12*:1238-1246.
5. Van Vlierberghe S, Dubruel P, Schacht E. Biopolymer-based hydrogels as scaffolds for tissue engineering applications: a review. *Biomacromolecules* [Internet. 2011;*12*:1387-1408. Available from. https://doi.org/10.1021/bm200083n.
6. Franz S, Rammelt S, Scharnweber D, Simon JC. Immune responses to implants—a review of the implications for the design of immunomodulatory biomaterials. *Biomaterials*. 2011;*32*:6692-6709. Available from:. https://doi.org/10.1016/j.biomaterials.2011.05.078.
7. Zhu J. Bioactive modification of poly(ethylene glycol) hydrogels for tissue engineering. *Biomaterials*. 2010;*31*:4639-4656.
8. Spicer CD. Hydrogel scaffolds for tissue engineering: the importance of polymer choice. *Polym Chem Royal Society of Chemistry*. 2020;*11*:184-219.
9. Lin C, Anseth KS. PEG hydrogels for the controlled release of biomolecules in regenerative medicine. *Pharm Res*. 2009;*26*:631-643.
10. Sargeant TD, Desai AP, Banerjee S, Agawu A, Stopek JB. An in situ forming collagen—PEG hydrogel for tissue regeneration. *Acta Materialia Inc*. 2012;*8*:124-132. https://doi.org/10.1016/j.actbio.2011.07.028.
11. Barros D, Conde-sousa E, Gonçalves AM, et al. Engineering hydrogels with affinity-bound laminin as 3D neural stem cell culture systems. *Biomater Sci Royal Soc Chem*. 2019;*7*:5338-5349.
12. Hern DL, Hubbell JA. Incorporation of adhesion peptides into nonadhesive hydrogels useful for tissue resurfacing. *J Biomed Mater Res*. 1998;*39*:266-276.
13. Ouyang L, Dan Y, Shao Z, et al. MMP—sensitive PEG hydrogel modified with RGD promotes bFGF, VEGF and EPC - mediated angiogenesis. *Exp Ther Med*. 2019;*18*:2933-2941.
14. Burdick JA, Anseth KS. Photoencapsulation of osteoblasts in injectable RGD-modified PEG hydrogels for bone tissue engineering. 2002;*23*:4315-4323.
15. Nemir S, West L. J. Synthetic materials in the study of cell response to substrate rigidity. *Ann Biomed Eng*. 2010;*38*:2-20.
16. Papavasiliou G, Sokic S, Turturro M. Synthetic PEG Hydrogels as Extracellular Matrix Mimics for Tissue Engineering Applications, Biotechnology - Molecular Studies and Novel Applications for Improved Quality of Human Life, Reda Helmy Sammour, IntechOpen. https://doi.org/10.5772/31695. Available from: https://www.intechopen.

com/books/biotechnology-molecular-studies-and-novel-applications-for-improved-quality-of-human-life/synthetic-peg-hydrogels-as-extracellular-matrix-mimics-for-tissue-engineering-applications.
17. Rizzi SC, Hubbell JA. Recombinant protein-co-PEG networks as cell-adhesive and Proteolytically degradable hydrogel matrixes. Part I: development and physicochemical characteristics. *Biomacromolecules*. 2005;*6*:1226-1238.
18. Wathier M, Jung PJ, Carnahan MA, Kim T, Grinstaff MW. Dendritic Macromers as in situ polymerizing biomaterials for securing cataract incisions. *J Am Chem Soc*. 2004;*126*:12744-12745.
19. Wathier M, Johnson CS, Kim T, Grinstaff MW. Hydrogels formed by multiple peptide ligation reactions to fasten corneal transplants. *Bioconjugate Chem*. 2006;*17*:873-876.
20. Kaga S, Arslan M, Sanyal R, Sanyal A. Dendrimers and Dendrons as versatile building blocks for the fabrication of functional hydrogels. *Molecules*. 2016;*21*(4):497. https://doi.org/10.3390/molecules21040497.
21. Oliveira JM, Salgado AJ, Sousa N, Mano JF, Reis RL. Dendrimers and derivatives as a potential therapeutic tool in regenerative medicine strategies—a review. Prog Polym Sci [internet]. *Elsevier*. 2010;*35*:1163-1194.
22. N. Desai P, Yuan Q, Yang H. Synthesis and characterization of Photocurable Polyamidoamine dendrimer hydrogels as a versatile platform for tissue engineering and drug delivery. *Biomacromolecules* 2011;*11*:666–73.
23. Navath RS, Menjoge AR, Dai H, Romero R, Kannan S, Kannan RM. Injectable PAMAM dendrimer - PEG hydrogels for the treatment of genital infections: formulation and in vitro and in vivo evaluation. *Mol Pharmaceutics*. 2011;*8*:1209-1223.
24. Unal B, Hedden RC. Gelation and swelling behavior of end-linked hydrogels prepared from linear poly (ethylene glycol) and poly (amidoamine) dendrimers. *Polymer*. 2006;*47*:8173-8182.
25. Labieniec-Watala M, Watala C. PAMAM dendrimers: destined for success or doomed to fail? Plain and modified PAMAM dendrimers in the context of biomedical applications. J pharm Sci [internet]. *Elsevier Masson SAS*. 2015;*104*:2-14. https://doi.org/10.1002/jps.24222.
26. Romestand B, Rolland J, Commeyras A, Desvignes I, Pascal R, Vandenabeele-trambouze O. Dendrigraft poly- L -lysine: a non-immunogenic synthetic carrier for antibody production. *Biomacromolecules*. 2010;*11*:1169-1173.
27. Francoia J, Vial L. Everything you always wanted to know about poly-l-lysine Dendrigrafts (but were afraid to ask). *Chem—Eur J*. 2018;*24*:1-10.
28. Huang R, Liu S, Shao K, et al. Evaluation and mechanism studies of PEGylated dendrigraft poly-L-lysines as novel gene delivery vectors. *Nanotechnology*. 2010;*21*:265101.
29. Lorion C, Faye C, Maret B, et al. Biosynthetic support based on dendritic poly(L-lysine) improves human skin fibroblasts attachment. *J Biomater Sci, Polym Ed* [Internet. 2014;*25*:136-149.
30. Collet H, Souaid E, Cottet H, et al. An expeditious multigram-scale synthesis of lysine dendrigraft (DGL) polymers by aqueous n-carboxyanhydride polycondensation. *Chem—A Eur J*. 2010;*16*:2309-2316.
31. Maret B, Crépet A, Faye C, Garrelly L, Ladavière C. Molar-mass analysis of dendrigraft poly(L-lysine) (DGL) polyelectrolytes by SEC-MALLS: the "cornerstone" refractive index increment. *Macromol Chem Phys*. 2015;*216*:95-105.
32. Schneider CA, Rasband WS, Eliceiri KW. NIH image to ImageJ: 25 years of image analysis. *Nat Methods*. Nature Publishing Group. 2012;*9*:671-675.
33. Ma PX, Choi PDJ. Biodegradable polymer scaffolds with well-defined interconnected spherical pore network. *Tissue Eng*. 2001;*7*:23-33.
34. Anseth KS, Bowman CN, Brannon-Peppas L. Mechanical properties of hydrogels and their experimental determination. *Biomaterials*. 1996;*17*:1647-1657.
35. Coussot G, Nicol E, Commeryras A, Desvignes I, Pascal R, Vandenabeele-trambouze O. Colorimetric quantification of amino groups in linear and dendritic structures. *Polym Int*. 2009;*58*:511-518.
36. Wang Y, Zhao Q, Zhang H, Yang S, Jia X. A novel poly(amido amine)-dendrimer-based hydrogel as a mimic for the extracellular matrix. *Adv Mater*. 2014;*26*:4163-4167.
37. Gitsov I, Zhu C. Amphiphilic hydrogels constructed by poly(ethylene glycol) and shape-persistent dendritic fragments. *Macromolecules*. 2002;*35*:8418-8427.
38. Quinton MP, Philpott CWA. Role for anionic sites in epithelial architecture: effects of cationic polymers on cell membrane structure. *J Cell Biol*. 1978;*56*:787-796.
39. Tang M, Dong H, Li Y, Ren T. Harnessing the PEG-cleavable strategy to balance cytotoxicity, intracellular release and the therapeutic effect of dendrigraft poly-L-lysine for cancer gene therapy. *J Mater Chem B*. 2016;*4*:1284-1295.
40. Jiang G, Huang AH, Cai Y, Tanase M, Sheetz MP. Rigidity sensing at the leading edge through avb3 Integrins and RPTPa. *Biophys J*. 2006;*90*:1804-1809.
41. Yeung T, Georges PC, Flanagan LA, et al. Effects of substrate stiffness on cell morphology, cytoskeletal structure, and adhesion. *Cell Motil Cytoskeleton*. 2005;*60*:24-34.
42. Ghosh K, Pan Z, Guan E, et al. Cell adaptation to a physiologically relevant ECM mimic with different viscoelastic properties. *Biomaterials*. 2007;*28*:671-679.
43. Lo CM, Wang HB, Dembo M, Wang YL. Cell movement is guided by the rigidity of the substrate. *Biophys J*. 2000;*79*:144-152.
44. Solon J, Levental I, Sengupta K, Georges PC, Janmey PA. Fibroblast adaptation and stiffness matching to soft elastic substrates. *Biophys J*. 2007;*93*:4453-4461.
45. Kono T, Tanii T, Furukawa M, et al. Cell cycle analysis of human dermal fibroblasts cultured on or in hydrated type I collagen lattices. *Arch Dermatol Res*. 1990;*282*:258-262.
46. Rhudy RW, McPherson JM. Influence of the extracellular matrix on the proliferative response of human skin fibroblasts to serum and purified platelet-derived growth factor. *J Cell Physiol*. 1988;*137*:185-191.
47. Sarber R, Hull B, Merrill C, Sorrano T, Bell E. Regulation of proliferation of fibroblasts of low and high population doubling levels grown in collagen lattices. *Mech Ageing Dev*. 1981;*17*:107-117.
48. Lynn AD, Kyriakides TR, Bryant SJ. Characterization of the in vitro macrophage response and in vivo host response to poly(ethylene glycol)-based hydrogels. *J Biomed Mater Res—Part A*. 2010;*93*:941-953.
49. Griffon DJ, Sedighi MR, Schaeffer DV, Eurell JA, Jonhnson AL. Chitosan scaffolds: interconnective pore size and cartilage engineering. *Acta Biomater*. 2006;*2*:313-320.
50. Rouwkema J, Rivron NC, Van BCA. Vascularization in tissue engineering. *Trends Biotechnol*. 2008;*26*:434-441.
51. Annabi N, Nichol JW, Zhong X, et al. Controlling the porosity and microarchitecture of hydrogels for tissue engineering. *Tissue Eng Part B Rev*. 2010;*16*:371-383.

SUPPORTING INFORMATION

Additional supporting information may be found online in the Supporting Information section at the end of this article.

How to cite this article: Carrancá M, Griveau L, Remoué N, et al. Versatile lysine dendrigrafts and polyethylene glycol hydrogels with inherent biological properties: in vitro cell behavior modulation and in vivo biocompatibility. *J Biomed Mater Res*. 2020;1–12. https://doi.org/10.1002/jbm.a.37083

Archives of Dermatological Research
https://doi.org/10.1007/s00403-019-01962-5

ORIGINAL PAPER

Substrate softness promotes terminal differentiation of human keratinocytes without altering their ability to proliferate back into a rigid environment

Choua Ya[1,2] · Mariana Carrancá[1] · Dominique Sigaudo-Roussel[1] · Philippe Faure[3] · Bérengère Fromy[1] · Romain Debret[1]

Received: 29 October 2018 / Revised: 13 May 2019 / Accepted: 15 June 2019

Abstract

Substrate stiffness is a key regulator of cell behavior. To investigate how mechanical properties of cell microenvironment affect the human keratinocyte, primary cells were seeded on polyacrylamide hydrogels of different compliances (soft: 4 kPa, medium: 14 kPa, rigid: 45 kPa) in comparison with glass coverslip (> GPa). Keratinocyte spreading and proliferation were strongly decreased on the softest hydrogel, while no significant difference was observed between medium, rigid hydrogels and glass coverslip, and cells' viability was comparable in all conditions after 72 h. We then performed a RNA-seq to compare the transcriptomes from keratinocytes cultured for 72 h on the softest hydrogel or on coverslips. The cells on the soft hydrogel showed a strong increase in the expression of late differentiation marker genes from the epidermal differentiation complex (1q21) and the antioxidant machinery. In parallel, these cells displayed a significant loss of expression of the matrix receptors (integrin α6 and β1) and the EGF receptor. However, when these cells were replated on a plastic culture plate (> GPa), they were able to re-engage the proliferation machinery with a strong colony-formation efficiency. Overall, using low-calcium differentiation monolayers at confluence, the lesser the rigidity, the stronger the markers of late differentiation are expressed, while the inverse is observed regarding the markers of early differentiation. In conclusion, below a certain rigidity, human keratinocytes undergo genome reprogramming indicating terminal differentiation that can switch back to proliferation in contact with a stiffer environment.

Keywords Mechanical properties · Keratinocytes · Differentiation · Proliferation · Transcriptome profiling

Introduction

In the epidermis, the balance between keratinocyte proliferation in the basal layer and terminal differentiation and shedding in the upper layers maintain normal tissue homeostasis [3]. The keratinocytes are interconnected via intercellular junctions and lie on a basal membrane at the interface of the epidermis and the dermis, the underlying extracellular matrix (ECM)-rich connective tissue. Mechanical, biophysical and biochemical factors regulate the keratinocyte function. Indeed, physical interactions are detected by the keratinocytes through mechanotransduction mechanisms transforming mechanical loads into biochemical cascades and have been involved in the regulation of keratinocyte proliferation, differentiation, morphology, and migration [27]. There has been extensive research into the measurement of the skin's elastic modulus via a multitude of in vitro and in vivo techniques with various values depending on

Bérengère Fromy and Romain Debret are co-last authors.

Electronic supplementary material The online version of this article (https://doi.org/10.1007/s00403-019-01962-5) contains supplementary material, which is available to authorized users.

✉ Romain Debret
romain.debret@ibcp.fr

[1] CNRS/UCBL, University Lyon 1, UMR 5305, Laboratory of Tissue Biology and Therapeutic Engineering, LBTI, IBCP, 7, passage du Vercors, 69367 Lyon cedex 7, France

[2] Isispharma, 29 Rue Maurice Flandin, 69003 Lyon, France

[3] Alpol Cosmétique, 140 Rue Pasteur, 01500 Château-Gaillard, France

Published online: 07 August 2019

the method used (see [6, 11] for comprehensive reviews). In vivo, the mechanical measurements obtained are generally attributed to those of the dermis because of its thickness with respect to the epidermis, with a rigidity of 5 and 10 kPa as measured by indentation [30]. The dermis is a connective tissue composed mainly of fibroblasts responsible for the synthesis of an ECM rich in collagen fibers, elastic fibers, glycosaminoglycans and the fundamental substance. Mechanically speaking, the dermis gives the skin its strength, firmness, elasticity and viscosity. Studies have attempted to measure the mechanical properties of the different histological layers of the skin, but high interconnections between the different layers rendered the discrimination challenging.

The mechanical properties of the skin can be altered by physiological phenomena such as aging or wounding [9, 30], or by pathological phenomena with consequences on the epidermal homeostasis [10]. During chronological aging, the expression level of ECM constituents, such as type I and III collagens [23] and elastin [7], decrease, while the synthesis and the activities of matrix metalloproteases increase [24]. Together, these alterations lead to age-related reduction of skin elastic modulus as reported in humans [30]. During the wound healing process, the composition and structure of the ECM are continuously modified during the formation of granulation tissue and remodeling [8], inducing drastic changes in the mechanical properties of the dermis. Indeed, the rigidity of the granulation tissue increased from 18 kPa at 7 days after wounding to 50 kPa at 12 days [9]. This increase is required for the initiation of keratinocyte migration. Persistent abnormal alterations in the mechanical properties of ECM would therefore contribute to healing defects such as chronic or hypertrophic wounds [12].

In vitro studies showed that keratinocytes are able to respond to the rigidity of the support. Studies on the HaCaT cell line have indeed shown that the rigidity of the support promotes proliferation and migration, leading to an increase in re-epithelization, whereas cell differentiation is inhibited [25]. The substrate stiffening promotes proliferation by activation of the EGF signaling pathway, as reported using primary human keratinocytes [13]. In addition, the rigidity of the substrate regulated the formation of adhesion junctions via activation of the Jun N-terminal kinase pathway [29]. Finally, stiffness affects the morphology of cells resulting in a decrease in cell spread and focal adhesions [22]. The changes in the dermal stiffness could thus explain the phenotypic disturbances observed in keratinocytes leading to an alteration of epidermal homeostasis.

However, data on the impact of skin stiffness on epidermal differentiation are still very sparse, particularly using primary human cells. In this study, we aimed to investigate how mechanical properties of the microenvironment affect primary human keratinocyte phenotype. For this purpose, we used primary human keratinocytes grown on substrates of different compliances.

Materials and methods

Ethical considerations

Infant foreskins were collected according to the Declaration of Helsinki Principles. Written informed consent was obtained from infants' parents according to French bioethical law of 2004.

Cell culture

The human epidermal keratinocyte cultures were obtained from child foreskin biopsies after enzymatic treatment [1]. Briefly, the biopsies were cut into small pieces and immersed overnight at 4 °C in a solution containing trypsin (Gibco, Life Technologies, Carlsbad, CA, USA) and dispase (Dispase II; Roche Diagnostics, Mannheim, Germany). Then, the dermis and epidermis were separated and the epidermis was incubated for 20 min at 37 °C with trypsin and 0.05% EDTA. The cells were resuspended and filtered through a 70 µm cell stainer (BD Biosciences) to remove the remaining aggregates. After extraction, keratinocytes were cultured in KGM2 medium (Keratinocyte Growth Medium 2, Promocell, Heidelberg, Germany) comprising 0.06 mM $CaCl_2$ and supplemented with 100 µg/ml of primocin at 37 °C and 5% CO_2. Cells were amplified on plastic dishes prior to seeding on different substrates for experimental assessments. To induce keratinocyte differentiation, at confluence, cells were cultured in KGM2 without growth factor supplement. The cells were used at early passage (passage 1 and 2) in subsequent experiments. All cell-based in vitro experiments were repeated in triplicate.

Generation of polyacrylamide hydrogels

The hydrogels were synthesized according to the principle described previously by Tse and Engler [2]. Briefly, 18 mm diameter coverslips were activated with 70 mM NaOH solution and heated at 80 °C. This step was repeated with milliQ water until NaOH forms a thin semi-transparent film. The coverslips were treated for 5 min with APES (3-aminopropyltriethoxysilane, Sigma) and thoroughly rinsed. Then, 0.5% glutaraldehyde (Sigma) was added onto the coverslips for 30 min and dried few minutes at room temperature. In parallel, 24×60 mm glass slides were chlorosilanized with DCDMS (dichlorodimethylsilane, Sigma) for 5 min, gently rinsed, and dried for 30 min at room temperature.

Polyacrylamide gels with different modulus of elasticity values were produced by mixing acrylamide/bis-acrylamide

solutions at final percentages (p/v) of 3/0.1, 4/0.225 and 10/0.225 for soft, medium and rigid hydrogels, respectively. The polymerization is initiated with APS (ammonium persulfate, Sigma) and TEMED (*N*,*N*,*N*′,*N*′-tetramethylethane-1,2-diamine, Sigma). The polyacrylamide solution is immediately pipetted onto the chlorosilanized slide and covered by the functionalized coverslip. After the completed polymerization, the top coverslip with the attached polyacrylamide gel is slowly peeled off and rinsed to take out DCDMS on gel surface.

To facilitate keratinocyte attachment, a heterobifunctional crosslinker, sulfo-SANPAH (sulfosuccinimidyl6(4-azido-2-nitrophenyl-amino)hexanoate, ThermoFisher Scientific), is used to crosslink extracellular matrix molecules onto the surface of the gel. 0.2 mg/mL sulfo-SANPAH solution is added to the gel surface, placed 3 inches under an ultraviolet lamp, irradiated for 10 min and rinsed with water. Then, 100 µg/mL of rat tail collagen I solution (ThermoFisher Scientific) is added to the gel and incubated for 2 h at room temperature under a 50 rpm agitation. Hydrogels were rinsed in PBS (phosphate buffered saline), placed in 12-well plates and immersed in culture media at 37 °C one night prior to cell seeding.

Mechanical characterization of polyacrylamide hydrogels

Viscoelastic properties of polyacrylamide gels (12 mm diameter and ~ 1.2 mm thick) were determined by Dynamical Mechanic Analysis (DMA 242 E Artemis, NEZSTCH, Germany). Samples were subject to compression tests under liquid immersion (PBS) water bath at room temperature. Strain-sweep measurements were performed to determine the elastic limit or linear domain of the gels. The tan delta, complex modulus (E^*) as well as storage (E') and loss modulus (E'') were determined from dynamic stress curves obtained for an amplitude of 55 µm, a frequency of 1 Hz and 10% constraint.

Immunofluorescence

Keratinocytes were plated on a glass coverslip or polyacrylamide gels in 12-well plates for 24 h to analyze cell morphology, or for 72 h to observe differentiation markers. Then, the cells were fixed in 4% paraformaldehyde for 10 min.

To visualize focal adhesion and actin cytoskeleton, cells were permeabilized with 0.1% Triton X-100 for 10 min, blocked with 5% of goat serum in PBS for 1 h at room temperature and incubated with anti- antibody (clone 8D4, Sigma) overnight at 4 °C. Secondary Alexa-488 anti-mouse (Invitrogen) was incubated 1 h at room temperature. Actin network was stained with TRITC phalloidin for 5 min at room temperature. Differentiation markers were immuno-detected with anti-K10 (Ab76318, Abcam, 1:500) or anti-involucrin (Ab53112, Abcam, 1:500) for 2 h at room temperature. Secondary Alexa-563 anti-rabbit (Invitrogen) was incubated for 1 h at room temperature.

All stainings were incubated with DAPI (4,6-diamidino-2-phenylindole) to visualize DNA and mounted with Permafluor™ Aqueous Mounting Medium (Labvision, Thermo Fisher Scientific). All images were acquired with a Nikon TiE inverted fluorescent microscope.

Cell proliferation and viability assay

Cells (5×10^3 per substrate) were seeded on glass coverslip or polyacrylamide hydrogels. Cells were fixed at 24 h, 48 h and 72 h with 4% paraformaldehyde for 10 min and stained with DAPI for 5 min. Cell proliferation was determined by nuclei count using ImageJ software. All experiments were repeated at least three times in triplicate.

To assess keratinocyte viability, cells were cultured on glass coverslip or on hydrogels for 3 days. Cells were then stained with LIVE/DEAD™ Cell Imaging Kit (Invitrogen), as described by the manufacturer's protocol. Green living cells and red dead cells were counted and the ratio of living cells/dead cells was expressed as a percentage of cell viability.

mRNA extraction and qRT-PCR

Total RNA was extracted from cells at indicated times using RNeasy mini kit (Qiagen, Valencia, CA) according to the manufacturer's instructions. Reverse transcription was performed using PrimeScript™ RT Reagent Kit (Takara, Tokyo, Japan). qRT–PCR was performed on a Mx3000P real-time PCR system (Stratagene, san Diego, CA, USA) using SYBR® Premix Ex Taq™ II (TaKaRa). Amplification was started at 95 °C for 30 s as the first step, followed by 40 successive cycles of PCR: at 95 °C for 5 s, at 60 °C for 30 s and at 72 °C for 30 s. Primers specific for RPL13 (ribosomal housekeeping gene), MKI67 (proliferation marker), KRT1 and KRT10 (early differentiation marker), IVL, TGM1, FLG and CDSN (late differentiation markers), ITGA6 and ITGB1 (cell adhesion), CDKN1A and CDKN2A (cell cycle progression), EREG and EGFR (epidermal growth factor signaling), MT1H, AKR1B10 and AKR1C2 (oxidative machinery) were used.

Western blot

To analyze protein expression, cells were washed briefly in PBS and lysed on ice in the RIPA buffer (50 mM Tris–HCl, pH 8, 150 mM NaCl, 1% Nonidet P-40, 0.1% sodium deoxycholate, 0.1% SDS, 1 mM orthovanadate and protease inhibitor cocktail (Thermo Fischer scientific). Lysates were

centrifuged for 10 min at 14,000*g* at 4 °C to eliminate cell debris. Proteins were separate by SDS–PAGE followed by transfer to polyvinylidene fluoride membrane (EMD-Millipore, Billerica, MA). The membrane was blocked with 5% non-fat milk in Tris-buffered saline (TBS) buffer containing 0.1% Tween-20, and incubated with rabbit anti-involucrin (SY5) antibody (SC-21,748, Santa Cruz, 1:1000) and mouse anti-actin (C4, MAB1501, Sigma-Aldrich, 1:5000), overnight at 4 °C. The membrane was incubated with secondary antibodies for 1 h at room temperature: goat anti-rabbit IgG (H + L)–HRP conjugate (170–6510, Biorad, 1:10,000) and goat anti-mouse IgG (H + L)–HRP conjugate (170–6516, Biorad, 1:10,000). Antibody binding was detected by the enhanced chemiluminescence system (Thermo Fischer Scientific), using the Fusion Fx system (Vilbert Lourmat).

RNA sequencing

Cells were cultured on glass substrate and soft hydrogel for 3 days and total RNA was extracted using RNeasy mini kit (Qiagen). RNA quantity and purity were verified using 2200 TapeStation system (Agilent Technologies). Library preparation was performed using mRNA-Seq Library Prep Kit Lexogen following manufacturer's instructions. Libraries were validated on TapeStation—HSD1000 ScreenTape®Dosage. Barecoded libraries were pooled together (three per run) on an equimolar basis and run using PI chips on an Ion Torrent™ PGM sequencer using HiQ chemistry. Library preparation and sequencing were achieved by the IGFL sequencing platform (Lyon, France).

Bioinformatic analyses

Reads were aligned to the human reference genome hg19 using the Ion Torrent RNASeqAnalysis plugin. Two consecutive alignments were achieved through the STAR and Bowtie2 programs to generate the BAM files. Reads over genes were determined using the R/Bioconductor "Rsubread" software package to create a count matrix [15]. Differential gene expression analysis was performed using R/Bioconductor "limma" and "edgeR" software packages [18, 20, 21]. Smear plot and heat map were generated from limma-voom normalized values in *R* [14]. Genes with a differential expression FDR ≤ 0.05 were considered significant. Two sets of significant genes, upregulated or downregulated, were subjected to gene ontology (GO) analysis using GOrilla tool [5] and enrichment analysis of the five top molecular functions are represented.

Clonogenic assay

Primary keratinocytes were plated on soft hydrogel or glass coverslip for 3 days then clonogenic assay was realized on three generations with plastic culture plate. For each generation, the cells were trypsinized, resuspended in the media and counted. The cells were re-seeded (500 cells/well) in 6-well plates and incubated for 10 days. On the 10th day, cells were trypsinized, counted and re-seeded (500 cells/well) in new 6-well plates. In parallel, cells were fixed with 4% paraformaldehyde solution for 10 min and the colonies were stained with 0.1% crystal violet for 1 h. The wells were rinsed three times with PBS and cells were lysed with 2% SDS solution. The absorbance (570 nm) was read with Tecan Infinite 1000 M. All experiments were performed in triplicate.

Statistical analysis

All data were presented as mean ± SD for three independent experiments. Statistical significance ($p < 0.05$) was determined by performing either unpaired *T* test when comparing two groups or one-way or two-way analysis of variance (ANOVA) followed by a Bonferroni post-test when comparing multiple groups. All analyses were performed with GraphPad Prism5 software.

Results

To investigate human keratinocyte behavior in response to substrate stiffness, we used polyacrylamide hydrogels (PAH) of different compliances and functionalized with type I collagen coating to allow cell adhesion. The three different PAH preparations displayed E^* of 3.91 ± 1.4 kPa (soft), 14.63 ± 3.7 kPa (medium) and 44.98 ± 3.6 kPa (rigid), respectively (Fig. 1a). 24 h post-seeding, the morphology of freshly isolated human keratinocytes was modified by the substrate stiffness (Fig. 1b). On soft PAH, the cell shape remained round with a thin distribution of the actin cytoskeleton at the plasma membrane, while no clear focal adhesion point was observed. On medium and rigid PAH, cells were much more spread as illustrated by a wider distribution of actin and the presence of well-defined focal adhesion points. Glass coverslip condition was characterized by the formation of stress fibers across the cytoplasm and well-defined focal adhesion points at the cell periphery leading to a polygonal cell shape. Since cells were present in all conditions, their proliferation was assessed by cell counting during 3 days (Fig. 1c). No significant difference was observed between medium PAH, rigid PAH and glass coverslip conditions. In contrast, no proliferation was noted on the soft substrate. Cell viability was then assessed in all conditions after 3 days and no significant difference was observed (Fig. 1d). These results show that the human keratinocyte gradually adapts to the substrate rigidity on which it adheres. On the softest substrate, although the cells were in the proliferative phase

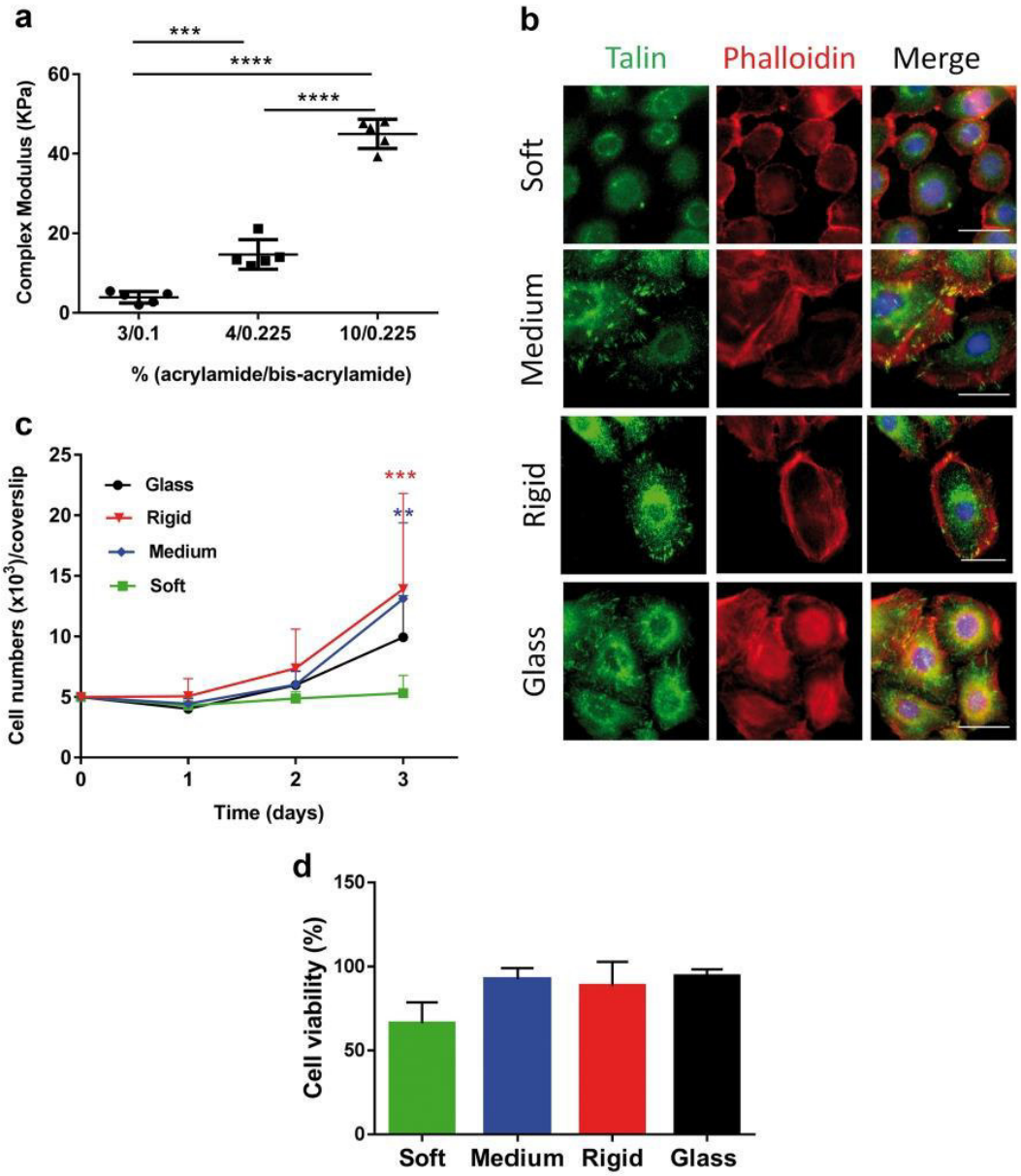

Fig. 1 Substrate mechanical properties affect keratinocyte behavior. **a** Viscoelastic properties of PAH were determined by dynamical mechanic analysis, using an amplitude of 55 µm, a frequency of 1 Hz and 10% constraint. (E^*) complex modulus. ($n=5$) The data are presented as mean ± SD; ***$P<0.001$ and ****$P<0.0001$ using one-way ANOVA with a Bonferroni post-test. **b** Human primary keratinocytes were cultured on glass and PAH with different rigidities. After 24 h, cells were stained for F-actin content (phalloidin staining: red) and nuclei were counterstained with DAPI (blue). Immunostained for talin (green) after 24 h in culture. Scale bar: 25 µm. **c** Human primary keratinocytes were cultured on glass (black dot), soft (green square), medium (blue diamond) and rigid (red triangle) PAH. Nuclei were counterstained with DAPI and proliferation rate was measured by cell counting after 1, 2 and 3 days in culture. ($n=3$) All data are presented as mean ± SD, **$P<0.01$ and ***$P<0.001$, using two-way ANOVA with a Bonferroni post-test, compared to soft PAH condition. **d** After 3 days in culture on PAH with different rigidities or glass coverslip, living cells and dead cells were visualized and counted by LIVE/DEAD™ Cell Imaging. Histograms represent cell viability as the percentage of living cells over dead cells. All data are presented as mean ± SD. A two-way ANOVA with a Bonferroni post-test was applied, compared to soft PAH condition

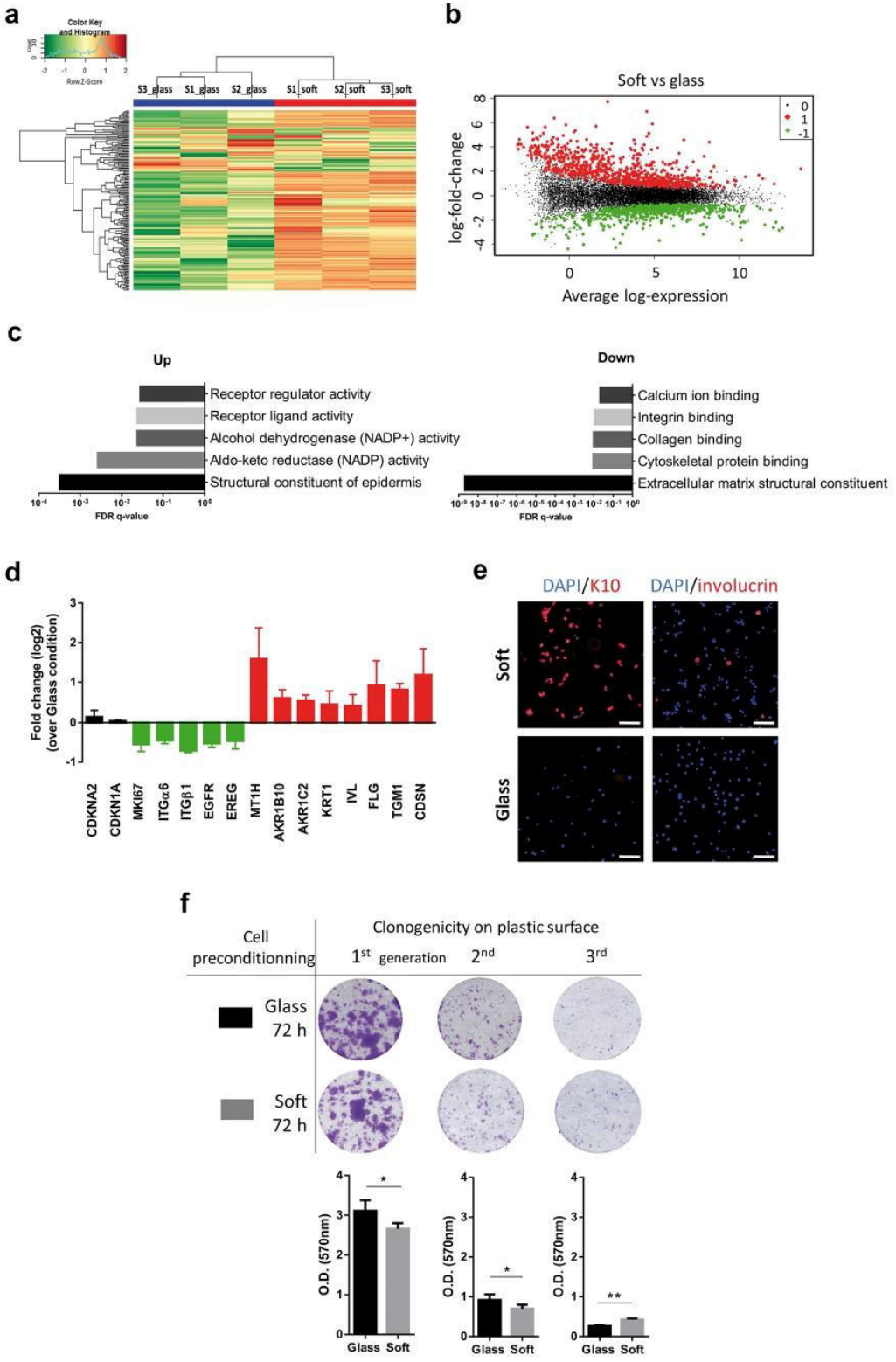

◂**Fig. 2** Transcriptomic profiling and colony-forming efficiency. **a** Hierarchical clustering of 200 most differentially expressed genes in keratinocytes cultured for 72 h on soft PAH (S_soft) or glass (S_glass). Green color corresponds to and red color to overexpressed genes. **b** Smear plot of RNA-seq data showing average log signal intensity (x axis) vs. log2 fold change in gene expression (soft PAH/glass). Differentially expressed genes (FDR $q \leq 0.05$) are shown in red for upregulated genes ($n = 808$), in green for downregulated genes (n = 584), and non-significant changes are shown in black. **c** Gene ontology enrichment analysis of the top five molecular functions (GOrilla). Significance of term enrichment by FDR q values is represented by log10 bar values. **d** qPCR validation of 2 unmodulated (black) and 13 modulated (green and red) genes on soft substrate. ($n = 3$) Data are presented as mean ± SD. **e** Human primary keratinocytes were cultured on glass and soft PAH. After 72 h, cells were immunostained for cytokeratin 10 or involucrin (red) and nuclei were counterstained with DAPI (blue). Scale bar: 100 µm. **f** Preconditioned cells grown for 72 h on soft PAH (black) or glass coverslips (gray) were replated on 6-well plates to evaluate colony-forming efficiency for three generations. ($n = 3$) Data are presented as mean ± SD, *P < 0.05, **$P < 0.01$, unpaired T test

during the isolation and amplification process on plastic (> GPa), the keratinocyte appears in a "quiescence-like" state, suggesting a very quick change of keratinocyte phenotype in response to the low compliance (below 15 kPa).

To investigate the particular "quiescience-like" state observed in response to the low compliance, the keratinocytes were cultured on soft PAH and on glass coverslip for 3 days and a phenotype-specific transcriptional profiling was undertaken by RNA-seq analysis (Fig. 2a–c). Consistent with a specific effect of the substrate, the heat map of 200 most differentially expressed genes showed a clustering of the samples by culture conditions over interindividual variability of the three donors (Fig. 2a). A total of 1392 genes were differentially expressed (FDR q value ≤ 0.05) between soft PAH and glass coverslip (Fig. 2b). Among these, 808 genes were expressed at significantly higher levels in soft PAH (gene list available in Online Resource 1), whereas 584 were expressed at significantly lower levels (gene list available in Online Resource 2) compared to glass coverslip. GO pathway analysis of these differentially expressed genes in soft PAH condition revealed an increase in the expression of genes involved in structural constituent of epidermis (23 genes belong to the epidermal differentiation complex located at 1q21 locus), metabolism and anti-oxidative machinery. In parallel, genes that decreased in expression level were preponderantly associated with extracellular matrix binding receptors and cytoskeleton (Fig. 2c). Using real-time RT-PCR on keratinocytes from three other donors, the level of expression of several hits observed in the various GO categories evoked was consistent with RNA-seq data, strengthening the results (Fig. 2d). The transcriptomic profile of the cells cultured on a soft substrate was therefore similar to differentiated keratinocytes. This observation was enhanced at the protein level, since the cells grown on the Soft PAH were all positive for the cytokeratin 10 marker and few cells started to express the involucrin late differentiation marker, while no staining was observed on glass coverslips (Fig. 2e). However, cell cycle-related gene expression levels (*CDKN1A* and *CDKNA2*) were also analyzed and a slight increase in expression level was observed for both genes (Fig. 2d). Hence, the lack of downregulation of genes linked to the cell cycle tended to show that these cells had not fully entered a terminal differentiation pathway and neither could they be related to a quiescent state. Then, preconditioned cells cultured for 3 days on soft PAH or on a glass coverslip were transplanted in 6-well plastic plates (> GPa) to observe colony-forming efficiency over three generations (Fig. 2f). The results showed that the cells previously engaged in the differentiation pathway on soft PAH were able to proliferate again once put back on a rigid substrate. During the two first generations, cells transplanted from soft PAH showed a slight but significant decrease of colony formation compared to cells transplanted from glass. This observation was reversed during the third generation showing that cells from the soft PAH kept an important proliferative potential. However, in both experimental conditions, an overall decrease in proliferative capacity was observed over successive generations.

Finally, since the keratinocyte proliferates normally above 4 kPa, we investigated whether intermediate rigidities could affect the keratinocyte differentiation program. To address this, the keratinocytes were seeded on the surface of medium, rigid PAH and glass coverslips at high density and differentiation was induced by cell confluence and growth factor deprivation at low-calcium concentration. The gene expression level for the proliferation marker *MKI67* was quickly repressed in medium PAH condition as the cells reached confluence, while it was sustained until growth factor depletion in rigid PAH and glass coverslip conditions (Fig. 3a). Regarding the early differentiation marker *KRT10*, its expression increased with time (post-confluence) in a substrate stiffness-dependent manner, reaching a strong expression level on glass coverslip, an intermediary expression on rigid PAH, and no expression on the medium PAH at day 5 (Fig. 3b). Considering the late differentiation markers, *IVL* and *CDSN* expression levels were prematurely increased in medium PAH condition compared to the two other groups (Fig. 3c, d). At day 5, cells cultured on the two PAH displayed a similar higher expression level of the late differentiation markers (*IVL* and *CDSN)* compared to the glass coverslip condition (Fig. 3c, d). These results therefore indicate an adaptive response of the human keratinocytes with respect to rigidity through their capacity to differentiate, the rigidity favoring the expression of early markers of differentiation to the detriment of later markers in contrast to low rigidity.

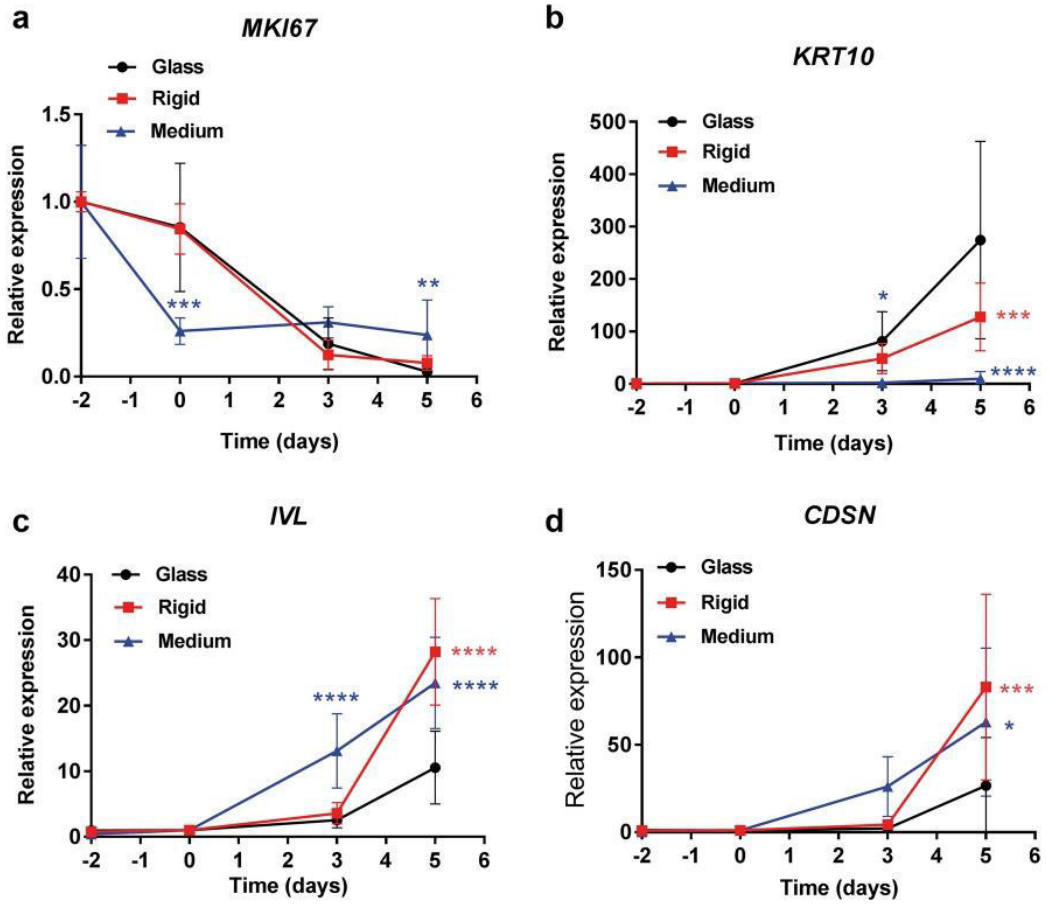

Fig. 3 Substrate stiffness impact on keratinocyte's differentiation. **a**–**d** Cells were plated on medium (blue triangle), rigid (red square) PAH and glass (black dot). mRNA expression was analyzed by qPCR at indicated time (day 0 corresponds to the moment cells reach confluence): proliferation marker *MKI67* (**a**), keratinocyte early differentiation marker *KRT10* (**b**) and keratinocyte late differentiation markers *IVL* (**c**) and *CDSN* (**d**) at the indicated points. ($n=3$) All data are presented as mean ± SD, $^{*}P<0.05$, $^{**}P<0.01$, $^{***}P<0.001$ and $^{****}P<0.0001$, using two-way ANOVA with a Bonferroni post-test, compared to glass condition

Discussion

In the present study, PAH of different rigidities were used to better understand primary human keratinocyte responses in situations where their biomechanical environment is modified. We have shown that soft (~4 kPa) PAH induced terminal differentiation, while rigid PAH (~45 kPa) favored a proliferative state similar to what is observed on glass coverslip or classical plastic culture dishes (> GPa). In addition, we demonstrated that keratinocytes committed in terminal differentiation on the softest environment could reactivate a proliferative response under a more rigid environment suggesting a strong conditioning of the genome by mechanical cell environment. Previous studies demonstrated that the adaptation of keratinocytes to the rigidity of their substrate relies mainly on the possibility for the cells to form focal adhesion points with the underlying ECM [12]. The number and the density of the focal points of adhesion decrease on soft substrates, but the occupation of the surface integrins is essential to prevent the entry into differentiation of the keratinocytes which results from the absence of activation of the signaling cascade focal adhesion kinase (FAK)/extracellular signal-related kinase (ERK)/mitogen-activated protein kinase (MAPK) [22, 26]. Stiffness also promotes proliferation through a synergistic interaction between FAK pathway and EGF receptor signaling [13]. Our observations trend in the same way showing a decrease of focal adhesion points accompanied by a stop of proliferation on the softest substrates (~4 kPa). However, we also emphasize the existence of a stiffness value (< 14 kPa) above which cells equally proliferate, suggesting a nonlinear response of keratinocyte proliferation rate to stiffness. Our results also showed that

the distribution of the focal adhesion points does not vary substantially above this proliferative stiffness value, reinforcing the interrelation between the focal adhesion point assemblies and the capacity for the cell to proliferate. Below the stiffness value allowing proliferation, the keratinocytes undergo an atypical very quick differentiation in response to the low compliance.

The impact of the substrate rigidity is much more progressive with respect to the differentiation capacity of the keratinocytes. Trappmann et al. reported a similar correlation between PAH stiffness increase and involucrin synthesis inhibition in keratinocytes at 24 h post-seeding [22]. Using monolayer keratinocyte cultures, we showed that the lesser the stiffness, the more the keratinocytes are able to express markers of late differentiation such as involucrin and corneodesmosin. In contrast, the early differentiation marker, cytokeratin 10, increases with increasing rigidity. Moving towards the critical proliferative stiffness value, *KRT10* gene expression is not observed at all after 3 days. However, this does not exclude the fact that this marker can be expressed at an earlier time, as evidenced by the presence of cytokeratin 10 in the softest hydrogels 3 days. Our results support the idea that on softer substrates, keratinocytes are quickly committed to terminal differentiation. Consistent with these observations, the mechanical measurements made on the human skin at different ages showed a reduced elastic modulus of 10 kPa at 30, 7.5 kPa at 60 years and 5.3 kPa at 80 year old [30]. Hence, changes in the dermis stiffness with aging could explain the phenotypic disturbances observed in keratinocytes leading to an alteration of epidermal homeostasis, and particularly the epidermal thinning [17].

The modulation of the differentiation being gradual according to rigidity, it cannot be directly related to the density of the focal adhesion points that were constant above the proliferative stiffness value. Indeed, differentiating keratinocytes are supposed to leave the basal membrane and no longer establish focal adhesion points. Our results showed that the cytoskeleton organization changes in a more gradual way with rigidity through the clustering of actin filaments in the peri-cytoplasmic region, beneath the plasma membrane, and across the cytoplasm. Interestingly, the spectrin cytoskeleton, a crosslinker of actin filaments and mainly implicated in cell shape maintenance [16], is abundant in differentiated keratinocytes, and the disorganization of this architecture prevents the correct differentiation of the keratinocyte [31]. Moreover, recent studies have shown that the spectrin cytoskeleton plays an important role in the mechanotransduction of osteocytes [28], so it would be interesting to explore the involvement of the stiffness related to spectrin cytoskeleton changes on keratinocyte differentiation.

Thus, there would be an optimal rigidity allowing to maintain a proliferative state of keratinocytes and their complete differentiation capacity as previously demonstrated in mouse skin wound healing using poly(amidoamine) and poly(*n*-isopropyl acrylamide) hydrogels of varying rigidity [4]. Indeed, the authors indicated that hydrogels of medium rigidity (in the order of the kPa) improve wound healing in vivo by promoting fibroblast transformation, wound closure and proliferation of keratinocytes; while very soft (< kPa) or more rigid (~ 50 kPa) hydrogels hinder these processes. Interestingly, our results are concordant with the delay of proliferation but also show a premature expression of late differentiation markers on soft substrates. These observations are consistent with the histological description of an aged epidermis in which the suprabasal layers decrease in number, giving rise to a thinner epidermis, although the aged cells are capable of forming a stratum corneum [17]. Together with our results, this suggests that soft substrate would confer an aged phenotype to cells obtained from young donors as is the case in our study.

We also studied the phenotype reversibility of cultured keratinocyte differentiation on the softest substrates. In the late 80s, Adams and Watt demonstrated that keratinocytes suspended in methylcellulose leave the cell cycle and express terminal differentiation genes such as involucrin after only 24 h [2]. The addition of fibronectin in the suspension abrogated the expression of the differentiation genes but did not allow re-inducing the cell cycle. These previous data suggest that the occupation of surface integrins by their ligand is not sufficient to promote proliferation and that it is necessary for the keratinocyte to supplement this signaling by other means of mechanical perception. In our study, we pushed keratinocyte culture up to 3 days on the softest substrates to commit them more downstream in the differentiation program despite low-calcium concentration and lack of cell–cell junctions. Gene expression profile is strongly modified, probably through epigenetic reprogramming insofar as a majority of the genes contained in the epidermal differentiation complex is expressed [1]. At the protein level, all the cells grown on Soft PAH express the cytokeratin 10 marker, and several cells already produce the involucrin late differentiation marker. Our results demonstrate that the differentiated cells replated on a rigid substrate were able to readapt to this new biomechanical environment and to start proliferating again with a colony-forming efficiency slightly lower during the two first generations than cells that have not been differentiated and even higher during the third generation. This increase during the third generation could be explained by the fact that cells from Soft PAH were less divided during the two first generations, thus preserving their proliferative potential compared to cells preconditioned on glass coverslips. It therefore appears that the keratinocytes initially grown at low density on soft substrates preserved an important proliferative potential despite the prior induction of differentiation. Previously, Poumay and Pittelkow showed that

an entry into differentiation induced by a high concentration of calcium or a depletion in growth factors does not alter the clonogenic capacity of keratinocytes and that a decrease is observed only if the keratinocytes are pushed to confluence [19]. This suggests that keratinocyte clonogenicity or proliferation potential is intimately related to their level of confluence, although the very early markers of cytokeratin 1 and 10 were only studied. However, this hypothesis remains plausible in our case.

In conclusion, we confirmed here the response of primary human keratinocytes to soft substrate by the decrease of their adhesion focal points and proliferation, and we demonstrated a quick commitment of these cells in terminal differentiation. Moreover, this study turns out that the induction of terminal differentiation on a soft substrate is reversible and open the way to interesting models to study the genome plasticity of keratinocytes. Extensive future studies of the reversible aspect of these reprogramming mechanisms would be helpful to discover new targets in pathophysiological situations displaying impaired epidermal differentiation, notably when dermal mechanical properties are modified.

Acknowledgements This work is supported by Isispharma France. Choua Ya is a recipient of a PhD grant from the French National Association of Research and Technology (ANRT). Mariana Carrancá is supported by a PhD grant from the Région Auvergne Rhône Alpes.

Compliance with ethical standards

Conflict of interest The authors have no conflict of interest to disclose.

References

1. Abhishek S, Palamadai Krishnan S (2016) Epidermal differentiation complex: a review on its epigenetic regulation and potential drug targets. Cell J 18:1–6
2. Adams JC, Watt FM (1989) Fibronectin inhibits the terminal differentiation of human keratinocytes. Nature 340:307–309. https://doi.org/10.1038/340307a0
3. Blanpain C, Fuchs E (2009) Epidermal homeostasis: a balancing act of stem cells in the skin. Nat Rev Mol Cell Biol 10:207–217. https://doi.org/10.1038/nrm2636
4. Chen S, Shi J, Xu X, Ding J, Zhong W, Zhang L, Xing M, Zhang L (2016) Study of stiffness effects of poly(amidoamine)-poly(*n*-isopropyl acrylamide) hydrogel on wound healing. Coll Surf B Biointerfaces 140:574–582. https://doi.org/10.1016/j.colsurfb.2015.08.041
5. Eden E, Navon R, Steinfeld I, Lipson D, Yakhini Z (2009) GOrilla: a tool for discovery and visualization of enriched GO terms in ranked gene lists. BMC Bioinform 10:48. https://doi.org/10.1186/1471-2105-10-48
6. Edwards C, Marks R (1995) Evaluation of biomechanical properties of human skin. Clin Dermatol 13:375–380
7. El-Domyati M, Attia S, Saleh F, Brown D, Birk DE, Gasparro F, Ahmad H, Uitto J (2002) Intrinsic aging vs. photoaging: a comparative histopathological, immunohistochemical, and ultrastructural study of skin. Exp Dermatol 11:398–405
8. Evans ND, Oreffo RO, Healy E, Thurner PJ, Man YH (2013) Epithelial mechanobiology, skin wound healing, and the stem cell niche. J Mech Behav Biomed Mater 28:397–409. https://doi.org/10.1016/j.jmbbm.2013.04.023
9. Hinz B, Mastrangelo D, Iselin CE, Chaponnier C, Gabbiani G (2001) Mechanical tension controls granulation tissue contractile activity and myofibroblast differentiation. Am J Pathol 159:1009–1020. https://doi.org/10.1016/S0002-9440(10)61776-2
10. Hsu CK, Lin HH, Harn HI, Hughes MW, Tang MJ, Yang CC (2018) Mechanical forces in skin disorders. J Dermatol Sci 90:232–240. https://doi.org/10.1016/j.jdermsci.2018.03.004
11. Jor JW, Parker MD, Taberner AJ, Nash MP, Nielsen PM (2013) Computational and experimental characterization of skin mechanics: identifying current challenges and future directions. Wiley Interdiscip Rev Syst Biol Med 5:539–556. https://doi.org/10.1002/wsbm.1228
12. Kenny FN, Connelly JT (2015) Integrin-mediated adhesion and mechano-sensing in cutaneous wound healing. Cell Tissue Res 360:571–582. https://doi.org/10.1007/s00441-014-2064-9
13. Kenny FN, Drymoussi Z, Delaine-Smith R, Kao AP, Laly AC, Knight MM, Philpott MP, Connelly JT (2018) Tissue stiffening promotes keratinocyte proliferation through activation of epidermal growth factor signaling. J Cell Sci 131:jcs215780. https://doi.org/10.1242/jcs.215780
14. Law CW, Chen Y, Shi W, Smyth GK (2014) voom: precision weights unlock linear model analysis tools for RNA-seq read counts. Genome Biol 15:R29. https://doi.org/10.1186/gb-2014-15-2-r29
15. Liao Y, Smyth GK, Shi W (2013) The Subread aligner: fast, accurate and scalable read mapping by seed-and-vote. Nucleic Acids Res 41:e108. https://doi.org/10.1093/nar/gkt214
16. Liem RK (2016) Cytoskeletal Integrators: the spectrin superfamily. Cold Spring Harb Perspect Biol 8:a018259. https://doi.org/10.1101/cshperspect.a018259
17. Mainzer C, Remoue N, Molinari J, Rousselle P, Barricchello C, Lago JC, Sommer P, Sigaudo-Roussel D, Debret R (2018) In vitro epidermis model mimicking IGF-1-specific age-related decline. Exp Dermatol 27:537–543. https://doi.org/10.1111/exd.13547
18. McCarthy DJ, Chen Y, Smyth GK (2012) Differential expression analysis of multifactor RNA-Seq experiments with respect to biological variation. Nucleic Acids Res 40:4288–4297. https://doi.org/10.1093/nar/gks042
19. Poumay Y, Pittelkow MR (1995) Cell density and culture factors regulate keratinocyte commitment to differentiation and expression of suprabasal K1/K10 keratins. J Invest Dermatol 104:271–276
20. Ritchie ME, Phipson B, Wu D, Hu Y, Law CW, Shi W, Smyth GK (2015) limma powers differential expression analyses for RNA-sequencing and microarray studies. Nucleic Acids Res 43:e47. https://doi.org/10.1093/nar/gkv007
21. Robinson MD, McCarthy DJ, Smyth GK (2010) edgeR: a Bioconductor package for differential expression analysis of digital gene expression data. Bioinformatics 26:139–140. https://doi.org/10.1093/bioinformatics/btp616
22. Trappmann B, Gautrot JE, Connelly JT, Strange DG, Li Y, Oyen ML, Cohen Stuart MA, Boehm H, Li B, Vogel V, Spatz JP, Watt FM, Huck WT (2012) Extracellular-matrix tethering regulates stem-cell fate. Nat Mater 11:642–649. https://doi.org/10.1038/nmat3339
23. Varani J, Dame MK, Rittie L, Fligiel SE, Kang S, Fisher GJ, Voorhees JJ (2006) Decreased collagen production in chronologically aged skin: roles of age-dependent alteration in fibroblast function and defective mechanical stimulation. Am J Pathol 168:1861–1868. https://doi.org/10.2353/ajpath.2006.051302
24. Waldera Lupa DM, Kalfalah F, Safferling K, Boukamp P, Poschmann G, Volpi E, Gotz-Rosch C, Bernerd F, Haag L,

Huebenthal U, Fritsche E, Boege F, Grabe N, Tigges J, Stuhler K, Krutmann J (2015) Characterization of skin aging-associated secreted proteins (SAASP) produced by dermal fibroblasts isolated from intrinsically aged human skin. J Invest Dermatol 135:1954–1968. https://doi.org/10.1038/jid.2015.120

25. Wang Y, Wang G, Luo X, Qiu J, Tang C (2012) Substrate stiffness regulates the proliferation, migration, and differentiation of epidermal cells. Burns 38:414–420. https://doi.org/10.1016/j.burns.2011.09.002
26. Watt FM, Kubler MD, Hotchin NA, Nicholson LJ, Adams JC (1993) Regulation of keratinocyte terminal differentiation by integrin-extracellular matrix interactions. J Cell Sci 106(Pt 1):175–182
27. Wong VW, Akaishi S, Longaker MT, Gurtner GC (2011) Pushing back: wound mechanotransduction in repair and regeneration. J Invest Dermatol 131:2186–2196. https://doi.org/10.1038/jid.2011.212
28. Wu XT, Sun LW, Yang X, Ding D, Han D, Fan YB (2017) The potential role of spectrin network in the mechanotransduction of MLO-Y4 osteocytes. Sci Rep 7:40940. https://doi.org/10.1038/srep40940
29. You H, Padmashali RM, Ranganathan A, Lei P, Girnius N, Davis RJ, Andreadis ST (2013) JNK regulates compliance-induced adherens junctions formation in epithelial cells and tissues. J Cell Sci 126:2718–2729. https://doi.org/10.1242/jcs.122903
30. Zahouani H, Pailler-Mattei C, Sohm B, Vargiolu R, Cenizo V, Debret R (2009) Characterization of the mechanical properties of a dermal equivalent compared with human skin in vivo by indentation and static friction tests. Skin Res Technol 15:68–76. https://doi.org/10.1111/j.1600-0846.2008.00329.x
31. Zhao KN, Masci PP, Lavin MF (2011) Disruption of spectrin-like cytoskeleton in differentiating keratinocytes by PKCdelta activation is associated with phosphorylated adducin. PLoS One 6:e28267. https://doi.org/10.1371/journal.pone.0028267

Bibliographical References

[1] F. Kemper, N. Loprieno, I. White, Notes of guidance for testing of cosmetic ingredients for their safety evaluation, 2000.

[2] S.H. Mathes, H. Ruffner, U. Graf-Hausner, The use of skin models in drug development, Adv. Drug Deliv. Rev. 69–70 (2014) 81–102. https://doi.org/10.1016/j.addr.2013.12.006.

[3] D.Y. Chau, C. Johnson, S. Macneil, J.W. Haycock, A.M. Ghaemmaghami, The development of a 3D immunocompetent model of human skin., Biofabrication. 5 (2013) 035011. https://doi.org/10.1088/1758-5082/5/3/035011.

[4] Y. Xie, S.C. Rizzi, R. Dawson, E. Lynam, S. Richards, D.I. Leavesley, Z. Upton, Development of a three-dimensional human skin equivalent wound model for investigating novel wound healing therapies., Tissue Eng. Part C. Methods. 16 (2010) 1111–23. https://doi.org/10.1089/ten.TEC.2009.0725.

[5] R. a. Kamel, J.F. Ong, E. Eriksson, J.P.E. Junker, E.J. Caterson, Tissue engineering of skin, J. Am. Coll. Surg. 217 (2013) 533–555. https://doi.org/10.1016/j.jamcollsurg.2013.03.027.

[6] A. Mieremet, M. Rietveld, S. Absalah, J. Van Smeden, J.A. Bouwstra, A. El Ghalbzouri, Improved epidermal barrier formation in human skin models by Chitosan modulated dermal matrices, PLoS One. 12 (2017) 1–20. https://doi.org/10.1371/journal.pone.0174478.

[7] N. Maas-szabowski, A. Shimotoyodome, N.E. Fusenig, Keratinocyte growth regulation in fibroblast cocultures via a double paracrine mechanism, J. Cell Sci. 1853 (1999) 1843–1853.

[8] B. Coulomb, L. Friteau, J. Baruch, J. Guibaud, B. Chretien-Marquet, J. Glicenstein, C. Lebreton-Decoster, E. Bell, L. Dubertret, Advantage of the presence of living dermal fibroblasts within in vitro reconstructed skin for grafting in humans., Plast. Reconstr. Surg. 101 (1998) 1891–1903.

[9] E. Bell, B. Ivarsson, C. Merrill, Production of a tissue-like structure by contraction of collagen lattices by human fibroblasts of different proliferative potential in vitro, Cell Biol. 76 (1979) 1274–1278.

[10] C. Collombel, O. Damour, C. Gagnieu, J. Marichy, F. Poinsignon, Biomaterials with a base of collagen, chitosan and glycosaminoglycans; process for preparing them and their application in human medicine, 1987.

[11] H.J. De Vries, E. Middelkoop, J.R. Meknes, R.P. Dumieux, Dermal regeneration in native non-cross-linked collagen sponges with different extracellular matrix molecules, Wound Repair Regen. 2 (1994) 37–47.

[12] L. Ma, C. Gao, Z. Mao, J. Zhou, J. Shen, X. Hu, C. Han, Collagen/chitosan porous

scaffolds with improved biostability for skin tissue engineering, Biomaterials. 24 (2003) 4833–4841. https://doi.org/10.1016/S0142-9612(03)00374-0.

[13] C. Lotz, F.F. Schmid, E. Oechsle, M.G. Monaghan, H. Walles, F. Groeber-becker, Cross-linked Collagen Hydrogel Matrix Resisting Contraction To Facilitate Full-Thickness Skin Equivalents, Appl. Mater. Interfaces. 9 (2017) 20417–20425. https://doi.org/10.1021/acsami.7b04017.

[14] G. Ramanathan, S. Singaravelu, T. Muthukumar, S. Thyagarajan, P.T. Perumal, U.T. Sivagnanam, Design and characterization of 3D hybrid collagen matrixes as a dermal substitute in skin tissue engineering, Mater. Sci. Eng. C. 72 (2017) 359–370. https://doi.org/10.1016/j.msec.2016.11.095.

[15] S. Franz, S. Rammelt, D. Scharnweber, J.C. Simon, Biomaterials Immune responses to implants - A review of the implications for the design of immunomodulatory biomaterials, Biomaterials. 32 (2011) 6692–6709. https://doi.org/10.1016/j.biomaterials.2011.05.078.

[16] S. Van Vlierberghe, P. Dubruel, E. Schacht, Biopolymer-based hydrogels as scaffolds for tissue engineering applications: a review., Biomacromolecules. 12 (2011) 1387–408. https://doi.org/10.1021/bm200083n.

[17] C. Lin, K.S. Anseth, PEG Hydrogels for the Controlled Release of Biomolecules in Regenerative Medicine, Pharm. Res. 26 (2009) 631–643. https://doi.org/10.1007/s11095-008-9801-2.

[18] J.A. Burdick, K.S. Anseth, Photoencapsulation of osteoblasts in injectable RGD-modified PEG hydrogels for bone tissue engineering, 23 (2002) 4315–4323.

[19] S.C. Rizzi, J.A. Hubbell, Recombinant Protein-co-PEG Networks as Cell-Adhesive and Proteolytically Degradable Hydrogel Matrixes. Part I: Development and Physicochemical Characteristics, Biomacromolecules. 6 (2005) 1226–1238. https://doi.org/10.1021/bm049614c.

[20] M. Wathier, P.J. Jung, M.A. Carnahan, T. Kim, M.W. Grinstaff, Dendritic Macromers as in Situ Polymerizing Biomaterials for Securing Cataract Incisions, J. Am. Chem. Soc. 126 (2004) 12744–12745. https://doi.org/10.1021/ja045870l.

[21] M. Wathier, C.S. Johnson, T. Kim, M.W. Grinstaff, Hydrogels Formed by Multiple Peptide Ligation Reactions To Fasten Corneal Transplants, Bioconjugate Chem. 17 (2006) 873–876. https://doi.org/10.1021/bc060060f.

[22] S. Kaga, M. Arslan, R. Sanyal, A. Sanyal, Dendrimers and Dendrons as Versatile Building Blocks for the Fabrication of Functional Hydrogels, Molecules. 21 (2016). https://doi.org/10.3390/molecules21040497.

[23] J.M. Oliveira, A.J. Salgado, N. Sousa, J.F. Mano, R.L. Reis, Dendrimers and derivatives as a potential therapeutic tool in regenerative medicine strategies—A review, Prog. Polym. Sci. 35 (2010) 1163–1194.

https://doi.org/10.1016/j.progpolymsci.2010.04.006.
[24] B. Romestand, J. Rolland, A. Commeyras, I. Desvignes, R. Pascal, O. Vandenabeele-trambouze, Dendrigraft Poly- L -lysine : A Non-Immunogenic Synthetic Carrier for Antibody Production, Biomacromolecules. 11 (2010) 1169–1173. https://doi.org/10.1021/bm9012056.
[25] J. Francoia, L. Vial, Everything You Always Wanted to Know about Poly-l-lysine Dendrigrafts (But Were Afraid to Ask), Chem. A Eur. J. 24 (2018) 1–10. https://doi.org/10.1002/chem.201704147.
[26] R. Huang, S. Liu, K. Shao, L. Han, W. Ke, Y. Liu, J. Li, S. Huang, C. Jiang, Evaluation and mechanism studies of PEGylated dendrigraft poly-L-lysines as novel gene delivery vectors., Nanotechnology. 21 (2010) 265101. https://doi.org/10.1088/0957-4484/21/26/265101.
[27] C. Lorion, C. Faye, B. Maret, T. Trimaille, T. Régnier, P. Sommer, R. Debret, Biosynthetic support based on dendritic poly(L-lysine) improves human skin fibroblasts attachment., J. Biomater. Sci. Polym. Ed. 25 (2014) 136–49. https://doi.org/10.1080/09205063.2013.843966.
[28] N. Annabi, S.M. Mithieux, E.A. Boughton, A.J. Ruys, A.S. Weiss, F. Dehghani, Synthesis of highly porous crosslinked elastin hydrogels and their interaction with fibroblasts in vitro, Biomaterials. 30 (2009) 4550–4557. https://doi.org/10.1016/j.biomaterials.2009.05.014.
[29] R. Brown, In the beginning there were soft collagen-cell gels: Towards better 3D connective tissue models?, Exp. Cell Res. 319 (2013) 2460–2469. https://doi.org/10.1016/j.yexcr.2013.07.001.
[30] W.F. Daamen, J.H. Veerkamp, J.C.M. Van Hest, T.H. Van Kuppevelt, Elastin as a biomaterial for tissue engineering, Biomaterials. 28 (2007) 4378–4398. https://doi.org/10.1016/j.biomaterials.2007.06.025.
[31] N. Annabi, S. M. Mithieux, G. Camci-Unal, M. R. Dokmeci, A. S. Weiss, A. Khademhosseini, Elastomeric Recombinant Protein-based Biomaterials, Biochem Eng. J. 77 (2013) 110–118. https://doi.org/10.1016/j.bej.2013.05.006.Elastomeric.
[32] C. Lorion, Development, characterization and therapeutic potential of Elactiv, a biomimetic elastic protein, inspired by the human tropoelastin, 2015.
[33] S. Tajima, H. Wachi, Y. Uemura, K. Okamoto, Modulation by elastin peptide VGVAPG of cell proliferation and elastin expression in human skin fibroblasts, Arch. Dermatol. Res. 289 (1997) 489–492.
[34] T.D. Sargeant, A.P. Desai, S. Banerjee, A. Agawu, J.B. Stopek, An in situ forming collagen – PEG hydrogel for tissue regeneration, Acta Biomater. 8 (2012) 124–132. https://doi.org/10.1016/j.actbio.2011.07.028.
[35] D. Barros, E. Conde-sousa, A.M. Gonçalves, W.M. Han, A.J. García, I.F. Amaral, A.P.

Pêgo, Engineering hydrogels with affinity-bound laminin as 3D neural stem cell culture systems, Biomater. Sci. 7 (2019) 5338–5349. https://doi.org/10.1039/c9bm00348g.

[36] J. Vacanti, Beyond transplantation, Arch Surg. 123 (1988) 545–549.

[37] Z. Zhang, B.B. Michniak-Kohn, Tissue engineered human skin equivalents, Pharmaceutics. 4 (2012) 26–41. https://doi.org/10.3390/pharmaceutics4010026.

[38] E. Cukierman, R. Pankov, K.M. Yamada, Cell interactions with three-dimensional matrices, Curr. Opin. Cell Biol. 14 (2002) 633–640. https://doi.org/10.1016/S0955-0674(02)00364-2.

[39] S. MacNeil, Biomaterials for tissue engineering of skin, Mater. Today. 11 (2008) 26–35. https://doi.org/10.1016/S1369-7021(08)70087-7.

[40] J.R. Yu, J. Navarro, J.C. Coburn, B. Mahadik, J. Molnar, J.H.H. Iv, A.J. Nam, J.P. Fisher, Current and Future Perspectives on Skin Tissue Engineering : Key Features of Biomedical Research, Translational Assessment, and Clinical Application, Adv. Healthc. Mater. 8 (2019) 1–19. https://doi.org/10.1002/adhm.201801471.

[41] E. Proksch, J.M. Brandner, J.M. Jensen, The skin: An indispensable barrier, Exp. Dermatol. 17 (2008) 1063–1072. https://doi.org/10.1111/j.1600-0625.2008.00786.x.

[42] C.A. Brohem, L.B. da Silva Cardeal, M. Tiago, M. S. Soengas, S. Berlanga de Moraes Barros, S.S. Maria-Engler, Artificial Skin in Perspective : Concepts and Applications, Pigment Cell Melanoma Res. 24 (2011) 35–50. https://doi.org/10.1111/j.1755-148X.2010.00786.x.Artificial.

[43] Z. Zhang, B.B. Michniak-kohn, Tissue Engineered Human Skin Equivalents, Pharmacutics. 4 (2012) 26–41. https://doi.org/10.3390/pharmaceutics4010026.

[44] J.A. Mcgrath, R.A.J. Eady, F.M. Pope, Anatomy and Organization of Human Skin, in: Rook's Textb. Dermatology, 2004: pp. 45–128.

[45] C.L. Simpson, D.M. Patel, K.J. Green, Deconstructing the skin: Cytoarchitectural determinants of epidermal morphogenesis, Nat. Rev. Mol. Cell Biol. 12 (2011) 565–580. https://doi.org/10.1038/nrm3175.

[46] D. Bikle, Z. Xie, C.-L. Tu, Calcium regulation of keratinocyte differentiation, Expert Rev. Endocrinol. Metab. 7 (2012) 461–472. https://doi.org/10.1586/eem.12.34.Calcium.

[47] C. Marchese, J. Rubin, D. Ron, A. Fagcioni, M.R. Torrisi, A. Messina, L. Frati, S.. Aaronson, Human Keratinocyte Growth Factor Activity on Proliferation and Differentiation of Human Keratinocytes : Differentiation Response Distinguishes KCF From EGF Family, J. Cell. Physiol. 144 (1990) 326–332.

[48] G.F. Odland, A submicroscopic granular component in human epidermis., J. Invest. Dermatol. 34 (1960) 11–15. https://doi.org/10.1038/jid.1960.4.

[49] T. Egelrud, Desquamation in the stratum corneum, Acta Dermato-Venereologica, Suppl. (2000) 44–45. https://doi.org/10.1080/000155500750042853.

[50] T. Agner, Skin Barrier Function, 2016.

[51] C.M. Beddoes, G.S. Gooris, J.A. Bouwstra, Preferential arrangement of lipids in the long-periodicity phase of a stratum corneum matrix model, J. Lipid Res. 59 (2018) 2329–2338.

[52] H.J. Yardley, R. Summerly, Lipid composition and metabolism in normal and diseased epidermis, Pharmacol. Ther. 13 (1981) 357–383. https://doi.org/10.1016/0163-7258(81)90006-1.

[53] J.A. Bouwstra, M. Ponec, The skin barrier in healthy and diseased state, Biochim. Biophys. Acta - Biomembr. 1758 (2006) 2080–2095. https://doi.org/10.1016/j.bbamem.2006.06.021.

[54] M. Ponec, E. Boelsma, S. Gibbs, M. Mommaas, Characterization of Reconstructed Skin Models, Ski. Pharmacol. Appl Ski. Physiol. 15 (2002) 4–17. https://doi.org/10.1159/000066682.

[55] M. Simard, P. Julien, J. Fradette, R. Pouliot, Modulation of the Lipid Profile of Reconstructed Skin Substitutes after Essential Fatty Acid Supplementation A ff ects Testosterone Permeability, Cells. 8 (2019) 1–15.

[56] D. Breitkreutz, I. Koxholt, K. Thiemann, R. Nischt, Skin Basement Membrane : The Foundation of Epidermal Integrity — BM Functions and Diverse Roles of Bridging Molecules Nidogen and Perlecan, Biomed Res. Int. 2013 (2013) 1–16.

[57] M. Hertl, R. Eming, C. Veldman, T cell control in autoimmune bullous skin disorders, J. Clin. Invest. 116 (2006) 1159–1166. https://doi.org/10.1172/JCI28547.

[58] A. El Ghalbzouri, M.F. Jonkman, R. Dijkman, M. Ponec, Basement membrane reconstruction in human skin equivalents is regulated by fibroblasts and/or exogenously activated keratinocytes, J. Invest. Dermatol. 124 (2005) 79–86. https://doi.org/10.1111/j.0022-202X.2004.23549.x.

[59] A. Kalra, A. Lowe, A. Al-Jumaily, Mechanical Behaviour of Skin : A Review, J. Mater. Sci. Eng. 5 (2016) 1–7. https://doi.org/10.4172/2169-0022.1000254.

[60] W.N. Meigel, S. Gay, L. Weber, Dermal architecture and collagen type distribution, Arch. Dermatological Res. 259 (1977) 1–10. https://doi.org/10.1007/BF00562732.

[61] G. Sriram, P.L. Bigliardi, M. Bigliardi-Qi, Fibroblast heterogeneity and its implications for engineering organotypic skin models in vitro, Eur. J. Cell Biol. 94 (2015) 483–512. https://doi.org/10.1016/j.ejcb.2015.08.001.

[62] H. Smola, G. Thieko, T. Krieg, N.E. Fusenig, Dynamics of Basement Membrane Formation by Keratinocyte – Fibroblast Interactions in Organotypic Skin Culture, Exp. Cell Res. 410 (1998) 399–410.

[63] P. Contard, R.L. Bartel, L. Jacobs, J.S. Perlish, E.D. MacDonald, L. Handler, D. Cone,

R. Fleischmajer, Culturing keratinocytes and fibroblasts in a three-dimensional mesh results in epidermal differentiation and formation of a basal lamina-anchoring zone, J. Invest. Dermatol. 100 (1993) 35–39. https://doi.org/10.1111/1523-1747.ep12349952.

[64] C. Frantz, K.M. Stewart, V.M. Weaver, The extracellular matrix at a glance., J. Cell Sci. 123 (2010) 4195–4200. https://doi.org/10.1242/jcs.023820.

[65] L.E. Tracy, R.A. Minasian, E.J. Caterson, Extracellular Matrix and Dermal Fibroblast Function in the Healing Wound., Adv. Wound Care. 5 (2016) 119–136. https://doi.org/10.1089/wound.2014.0561.

[66] B. Eckes, R. Nischt, T. Krieg, Cell-matrix interactions in dermal repair and scarring, Fibrogenes. Tissue Repair. 3 (2010) 1–11. https://doi.org/10.1186/1755-1536-3-4.

[67] D. Hun, J. Oh, J. Ho, Glycosaminoglycan and proteoglycan in skin aging, J. Dermatol. Sci. 83 (2016) 174–181.

[68] E.C. Naylor, R.E.B. Watson, M.J. Sherratt, Molecular aspects of skin ageing, Maturitas. 69 (2011) 249–256. https://doi.org/10.1016/j.maturitas.2011.04.011.

[69] G.D. Weinstein, R.J. Boucek, Collagen and elastin of human dermis., J. Invest. Dermatol. 35 (1960) 227–229. https://doi.org/10.1038/jid.1960.109.

[70] D.J.S. Hulmes, Collagen diversity, synthesis and assembly, Collagen Struct. Mech. (2008) 15–47. https://doi.org/10.1007/978-0-387-73906-9_2.

[71] J. Aziz, H. Shezali, Z. Radzi, N.A. Yahya, N. Hayaty, A. Kassim, J. Czernuszka, M.T. Rahman, Molecular Mechanisms of Stress-Responsive Changes in Collagen and Elastin Networks in Skin, Skin Pharmacol. Physiol. 29 (2016) 190–203. https://doi.org/10.1159/000447017.

[72] J.E. Wagenseil, R.P. Mecham, New insights into elastic fiber assembly, Birth Defects Res. Part C - Embryo Today Rev. 81 (2007) 229–240. https://doi.org/10.1002/bdrc.20111.

[73] J.F. Almine, S.G. Wise, A.S. Weiss, Elastin signaling in wound repair, Birth Defects Res. Part C. 96 (2012) 248–257. https://doi.org/10.1002/bdrc.21016.

[74] S.G. Wise, A.S. Weiss, Tropoelastin, Int. J. Biochem. Cell Biol. 41 (2009) 494–497. https://doi.org/10.1016/j.biocel.2008.03.017.

[75] B.A. Kozel, H. Wachi, E.C. Davis, R.P. Mecham, Domains in tropoelastin that mediate elastin deposition in vitro and in vivo, J. Biol. Chem. 278 (2003) 18491–18498. https://doi.org/10.1074/jbc.M212715200.

[76] C.B. Saitow, S.G. Wise, A.S. Weiss, J.J.C. Jr, D.L. Kaplan, Elastin biology and tissue engineering with adult cells, Biomol. Concepts. 4 (2013) 173–185. https://doi.org/10.1515/bmc-2012-0040.

[77] F. Sato, H. Wachi, M. Ishida, R. Nonaka, S. Onoue, Z. Urban, B.C. Starcher, Y. Seyama, Distinct Steps of Cross-linking, Self-association, and Maturation of

Tropoelastin Are Necessary for Elastic Fiber Formation, J. Mol. Biol. 369 (2007) 841–851. https://doi.org/10.1016/j.jmb.2007.03.060.

[78] N. Annabi, S.M. Mithieux, G. Camci-unal, M.R. Dokmeci, A.S. Weiss, A. Khademhosseini, Elastomeric recombinant protein-based biomaterials, Biochem. Eng. J. 77 (2013) 110–118. https://doi.org/10.1016/j.bej.2013.05.006.

[79] Q. Wen, S.M. Mithieux, A.S. Weiss, Elastin Biomaterials in Dermal Repair, Trends Biotechnol. (2019) 1–12. https://doi.org/10.1016/j.tibtech.2019.08.005.

[80] A.M.J. Coenen, K. V. Bernaerts, J.A.W. Harings, S. Jockenhoevel, S. Ghazanfari, Elastic materials for tissue engineering applications: Natural, synthetic, and hybrid polymers, Acta Biomater. 79 (2018) 60–82. https://doi.org/10.1016/j.actbio.2018.08.027.

[81] L. Duca, N. Floquet, A.J.P. Alix, B. Haye, L. Debelle, Elastin as a matrikine, Crit. Rev. Oncol. Hematol. 49 (2004) 235–244. https://doi.org/10.1016/j.critrevonc.2003.09.007.

[82] M.P. Lutolf, J.A. Hubbell, Synthetic biomaterials as instructive extracellular microenvironments for morphogenesis in tissue engineering, 23 (2005) 47–55. https://doi.org/10.1038/nbt1055.

[83] M. Barczyk, S. Carracedo, D. Gullberg, Integrins, Cell Tissue Res. 339 (2010) 269–280. https://doi.org/10.1007/s00441-009-0834-6.

[84] U. Hersel, C. Dahmen, H. Kessler, RGD modified polymers: Biomaterials for stimulated cell adhesion and beyond, Biomaterials. 24 (2003) 4385–4415. https://doi.org/10.1016/S0142-9612(03)00343-0.

[85] A. Howe, A.E. Aplin, S.K. Alahari, R. Juliano, Integrin signaling and cell growth control, Curr. Opin. Cell Biol. 10 (1998) 220–231. https://doi.org/10.1016/S0955-0674(98)80144-0.

[86] F.M. Watt, H. Fujiwara, Cell-Extracellular Matrix Interactions in Normal and Diseased Skin, Cold Spring Harb Perspect Biol. 3 (2011) 1–14.

[87] L.C. Biggs, C.S. Kim, Y.A. Miroshnikova, S.A. Wickstro, Mechanical Forces in the Skin : Roles in Tissue Architecture , Stability , and Function, J. Invest. Dermatol. (2019) 1–7. https://doi.org/10.1016/j.jid.2019.06.137.

[88] C. Pailler-Mattei, R. Debret, R. Vargiolu, P. Sommer, H. Zahouani, In vivo skin biophysical behaviour and surface topography as a function of ageing, J. Mech. Behav. Biomed. Mater. 28 (2013) 474–483. https://doi.org/10.1016/j.jmbbm.2013.04.008.

[89] P.G. Agache, C. Monneur, J.L. Leveque, J. De Rigal, Mechanical Properties and Young's Modulus of Human Skin in Vivo, Arch Dermatol Res. 269 (1980) 221–232. https://link.springer.com/content/pdf/10.1007%2FBF00406415.pdf.

[90] G. Boyer, C.P. Mattei, J. Molimard, M. Pericoi, S. Laquieze, H. Zahouani, Non contact

method for in vivo assessment of skin mechanical properties for assessing effect of ageing, Med. Eng. Phys. 34 (2012) 172–178. https://doi.org/10.1016/j.medengphy.2011.07.007.

[91] G. Boyer, L. Laquièze, A. Le Bot, S. Laquieze, H. Zahouani, Dynamic indentation on human skin in vivo : ageing effects, Ski. Res. Technol. 15 (2009) 55–67. https://doi.org/10.1111/j.1600-0846.2008.00324.x.

[92] C. Jacquemoud, K. Bruyere-Garnier, M. Coret, Methodology to determine failure characteristics of planar soft tissues using a dynamic tensile test, J. Biomech. 40 (2007) 468–475. https://doi.org/10.1016/j.jbiomech.2005.12.010.

[93] A.. Gallagherm, A. Ni Annaidh, K. Bruyere, Dynamic Tensile Properties of Human Skin, in: IRCOBI Conf. Proc. IRCOBI, 2012: pp. 484–502.

[94] M. Ottenio, D. Tran, A. Ní Annaidh, M.D. Gilchrist, K. Bruyère, Strain rate and anisotropy effects on the tensile failure characteristics of human skin, J. Mech. Behav. Biomed. Mater. 41 (2015) 241–250. https://doi.org/10.1016/j.jmbbm.2014.10.006.

[95] S. Diridollou, F. Patat, F. Gens, L. Vaillant, D. Black, J.M. Lagarde, Y. Gall, M. Berson, In vivo model of the mechanical properties of the human skin under suction, Ski. Res. Technol. 6 (2000) 214–221. https://doi.org/10.1034/j.1600-0846.2000.006004214.x.

[96] F.M. Hendriks, D. Brokken, J.T.W.M. van Eemeren, C.W.J. Oomens, F.P.T. Baaijens, J.B.A.M. Horsten, A numerical-experimental method to characterize the non-linear mechanical behavior of human skin, Ski. Res. Technol. 9 (2003) 274–283. https://doi.org/10.1034/j.1600-0846.2003.00019.x.

[97] X. Liang, Biomechanical Properties of In Vivo Human Skin From Dynamic Optical Coherence Elastography, IEEE Trans Biomed Eng. 57 (2013) 953–959. https://doi.org/10.1109/TBME.2009.2033464.Biomechanical.

[98] R. Sanders, Torsional elasticity of human skin in vivo, Pflügers Arch. Eur. J. Physiol. 342 (1973) 255–260. https://doi.org/10.1007/BF00591373.

[99] L. Falland-Cheung, M. Scholze, P.F. Lozano, B. Ondruschka, D.C. Tong, P.A. Brunton, J.N. Waddell, N. Hammer, Mechanical properties of the human scalp in tension, J. Mech. Behav. Biomed. Mater. 84 (2018) 188–197. https://doi.org/10.1016/j.jmbbm.2018.05.024.

[100] K.M. Jeong, K. Bo-seung, H. Sejin, Y.H. Hee, Experimentally derived viscoelastic properties of human skin and muscle in vitro, Med. Eng. Phys. 61 (2018) 25–31. https://doi.org/10.1016/j.medengphy.2018.08.001.

[101] Y. An, C. Ji, Y. Li, J. Wang, X. Zhang, Y. Huang, In vivo measurements of human neck skin elasticity using MRI and fi nite element modeling, J. Med. Phys. 44 (2017) 1402–1407. https://doi.org/10.1002/mp.12154.

[102] Y. Yang, L. Wang, F. Yan, X. Xiang, Y. Tang, L. Zhang, J. Liu, L. Qui, Determination of Normal Skin Elasticity by Using Real-time Shear Wave Elastography, J. Ultrasound Med. 37 (2018) 2507–2516. https://doi.org/10.1002/jum.14608.

[103] B. Holt, A. Tripathi, J. Morgan, Viscoelastic response of human skin to low magnitude physiologically relevant shear, J. Biomech. 41 (2008) 2689–2695. https://doi.org/10.1016/j.jbiomech.2008.06.008.

[104] C. Pailler-Mattei, S. Nicoli, F. Pirot, R. Vargiolu, H. Zahouani, A new approach to describe the skin surface physical properties in vivo, Colloids Surfaces B Biointerfaces. 68 (2009) 200–206. https://doi.org/10.1016/j.colsurfb.2008.10.005.

[105] R. Akhtar, M.J. Sherratt, J.K. Cruickshank, B. Derby, Characterizing the elastic properties of tissues, Mater. Today. 14 (2011) 96–105. https://doi.org/10.1016/S1369-7021(11)70059-1.

[106] W. Guo, M.T. Frey, N.A. Burnham, Y. Wang, Substrate Rigidity Regulates the Formation and Maintenance of Tissues, Biophys. J. 90 (2006) 2213–2220. https://doi.org/10.1529/biophysj.105.070144.

[107] S. Bottcher-Haberzeth, T. Biedermann, E. Reichmann, Tissue engineering of skin substitutes., Burns. 36 (2010) 450–460. https://doi.org/10.1016/j.burns.2009.08.016.

[108] S. MacNeil, Progress and opportunities for tissue-engineered skin, Nature. 445 (2007) 874–880. https://doi.org/10.1038/nature05664.

[109] F. Groeber, M. Holeiter, M. Hampel, S. Hinderer, K. Schenke-Layland, Skin tissue engineering - In vivo and in vitro applications, Adv. Drug Deliv. Rev. 63 (2011) 352–366. https://doi.org/10.1016/j.addr.2011.01.005.

[110] H. Kandarova, Evaluation and Validation of Reconstructed Human Skin Models as Alternatives to Animal Tests in Regulatory Toxicology, 2006.

[111] K. Ackermann, S.L. Borgia, H.. Korting, K.. Mewes, M. Schäfer-Korting, The Phenion Full-Thickness Skin Model for Percutaneous Absorption Testing, Skin Pharmacol. Physiol. 23 (2010) 105–112. https://doi.org/10.1159/000265681.

[112] G.E. Flaten, Z. Palac, A. Engesland, J. Filipovic-Grcic, Z. Vanic, N. Skalko-Basnet, In vitro skin models as a tool in optimization of drug formulation, Eur. J. Pharm. Sci. 75 (2015) 10–24. https://doi.org/10.1016/j.ejps.2015.02.018.

[113] D.Y. Lee, K.H. Cho, The effects of epidermal keratinocytes and dermal fibroblasts on the formation of cutaneous basement membrane in three-dimensional culture systems, Arch. Dermatol. Res. 296 (2005) 296–302. https://doi.org/10.1007/s00403-004-0529-5.

[114] A. El-Ghalbzouri, S. Gibbs, E. Lamme, C.A. Van Blitterswijk, Effect of fibroblasts on epidermal regeneration, Br. J. Dermatol. 147 (2002) 230–243.

[115] K. Boehnke, N. Mirancea, A. Pavesio, N.E. Fusenig, P. Boukamp, H.J. Stark, Effects

of fibroblasts and microenvironment on epidermal regeneration and tissue function in long-term skin equivalents, Eur. J. Cell Biol. 86 (2007) 731–746. https://doi.org/10.1016/j.ejcb.2006.12.005.

[116] C. Duval, R. Schmidt, M. Regnier, V. Facy, D. Asselineau, F. Bernerd, The use of reconstructed human skin to evaluate UV-induced modifications and sunscreen efficacy, Exp. Dermatology, Suppl. 12 (2003) 64–70. https://doi.org/10.1034/j.1600-0625.12.s2.10.x.

[117] S.E. Lightfoot, K.A. Tamamoto, H. Nguyen, R.D. Abbott, D.M. Cairns, D.L. Kaplan, Biomaterials 3D biomaterial matrix to support long term , full thickness , immuno-competent human skin equivalents with nervous system components, Biomaterials. 198 (2019) 194–203. https://doi.org/10.1016/j.biomaterials.2018.04.044.

[118] A.F. Black, V. Hudon, O. Damour, L. Germain, F.A. Auger, A novel approach for studying angiogenesis: A human skin equivalent with a capillary-like network, Cell Biol. Toxicol. 15 (1999) 81–90. https://doi.org/10.1023/A:1007541713398.

[119] B.S. Kim, G. Gao, J.Y. Kim, D. Cho, 3D Cell Printing of Perfusable Vascularized Human Skin Equivalent Composed of Epidermis , Dermis , and Hypodermis for Better Structural Recapitulation of Native Skin, Adv. Healthc. Mater. 8 (2019) 1801019. https://doi.org/10.1002/adhm.201801019.

[120] J.W.J. Van Kilsdonk, M. Bergers, L.C.L.T. Van Kempen, J. Schalkwijk, G.W.M. Swart, Keratinocytes drive melanoma invasion in a reconstructed skin model, Melanoma Res. 20 (2010) 372–380. https://doi.org/10.1097/CMR.0b013e32833d8d70.

[121] D.S. Hill, N.D.P. Robinson, M.P. Caley, M. Chen, E.A.O. Toole, L. Jane, A novel fully-humanised 3D skin equivalent to model early melanoma invasion, Mol. Cancer Ther. 14 (2015) 2665–2673. https://doi.org/10.1158/1535-7163.MCT-15-0394.A.

[122] H.C. Korting, U. Patzak, M. Schaller, H.I. Maibach, A model of human cutaneous candidosis based on reconstructed human epidermis for the light and electron microscopic study of pathogenesis and treatment, J. Infect. 36 (1998) 259–267. https://doi.org/10.1016/S0163-4453(98)94063-4.

[123] G. Andrei, J. Van Den Oord, P. Fiten, G. Opdenakker, C. De Wolf-Peeters, E. De Clercq, R. Snoeck, Organotypic epithelial raft cultures as a model for evaluating compounds against alphaherpesviruses, Antimicrob. Agents Chemother. 49 (2005) 4671–4680. https://doi.org/10.1128/AAC.49.11.4671-4680.2005.

[124] F. Rademacher, M. Simanski, R. Gläser, J. Harder, Skin microbiota and human 3D skin models, Exp. Dermatol. 27 (2018) 489–494. https://doi.org/10.1111/exd.13517.

[125] M. Roger, N. Fullard, L. Costello, S. Bradbury, E. Markiewicz, S. O'Reilly, N. Darling, P. Ritchie, A. Määttä, I. Karakesisoglou, G. Nelson, T. von Zglinicki, T. Dicolandrea, R. Isfort, C. Bascom, S. Przyborski, Bioengineering the microanatomy of human skin,

J. Anat. 234 (2019) 438–455. https://doi.org/10.1111/joa.12942.

[126] L. Shahabeddin, F. Berthod, O. Damour, C. Collombel, Characterization of skin reconstructed on a chitosan-cross-linked collagen-glycosaminoglycan matrix., J. Ski. Pharmacol. Soc. 3 (1990) 107–14. http://www.ncbi.nlm.nih.gov/pubmed/2078342.

[127] M. Prunieras, M. Regnier, D. Woodley, Methods for Cultivation of Keratinocytes with an Air-Liquid Interphase, J. Invest. Dermatol. 81 (1983) 28–33.

[128] R.. Isseroff, K.T. Chun, R.M. Rosenberg, Triiodothyronine alters the cornification of cultured human keratinocytes, Br. J. Dermatol. 120 (1989) 503–510.

[129] S. Sorensen, H. Solvsten, Y. Politi, K. Kragballe, Effects of Vitamin D3 on Keratinocyte Proliferation and Differentiation in Vitro: Modulation by Ligands for Retinoic Acid and Retinoid X Receptors, Skin Pharmacol. 10 (1997).

[130] I. Savini, M.V. Catani, A. Rossi, G. Duranti, G. Melino, Characterization of Keratinocyte Differentiation Induced by Ascorbic Acid: Protein Kinase C Involvement and Vitamin C Homeostasis, J. Invest. Dermatol. 118 (2002) 372–379. https://doi.org/10.1046/j.0022-202x.2001.01624.x.

[131] C. Reuter, H. Walles, F. Groeber, Preparation of a Three-Dimensional Full Thickness Skin Equivalent, in: Methods Mol. Biol., 2017: pp. 191–198. https://doi.org/10.1007/978-1-4939-7021-6.

[132] Instructions for Use, in: Phenion® FT Ski. Model Kit, n.d.: pp. 1–8.

[133] J.A. Bouwstra, G.S. Gooris, The Lipid Organisation in Human Stratum Corneum and Model Systems, Open Dermatol. J. 4 (2010) 10–13. https://doi.org/10.2174/1874372201004010010.

[134] E. Boelsma, M.C.H. Verhoeven, M. Ponec, Reconstruction of a Human Skin Equivalent Using a Transformed Keratinocyte Cell Line (HaCaT), J. Invest. Dermatol. 112 (1999) 489–498. https://doi.org/10.1046/j.1523-1747.1999.00545.x.

[135] N. Maas-Szabowski, A. Stärker, N.E. Fusenig, Epidermal tissue regeneration and stromal interaction in HaCaT cells is initiated by TGF-α, J. Cell Sci. 116 (2003) 2937–2948. https://doi.org/10.1242/jcs.00474.

[136] C.M.A. Reijnders, A. Van Lier, S. Roffel, D. Kramer, R.J. Scheper, S. Gibbs, Development of a Full-Thickness Human Skin Equivalent In Vitro Model Derived from TERT-Immortalized Keratinocytes and Fibroblasts, Tissue e Eng. Part A. 21 (2015) 2448–2459. https://doi.org/10.1089/ten.tea.2015.0139.

[137] S.N. Park, J.C. Park, H.O. Kim, M.J. Song, H. Suh, Characterization of porous collagen/hyaluronic acid scaffold modified by 1-ethyl-3-(3-dimethylaminopropyl)carbodiimide cross-linking, Biomaterials. 23 (2002) 1205–1212. https://doi.org/10.1016/S0142-9612(01)00235-6.

[138] D.P. Speer, M. Chvapil, C.D. Eskelson, J. Ulreich, Biological effects of residual glutaraldehyde in glutaraldehyde-tanned collagen biomaterials, J. Biomed. Mater.

Res. 14 (1980) 753–764. https://doi.org/10.1002/jbm.820140607.
[139] D.M. Casali, M.J. Yost, M.A. Matthews, Eliminating glutaraldehyde from crosslinked collagen films using supercritical CO2, J. Biomed. Mater. Res. - Part A. 106 (2018) 86–94. https://doi.org/10.1002/jbm.a.36209.
[140] N. Davidenko, C.F. Schuster, D. V. Bax, N. Raynal, R.W. Farndale, S.M. Best, R.E. Cameron, Control of crosslinking for tailoring collagen-based scaffolds stability and mechanics, Acta Biomater. 25 (2015) 131–142. https://doi.org/10.1016/j.actbio.2015.07.034.
[141] L. Gu, T. Shan, Y. xuan Ma, F.R. Tay, L. Niu, Novel Biomedical Applications of Crosslinked Collagen, Trends Biotechnol. 37 (2019) 464–491. https://doi.org/10.1016/j.tibtech.2018.10.007.
[142] N. Davidenko, D. V. Bax, C.F. Schuster, R.W. Farndale, S.W. Hamaia, S.M. Best, R.E. Cameron, Optimisation of UV irradiation as a binding site conserving method for crosslinking collagen-based scaffolds, J. Mater. Sci. Mater. Med. 27 (2016) 1–17. https://doi.org/10.1007/s10856-015-5627-8.
[143] M.G. Haugh, M.J. Jaasma, F.J. O'Brien, The effect of dehydrothermal treatment on the mechanical and structural properties of collagen-GAG scaffolds, J. Biomed. Mater. Res. - Part A. 89 (2009) 363–369. https://doi.org/10.1002/jbm.a.31955.
[144] H. Schoof, J. Apel, I. Heschel, G. Rau, Control of pore structure and size in freeze-dried collagen sponges, J. Biomed. Mater. Res. 58 (2001) 352–357. https://doi.org/10.1002/jbm.1028.
[145] T. Heck, G. Faccio, M. Richter, L. Thöny-Meyer, Enzyme-catalyzed protein crosslinking, Appl. Microbiol. Biotechnol. 97 (2013) 461–475. https://doi.org/10.1007/s00253-012-4569-z.
[146] A. León-López, A. Morales-Peñaloza, V.M. Martínez-Juárez, A. Vargas-Torres, D.I. Zeugolis, G. Aguirre-Álvarez, Hydrolyzed Collagen—Sources and Applications, Molecules. 24 (2019) 1–16.
[147] J. Singh, The national centre for the replacement, refinement, and reduction of animals in research, J. Pharmacol. Pharmacother. 3 (2012) 87–89.
[148] S.P. Zhong, Y.Z. Zhang, C.T. Lim, Tissue scaffolds for skin wound healing and dermal reconstruction, Wiley Interdiscip. Rev. Nanomedicine Nanobiotechnology. 2 (2010) 510–525. https://doi.org/10.1002/wnan.100.
[149] A. Glalbzouri, E.N. Lamme, C. Van Blitterswijk, J. Koopman, M. Ponec, The use of PEGT / PBT as a dermal scaffold for skin tissue engineering, Biomaterials. 25 (2004) 2987–2996. https://doi.org/10.1016/j.biomaterials.2003.09.098.
[150] P. Bruin, J. Smedinga, A.. Pennings, M.. Jonkman, Biodegradable lysine diisocyanate-based poly(glycolide-co-epsilon-caprolactone)-urethane network in artificial skin, Biomaterials. 11 (1990) 291–295.

[151] N.T. Dai, M.K. Yeh, C.H. Chiang, K.C. Chen, T.H. Liu, A.C. Feng, L.L. Chao, C.M. Shih, H.K. Sytwu, S.L. Chen, T.M. Chen, E. Adams, Human single-donor composite skin substitutes based on collagen and polycaprolactone copolymer, Biochem. Biophys. Res. Commun. 386 (2009) 21–25. https://doi.org/10.1016/j.bbrc.2009.05.123.

[152] C.E. Hart, A. Loewen-Rodriguez, J. Lessem, Dermagraft : Use in the Treatment of Chronic Wounds, Adv. Wound Care. 1 (2012) 138–141. https://doi.org/10.1089/wound.2011.0282.

[153] A.G. Van Dorp, M.C. Verhoeven, H.K. Koerten, C.A. van Blitterswijk, M. Ponec, Bilayered biodegradable poly (ethylene glycol)/ poly (butylene terephthalate) copolymer (Polyactive ™) as substrate for human fibroblasts and keratinocytes, J. Biomed. Mater. Res. 47 (1999) 292–300.

[154] K. Ng, H. Khor, D. Hutmacher, In vitro characterization of natural and synthetic dermal matrices cultured with human dermal fibroblasts, Biomaterials. 25 (2004) 2807–2818. https://doi.org/10.1016/j.biomaterials.2003.09.058.

[155] M.L. Cooper, J.F. Hansbrough, R.L. Spielvogel, R. Cohen, R.L. Bartel, G. Naughton, In vivo optimization of a living dermal substitute employing cultured human fibroblasts on a biodegradable polyglycolic acid or polyglactin mesh, Biomaterials. 12 (1991) 243–248. https://doi.org/10.1016/0142-9612(91)90207-Q.

[156] G.J. Beumer, C.A. van Blitterswijk, D. Bakker, M. Ponec, Cell-seeding and in vitro biocompatibility evaluation of polymeric matrices of PEO/PBT copolymers and PLLA, Biomaterials. 14 (1993) 598–604. https://doi.org/10.1016/0142-9612(93)90178-5.

[157] S.G. Kumbar, S.P. Nukavarapu, R. James, L.S. Nair, C.T. Laurencin, Electrospun poly(lactic acid-co-glycolic acid) scaffolds for skin tissue engineering, Biomaterials. 29 (2008) 4100–4107. https://doi.org/10.1016/j.biomaterials.2008.06.028.

[158] W. Cui, X. Zhu, Y. Yang, X. Li, Y. Jin, Evaluation of electrospun fibrous scaffolds of poly(dl-lactide) and poly(ethylene glycol) for skin tissue engineering, Mater. Sci. Eng. C. 29 (2009) 1869–1876. https://doi.org/10.1016/j.msec.2009.02.013.

[159] T. Sun, S. Mai, D. Norton, J.W. Haycock, A.J. Ryan, S. MacNeil, Self-Organization of Skin Cells in Three-Dimensional Electrospun Polystyrene Scaffold, Tissue Eng. 11 (2005) 1023–1033.

[160] B. Subia, J. Kundu, S. Kundu, Biomaterial scaffold fabrication techniques for potential tissue engineering applications, Tissue Eng. (2010) 141–159. http://cdn.intechopen.com/pdfs-wm/9798.pdf.

[161] A. Dolcimascolo, G. Cabrese, S. Conoci, R. Parenti, Innovative Biomaterials for Tissue Engineering, in: Biomater. Tissue Reconstr. or Regen., 2019. https://doi.org/http://dx.doi.org/10.5772/57353.

[162] M.W. Tibbitt, K.S. Anseth, Hydrogel as Extracellular Matrix Mimics for 3D Cell

Culture, Hydrogel as Extracell. Matrix Mimics 3D Cell Cult. 103 (2010) 655–663. https://doi.org/10.1002/bit.22361.Hydrogels.

[163] X. Jia, K.L. Kiick, Hybrid multicomponent hydrogels for tissue engineering, Macromol. Biosci. 9 (2009) 140–156. https://doi.org/10.1002/mabi.200800284.

[164] S. Park, K. Park, Engineered Polymeric Hydrogels for 3D Tissue Models, Polymers (Basel). 8 (2016) 23. https://doi.org/10.3390/polym8010023.

[165] L. Figueiredo, R. Pace, C. D'Arros, G. Réthoré, J. Guicheux, C. Le Visage, P. Weiss, Assessing glucose and oxygen diffusion in hydrogels for the rational design of 3D stem cell scaffolds in regenerative medicine, J. Tissue Eng. Regen. Med. 12 (2018) 1238–1246. https://doi.org/10.1002/term.2656.

[166] G.N. Tew, N. Sanabria-delong, K. Agrawal, S.R. Bhatia, New properties from PLA–PEO –PLA hydrogels, Soft Matter. 1 (2005) 253–258. https://doi.org/10.1039/b509800a.

[167] C. Lin, K.S. Anseth, PEG Hydrogels for the Controlled Release of Biomolecules in Regenerative Medicine, Pharm. Res. 26 (2009) 631–643. https://doi.org/10.1007/s11095-008-9801-2.PEG.

[168] A. Kumar, S.S. Han, PVA-based hydrogels for tissue engineering: A review, Int. J. Polym. Mater. Polym. Biomater. 66 (2017). doi.org/10.1080/00914037.2016.1190930.

[169] Z. Jing, A. Xu, Y.Q. Liang, Z. Zhang, C. Yu, P. Hong, Y. Li, Biodegradable poly(acrylic acid-co-acrylamide)/ poly(vinyl alcohol) double network hydrogels with tunable mechanics and high self-healing performance, Polymers (Basel). 11 (2019). https://doi.org/10.3390/polym11060952.

[170] C.D. Spicer, Hydrogel scaffolds for tissue engineering: the importance of polymer choice, Polym. Chem. 11 (2020) 184–219. https://doi.org/10.1039/c9py01021a.

[171] J.L. Drury, D.J. Mooney, Hydrogels for tissue engineering: Scaffold design variables and applications, Biomaterials. 24 (2003) 4337–4351. https://doi.org/10.1016/S0142-9612(03)00340-5.

[172] R. Wieduwild, Y. Xu, S. Ostrovidov, A. Khademhosseini, Y. Zhang, G. Orive, Engineering Hydrogels beyond a Hydrated Network, Adv. Healthc. Mater. 8 (2019) 1–7. https://doi.org/10.1002/adhm.201900038.

[173] S.R. Macewan, A. Chilkoti, Elastin-like Polypeptides: Biomedical applications of Tunable Biopolymers, Biomed. Appl. Tunable Biopolym. 94 (2010) 60–77. https://doi.org/10.1002/bip.21327.

[174] A. Sivashanmugam, R. Arun Kumar, M. Vishnu Priya, S. V. Nair, R. Jayakumar, An overview of injectable polymeric hydrogels for tissue engineering, Eur. Polym. J. 72 (2015) 543–565. https://doi.org/10.1016/j.eurpolymj.2015.05.014.

[175] M.P. Lutolf, G.P. Raeber, A.H. Zisch, N. Tirelli, J.A. Hubbell, Cell-responsive synthetic

hydrogels, Adv. Mater. 15 (2003) 888–892. https://doi.org/10.1002/adma.200304621.

[176] N. Annabi, J.W. Nichol, X. Zhong, C. Ji, S. Koshy, A. Khademhosseini, F. Dehghani, Controlling the porosity and microarchitecture of hydrogels for tissue engineering., Tissue Eng. Part B. Rev. 16 (2010) 371–83. https://doi.org/10.1089/ten.TEB.2009.0639.

[177] D. J. Griffon, M.R. Sedighi, D. V. Schaeffer, J.A. Eurell, A.L. Jonhnson, Chitosan scaffolds : Interconnective pore size and cartilage engineering, Acta Biomater. 2 (2006) 313–320. https://doi.org/10.1016/j.actbio.2005.12.007.

[178] J. Rouwkema, N.C. Rivron, C.A. Van Blitterswijk, Vascularization in tissue engineering, Trends Biotechnol. 26 (2008) 434–441. https://doi.org/10.1016/j.tibtech.2008.04.009.

[179] H.W. Kang, Y. Tabata, Y. Ikada, Fabrication of porous gelatin scaffolds for tissue engineering., Biomaterials. 20 (1999) 1339–1344. https://doi.org/10.1016/S0142-9612(99)00036-8.

[180] C. Palocci, A. Barbetta, A. La Grotta, M. Dentini, Porous biomaterials obtained using supercritical CO2- water emulsions., Langmuir. 23 (2007) 8243–51. https://doi.org/10.1021/la700947g.

[181] Y.S. Nam, J.J. Yoon, T.G. Park, A novel fabrication method of macroporous biodegradable polymer scaffolds using gas foaming salt as a porogen additive., J. Biomed. Mater. Res. 53 (2000) 1–7. http://www.ncbi.nlm.nih.gov/pubmed/10634946 (accessed February 7, 2016).

[182] M.J. Gupte, W.B. Swanson, J. Hu, X. Jin, H. Ma, Z. Zhang, Z. Liu, K. Feng, G. Feng, G. Xiao, N. Hatch, Y. Mishina, P.X. Ma, Pore size directs bone marrow stromal cell fate and tissue regeneration in nanofibrous macroporous scaffolds by mediating vascularization, Acta Biomater. 82 (2018) 1–11. https://doi.org/10.1016/j.actbio.2018.10.016.

[183] P.X. Ma, P.D.J. Choi, Biodegradable Polymer Scaffolds with Well-Defined Interconnected Spherical Pore Network, Tissue Eng. 7 (2001) 23–33.

[184] N. Joshi, M. Grinstaff, Applications of Dendrimers in Tissue Engineering, Curr. Top. Med. Chem. 8 (2008) 1225–1236. https://doi.org/10.2174/156802608785849067.

[185] H. Collet, E. Souaid, H. Cottet, A. Deratani, L. Boiteau, G. Dessalces, J.C. Rossi, A. Commeyras, R. Pascal, An expeditious multigram-scale synthesis of lysine dendrigraft (DGL) polymers by aqueous n-carboxyanhydride polycondensation, Chem. - A Eur. J. 16 (2010) 2309–2316. https://doi.org/10.1002/chem.200901734.

[186] N.P. Desai, Q. Yuan, H. Yang, Synthesis and Characterization of Photocurable Polyamidoamine Dendrimer Hydrogels as a Versatile Platform for Tissue Engineering and Drug Delivery, Biomacromolecules. 11 (2010) 666–673.

https://doi.org/10.1021/bm901240g.Synthesis.

[187] B. Unal, R.C. Hedden, Gelation and swelling behavior of end-linked hydrogels prepared from linear poly(ethylene glycol) and poly(amidoamine) dendrimers, Polymer (Guildf). 47 (2006) 8173–8182. https://doi.org/10.1016/j.polymer.2006.09.048.

[188] R.S. Navath, A.R. Menjoge, H. Dai, R. Romero, S. Kannan, R.M. Kannan, Injectable PAMAM Dendrimer - PEG Hydrogels for the Treatment of Genital Infections : Formulation and in Vitro and in Vivo Evaluation, Mol. Pharm. 8 (2011) 1209–1223. https://doi.org/10.1021/mp200027z.

[190] Y. Wang, Q. Zhao, H. Zhang, S. Yang, X. Jia, A novel poly(amido amine)-dendrimer-based hydrogel as a mimic for the extracellular matrix, Adv. Mater. 26 (2014) 4163–4167. https://doi.org/10.1002/adma.201400323.

[191] M. Labieniec-Watala, C. Watala, PAMAM dendrimers: Destined for success or doomed to fail? Plain and modified PAMAM dendrimers in the context of biomedical applications, J. Pharm. Sci. 104 (2015) 2–14. https://doi.org/10.1002/jps.24222.

[192] J. Francoia, L. Vial, Everything You Always Wanted to Know about Poly- l -lysine Dendrigrafts (But Were Afraid to Ask), (2018) 1–10. https://doi.org/10.1002/chem.201704147.

[193] P. N. Desai, Q. Yuan, H. Yang, Synthesis and Characterization of Photocurable Polyamidoamine Dendrimer Hydrogels as a Versatile Platform for Tissue Engineering and Drug Delivery, Biomacromolecules. 11 (2011) 666–673. https://doi.org/10.1021/bm901240g.Synthesis.

[194] R.S. Navath, A.R. Menjoge, H. Dai, R. Romero, S. Kannan, R.M. Kannan, Injectable PAMAM Dendrimer À PEG Hydrogels for the Treatment of Genital Infections : Formulation and in Vitro and in Vivo Evaluation, Mol. Pharm. 8 (2011) 1209–1223. https://doi.org/10.1021/mp200027z.

[195] N. Yevlampieva, A. Dobrodumov, O. Nazarova, O. Okatova, Hydrodynamic Behavior of Dendrigraft Polylysines in Water and Dimethylformamide, Polymers (Basel). 4 (2012) 20–31. https://doi.org/10.3390/polym4010020.

[196] R.J. Pelham, Y. Wang, Cell locomotion and focal adhesions are regulated by substrate flexibility, Proc. Natl. Acad. Sci. 94 (1997) 13661–13665.

[197] A.J. Engler, S. Sen, H.L. Sweeney, D.E. Discher, Matrix Elasticity Directs Stem Cell Lineage Specification, (2006) 677–689. https://doi.org/10.1016/j.cell.2006.06.044.

[198] N. Wang, Review of cellular mechanotransduction, J. Phys. D. Appl. Phys. 50 (2017). https://doi.org/10.1088/1361-6463/aa6e18.

[199] F. Martino, A.R. Perestrelo, V. Vinarský, S. Pagliari, G. Forte, L.A. Peyré-tartaruga, Cellular Mechanotransduction : From Tension to Function, Front. Physiol. 9 (2018) 1–21. https://doi.org/10.3389/fphys.2018.00824.

[200] G. Jiang, A.H. Huang, Y. Cai, M. Tanase, M.P. Sheetz, Rigidity Sensing at the Leading Edge through avb3 Integrins and RPTPa, Biophys. J. 90 (2006) 1804–1809. https://doi.org/10.1529/biophysj.105.072462.

[201] C.M. Lo, H.B. Wang, M. Dembo, Y.L. Wang, Cell movement is guided by the rigidity of the substrate, Biophys. J. 79 (2000) 144–152. https://doi.org/10.1016/S0006-3495(00)76279-5.

[202] S. Nemir, J. L. West, Synthetic Materials in the Study of Cell Response to Substrate Rigidity, Ann. Biomed. Eng. 38 (2010) 2–20. https://doi.org/10.1007/s10439-009-9811-1.

[203] T. Yeung, P.C. Georges, L.A. Flanagan, B. Marg, M. Ortiz, M. Funaki, N. Zahir, W. Ming, V. Weaver, P.A. Janmey, Effects of Substrate Stiffness on Cell Morphology , Cytoskeletal Structure , and Adhesion, Cell Motil. Cytoskeleton. 60 (2005) 24–34. https://doi.org/10.1002/cm.20041.

[204] S. Nemir, J.L. West, Synthetic materials in the study of cell response to substrate rigidity, Ann. Biomed. Eng. 38 (2010) 2–20. https://doi.org/10.1007/s10439-009-9811-1.

[205] C. Ya, M. Carrancá, D. Sigaudo-roussel, B. Fromy, Substrate softness promotes terminal differentiation of human keratinocytes without altering their ability to proliferate back into a rigid environment, Arch. Dermatol. Res. 311 (2019) 741–751. https://doi.org/10.1007/s00403-019-01962-5.

[206] S.R. Caliari, J.A. Burdick, A practical guide to hydrogels for cell culture, Nat. Methods. 13 (2016) 405–414. https://doi.org/10.1038/nmeth.3839.

[207] D.L. Hern, J.A. Hubbell, Incorporation of adhesion peptides into nonadhesive hydrogels useful for tissue resurfacing, 1998.

[208] L. Ouyang, Y. Dan, Z. Shao, S. Yang, C. Yang, G. Liu, D. Duan, MMP - sensitive PEG hydrogel modified with RGD promotes bFGF , VEGF and EPC - mediated angiogenesis, Exp. Ther. Med. 18 (2019) 2933–2941. https://doi.org/10.3892/etm.2019.7885.

[209] R.O. Hynes, Cell adhesion : old and new questions, Trends Genet. 15 (1999) 33–37.

[210] J.H. Lee, H.W. Jung, I.K. Kang, H.B. Lee, Cell behaviour on polymer surfaces with different functional groups, Biomaterials. 15 (1994) 705–711. https://doi.org/10.1016/0142-9612(94)90169-4.

[211] O.F. Zouani, J. Kalisky, E. Ibarboure, M. Durrieu, Biomaterials Effect of BMP-2 from matrices of different stiffnesses for the modulation of stem cell fate, Biomaterials. 34 (2013) 2157–2166. https://doi.org/10.1016/j.biomaterials.2012.12.007.

[212] Y. Ito, Growth Factor Engineering for Biomaterials, ACS Biomater. Sci. Eng. 5 (2019) 5597–5609. https://doi.org/10.1021/acsbiomaterials.8b01649.

[213] S.C. Rizzi, M. Ehrbar, S. Halstenberg, G.P. Raeber, H.G. Schmoekel, H. Hagenmu, R. Mu, F.E. Weber, J.A. Hubbell, Recombinant Protein-co-PEG Networks as Cell-

Adhesive and Proteolytically Degradable Hydrogel Matrixes, Biomacromolecules. 7 (2006) 3019–3029. https://doi.org/10.1021/bm060504a.

[214] A.H. Zisch, M.P. Lutolf, M. Ehrbar, G.P. Raeber, S.C. Rizzi, N. Davies, H. Schmökel, D. Bezuidenhout, V. Djonov, P. Zilla, J.A. Hubbell, Cell-demanded release of VEGF from synthetic, biointeractive cell-ingrowth matrices for vascularized tissue growth, FASEB J. (2003) 2260–2262.

[215] R.O. Hynes, The Extracellular Matrix: Not Just Pretty Fibrils, Science (80-.). 326 (2009) 1216–1219. https://doi.org/10.1126/science.1176009.Extracellular.

[216] M. Ehrbar, S.C. Rizzi, R. Hlushchuk, V. Djonov, A.H. Zisch, J.A. Hubbell, F.E. Weber, M.P. Lutolf, Enzymatic formation of modular cell-instructive fibrin analogs for tissue engineering, Biomaterials. 28 (2007) 3856–3866. https://doi.org/10.1016/j.biomaterials.2007.03.027.

[217] S. Khan, M.W. Ullah, R. Siddique, G. Nabi, S. Manan, M. Yousaf, H. Hou, Role of Recombinant DNA Technology to Improve Life, Int. J. Genomics. (2016) 1–14.

[218] K. Hosoyama, C. Lazurko, M. Muñoz, C.D. Mctiernan, E.I. Alarcon, Peptide-Based Functional Biomaterials for Soft-Tissue Repair, Front. Bioeng. Biotechnol. 7 (2019) 1–19. https://doi.org/10.3389/fbioe.2019.00205.

[219] P. Katyal, F. Mahmoudinobar, J.K. Montclare, Recent trends in peptide and protein-based hydrogels, Curr. Opin. Struct. Biol. 63 (2020) 97–105. https://doi.org/10.1016/j.sbi.2020.04.007.

[220] M.B. Van Eldijk, C.L. Mcgann, Elastomeric Polypeptides, Top. Curr. Chem. (2013) 71–116. https://doi.org/10.1007/128.

[221] J.A.M. Ramshaw, J.A. Werkmeister, V. Glattauer, Recent progress with recombinant collagens produced in Escherichia coli, Curr. Opin. Biomed. Eng. 10 (2019) 149–155. https://doi.org/10.1016/j.cobme.2019.06.001.

[222] M. Meyer, Processing of collagen based biomaterials and the resulting materials properties, Biomed. Eng. Online. 18 (2019) 1–74. https://doi.org/10.1186/s12938-019-0647-0.

[223] Y. He, Z. Hou, J. Wang, Z. Wang, X. Li, J. Liu, Q. Liang, J. Zhao, Assessment of biological properties of recombinant collagen-hyaluronic acid composite scaffolds, Int. J. Biol. Macromol. 149 (2020) 1275–1284. https://doi.org/10.1016/j.ijbiomac.2020.02.023.

[224] S.M. Mithieux, A.S. Weiss, Design of an elastin-layered dermal regeneration template, Acta Biomater. 52 (2017) 33–40. https://doi.org/10.1016/j.actbio.2016.11.054.

[225] A. Pirayesh, H. Hoeksema, C. Richters, J. Verbelen, S. Monstrey, Glyaderm W dermal substitute : Clinical application and long-term results in 55 patients, Burns. 41 (2014) 132–144. https://doi.org/10.1016/j.burns.2014.05.013.

[226] Y. Wang, S.M. Mithieux, Y. Kong, X. Wang, C. Chong, A. Fathi, F. Dehghani, E. Panas, J. Kemnitzer, R. Daniels, R.M. Kimble, P.K. Maitz, Z. Li, A.S. Weiss, Tropoelastin Incorporation into a Dermal Regeneration Template Promotes Wound Angiogenesis, Adv. Healthc. Mater. 4 (2015) 577–584. https://doi.org/10.1002/adhm.201400571.

[227] P. Lee, G.C. Yeo, A.S. Weiss, A cell adhesive peptide from tropoelastin promotes sequential cell attachment and spreading via distinct receptors, Fed. Eur. Biochem. Soc. 284 (2017) 2216–2230. https://doi.org/10.1111/febs.14114.

[228] J.F. Almine, S.G. Wise, M. Hiob, N.K. Singh, K.K. Tiwari, S. Vali, T. Abbasi, A.S. Weiss, Elastin sequences trigger transient proinflammatory responses by human dermal fibroblasts, FASEB J. 27 (2013) 3455–3465. https://doi.org/10.1096/fj.13-231787.

[229] E.R. Wright, V.P. Conticello, Self-assembly of block copolymers derived from elastin-mimetic polypeptide sequences, Adv. Drug Deliv. Rev. 54 (2002) 1057–1073.

[230] J. Hoffmann, E. Heisler, S. Karpinski, J. Losse, D. Thomas, W. Siefken, H.J. Ahr, H.W. Vohr, H.W. Fuchs, Epidermal-skin-test 1000 (EST-1000)— A new reconstructed epidermis for in vitro skin corrosivity testing, Toxicol. Vitr. 19 (2005) 925–929. https://doi.org/10.1016/j.tiv.2005.06.010.

[231] R. Greek, A. Menache, Systematic Reviews of Animal Models : Methodology versus Epistemology, Int. J. Med. Sci. 10 (2013) 206–221. https://doi.org/10.7150/ijms.5529.

[232] Z. Ma, C. Gao, Y. Gong, J. Shen, Paraffin spheres as porogen to fabricate poly(L-lactic acid) scaffolds with improved cytocompatibility for cartilage tissue engineering., J. Biomed. Mater. Res. Part B. 67 (2003) 610–617. https://doi.org/10.1002/jbm.b.10049.

[233] C. Pailler-Mattei, L. Laquièze, R. Debret, S. Tupin, G. Aimond, P. Sommer, H. Zahouani, Rheological behaviour of reconstructed skin, J. Mech. Behav. Biomed. Mater. 37 (2014) 251–263. https://doi.org/10.1016/j.jmbbm.2014.05.030.

[234] Y. Yuan, R.T. Lee, Contact Angle and Wetting Properties, in: Surf. Sci. Tec., 2013: pp. 3–34. https://doi.org/10.1007/978-3-642-34243-1.

[235] Y.E. Shapiro, Progress in Polymer Science Structure and dynamics of hydrogels and organogels : An NMR spectroscopy approach, Prog. Polym. Sci. 36 (2011) 1184–1253. https://doi.org/10.1016/j.progpolymsci.2011.04.002.

[236] M. Balci, Chemical Shift, in: Basic 1H- 13C-NMR Spectrosc., 2005: pp. 283–292.

[237] B. Elena, A. Lesage, S. Steuernagel, A. Bockmann, L. Emsley, Proton to Carbon-13 INEPT in Solid-State NMR Spectroscopy, J. Am. Ceram. Soc. 120 (2005) 17296–17302. https://doi.org/10.1021/ja054411x.

[238] W.F. Vranken, W. Boucher, T.J. Stevens, R.H. Fogh, A. Pajon, M. Llinas, E.L. Ulrich, J.L. Markley, J. Ionides, E.D. Laue, The CCPN Data Model for NMR Spectroscopy :

Development of a Software Pipeline, Proteins Struct. Funct. Bioinforma. 59 (2005) 687–696. https://doi.org/10.1002/prot.20449.

[239] G. Coussot, E. Nicol, A. Commeryras, I. Desvignes, R. Pascal, O. Vandenabeele-trambouze, Colorimetric quantification of amino groups in linear and dendritic structures, Polym Int. 58 (2009) 511–518. https://doi.org/10.1002/pi.2560.

[241] K.S. Anseth, C.N. Bowman, L. Brannon-Peppas, Mechanical properties of hydrogels and their experimental determination, Biomaterials. 17 (1996) 1647–1657. https://doi.org/10.1016/0142-9612(96)87644-7.

[242] B.D. Johnson, D.J. Beebe, W.C. Crone, Effects of swelling on the mechanical properties of a pH-sensitive hydrogel for use in microfluidic devices, Mater. Sci. Eng. C. 24 (2004) 575–581. https://doi.org/10.1016/j.msec.2003.11.002.

[243] I. Gitsov, C. Zhu, Amphiphilic hydrogels constructed by poly(ethylene glycol) and shape-persistent dendritic fragments, Macromolecules. 35 (2002) 8418–8427. https://doi.org/10.1021/ma020935v.

[244] J.D. Robert, M.C. Caserio, Organonitrogen compounds I: Amines, in: Basic Princ. Org. Chem., 1977: pp. 1095–1166.

[245] K. Von der Mark, V. Gauss, H. Von der Mark, P. Müller, Relationship between cell shape and type of collagen synthesised as chondrocytes lose thier cartilage phenotype in culture, Nature. 267 (1977) 531–532.

[246] P.D. Benya, J.D. Shaffer, Dedifferentiated chondrocytes reexpress the differentiated collagen phenotype when cultured in agarose gels, Cell. 30 (1982) 215–224. https://doi.org/10.1016/0092-8674(82)90027-7.

[247] E. Schuh, M. Sc, J. Kramer, D. Ph, H. Notbohm, D. Ph, R. Mu, D. Ph, T. Gutsmann, D. Ph, N. Rotter, Effect of Matrix Elasticity on the Maintenance of the Chondrogenic Phenotype, Tissue e Eng. Part A. 16 (2010).

[248] M.P. Quinton, C.W. Philpott, A Role for Anionic Sites in Epithelial Architecture: Effects of Cationic Polymers on Cell Membrane Structure, J. Cell Biol. 56 (1978) 787–796.

[249] M. Tang, H. Dong, Y. Li, T. Ren, Harnessing the PEG-cleavable strategy to balance cytotoxicity, intracellular release and the therapeutic effect of dendrigraft poly-L-lysine for cancer gene therapy, 1284 | J. Mater. Chem. B. 4 (2016) 1284. https://doi.org/10.1039/c5tb02224j.

[250] R. Sarber, B. Hull, C. Merrill, T. Sorrano, E. Bell, Regulation of proliferation of fibroblasts of low and high population doubling levels grown in collagen lattices, Mech. Ageing Dev. 17 (1981) 107–117. https://doi.org/10.1016/0047-6374(81)90077-4.

[251] T. Kono, T. Tanii, M. Furukawa, N. Mizuno, J. Kitajima, M. Ishii, T. Hamada, K. Yoshizato, Cell cycle analysis of human dermal fibroblasts cultured on or in hydrated type I collagen lattices, Arch. Dermatol. Res. 282 (1990) 258–262.

https://doi.org/10.1007/BF00371646.

[252] R.W. Rhudy, J.M. McPherson, Influence of the extracellular matrix on the proliferative response of human skin fibroblasts to serum and purified platelet-derived growth factor, J. Cell. Physiol. 137 (1988) 185–191. https://doi.org/10.1002/jcp.1041370123.

[253] M. Mekhail, K. Jahan, M. Tabrizian, Genipin-crosslinked chitosan/poly-l-lysine gels promote fibroblast adhesion and proliferation, Carbohydr. Polym. 108 (2014) 91–98. https://doi.org/10.1016/j.carbpol.2014.03.021.

[254] K. Ghosh, Z. Pan, E. Guan, S. Ge, Y. Liu, T. Nakamura, X.D. Ren, M. Rafailovich, R.A.F. Clark, Cell adaptation to a physiologically relevant ECM mimic with different viscoelastic properties, Biomaterials. 28 (2007) 671–679. https://doi.org/10.1016/j.biomaterials.2006.09.038.

[255] E. Hadjipanayi, V. Mudera, R. Brown, Close dependence of fibroblast proliferation on collagen scaffold matrix stiffness, J. Tissue Eng. Regen. Med. 3 (2009) 77–84. https://doi.org/10.1002/term.

[256] C. Lo, H. Wang, M. Dembo, Y. Wang, Cell Movement Is Guided by the Rigidity of the Substrate, Biophys. J. 79 (2000) 144–152. https://doi.org/10.1016/S0006-3495(00)76279-5.

[257] J. Solon, I. Levental, K. Sengupta, P.C. Georges, P.A. Janmey, Fibroblast Adaptation and Stiffness Matching to Soft Elastic Substrates, Biophys. J. 93 (2007) 4453–4461. https://doi.org/10.1529/biophysj.106.101386.

[258] Q. Tan, S. Li, J. Ren, C. Chen, Fabrication of Porous Scaffolds with a Controllable Microstructure and Mechanical Properties by Porogen Fusion Technique, Int. J. Mol. Sci. 12 (2011) 890–904. https://doi.org/10.3390/ijms12020890.

[259] G. Rolin, V. Placet, E. Jacquet, H. Tauzin, S. Robin, L. Pazart, C. Viennet, P. Saas, P. Muret, D. Binda, P. Humbert, Development and characterization of a human dermal equivalent with physiological mechanical properties, Ski. Res. Technol. 18 (2012) 251–258. https://doi.org/10.1111/j.1600-0846.2011.00564.x.

[260] H.E. White, S.F. Walton, Particle Packing and Particle Shape, J. Am. Ceram. Soc. 20 (1937) 155–166. https://doi.org/10.1111/j.1151-2916.1937.tb19882.x.

[261] C. Collombel, O. Damour, C. Gagnieu, F. Poinsignon, C. Echinard, J. Marichy, Artificial skin and process for preparing the same, 8708752, 1987.

[262] F. Duplan-Perrat, O. Damour, C. Montrocher, S. Peyrol, G. Grenier, M.P. Jacob, F. Braye, Keratinocytes influence the maturation and organization of the elastin network in a skin equivalent., J. Invest. Dermatol. 114 (2000) 365–70. https://doi.org/10.1046/j.1523-1747.2000.00885.x.

[263] M. Sevcova, J. Horacek, J. Sevc, On the thickness of the epidermis, Ces. Dermatologie. 53 (1978) 223–228.

[264] T. Nishiyama, S. Amano, M. Tsunenaga, The importance of laminin 5 in the dermal – epidermal basement membrane, 1 (2000) 51–59.

[265] J. Rnjak, Z. Li, P.K.M. Maitz, S.G. Wise, A.S. Weiss, Biomaterials Primary human dermal fibroblast interactions with open weave three-dimensional scaffolds prepared from synthetic human elastin, Biomaterials. 30 (2009) 6469–6477. https://doi.org/10.1016/j.biomaterials.2009.08.017.

[266] J.C. Rodirguez-Cabello, L. Martin, A. Girotti, C. García-Arévalo, F.J. Arías, M. Alonso, Emerging applications of multifunctional elastin-like recombinamers, Nanomedicine. 6 (2011) 111–122.

[267] C. Hui, T. Liu, T. Salez, E. Raphael, A. Jagota, Indentation of a rigid sphere into an elastic substrate with surface tension and adhesion, Proc. R. Soc. A. 471 (2015) 1–16.

[268] C.C. Miller, G. Godeau, C. Lebreton-DeCoster, A. Desmoulière, B. Pellat, L. Dubertret, B. Coulomb, Validation of a morphometric method for evaluating fibroblast numbers in normal and pathologic tissues, Exp. Dermatol. 12 (2003) 403–411. https://doi.org/10.1034/j.1600-0625.2003.00023.x.

[269] L. Besseau, B. Coulomb, C. Lebreton-decoster, Production of ordered collagen matrices for three-dimensional cell culture, Biomaterial. 23 (2002) 27–36.

[270] C. Helary, A. Foucault-bertaud, G. Godeau, B. Coulomb, M. Madeleine, G. Guille, Fibroblast populated dense collagen matrices : cell migration , cell density and metalloproteinases expression, Biomaterials. 26 (2005) 1533–1543. https://doi.org/10.1016/j.biomaterials.2004.05.016.

[271] K.R. Mewes, M. Raus, A. Bernd, N.. Zöller, A. Sättler, R. Graf, Elastin Expression in a Newly Developed Full-Thickness Skin Equivalent, Skin Pharmacol. Physiol. 20 (2007) 85–95. https://doi.org/10.1159/000097655.

[272] Y. Mao, J.E. Schwarzbauer, Fibronectin fibrillogenesis, a cell-mediated matrix assembly process, Matrix Biol. 24 (2005) 389–399. https://doi.org/10.1016/j.matbio.2005.06.008.

[273] I. a. Darby, B. Laverdet, F. Bonté, A. Desmouliére, Fibroblasts and myofibroblasts in wound healing, Clin. Cosmet. Investig. Dermatol. 7 (2014) 301–311. https://doi.org/10.2147/CCID.S50046.

[274] V. Bouvard, L. Germain, P. Rompré, B. Roy, F.A. Auger, Influence of dermal equivalent maturation on the development of a cultured skin equivalent, Biochem. Cell Biol. 70 (1992) 34–42.

[275] R. Visse, H. Nagase, Matrix metalloproteinases and tissue inhibitors of metalloproteinases: Structure, function, and biochemistry, Circ. Res. 92 (2003) 827–839. https://doi.org/10.1161/01.RES.0000070112.80711.3D.

[276] J.L. Seltzer, A.-Y. Lee, K.T. Akers, B. Sudbeck, E.A. Southon, E.A. Wayner, A.Z.

Eisen, Activation of 72 kDa collagenase by normal fibroblasts in collagen lattices is mediated by integrin receptors, Exp. Cell Res. 213 (1994) 365–374.

[277] B. Brassart, A. Randoux, W. Hornebeck, H. Emonard, Regulation of matrix metalloproteinase-2 (gelatinase A, MMP-2), membrane-type matrix metalloproteinase-1 (MT1-MMP) and tissue inhibitor of metalloproteinases-2 (TIMP-2) expression by elastin-derived peptides in human HT-1080 fibrosarcoma cell line, Clin. Exp. Metastasis. 16 (1998) 489–500. https://doi.org/10.1023/A:1006550503612.

[278] C. Ntayi, A.L. Labrousse, R. Debret, P. Birembaut, G. Bellon, F. Antonicelli, W. Hornebeck, P. Bernard, Elastin-Derived Peptides Upregulate Matrix Metalloproteinase-2-ediated Melanoma Cell Invasion Through Elastin-Binding Protein, J. Invest. Dermatol. 122 (2004) 256–265. https://doi.org/10.1046/j.0022-202X.2004.22228.x.

[279] S. Toupance, B. Brassart, F. Rabenoelina, L. Debelle, P. Birembaut, Elastin-derived peptides increase invasive capacities of lung cancer cells by post-transcriptional regulation of MMP-2 and uPA, Clin. Exp. Metastasis. 29 (2012) 511–522. https://doi.org/10.1007/s10585-012-9467-3.

[280] A. Kamoun, J.-M. Landeau, G. Godeau, J. Wallach, A. Duchesnay, B. Pellat, W. Hornebeck, Growth Stimulation of Human Skin Fibroblasts by Elastin-Derived Peptides, Cell Adhes. Commun. 3 (1995) 273–281. https://doi.org/10.3109/15419069509081013.

[281] N. Fujimoto, S. Tajima, A. Ishibashi, Elastin peptides induce migration and terminal differentiation of cultured keratinocytes via 67 kDa elastin receptor in vitro: 67 kDa elastin receptor is expressed in the keratinocytes eliminating elastic materials in elastosis perforans serpiginosa, J. Invest. Dermatol. 115 (2000) 633–639. https://doi.org/10.1046/j.1523-1747.2000.00117.x.

[282] A.D. Lynn, T.R. Kyriakides, S.J. Bryant, Characterization of the in vitro macrophage response and in vivo host response to poly(ethylene glycol)-based hydrogels, J. Biomed. Mater. Res. - Part A. 93 (2010) 941–953. https://doi.org/10.1002/jbm.a.32595.

[283] J.M. Anderson, A. Rodriguez, D.T. Chang, Foreigne body reaction to biomaterials, Semin. Immunol. 20 (2008) 86–100.

[284] C.M. Wake, C.W. Patrick, A.G. Mikos, Pore Morphology Effects on the Fibrovascular Tissue Growth in Porous Polymer Substrates, Cell Transplant. 3 (1994) 339–343.

[285] I. V Yannas, E. Lee, D.P. Orgill, E.M. Skrabut, G.F. Murphyt, Synthesis and characterization of a model extracellular matrix that induces partial regeneration of adult mammalian skin, Proc. Natl. Acad. Sci. 86 (1989) 933–937.

[286] H. Wang, J. Pieper, F. Peters, C.A. Van Van Blitterswijk, E.N. Lamme, Synthetic

scaffold morphology controls human dermal connective tissue formation, J. Biomed. Mater. Res. Part A. 74 (2005) 523–532. https://doi.org/10.1002/jbm.a.30232.

[287] G. Papavasiliou, S. Sokic, M. Turturro, Synthetic PEG Hydrogels as Extracellular Matrix Mimics for Tissue Engineering Applications, in: Biotechnol. - Mol. Stud. Nov. Appl. Improv. Qual. Hum. Life, 2012: pp. 112–134.